JOURNAL OF APPLIED PHYSICS

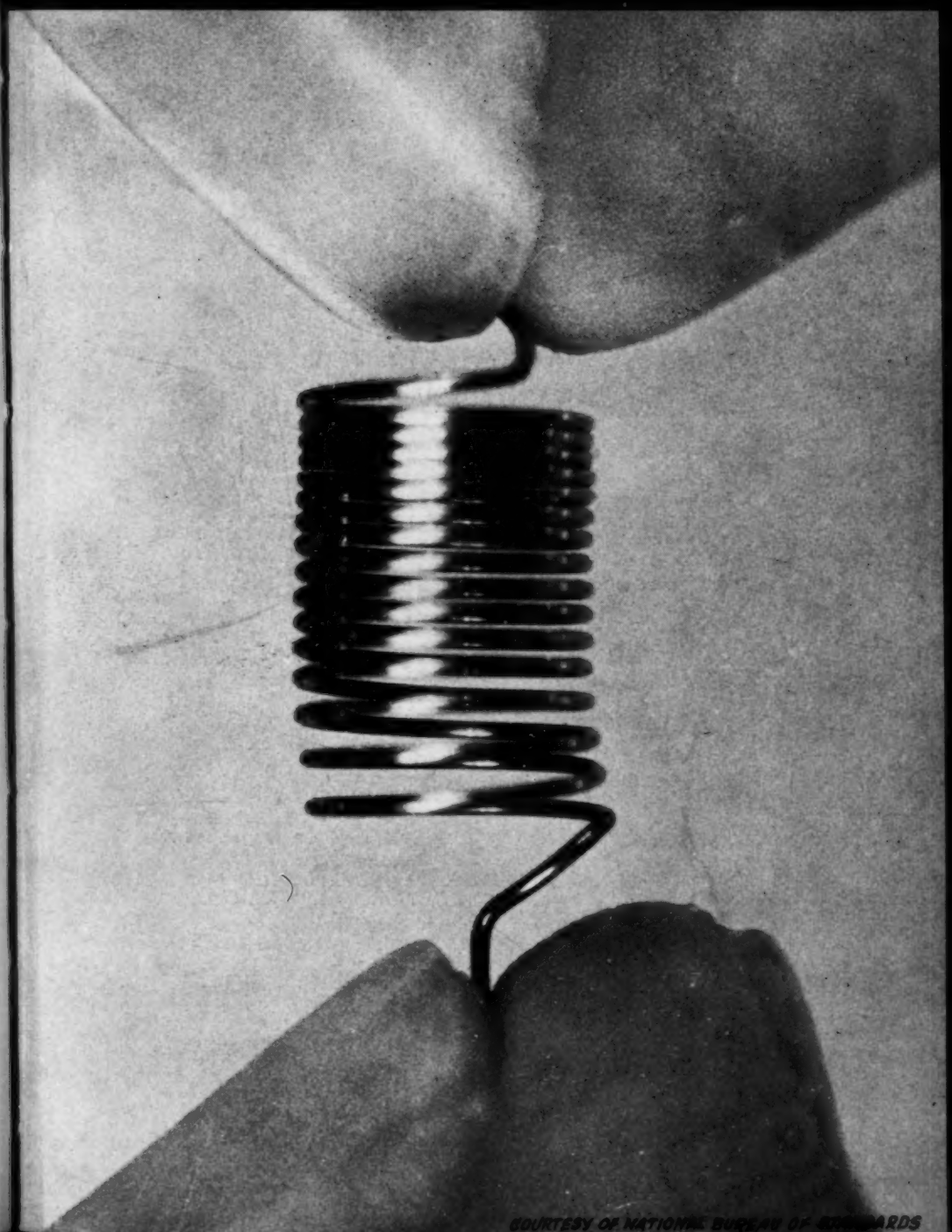

JOURNAL OF APPLIED PHYSICS

Vol. 19, No. 10 OCTOBER, 1948

In This Issue

	Page
Magnetic Properties of Ordered Nickel-Manganese Alloys — Robert I. Jaffee	867
Gains and Effective Areas of Horn Antennas — R. B. Watson and C. M. McKinney	871
Theory of Formation of Metal Chips — Väinö Piispanen	876
Recent Developments in Analysis of the Mechanisms of Positive and Negative Coronas in Air — Leonard B. Loeb	882
Alloying of Metal Powders by Diffusion — Sidney Weinbaum	897
Scattering of Ultrasonic Radiation in Polycrystalline Metals — W. Roth	901
Bridge Erosion of Electrical Contacts. Part I. — J. J. Lander and L. H. Germer	910
Twinning in Tetragonal Alloys of Copper and Manganese — Francis T. Worrell	929
Cavity Drag in Two and Three Dimensions — Milton S. Plesset and Philip A. Shaffer, Jr.	934
Energy Losses of Sound Waves in Metals Due to Scattering and Diffusion — W. P. Mason and H. J. McSkimin	940
Probability That a Meteorite Will Hit or Penetrate a Body Situated in the Vicinity of the Earth — G. Grimminger	947
On the Canonical Form of the Equations of Steady Motion of a Perfect Gas — Max M. Munk and Robert C. Prim	957
Letter to the Editor:	
Production of Ice Crystals by the Adiabatic Expansion of Gas — Bernard Vonnegut	959
Recent Books	959
In Every Issue	
Calendar of Meetings	956
New Booklets	971
Here and There	971
Index to Advertisers	xxxviii

BOARD OF EDITORS

Elmer Hutchisson, *Editor*

Associate Editors

R. Bowling Barnes
Otto Beeck
W. F. Busse
W. James Lyons
Philip Morrison
Paul E. Sabine
Frederick Seitz
J. R. Townsend
John Von Neumann

Publication of the American Institute of Physics

ADMINISTRATIVE STAFF

Henry A. Barton, *Director*
Cleveland Norcross, *Assistant Director*
Ruth F. Bryans, *Publication Manager*
Theodore Vorburger, *Business Manager*
John T. Tate, *Adviser on Publications*

GOVERNING BOARD

George R. Harrison, *Chairman*
Wallace Waterfall, *Secretary*
George B. Pegram, *Treasurer*

Luis W. Alvarez
Robert B. Brode
E. U. Condon
A. J. Dempster
W. F. Fair, Jr.
Harvey Fletcher
R. C. Gibbs
W. V. Houston
Paul E. Klopsteg
F. W. Loomis
Philip M. Morse
A. H. Pfund
John T. Tate
M. W. White
A. G. Worthing

The Journal of Applied Physics, published monthly at Prince and Lemon Sts., Lancaster, Pa., is devoted to physics in its role as the science basic to other natural sciences and to the arts and industries. Previous to 1937 this publication was known as Physics. The Journal of Applied Physics publishes editorials, news of physicists, and reviews, as well as technical papers of applied physics.

Manuscripts should be submitted to Elmer Hutchisson, Editor, Case Institute of Technology, Cleveland 6, Ohio.

Subscriptions and orders for back numbers should be addressed to Prince and Lemon Streets, Lancaster, Pa. or to the American Institute of Physics, 57 East 55 Street, New York 22, N. Y.

Subscription Price

	U.S. and Canada	Elsewhere
To members and associate members of the American Institute of Physics	$7.00	$ 8.00
To all others	9.00	10.00

Back Number Prices

Complete set: Vol. 1, July, 1931–Vol. 18, 1947—$132.00
Yearly back number rate: $10.00
Single copies: $1.00 each.

Changes of address should be sent to the Business Manager, American Institute of Physics; **corrected proofs** should be sent to the Publication Manager, American Institute of Physics.

Advertising rates supplied on request. Orders, advertising copy, and cuts should be sent to the American Institute of Physics.

Entered as second class matter January 22, 1937, at the Post Office at Lancaster, Pennsylvania, under the Act of March 3, 1879. Accepted for mailing at the special rate of postage provided for in the Act of February 28, 1925, authorized May 2, 1932.

Copyright 1948, by the American Institute of Physics.

Journal
of
Applied Physics

Volume 19, Number 10 October, 1948

The Magnetic Properties of Ordered Nickel-Manganese Alloys

ROBERT I. JAFFEE
Battelle Memorial Institute, Columbus, Ohio
(Received January 15, 1948)

Nickel-manganese alloys containing 20.1 percent, 21.4 percent, and 25.3 percent Mn in the form of Rowland rings were put into an ordered condition by very slow cooling to 380°C, and long annealing at that temperature. Magnetization curves and hysteresis loops at room temperature showed that the 21.4 percent Mn alloy was very soft magnetically, while the 25.3 percent Mn alloy was relatively hard magnetically. The 20.1 percent Mn alloy was magnetically soft, but not so soft as the 21.4 percent alloy. The magnetic properties of the ordered 21.4 percent Mn alloy changed markedly from room temperature to about 120°C. Induction at 30 oersteds decreases very rapidly, and the maximum permeability goes through a sharp maximum at 91°C. Coercive force and remanence also decrease during the same temperature interval.

ALLOYS of nickel and manganese in the region of the composition Ni_3Mn (23.78 percent by weight manganese) undergo an order-disorder reaction by annealing at temperatures below 500°C or by very slow cooling through the ordering range from 500°C to about 300°C.[1-3] Higher degrees of order are developed by long annealing at temperatures low in the ordering range or by extremely slow cooling through the ordering range. Ordered alloys are ferromagnetic, whereas disordered alloys are paramagnetic. The ferromagnetic Curie point of ordered Ni_3Mn is reported to be about 450°C; at lower manganese contents of the Curie points are lower than 450°C, and at high manganese contents they are somewhat higher.

Most investigators of the order-disorder transformation in Ni_3Mn have used saturation magnetization as a measure of magnetic quality. Little work appears to have been done on the type of ferromagnetism developed, whether "hard" or "soft," or on the variation with composition around Ni_3Mn.

This paper will report magnetization curves and hysteresis loops for three highly ordered nickel-manganese alloys containing 20.1 percent Mn, 21.4 percent Mn, and 25.3 percent Mn (two alloys on the nickel side of Ni_3Mn and one alloy on the manganese side). Also, the temperature dependence of the magnetization and hysteresis curves of the 21.4 percent Mn alloy will be reported.

TABLE I. Chemical analyses of ring specimens.

Specimen No.	Weight percent		Atomic percent	
	Manganese	Nickel	Manganese	Nickel
B 12	20.1	79.5	21.3	78.7
B 31	21.4	78.6	22.6	77.4
B 22	25.3	74.4	26.7	73.3

[1] S. Kaya and A. Kussmann, Zeits. f. Physik **72**, 293–309 (1931).
[2] N. Thompson, Proc. Phys. Soc. (London) **52**, 217–228 (1940).
[3] S. Kaya and M. Nakayama, Proc. Phys. Math. Soc. Japan **22**, 126–141 (1940).

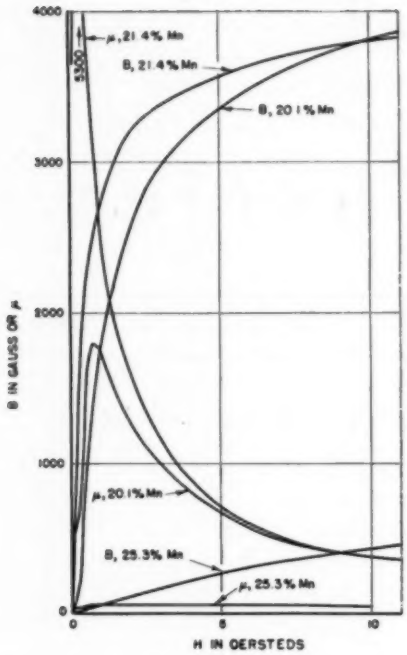

FIG. 1. Normal magnetization and permeability curves of ordered nickel-manganese alloys.

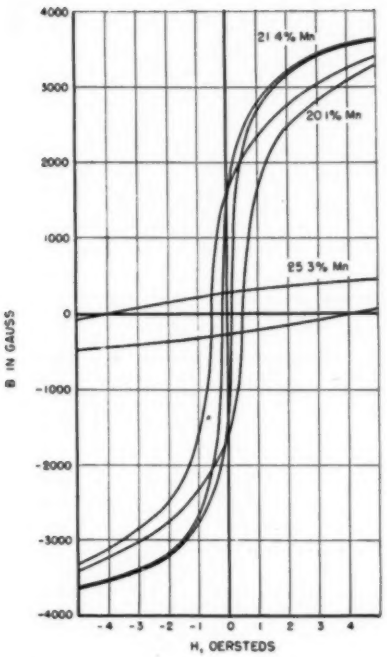

FIG. 2. Hysteresis at room temperature of ordered nickel-manganese alloys. Maximum field strength—30 oersteds.

SPECIMENS

Electrolytic manganese and electrolytic nickel were melted together in an induction furnace in an Alundum crucible, and chill-cast into plates, which were cold-rolled, with intermediate annealing at 900°C, to final size. The plates were quenched into water from 900°C as a final operation. From these plates were machined Rowland rings of the approximate dimensions 7 cm in o.d., $5\frac{3}{4}$ cm in i.d., and 1 cm thick. Chemical analyses of the millings are given in Table I.

All of the alloys were paramagnetic as quenched from 900°C, except the 20.1 percent Mn alloy, which was slightly ferromagnetic, having an induction of 330 gauss at 30 oersteds and a maximum permeability of 50 at 0.5 oersted.

ORDERING HEAT TREATMENT

The rings were heated at 600°C for one-half hour and air-quenched. They were then heated in vacuum to 560°C and slowly cooled to 440°C in 13 hours, cooled from there to 400°C in six hours, held at 380°C for sixty hours, and furnace-cooled to room temperature. This heat treatment must have allowed the alloys to approach order-disorder equilibrium at 380°C, which is low as an ordering temperature goes, and, consequently, the degree of order attained by these specimens must have been high.

MAGNETIC MEASUREMENTS

The ballistic methods described by T. F. Wall[4] were followed in carrying out the magnetic measurements. About 260 primary turns and 100 secondary turns were wound on the rings. By means of suitable resistances and switches, magnetization values were taken at suitable field strengths to 30 oersteds. Hysteresis loops were measured from 30 oersteds to −30 oersteds.

MAGNETISM AT ROOM TEMPERATURE

Results of magnetization and hysteresis of the three-ordered nickel-manganese alloys as annealed at 380°C are shown in Figs. 1 and 2. A summary of the magnetic constants is given in Table II.

It is seen that the 21.4 percent Mn alloy is magnetically very soft, and the 25.3 percent Mn

[4] T. F. Wall, *Applied Magnetism* (E. Benn, Ltd., London, 1927).

alloy is magnetically very hard. The alloy with 20.1 percent Mn, although soft magnetically, is not nearly so soft as the 21.4 percent Mn alloy. The fact that the two magnetically soft alloys are on the nickel side of the compound Ni_3Mn, whereas the magnetically hard alloy is on the manganese side of Ni_3Mn, appears to be significant.

Although only three alloy comparisons were studied, it is extremely interesting that a maximum in permeability and minimum in coercive force should be found at 2.14 percent Mn, 78.6 percent Ni. The case of permalloy in the nickel-iron system at 21.5 percent Fe, 78.5 percent Ni at once comes to mind. Elmen[5] found that the initial permeability of nickel-iron alloys air-quenched from 600°C, approximately the Curie point, reached a maximum at 78.5 percent Ni. Long annealing at 425°C produced much lower permeabilities. S. Kaya[6] has found that the critical ordering temperature for Ni_3Fe is 490°C. Therefore, the point of similarity in the two cases is a maximum in magnetic softness at 78.5 percent Ni, and the point of dissimilarity is that quenching through the ordering range brings out the highest permeability in Ni_3Fe, whereas long annealing within the ordering range brings out highest permeability in Ni_3Mn. Actually, quenching through the ordering range results in a paramagnetic condition in the Ni_3Mn alloys.

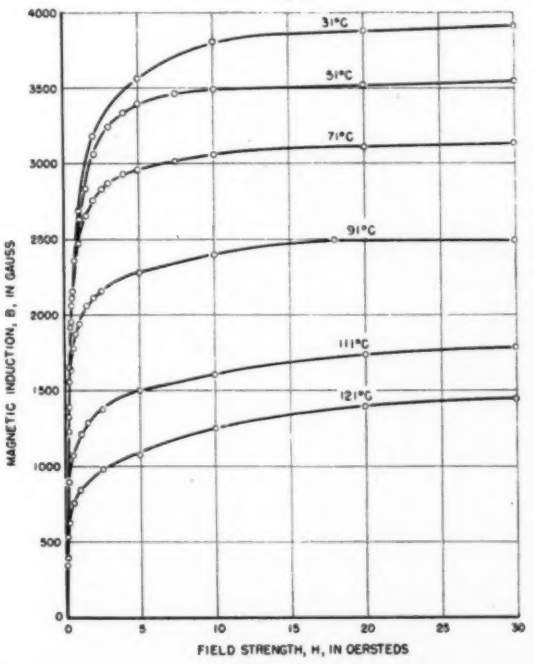

FIG. 3. Magnetization curves of ordered 21.4 percent manganese alloy from 31° to 121°C.

TABLE II. Magnetic properties of ordered nickel-manganese alloys at room temperature.

Property	Composition 20.1 percent Mn	21.4 percent Mn	25.3 percent Mn
Normal Magnetization			
Maximum permeability	1800	5300	60
Field strength at maximum permeability, oersteds	0.75	0.25	1
Induction in gauss at 30 oersteds	4130	3910	885
Hysteresis			
Remanence, gauss	1590	1420	260
Coercive force, oersteds	0.52	0.15	4.0

EFFECT OF TEMPERATURE ON MAGNETIC PROPERTIES

Since the highest permeabilities and lowest coercive forces were found with the ordered 21.4

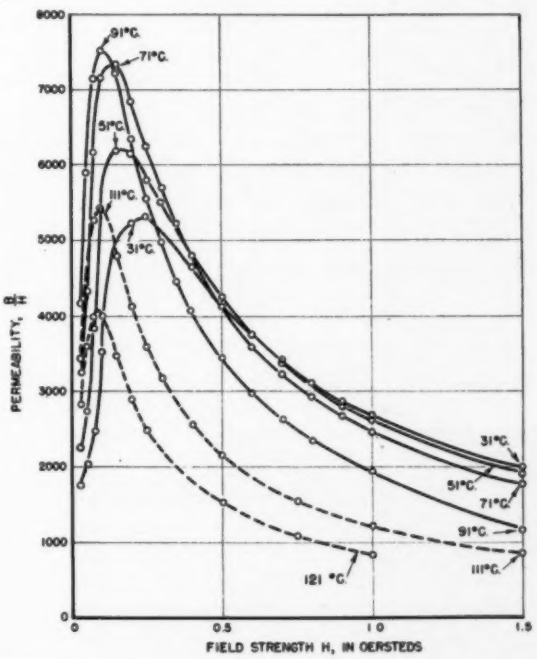

FIG. 4. Permeability of ordered 21.4 percent manganese alloy from 31° to 121°C.

[5] G. W. Elmen, "Magnetic alloys of iron, nickel, and cobalt," J. Franklin Inst. **207**, 583–617 (1929).
[6] S. Kaya, J. Faculty Sci., Hokkaido Imp. Univ., **2**, 29–53 (1938).

TABLE III. Hysteresis constants of 21.4 percent Mn annealed at 405°C for 170 hours.

Temperature, °C	Induction at 30 oersteds, gauss	Remanence, B_r gauss	Coercive force, H_c, oersteds
32	4510	1590	0.24
51	4090	1430	0.20
66	3800	1330	0.18
77	3525	1190	0.17
95	2980	930	0.15
115	2530	730	0.12

percent Mn alloy, it was of interest to investigate the effect of temperature on the magnetic properties of this alloy. Figure 3 shows magnetization curves from 31° to 121°C, and Fig. 4 shows the corresponding permeability curves at the same temperatures. A most interesting feature of these curves is the rapid decrease in induction at 30 oersteds as the temperature increases, an over-all drop of about 28 gauss per degree centigrade. Also, the maximum permeability goes through a maximum in this temperature interval, rising to a peak value of 7520 at 0.1 oersted and 91°C.

Hysteresis data at various temperatures were not obtained on the 21.4 percent Mn alloy as annealed at 380°C, for which all previous data apply. However, hysteresis data were obtained for the same alloy as annealed 170 hours at 405°C. The variation in the hysteresis constants, remanence, and coercive force from 32°C to 115° for the 405°C anneal are listed in Table III. The trend of both remanence and coercive force is downward as temperature increases, but not at so rapid a rate as the induction at 30 oersteds.

The rapid decrease of induction with temperature is indicative that the Curie point is being approached, although other data, not being reported here, show that it will not be reached until 280°–300°C. The phenomenon would appear to have potential utility in temperature-sensitive magnetic instruments.

SUMMARY

Nickel-manganese alloys containing 20.1 percent, 21.4 percent, and 25.3 percent Mn in the form of Rowland rings were put into an ordered condition by very slow cooling to 380°C and long annealing at that temperature. Magnetization curves and hysteresis loops at room temperature showed that the 21.4 percent Mn alloy was very soft magnetically, while the 25.3 percent Mn alloy was relatively hard magnetically. The 20.1 percent Mn alloy was magnetically soft, but not so soft as the 21.4 percent alloy. The magnetic properties of the ordered 21.4 percent Mn alloy changed markedly from room temperature to about 120°C. Induction at 30 oersteds decreases very rapidly, and the maximum permeability goes through a sharp maximum at 91°C. Coercive force and remanence also decrease during the same temperature interval.

ACKNOWLEDGMENT

This work was carried out during 1940–1942 at the Eastern Experiment Station of the Bureau of Mines, College Park, Maryland, and was part of a thesis on the order-disorder transformation in Ni_3Mn, submitted in partial fulfillment of the Ph.D. degree at the University of Maryland.

The author is grateful to Battelle Memorial Institute for aid in preparing this article for publication.

Gains and Effective Areas of Horn Antennas*

R. B. Watson and C. M. McKinney
Department of Physics and Defense Research Laboratory, The University of Texas, Austin, Texas
(Received February 5, 1948)

Two methods are described for determining the gain and effective area of an electromagnetic horn antenna. The first of these is an experimental method based on the reciprocal properties of antennas. The second method uses data obtained from measured receiving patterns, and from theoretical patterns, for calculation of values for gain and effective area. Comparable values are found from experiment and calculation for eight different horn antennas. It is concluded that the calculations described give satisfactory values of gain and effective area, taking the reciprocity values as standards.

PART I. RECIPROCITY MEASUREMENTS OF GAIN

A. Theory

FRIIS and Lewis[1] have defined absolute gain as being a number which provides a quantitative measure of the ability of an antenna to project a signal to a distant target. The gain is defined by the ratio

$$G=P/P_0, \tag{1}$$

where P is the power flow per unit area in a plane linearly polarized electromagnetic wave which the antenna causes in a distant region, and P_0 is the power flow per unit area which would have been produced if all the power fed into the antenna had been radiated equally in all directions in space. The value of gain is often particularized by choosing the value of P in the direction of maximum radiation. This definition of gain refers only to transmitting antennas; but it can be used to describe the corresponding property for any antenna.

The effective area of an antenna is defined as the quantitative measure of the ability of an antenna to collect power. This quantity is defined by the ratio:

$$A=P_R/P', \tag{2}$$

where P_R is the received power at the antenna, and P' is the power per unit area in the incident wave. Friis and Lewis further show, using the theory of reciprocity, that the ratio of gain to effective area at a given wave-length is constant for all antennas and is given by

$$(G/A)=(4\pi/\lambda^2), \tag{3}$$

where λ is the free space wave-length.

The reciprocity method[2] described herein allows the determination of the absolute gain of an antenna. The following development of the theory is primarily for electromagnetic horn type radiators but is equally applicable to other types of antennas.

Consider two electromagnetic horns, A and B (see Fig. 1) used as transmitter and receiver, respectively. The received power is

$$P_R=PA_B=\frac{P_T G_A A_B}{4\pi R^2}, \tag{4}$$

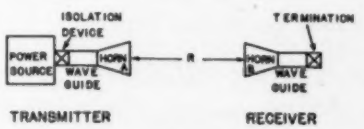

FIG. 1. Free space radio circuit.

* Part I of this paper is taken from the thesis entitled "A method of measuring the gain of electromagnetic horns at ultra-high frequencies," presented by Mr. McKinney in August, 1947, in partial fulfillment of the requirements for the M. A. degree at the University of Texas.

The work herein reported was carried out at the Defense Research Laboratory, operating under the sponsorship of the Bureau of Ordnance, Navy Department, Contract NOrd-9195.

[1] H. T. Friis and W. D. Lewis, "Radar antennas," Bell Sys. Tech. J. **26**, 220 (1497).

[2] The reciprocity method is well known and well documented in the literature. Early work describing the method known as the "three-antenna method" is found in: Carson, Bell Sys. Tech. J. **3**, 393 (1924); Sommerfeld, Zeits. f. Hochfrequenz. **26**, 93 (1925); Ballantine, Proc. I.R.E. **16**, 513 (1928); Ballantine, Proc. I.R.E. **17**, 929 (1929); Carson, Proc. I.R.E. **17**, 952 (1929). Subsequent work has resulted in a brief description of the method reported here in: King, Mimno, and Wing, *Transmission Lines, Antennas and Wave Guides* (McGraw-Hill Book Company, Inc., New York, 1945), pp. 185 and 216; *Technique of Microwave Measurements*, Radiation Laboratory Series (McGraw-Hill Book Company, Inc., New York, 1947), Vol. 11, pp. 907–915.

TABLE I. Dimensions of the electromagnetic horns.

Horn number	Description	Flare angle E-plane	Flare angle H-plane	Dimensions of mouth (cm) E-plane	Dimensions of mouth (cm) H-plane	Area of mouth (cm²)	Axial length (cm)
1	Small conical horn	Half angle of cone 10°50′		Diameter: 6.1		29.4	16.0
2	Same as no. 1	Half angle of cone 10°50′		Diameter: 6.1		29.4	16.0
3	H-flare sectoral	0°	43°30′	1.15	28.95	29.4	15.25
4	E-flare sectoral	22°40′	0°	12.7	2.28	29.4	15.25
5	Short pyramidal	31°30′	32°	6.98	8.25	57.5	4.44
6	Long pyramidal	10°50′	10°50′	4.82	6.10	29.4	10.18
7	Large conical	Half angle of cone 13°30′		Diameter: 11.5		81.0	18.40
8	Open wave guide	0°	0°	1.15	2.28	2.3	0

where P_T is the total transmitted power, G_A is the gain of antenna A, A_B is the effective area of antenna B, and R is the separation of antennas A and B. Replacing A_B by its value in terms of gain from Eq. (3) gives

$$P_R = P_T G_A G_B \lambda^2 / 16\pi^2 R^2. \tag{5}$$

This is a very important relationship in antenna work, allowing evaluation of the power received by an antenna in terms of the transmitted power, the antenna gains, and the distance of separation.

The measured power level P_A in the transmitting wave guide differs from the power transmitted into space through horn A by a factor D_{A1} caused by the discontinuity between the wave guide proper and the horn and by a factor D_{A2} caused by the discontinuity between the end of the horn and space. Similarly, the measured power level P_B in the receiving wave guide differs from the power at the horn B by two factors D_{B1} and D_{B2}. The various power levels and transfer constants may be related as follows:

$$P_A(D_{A1}D_{A2}) = P_T \tag{6}$$

$$P_R(D_{B1}D_{B2}) = P_B. \tag{7}$$

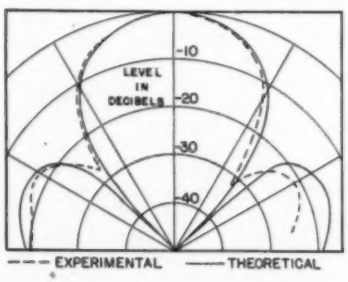

FIG. 2. Directional pattern for small conical horn (No. 1): E-plane.

More general gain constants then are

$$D_A = D_{A1}D_{A2}G_A \tag{8}$$

$$D_B = D_{B1}D_{B2}G_B. \tag{9}$$

Using these forms, Eq. (5) may be rewritten

$$P_B = P_A D_A D_B \lambda^2 / 16\pi^2 R^2. \tag{10}$$

Now consider a third horn, C, which is the horn whose absolute gain is to be measured. Horn C is used as the receiving horn, replacing horn B, and the power level in the receiving wave guide is again measured. P_A and R are held constant. Then

$$P_C = P_A D_A D_C \lambda^2 / 16\pi^2 R^2. \tag{11}$$

Horn A is replaced by horn B which now becomes the transmitter with horn C continuing as the receiver. The powers are measured again at the transmitter and receiver and designated P_B' and P_C', respectively. Then

$$P_C' = P_B' D_B D_C \lambda^2 / 16\pi^2 R^2. \tag{12}$$

Combining (10), (11), and (12) gives

$$D_C = \frac{4\pi R}{\lambda}\left(\frac{P_C P_C'}{P_B P_B'}\right)^{\frac{1}{2}}. \tag{13}$$

The gain factor D_C, a dimensionless constant characteristic of horn C alone, is thus determined in terms of measured power levels, free space wave-length, and separation between transmitter and receiver, and is completely independent of the characteristics of the auxiliary horns A and B.

B. Experimental Work

The gains of eight horns were measured for a wave-length of 3.2 centimeters. The horns were connected to standard rectangular guides excited in the $TE_{0,1}$ mode. The dimensions of the horns are given in Table I. Horns No. 1 and No. 2 were identical small conical horns. Horn No. 3 was a sectoral horn flared in the H-plane, the plane containing the direction of the magnetic vector in the wave guide. Horn No. 4 was a sectoral horn flared in the E-plane, the plane containing the direction of the electric vector in the wave guide. Horn No. 5 was a short pyramidal horn, that is, flared in both E- and H-

planes. Horn No. 6 was a somewhat longer pyramidal horn, of about the same aperture opening as No. 5. Horn No. 7 was a conical horn of the same general shape as No. 1 and No. 2, but considerably longer. "Horn" No. 8 was a 7-inch section of standard $1''\times1\frac{1}{2}''$ wave guide. Horns No. 1–4, and No. 6 all had the same aperture area. From Table I it is seen that all of the horns were relatively small, and therefore high gains were not to be expected.

The test equipment was mounted on the roof of a three story building to obtain reasonably good free space conditions. The horns were mounted about two and a half feet above the roof, with a separation of six feet between transmitter and receiver for most measurements. This distance was sufficient to produce plane waves at the receiver and to avoid any effect from the induction field of the transmitter. The transmitting horn was driven from a power source using a $723A/B$ reflex velocity modulated tube. A slotted wave guide was inserted between the signal generator and the horn to allow power level measurements by means of a traveling probe, whose output was amplified by a tuned amplifier. The same probe and amplifier were used for power level measurements at the receiving station. The receiving station consisted of the horn being used as a receiver connected through a section of slotted wave guide to a resistive-load termination. Standing wave measurements were made at both transmitting and receiving positions with a traveling probe to assure proper wave-guide arrangements.

The gain of a particular horn was calculated from Eq. (13) after measuring the power levels P_B, P_B', P_C, P_C', the frequency, and the separation between the transmitter and receiver. Numerous gain values were determined for each horn, using various power levels, separations, and combinations of auxiliary horns. The mean values of absolute gain are given in Table II.

Experimental errors may arise from reflections from the roof, incorrect power measurements due to the detector probe, instability of power output from the source, noise in the amplifier for the signal from the detector, and improper termination of horns. Calibrating procedures indicated that non-linearity of the detector probe for large signals, and a poor signal-to-noise ratio in the amplifier were the only errors of importance.

TABLE II. Summary of gain and effective area values for horn antennas.

Horn number	Reciprocity method gain	Reciprocity method effective area (cm²)	Experimental patterns gain	Experimental patterns effective area (cm²)	Theoretical patterns gain	Theoretical patterns effective area (cm²)	Geometrical area (cm²)
1	36.3	29.6	32.0	26.1	31.9	26.0	29.4
2	35.0	28.6	32.0	26.1	31.9	26.0	29.4
3	17.7	14.5	9.0	7.4	14.8	12.1	29.7
4	26.5	21.6	21.8	17.8	20.1	16.4	29.0
5	32.9	26.8	34.3	28.6			57.5
6	32.1	26.2	25.4	20.7	28.5	23.3	29.4
7	83.7	68.4	78.5	64.1			81.0
8	8.8	7.2	4.9	4.0			2.32

Directional patterns of these eight horns were made using the horns as receivers, taken in the E- and H-planes for each horn. These patterns assist in comparison of gain values, and are used in the second part of this work for gain computations. Sample directional patterns are shown in Figs. 2 and 3.

PART II. GAIN CALCULATIONS FROM PATTERNS

The gain and effective area of an antenna may be computed from the receiving patterns measured in the E- and H-planes. Gain and effective area have been defined previously by Eqs. (1) and (2) in Part I. The transmitting pattern, a plot of power radiated at a given radius *versus* angle measured from a reference axis through the antenna, defines the function P. Since the antenna is a reciprocal device, the receiving pattern likewise defines P. If the power received is P_R, then the power per unit area P is

$$P=P_R/A. \tag{14}$$

The isotropic value of power, P_0, may be obtained by finding the total energy received by integration of the receiving pattern over all

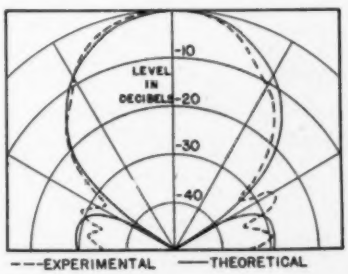

FIG. 3. Directional pattern for small conical horn (No. 1): H-plane.

TABLE III. Gain and effective area for horn antennas for E- and H-planes.

Horn number	Experimental patterns: gain		Experimental patterns: effective area (cm²)		Theoretical patterns: gain		Theoretical patterns: effective area (cm²)	
	E-plane	H-plane	E-plane	H-plane	E-plane	H-plane	E-plane	H-plane
1	38.0	28.3	31.0	23.1	39.3	26.5	32.1	21.6
2	38.0	28.3	31.0	23.1	39.3	26.5	32.1	21.6
3	4.2	29.8	3.44	24.3	3.7	526.0	3.02	429.0
4	82.8	9.71	67.6	7.92	164.0	5.38	134.0	4.39
5	40.1	30.5	32.7	24.9				
6	25.4	25.4	20.7	20.7	28.5	28.4	23.3	23.2
7	72.8	85.5	59.4	69.8				
8	2.21	17.9	1.8	14.6				

angles, and redistributing this energy uniformly. The geometry of the situation is shown in Fig. 4. Assuming that the pattern is independent of ϕ, the value of P_0 is

$$P_0=\frac{1}{2}\int_0^{\pi}(P_R/A)\sin\theta d\theta. \tag{15}$$

Calculation of gain values proceeds by graphical evaluation of this integral from the receiving patterns. Experimentally, power levels are referred to the maximum value for the receiving pattern, P_{RM}. Hence the expression used for computation takes the form

$$G=\frac{1}{\frac{1}{2}\sum_{i=1}^{N}(P_{Ri}/P_{RM})\sin\theta_i\Delta\theta_i}, \tag{16}$$

where the summation extends from $\theta=0$ to $\theta=\pi$. The effective area A may be obtained further from computed values of G by use of Eq. (3).

The values of G and A obtained by this process refer to a pattern taken in a single plane. The derivation assumes patterns in all other planes are the same, by assuming no dependence on ϕ. In practice two patterns are usually taken: a pattern in the E-plane and a second pattern in the H-plane. The actual gain of the horn may be found approximately by suitably averaging the two values computed from these patterns. Best agreement with the reciprocity values of gain as

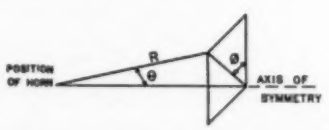

FIG. 4. Geometry for pattern computation.

determined in Part I was found by an elliptical average of the two computed values. This elliptical average was formed by assuming that the gain in planes other than the E- and H-planes takes on such values that a polar plot of gain *versus* the angles of these planes forms an ellipse whose semi-axes equal the gain values of the E- and H-planes, and then performing a suitable integration. The gain values and effective areas were computed from experimental E- and H-plane patterns for the group of horns described in Part I. In addition, calculations have been made using theoretical patterns for some of these horns. The resultant values are summarized in Table III for the E- and H-planes separately. The elliptical averages are compared with the reciprocity method values in Table II.

The values of effective area calculated from the theoretical patterns for the several horns all lie at about the same value of geometrical area. To extend this information to give further comparisons between theory and experiment, gains and effective areas were calculated from theoretical patterns for several horns with square apertures, the sides of the square being assigned the values 0.5λ, 1.0λ, 1.5λ, 2.0λ, 2.5λ, 3.0λ, and 4.0λ. The variation of effective area for these horns is shown in Fig. 5. On this same graph are plotted areas computed and measured for those horns most nearly symmetrical, as the unsymmetrical horns clearly have effective areas falling below the theoretical curve, and should not be comparable to the symmetrical horns.

ANALYSIS OF EXPERIMENTAL AND CALCULATED DATA

The values of gain determined by the reciprocity method are shown in Table II, and are plotted *versus* the aperture area of the horns in Fig. 6. On this figure is also plotted the relationship between gain and effective area, taken from Eq. (3).

The presence of losses in these horns causes all the points to lie below the straight line. It is seen that horns No. 1, No. 2, No. 6, and No. 7 have gains nearly equal to the values predicted by Eq. (3). Horns No. 3, No. 4, and No. 5 have much lower gain values than predicted, in spite of their large apertures; too large flare angles for these horns cause field distortions at their open-

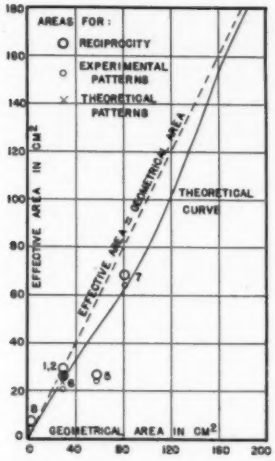

FIG. 5. Effective area *versus* geometrical area for symmetrical horns.

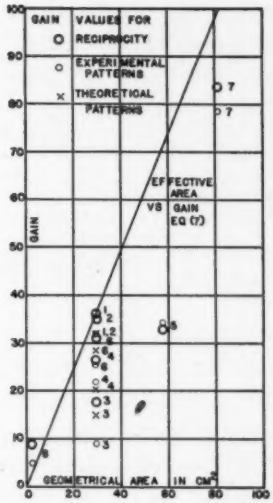

FIG. 6. Gain *versus* aperture area of horns.

ings leading to the lowered gains. Horn No. 8 has a gain greater than the straight line value. This large value is due in part to experimental error; receiver noise was nearly as large as the signal for this horn, leading therefore to an erroneous value of gain. Also, the value of gain for small apertures does not reduce toward zero but reaches a limiting value of unity; correspondingly, the effective area for small apertures approaches the limit of $\lambda^2/4\pi$. Hence the value for horn No. 8 might well lie above the straight line because of its small size.

The gain values calculated from experimental and theoretical patterns are also shown in Table II and plotted in Fig. 6. The gains calculated from theoretical patterns lie, in general, below the reciprocity values or the values obtained from experimental patterns. This is unexpected since the experimental work perforce includes the effect of incidental losses while the theory does not. The experimental values are high because of two previously mentioned experimental difficulties: the presence of high noise level and inaccuracy of the power detector for large signals. The values from theoretical (and experimental) patterns are open to some question because of the use of the elliptical averaging process in the absence of detailed patterns in planes other than the *E*- and *H*-planes.

The computed curve for symmetrical square horns agrees somewhat better with the experimental and computed values than the straight line of Eq. (7), as is seen in Fig. 5. This effect is to be expected since the values for the computed curve are obtained from theoretical patterns in the same way as the points calculated from the experimental patterns. It is seen that the areas for the three conical horns (No. 1, No. 2, and No. 7) lie somewhat above the curve, indicating a slightly greater effective area than for a square horn; the two nearly square horns (No. 5 and No. 6) have values lying below the curve because of losses and reflections at the junction between horn and wave guide. The data for the open wave guide (horn No. 8) lie somewhat above the curve, presumably due to the fact that the wave guide is unsymmetrical with a 2.5:1 ratio between its two dimensions, and also due to experimental errors for the reciprocity measurement.

It is concluded that the values of gain and effective area for horn antennas computed from experimental and theoretical patterns are comparable with the values obtained by the reciprocity method, being very nearly the same for symmetrical horns and not far different for unsymmetrical horns if an elliptical average is taken of the two available gain values.

ACKNOWLEDGMENT

The authors are greatly indebted to the Defense Research Laboratory at the University of Texas for making available the equipment and

facilities necessary for taking the experimental data described in this paper. Mr. C. W. Horton of the Defense Research Laboratory assisted materially by providing the theoretical patterns for horns No. 1 through No. 4, and No. 6, and by providing the theoretical patterns for the symmetrical square horns described in Part II. Mr. Horton was also very generous in devoting much of his time to discussions of the several aspects of the problem treated in this paper.

Theory of Formation of Metal Chips

VÄINÖ PIISPANEN
Oy. Billnäs Ab., Billnäs, Finland
(Received February 10, 1948)

In this article values for the angles β and ν have been deduced (compare Fig. 3 and Eqs. (2) and (3)). New values have been deduced for the shear angle ϕ, Eqs. (16), (20), and (21). The increasing of the internal friction and the strain hardening have been considered.

Equations for the work done in cutting per unit of length (6) and (13) have been deduced. For the cutting force Eqs. (14), (15), and (19) have been deduced. A high cutting speed decreases the friction angle τ between the chip and the face of the tool, by which the forces loading the machine tool steeply may be decreased. These forces are very highly dependent on the friction angle τ, since the rake angle α is negative.

A new theory of the formation of a discontinuous chip is presented.

I. GENERAL

IN this discussion only orthogonal cutting is treated. Accordingly, the cutting edge is normal to the direction of motion of the tool. Only one edge is cutting, and consequently the tool is wider than the machining surface. The lateral expansion of the chip is disregarded.

Among the modes of formation of chips the following are the most important:

(I) Continuous chip without built-up edge. The chip is of uniform thickness, unitary.

(II) Continuous chip with built-up edge. At the cutting edge a built-up edge is formed, which may change continually with regard to its volume. In this case the chip is also continuous, but the thickness of the chip and the nature of the surface are varying.

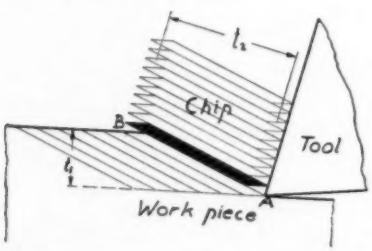

FIG. 1. Chip formation: a lamella just removed is marked black. In reality, the lamellas are very thin.

(III) Discontinuous chip. The chip is formed of chip parts, which generally are connected. The machined surface usually shows a frequency similar to the frequency of the chip. The surface machined is bad.

(IV) Broken chip occurs by machining fragile materials.

Here the chips under (I) and (III) will be considered.

II. CONTINUOUS CHIP WITHOUT BUILT-UP EDGE

A. Low Cutting Speed

1. *Theory*

The theory and some of the mathematical equations presented here were published by the writer in 1937.[1]

The formation of chips is assumed to proceed so that thin lamellas of metal move as shown in Fig. 1, in which the lamella just moved is marked black. In reality the lamellas are quite thin, and the chip is of uniform thickness.

Figure 2 shows the same matter in a somewhat different way. The formation of chips goes so that the parallelogram $ABCD$ turns into the

[1] Väinö Piispanen, Teknillinen Aikakauslenti **27**, 315–322 (1937).

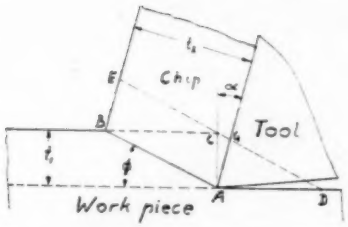

FIG. 2. Chip formation: the parallelogram $ABCD$ changes into the parallelogram $ABEG$.

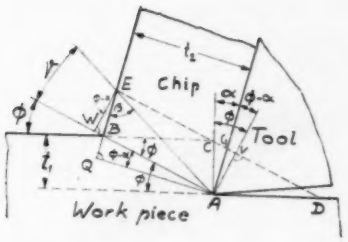

FIG. 3. Shear angles.

parallelogram $ABEG$. The depth of cut on the figures is equal to t_1 and the thickness of the chip is t_2. The shear angle is ϕ. It is easy to make evident that

$$t_2 = t_1[\cos(\phi-\alpha)/\sin\phi].^{1,2} \quad (1)$$

In Fig. 3 the angles required for deducing the formulas are shown.

In Fig. 4 the same formation of chips is shown in a diverging way. The square H in the work piece changes in the chip into the parallelogram K. The screw LM driven in the work piece changes into the screw TU.

The values of the angles β and γ will be:

$$\cot\beta = [\sin\phi\cos\phi/\cos^2(\phi-\alpha)] + \tan(\phi-\alpha),^1 \quad (2)$$

$$\cot\gamma = [1/\cos\phi\sin\phi] + \tan(\phi-\alpha). \quad (3)$$

2. *The Forces, Work, and Shear Angle* ϕ

The most essential of the shear angles is the angle ϕ. The working out of the value of the angle is based upon the following presumption: *the value of the angle* ϕ *is such that the shear resistance is at its minimum and the work done in cutting at its minimum.*

To calculate the work done in cutting it is at first necessary to clear up the forces which affect the shear point. Figure 5a shows these forces.

The force R, which the tool exerts on the chip, can be divided into two components. One of these, the force N, works normal to the face of the tool and does not do any cutting work. The other of the components, the force F, is a friction force, and works counter to the motion of the chip along the face of the tool. To subdue force F a part of the work done in cutting is required.

The formation of the chip takes place in the plane AB and the reaction of the force R can here be divided into two components, F_n and F_s. The former acts in the shear plane, and this force alone resists the removal of the lamellas of material. The other of the components, the force F_n, affects normal to the shear plane, and, to begin with, it is supposed that it does not increase the cutting work.

The value of the force F will be

$$F = F_s[\sin\tau/\cos(\phi+\tau-\alpha)]. \quad (4)$$

In Fig. 5a an exaggerated, thick, just-removed lamella is drawn in black. The tool moves the distance GO, the lamella slides the distance AO, and the chip moves along the face of the tool the distance AG. The work done in cutting per unit of length is equal to P and for this we get the following equation:

$$P = [F\cdot(AG) + F_s\cdot(AO)]/(GO). \quad (5)$$

By substituting the values herein we get

$$P = F_s\frac{\sin\phi}{\cos(\phi-\alpha)}\left[\frac{\sin\tau}{\cos(\phi+\tau-\alpha)} + \frac{\cos\alpha}{\sin\phi}\right]. \quad (6)$$

The value of the force F_s is dependent on the dimensions of the surface AB. If the chip width

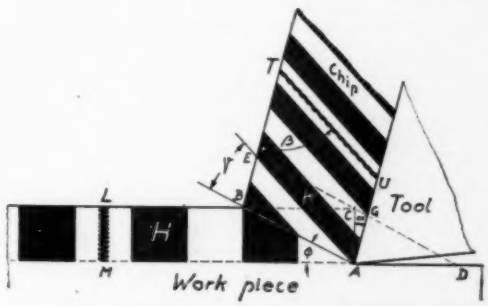

FIG. 4. Chip formation: the square H changes into the parallelogram K.

[2] M. Eugene Merchant, J. App. Phys. **16**, 318–324 (1945).

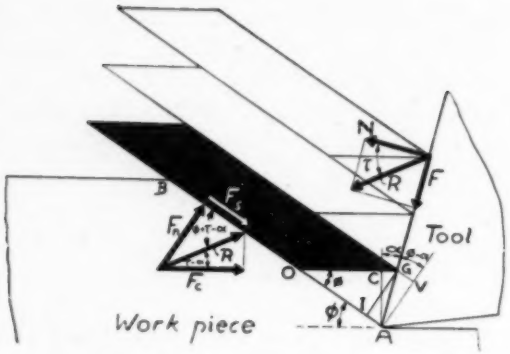

FIG. 5a. Cutting forces (without increase of the internal friction).

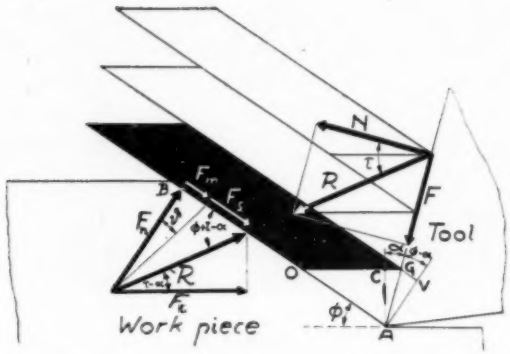

FIG. 5b. Cutting forces (with increase of the internal friction).

equals t_3, the dimensions of the shear plane $AB=t_1\cdot t_3/\sin\phi$.

The value of the force F_s further is dependent on the shear strength of the material S which is supposed to be constant. Accordingly, we get

$$F_s=t_1\cdot t_3\cdot S/\sin\phi=\text{constant}/\sin\phi, \tag{7}$$

and by substituting this value into Eq. (6):

$$P=\frac{\text{const.}}{\cos(\phi-\alpha)}\left[\frac{\sin\tau}{\cos(\phi+\tau-\alpha)}+\frac{\cos\alpha}{\sin\phi}\right]. \tag{8}$$

This work P attains its minimum when the derivate of the same in proportion to $\phi=0$. The ciphering gives

$$\phi=45°+(\alpha/2)-(\tau/2). \tag{9}$$

Equation (9) is published in several excellent articles.[2,3]

a. *The increase of the internal friction.*—It seems, however, very likely that the effect of the force F_n is to be taken into consideration. This force effects normal to the shear plane thus: the friction between the lamellas increases. It would be a great object of research to investigate if this is really so. It would be necessary to settle how the force pressing upon the surface of the work piece affects the (internal) shearing strength of the material. For this laboratory experiments should be done, and for such the writer does not have the opportunity. Here it is assumed that the force F_n causes the additional force F_m (Fig. 5b) and that

$$F_m=F_n\cdot\tan\vartheta. \tag{10}$$

The values of the forces will then be found as follows:

$$F_m+F_s=\frac{F_s}{1-\tan\vartheta\,\tan(\phi+\tau-\alpha)}, \tag{11}$$

$$F=\left[\frac{F_s}{1-\tan\vartheta\,\tan(\phi+\tau-\alpha)}\right]\times\left[\frac{\sin\tau}{\cos(\phi+\tau-\alpha)}\right], \tag{12}$$

and the work per unit of length

$$P=F_s\cdot\frac{\sin\phi}{[1-\tan\vartheta\,\tan(\phi+\tau-\alpha)]\cos(\phi-\alpha)}\times\left[\frac{\sin\tau}{\cos(\phi+\tau-\alpha)}+\frac{\cos\alpha}{\sin\phi}\right]. \tag{13}$$

For the force F_c we get the following equations:

$$F_c=\frac{\text{constant}\cdot\cos(\tau-\alpha)}{\sin\phi[1-\tan\vartheta\,\tan(\phi+\tau-\alpha)]\times\cos(\phi+\tau-\alpha)} \tag{14}$$

and

$$F_c=\frac{\text{constant}\cdot\cos\vartheta\,\cos(\tau-\alpha)}{\sin\phi\,\cos(\phi+\tau-\alpha+\vartheta)}. \tag{15}$$

When the work done in cutting reaches its minimum, F_c also gets its minimum, because the work done in cutting per unit of length $P=t_1\cdot t_3\cdot S\cdot 1\cdot F_c=\text{constant}\cdot F_c$.

[3] Hans Ernst and M. Eugene Merchant, *Chip Formation, Friction and Finish* (Cincinnati Milling Machine Company, Cincinnati, 1940).

F_c again attains its minimum when the derivate of the force in proportion to $\phi=0$. The shear angle ϕ may be found as follows

$$\phi=45°+(\alpha/2)-(\tau/2)-(\vartheta/2). \quad (16)$$

b. *Strain hardening.*—Furthermore, we wish to indicate that the value of the angle ϕ is dependent on the strain hardening of the material. As is known, a material hardens by machining. The unit of the machining of the material is the ratio AO/AV (Fig. 5b). The shear strength of the material S thus is a function of this, or

$$S=f(AO/AV)=f[\cos\alpha/\sin\phi\cos(\phi-\alpha)]. \quad (17)$$

Of what kind this correlation is should be determined by special investigations. The hardening of the material affects the strength qualities and beyond this the temperature, etc.

Equation (17) includes the ratio $\cos\alpha/\cos(\phi-\alpha)$, which is almost constant (the angle $(\phi-\alpha)$ is near to zero and the cosine of the same varies only a little). To get some conception of the effect of the hardening of the material upon the value of the shear angle ϕ, it was assumed that $S=\text{const.}/\sin\phi$. By substituting this into Eq. (7) we get

$$F_s=(t_1\cdot t_3/\sin\phi)\cdot(\text{const.}/\sin\phi)$$
$$=\text{const.}/\sin^2\phi \quad (18)$$

and the value of F_c will be

$$F_c=\frac{\text{const.}\cos\vartheta\cos(\tau-\alpha)}{\sin^2\phi\cos(\phi+\tau-\alpha+\vartheta)}. \quad (19)$$

The shear force F_c attains its minimum when the derivate of the same in proportion to $\phi=0$. The ciphering leads to the following result:

$$2\phi=\alpha-\tau-\vartheta+\text{arc}\cos[-\tfrac{1}{3}\cos(\tau-\alpha+\vartheta)]. \quad (20)$$

The formula surely is not for general application, and it is not certain as to whether or not it is valid by chip formation condition and thus within ranges in which the ratio AO/AV is always important.

As mentioned above, Eq. (20) is not based upon necessary investigations of material, etc. The writer suggests the following equation for the shear angle ϕ:

$$2\phi=90°+\alpha-\tau-\vartheta+\delta, \quad (21)$$

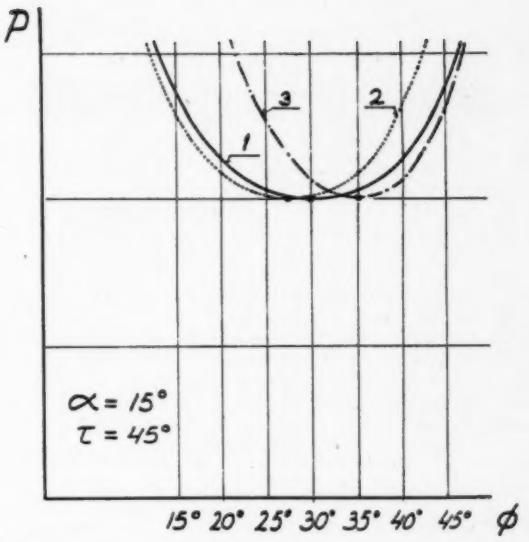

FIG. 6. The work done in cutting P is dependent on the shear angle ϕ, and on whether the increase of the internal friction and the strain hardening are regarded.

	Curve 1	Curve 2	Curve 3
Increase of the internal friction	Disregarded	Regarded	Regarded
Strain hardening	Disregarded	Disregarded	Regarded

in which the value of the angle δ is dependent on the strain hardening. Researches should be made to fix the same and the results presented in form of a table or nomogram.

Figure 6 shows how the increase of the internal

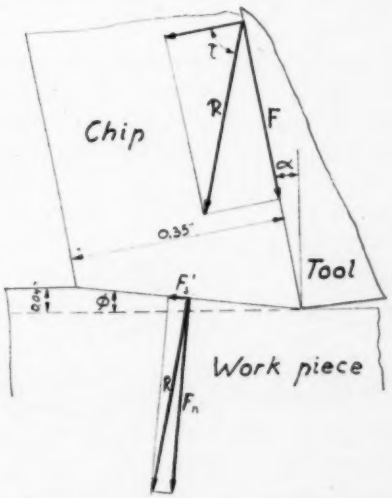

FIG. 7. When the angle $\alpha=-10°$ and the cutting speed is low, the chip is thick, the friction angle τ great, and the force R straining the machine great.

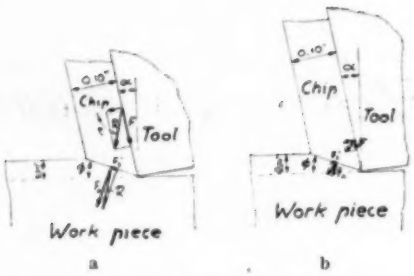

FIG. 8. a. The cutting speed is great and the chip thin. If the friction angle τ should be great, formation of chips would not be possible (the force F_s' which removes the chip outward would be negative). b. High cutting speed, thin chip, the friction angle τ smaller, machine loading forces steeply decreased.

friction of the material and the strain hardening affect the work done in cutting P. To facilitate the comparison the minima of all the curves have been placed on the same height.

B. High Cutting Speed

The writer has not had the opportunity to make experiments with high cutting speeds, and an investigation carried out by Hans Ernst[4] is used as a basis. His photographs have also been used as the basis for the drawing of Figs. 7, 8a, and 8b. In all of this the cutting depth $t_1=0.04''$ and the rake angle $\alpha=-10°$.

In the case shown in Fig. 7 (the chip probably will be discontinuous) the thickness of the chip $t_2=0.35''$ and the cutting speed is 140 feet per minute. By applying Eq. (9) the value of the angle τ will be $\sim 67.5°$. The force R is, as appears, great.

In the case shown in Figs. 8a and 8b the cutting speed is 780 feet per minute. The thickness of the chip $t_2=0.10''$. If the friction angle τ would be 67.5°, the force F_s' (Fig. 8a) which moves the lamellas would affect in the wrong direction and the formation of chips would not be possible. If also in this case the value of the friction angle τ is calculated according to Eq. (9) we get $\tau \sim 39.5°$ and this angle is shown in Fig. 8b. (May it cursorily be mentioned that the mass forces by a cutting speed of 780 feet per minute are small in comparison to the strength of the material.)

By comparing Figs. 7 and 8b we find that the decreasing of the friction angle τ affects a steep reduction of the forces (R) which strain the machine. If we get the angle τ small, the machine could be of a much lighter and less power-consuming construction. To find out other ways of reducing the friction angle τ (and this is of special importance if the rake angle α is negative) would, in the writer's opinion, be an important task for inventors and scientists. Possibilities: pressing out the lubricant at the shearing point; lapping the face of the tool super-smooth; covering the face of the tool with a material of low friction; changing the analysis of the tool and the machining materials; using such an immovable or rotating (roll-formed) tool, the cutting edge of which should be placed distinct obliquely to the direction of motion of the tool, etc.

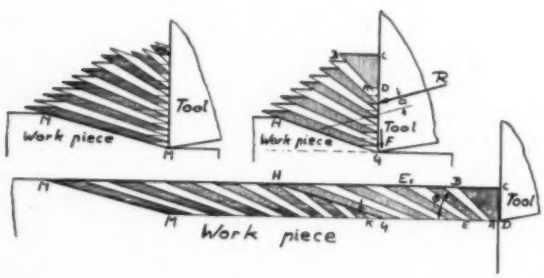

FIG. 9. When a discontinuous chip is formed, the angle ϕ changes under the process.

[4] Hans Ernst, Mech. Eng., 295–300 (May, 1944).

III. DISCONTINUOUS CHIP

Since the rake angle α is small and (or) the friction angle τ great, the chip formed is often discontinuous. Here we try to give the theory behind this. The writer has had at his disposal only primitive research materials.

Figure 9 shows schematically the formation of chips when the angle $\alpha=0°$. On the lower part of the figure is shown the work piece before the chip is formed and on the upper part two chip particles formed. As the tool has touched the one end of the work piece, the piece $ABCD$ slides at first. As this has slidden, the following piece (lamella) begins to slide. The more lamellas there are rubbing against the face of the tool, the greater the friction force F grows. The share of the friction force F in the work done in cutting equals $F\cdot(AG)$ (see Fig. 5a, Eq. (5)). If the share of the friction force in the work done in cutting would steeply increase, the work done

in cutting P would also steeply increase. The work done in cutting P, however, automatically tries to find its minimum and it will find, as the force F has increased, its minimum so that the denominator GO of Eq. (5) increases or, accordingly, *the angle ϕ decreases*. (The increasing of the work $F_s \cdot (AO)$ limits that.) The angle ϕ decreases continually and the lengths of the lamellas increase. The angle ϕ decreases until the sliding distance of the lamellas (=ratio AO/AV, Fig. 5a) grows so great that the shearing stress of the material is exceeded and the chip particle is cut off from the work piece. The cutting off of the chip particle is facilitated by the increasing of the force R (the compressive stress increases in the sliding plane) and the increasing of the lever a of the same (the bending stress increases in the sliding plane). In Fig. 9 GH shows the surface, along which the first chip particle is cut off.

The direction of the following slide plane is, however, not the same as the direction of the plane GH, because the force $F=0$. The angle ϕ is again great and the sliding plane has the direction KL. As further lamellas are rubbing against the face of the tool, the angle ϕ decreases anew and the lengths of the lamellas again increase until that following chip particle is cut off (along the plane MN). That second chip particle has been formed of the part $GHMN$.

Figure 10a shows a result of an experiment. The work piece is mild steel. The chip particle formed is marked I in the figure. AD indicates the machined surface. It was assumed that the chip particle is formed of the part $ABCD$ of the work piece. With the means at our disposal it could not be proved whether or not the chip was formed of strings of lamellas (e.g., $EFGH$).

In Fig. 10b an attempt is made to visualize the writer's theory of formation of a discontinuous chip. The proceeding is as described above and the squares Q of the work piece change, after the cutting, into long lamellas T. $ABCD$ is the part of the work piece of which the chip particle is formed. K and L show varying phases of the formation and $CDMN$ a chip particle which is just removed from the work piece.

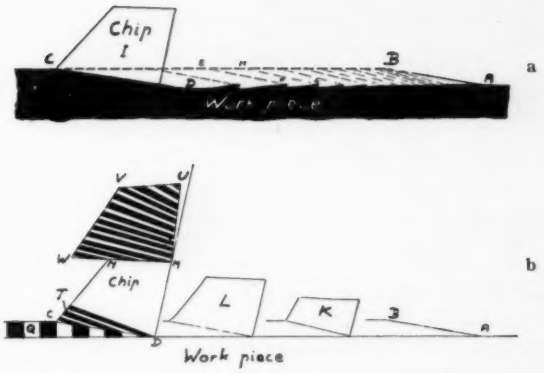

FIG. 10. a. The machined surface of a discontinuous chip and a chip particle. b. Forming of a discontinuous chip: the square Q changes in the chip into the lamella T.

IV. SUMMARY

There are the following equations for the shear angle ϕ:

$$\phi = 45° + (\alpha/2) - (\tau/2) - (\vartheta/2) \quad (16)$$

(the increasing of the internal friction is regarded),

$$2\phi = \alpha - \tau - \vartheta + \arccos\left[-\tfrac{1}{3}\cos(\tau - \alpha + \vartheta)\right] \quad (20)$$

(besides the foregoing strain hardening also regarded).

Work done in cutting per unit of length equals P and

$$P = \frac{F_s \sin\phi}{[1 - \tan\vartheta \tan(\phi + \tau - \alpha)]\cos(\phi - \alpha)} \times \left[\frac{\sin\tau}{\cos(\phi + \tau - \alpha)} + \frac{\cos\alpha}{\sin\phi}\right]. \quad (13)$$

Cutting force equals F_c and for that the following equations are given:

$$F_c = \frac{\text{constant} \cdot \cos(\tau - \alpha)}{\sin\phi[1 - \tan\vartheta \tan(\phi + \tau - \alpha)] \times \cos(\phi + \tau - \alpha)}, \quad (14)$$

$$F_c = \frac{\text{constant} \cdot \cos\vartheta \cos(\tau - \alpha)}{\sin\phi \cos(\phi + \tau - \alpha + \vartheta)}. \quad (15)$$

Making clear the theory of formation of chips is the basis of the whole machining problem and of the developing of the machine tools. Every possible progress on the range of theory is of use in practice for the manufacturers of machine tools as well as for the users of them.

Recent Developments in Analysis of the Mechanisms of Positive and Negative Coronas in Air*

LEONARD B. LOEB
Department of Physics, University of California, Berkeley, California
(Received March 3, 1948)

The nature of the detailed mechanism of the negative Trichel corona pulses in air at atmospheric pressures is reanalyzed on the basis of recent data of English giving the time duration of the pulse and details of its structure. The onset of corona from a negative point is shown to consist of pulses of about 4 μsec. duration with a rise time of about 1 μsec. It is shown to initiate according to the classical Townsend equation, building up a positive space charge of increasing intensity at the point surface, and an electronic and beyond this, an ionic space charge further out in the gap. The intense positive space charge leads to an auto-accelerative ionizing mechanism with Morton-Johnson ionization near the point. The magnitude of these space charge fields account for the sputtering previously observed. On the basis of the field distributions which can be deduced, the course of the growth of the visual and electrical phenomena can be traced to the point where the space charge distortion by negative ion formation out in the gap causes the pulse to choke off. New pulses will then start as soon as the field has cleared away the inhibiting negative ion space charge, if triggering electrons are present. The rate of removal of the negative ions depends on the clearing time for negative ions across the gap, and the rate increases as the applied potential increases. The duration of the pulse depends on the rate of electron production by the auto-accelerative process and the negative ion accumulation appears to require nearly the same total number of negative ions to choke itself off as does the positive corona. The axial space charge gradients account for the constrictions and flaring characteristics of the discharge. These findings are correlated with the coronas in very pure N_2 and H_2. The observed near equality of the thresholds for positive burst pulse corona onset and Trichel pulses is analyzed and shown to be caused only by a fortuitous and exceptionally high work function of the metal point for electron emission by positive ion bombardment in the presence of O_2. The difference in positive and negative corona currents at the same potential above onset in the linear regime is ascribable to differences in ion mobility, since both signs of pulses give about the same number of ions. The character of the positive point corona is briefly analyzed by means of the same criteria of field distortion used for the negative corona and the transient character of the streamer pulses is described through a diagram of successive field distortions. In comparing positive and negative pre-onset coronas, it is emphasized that despite similarities introduced by the choking off of the discharge through space charge accumulations, the positive point removes electrons quite effectively, giving a field distorted by only one sign of space charge, while the negative point has a much more complicated distortion caused by accumulations of positive and negative ions. The negative point has also a much smaller sensitive volume than the positive point, which introduces differences caused by lack of triggering electrons, making the negative point useless as a Geiger counter.

INTRODUCTION

THE first clear insight into the basic mechanisms of the positive and negative point coronas in air at atmospheric pressure began with the results from combined oscillographic and other studies initiated in the writer's laboratory around 1937 with the work of A. F. Kip[1] and G. W. Trichel.[2] As is usual in newly developed fields of research, it was possibly only to hit the high spots in the years before the war. Thus the pictures of the mechanisms developed, while in general correct, were rather inadequate in detail leaving many apparent contradictions and unanswered questions. Subsequent investigations and results with the improved high speed postwar oscilloscopes have now given the basis for a clarified summary of the mechanisms at work which it seems desirable to publish at this time. It may be added that while the studies utilize what we have chosen to designate as a standard point to plane geometry, the mechanisms are equally applicable to other geometries and dimensions due regard being given to the consequent changes in potential distribution. Thus for example, the concentric, cylindrical, negative wire corona shows the same characteristics in

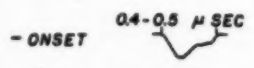

FIG. 1. Oscilloscope of negative Trichel pulse.

* Acknowledgment must be made to the Research Corporation of New York and to a contract with the Office of Naval Research for furnishing the necessary assistants to obtain the data needed in compiling this recent summary.

[1] A. F. Kip, Phys. Rev. **54**, 139 (1938).

[2] G. W. Trichel, Phys. Rev. **54**, 1078 (1938); **55**, 382 (1939).

FIG. 2. Photograph of Trichel pulses with moving film camera. Still photograph on right. Separate bursts and pulses can be discerned by fluctuations in intensity.

behavior and structure except that active spots for finer wires now show radial symmetry instead of point symmetry as might be expected.

THE NEGATIVE CORONA

The corona from a negative hemispherically capped cylindrical platinum point of 0.038 cm diameter with a positive plate at some 3 cm distance in air at atmospheric pressure, represents a convenient experimental norm for discussion. With such a point corona onset begins at about 5050 volts with a current of the order of 0.3 to 0.4 microampere.[3] Before this the clean point shows no light, and currents are several orders of magnitude smaller. The onset current oscillographically is observed to consist either of occasional random single pulses, negative Trichel pulses, or a regular rapid succession of a large number of such pulses, up to 100, at intervals of the order of 10^{-3} second. Increasing the potential causes an almost proportional increase in current (Ohm's law regime), which is accompanied by an increase of pulse frequency and greater continuity of sequential bursts but not of amplitude or basic character of pulses. In the past the duration of the pulse has been masked by instrumental characteristics of the oscilloscope. Recently, however, W. N. English[3] has shown that the time structure of the pulses is that seen in Fig. 1 and that the total duration is of the order of 4×10^{-7} sec. with a gradual rise and a fairly slow decline. Both by comparison of the pulse with a positive streamer pulse for which the total ionization is known and from the current and frequency one can estimate that during the negative Trichel pulse there are a total of about 2×10^{9} ions and electrons created.** A photograph of the corona with slowly moving camera shows the intermittent character of the discharge near onset as seen in Fig. 2. The isolated random pulses are seen in the faint traces with the rapid succession of pulses during some 0.01 to 0.1 second giving the brighter spots. Visually and photographically the discharge appears, as originally indicated by Trichel, Kip, and G. G. Hudson,[4] as a bright bluish purple button glow of some 0.01 cm diameter close to the point, yet giving the *impression* of being detached in contrast to the positive point burst pulse glow which adheres to the surface. This glow is separated by a narrow dark space from a fainter shaving-brush-like violet glow. A photograph is shown in Fig. 3. By increasing the potential to 8000 volts and the current to some 30 microamperes, the luminosity is more intense and distinct but the structure is otherwise unchanged. In order properly to identify the phenomena, the pressure was gradually reduced to 2 cm of Hg and estimates of the extent of the glows and dark spaces were made at various pressures.[3] While accuracy was not high, sufficient data were obtained so that in the middle pressure range the dimensions could be reduced to atmospheric pressure by the inverse pressure relation. The reduced values in the middle range of observation were quite consistent and average values of these dimensions are shown in the enlarged sketch of Fig. 4. The reduced data for highest and lowest pressures were the poorest as at low pressures edges were blurred while at high pressures the distances were too small. The glows and spaces, except the width of the button and the extension of the brush into the gap, where fading made measurement impossible, followed the pressure law. The diameter of the button was nearly constant with values gradually increasing from 0.01 to 0.02 cm down to 10 cm pressure. Below this pressure the button spread rapidly as pressure decreased. The data given in Fig. 4 are of great importance in the further discussion of the mechanism, since they furnish evidence

[3] W. N. English, Phys. Rev. **74**, 170, 179 (1948), and other data collected by English for this paper being now first reported.

** English (see reference 3) actually finds two "modes" of operation by pulses that shift from one to the other, probably associated with the work function of the surface as modified by the discharge. One mode has amplitudes which are $\frac{2}{3}$ those of the other, but are more closely spaced in time. The total ionization per pulse and its amplitude do not differ significantly in the two cases.

[4] L. B. Loeb, A. F. Kip, G. G. Hudson, W. N. Bennett, Phys. Rev. **60**, 714 (1941).

where calculation no longer applies. It is to be noticed that there is present a Crookes dark space of 2×10^{-4} cm thickness corresponding to some five electronic free paths at atmospheric pressure. The negative glow has a diameter of 0.01 cm and is about 5×10^{-3} cm thick, with a Faraday dark space of 3×10^{-3} cm thick and a flaring positive column extending roughly some 0.15 cm into the gap. At lower pressures a cathode glow can be seen as a dull grayish glow on the electrode surface. It is not visible at higher pressures.

It has been stated elsewhere that in the undistorted field, about a point under the conditions indicated, the electrons practically maintain equilibrium with the varying electrical field.[5] Hence one may *initially* use the undistorted field about the point and Townsend's primary ionizing coefficient α in calculation. Trichel[1] has calculated the axial values of the ratio X/p and values of Townsend's coefficient and integrals for such a point.*** The actual potential fall near the point obtained from model studies is represented as the broken curve of Fig. 6. It is to be noted that at a distance from the point of 0.04 cm the field gradient is so low that already ionization by collision is negligible. Using F. H. Sanders[6] data the ionization by a single electron calculated as a function of distance out from the point using Trichel's field*** is indicated by the broken curve of Fig. 5. The electrons moving out from the point in the first avalanche thus form a cloud which reaches its maximum density at about 0.05 cm out. It moves outward at first with a high speed, but later slows down as the field decreases. The total number of electrons in the avalanche is of the order of 3×10^4.*** As the electron cloud moves out it leaves behind a space charge distribution of positive ions slowly moving towards the point relative to the electrons. The spatial distribution of these ions is shown by the full curve of Fig. 5 whose integral gives the broken curve. It is noted that the space charge is sharply peaked at about 0.018 cm from the point and declines rapidly indicating that most of the ions are formed within 0.03 cm of the point.

FIG. 3. Still photograph of negative point corona near onset. Outline of point dashed in. Note detached appearance of negative glow button, Faraday Dark Space, and flaring fan-shaped Positive Column.

The calculation above was carried out for the 0.038 cm diameter point at -5000 volts as given by Trichel and the calculations to follow will use this value. Now the assumed -5000 volts sets the threshold for the corona onset which is given on the Townsend theory by the condition $\gamma(\exp\int_r^{r+a}\alpha dx)=1$. Here α is the first Townsend coefficient for ionization by collision by electrons in the gas, r is the point radius, $r+a$ is the distance from the point at which α becomes negligible in the undistorted field (here about 0.04 cm) and γ is Townsend's second coefficient. The coefficient γ is probably largely one giving the chance of electron liberation by positive ion bombardment of the surface. Photoelectric emis-

[5] L. B. Loeb, Phys. Rev. **71**, 712 (1947); also P. L. Morton, Phys. Rev. **70**, 358 (1946), and G. W. Johnson, Phys. Rev. **72**, 284 (1948).

*** Hemispherically capped cylindrical point to plane geometry has experimental advantages such that it has been and will be used in future corona studies. It has the disadvantage that the fields are not amenable to direct accurate calculation. Studies under difficulties have been made for the various positive corona onsets in confocal paraboloid gaps (see reference 1 and K. E. Fitzsimmons, Phys. Rev. **61**, 175 (1942)) where the fields are well defined and further studies may be made with this geometry if model studies fail to give a satisfactory solution to the field calculations. Comparison of onsets for positive streamers with both geometries and rough model studies have made possible more accurate evaluations than those taken from Trichel's curves (see reference 2). The differences in field variation as regards the Townsend integral are small and at most introduce differences in the evaluation of the integrals giving the ionization at negative corona onset of the order of definitely less than a factor of 2. Thus the total ionization is more nearly 6×10^4 ions in a single avalanche at onset rather than the value of 3×10^4 computed from Trichel's curves. This has been confirmed from a preonset burst pulse threshold measurement with a confocal paraboloid system as well as by electrolytic trough studies with point to plane geometry (see reference 3). The distances for maximum ionization and where ionization ceases to be effective are not materially changed and it makes little difference whether the initiating avalanche has 3 or 6×10^4 ions in the conclusions to be drawn. Thus since the curves to be discussed were drawn up for Trichel's computations, these will be used in place of possibly more precise later evaluations.

[6] F. H. Sanders, Phys. Rev. **41**, 667 (1932); **44**, 1020 (1933).

sion from the surface is also possible, active and perhaps very efficient here. It is, however, not essential to differentiate these modes of action. The condition $\gamma(\exp\int_r^{a+r}\alpha dx)=1$ states that the imposed field must be such that out of the $(\exp\int_r^{r+a}\alpha dx)$ positive ions created by an avalanche γ must be such that at least one new avalanche will follow. Owing to statistical fluctuations in $\gamma(\exp\int_r^{a+r}\alpha dx)$ in individual events about the mean values derived by experiment the exact threshold will be somewhat indefinite.[7] This indefinite character of the threshold of some 100 volts is well known to observers. Actually the observer will, in general, tend to choose values of the field slightly above that exactly satisfying this condition as his *experimentally observed threshold* because of these uncertainties. At such values $\gamma(\exp\int_r^{a+r}\alpha dx)>1$, a cumulative ionization process then takes place leading to self-sustaining currents of considerable magnitude whose further growth, as indicated by the inequality sign, is regulated by space charge limitations.

Since it is under such conditions that the corona is observed, this situation will be assumed to exist and one can proceed as follows. After the first avalanche described above, and illustrated in Fig. 5, has passed, it is clear that the positive space charge has somewhat distorted the potential indicated by the dashed curve of Fig. 6. The initial distortion is small and will at first be neglected in the considerations to follow. In this field the positive ions move towards the point in such a fashion that in the first 10^{-8} sec. the ions to the left of the line A on the full curve of Fig. 5 have moved to the point. *Neglecting* the later important distortion which accelerates the process, one would expect that in 10^{-7} sec., the positive ions lying to the left of line B, will reach the point. Now if one assumes as low a value for Townsend's second coefficient γ as 0.01 for + ions and photoelectrons in the high field of 120,000 volts/cm at the surface, one can estimate that some 170 new avalanches have been created and a total of at least 5×10^7 positive ions will have been formed in 10^{-7} sec. The process of generation of new avalanches is continuous and cumulative in this interval. For

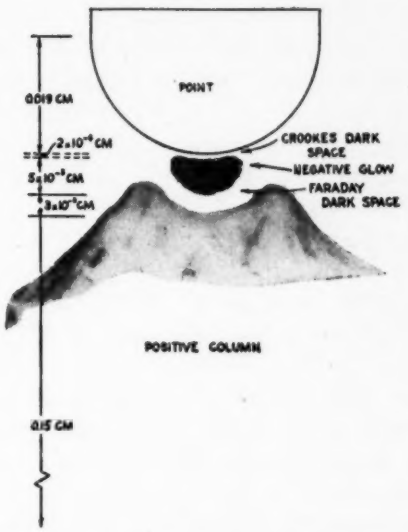

FIG. 4. Enlarged cross-sectional view of the Trichel pulse corona as derived from reduced pressure measurements.

as more positive ions move in, the new avalanches create new ions. Thus in place of the initial positive space charge distribution one has in some 4×10^{-8} sec. a continuous sheet of positive ions extending 0.04 cm out into the gap and moving into the point increasing in density as time goes on. If the distortion did not alter processes within some 10^{-7} sec., the first quarter of a Trichel pulse, the field within the first 10^{-3} cm of the cathode would have reached of the order of 4×10^5 volts per cm, with a potential fall in that layer of the order of some 400 volts. This classically considered and oversimplified analysis thus sets a *lower* limit for the ionization and potential gradients resulting. Actually they will be greater and grow more rapidly as will be seen. The simplified classical calculations above after 10^{-7} sec. lead to a potential gradient pictured in the full curve of Fig. 6 in contrast to that represented by the broken curve for the undistorted field. It is noted that this would give a dark space of 0.001 cm thick with a single glow extending out to 0.02 cm. Such an arrangement of glows is *not* observed. It must occur as a transient and dim phase early in each pulse but is masked by the more intense manifestations caused by later events and depicted in Figs. 3 and 4. Under the conditions pictured above, however, the gradients at the point as the discharge builds up rapidly become

[7] L. B. Loeb, Rev. Mod. Phys. **20**, 151 (1948).

so steep and are confined so closely to the point that the electrons cease to be in equilibrium with the field. Thus the *Townsend coefficients can no longer be applied.*[5] It is to be expected that the ionization as studied by Morton and by Johnson must set in well before 5×10^{-8} second has elapsed. Under these conditions the electrons gain energies of some hundred volts in the first few free paths. They then dissipate this energy in ionization beyond this region with greater ionizing efficiency by a considerable factor than is yielded by the Townsend mechanism. Calculations of the ionization under these conditions are at present impossible. It is, however, possible to infer what has occurred from the visual data reported above.

From what has preceded one must expect that well *before* the first quarter of the duration of the Trichel pulse is reached the positive space charge has ushered in the Morton regime. From the distribution of glows in Fig. 4 in the observed distance of 2×10^{-4} cm of dark space, or within some 5 electron free paths, the secondary electrons from the positive ion impacts on the cathode gain energy which enables them to ionize very efficiently in the succeeding 5×10^{-3} cm of the observed negative glow. Beyond this region they cease to ionize intensely. They have lost their ionizing energy in a *distance* of some 25 electron free paths in the field direction in the negative glow. Actually their paths are very tortuous and they may make 100 or so collisions in this zone. The ionization produced in the first

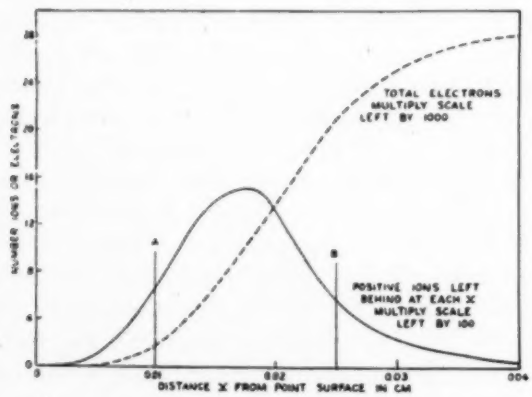

FIG. 5. Townsend ionization by one avalanche as a function of distance from the point surface. Solid curve positive ion distribution, multiply scale left by 100. Broken curve total electrons, multiply scale left by 1000. Note that ionization beyond 0.04 cm is negligible.

10^{-7} second of the pulse is probably well in excess of the 5×10^{7} ions previously estimated by Townsend's coefficients with undistorted field. The large fields about the point surface increase γ rapidly as well as producing a more effective primary process probably including field emission. It would not be far off to assume that some 2×10^{8} ions have been created in the first 10^{-7} second in the observed discharge.

It is also to be noted that all actions discussed lead to increased fields at the point and these in turn lead to increased ionization. Hence, were it not for some interrupting agency this autocatalytically cumulative process would continue indefinitely. Two possible inhibitory processes can occur to interrupt this increase. One of these is a destruction of the surface and a reduction of its emitting properties by ion bombardment. The other is the creation of an inhibiting space charge of some sort. Now the work of G. L. Weissler[5] and of W. H. Bennett[4] has shown that in air, where the heavy Trichel pulses occur, it is the presence of *negative ion forming* O_2 molecules that causes the pulses. Pulses are *not* observed in pure H_2 and N_2 gases, but appear at once when O_2 is added. Thus we must look to the negative ion produced space charge as the active interrupting agency.

To understand this, a further analysis of the discharge structure must be made. It may be recalled that space charge regions are regions of enhanced potential gradients. Such regions are normally regions where electrons are accelerated and thus are relatively dark. Regions of intense ionization with conducting plasma have low potential gradients and are relatively bright. Figure 6 shows the potential distribution to be expected on the basis of a continuation of the *Townsend* ionization for some 10^{-7} second in the full curve as previously indicated. It was seen that this calculation leads to a single dark space of some 5×10^{-3} cm thickness and a glow extending out some 3×10^{-2} cm. This particular calculated structure as stated does *not* appear in the *observed* corona as it is only a transient phase as a result of the first avalanche. It is masked by the much more intense luminosity of the later Morton regime pictured by the full curve on a

[5] G. L. Weissler, Phys. Rev. **63**, 93 (1943).

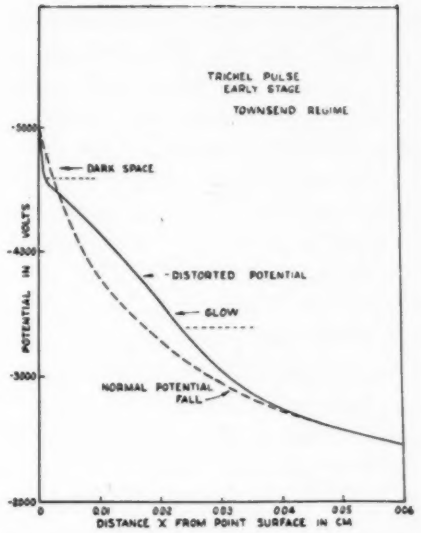

FIG. 6. Space charge distortion by avalanches in early phases of the Trichel pulse. Full curve the distorted field, broken curve the undistorted field.

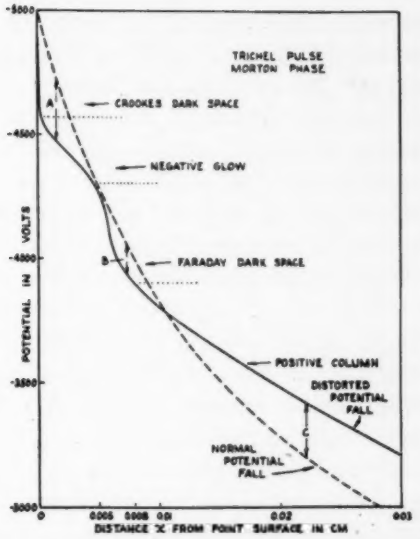

FIG. 7. Later phase of the Trichel pulse. The Morton regime is active. The light and dark regions correspond to the luminous visible distribution shown in Fig. 4.

similar diagram in Fig. 7, to a much enlarged scale, derived from observations as shown in Fig. 4. The broken curve as before represents the undistorted field. In the first 2×10^{-4} cm from the point there is a steep fall of potential as indicated by the dark space of Fig. 4. The value of the potential drop is not known. Over the distance of some 2×10^{-4} cm from the point it varies in time from an initial value of about 100 kv/cm to at least 400 kv/cm using calculations on the Townsend mechanism. It unquestionably reaches several times this value with the Morton mechanism active. This circumstance, together with the constriction of the discharge in the negative glow region and a flaring of the discharge in the column, indicates, as will later become clear, that throughout the region of the negative glow the distorted potential curve *during the period of greatest luminosity* lies *below* the curve for the undistorted field. This sets certain limitations on the potential fall if taken in conjunction with Fig. 4. Thus one can estimate that the potential distribution corresponding to the observed corona has the form shown in Fig. 7 with an initial drop of at least some 300 volts in the dark space. The conductivity of the plasma in the glow could cause a larger drop at the electrode with a lower slope in the glow, but it is doubtful whether one could expect a much lower potential fall in the dark space. The various regions corresponding to Fig. 4 are clearly indicated in Fig. 7. It is to be noted that following the very intense ionization in the negative glow, with its low gradient, there *must follow* a second steep gradient in a region where even the normal gradient gives appreciable values of Townsend's first coefficient which also lie below that in the undistorted curve. The region of the Faraday dark space is thus the second region of lowered luminosity. This dark space is relatively broad and is readily seen at atmospheric pressure. Beyond it lies the dull violet glow of diffuse character called the positive column. All visual manifestiations of the glow are the composite of the thousand or so separate Trichel pulses producing the visual image. The glow is thus a region of ionization not only along the lines of force of the undistorted field with slight radial compotents for points off the extended axis of the needle, but also of ionization caused by space charge field gradients as a consequence of a large number of Trichel pulses.

One may now look at the region of the discharge marked *A* in Fig. 7. Along the axis, at a distance of 0.002 cm from the point, in the glow, the distorted potential is -4580 volts. At the same radial distance from the point, *at* 0.005 *cm from the axis*, there is no discharge and the potential is -4740 volts. Between the two extreme ends of the line *A* there is, therefore, a potential

difference of 160 volts over 5×10^{-3} cm, or a gradient of 32,000 volts/cm at *right angles to the axis* and acting to *drive the ionizing electrons towards the axis*. There is, in consequence, of space charge distortion a *horizontal component* of the *electrical field acting to compress the discharge* and confine ionization to the region of the small button of negative glow. This accounts for the shape of this section of the discharge and its reluctance to spread as pressure decreases until the densities of ionization cease to produce strong gradients. It is probable that similar considerations apply to the Faraday dark space at B as well. Beyond this region, in the column where ionization and luminosity again appear, the situation is clearly reversed for the discharge flares radially far more in the column than any component of the field would warrant, i.e., the discharge does not follow the lines of force for an undistorted field. Thus in the region C the potential of the axial distorted field is indicated as -3680 while the undistorted field off the axis is -3520 volts. Hence in addition to the natural radial component of the off-axis field there is a potential between the discharge and the off-axis discharge-less regions of some 160 volts, which can lead to gradients driving electrons away from the axis. These can still cause ionization, and thus cause the glow to flare. Whether the gaseous turbulence set up by the electrical wind is also involved in the flaring is as yet an unsettled question. It is, however, not necessary to invoke its aid in accounting for the shape of the discharge.

The cause for the crossing of the distorted potential curve above that for the undistorted field is to be associated first with the two very sharp potential drops followed by a short and a relatively very extensive region of low gradient resulting from ionization and to the existence of both negative and positive space charges. It is further to be associated with the accumulation of a negative space charge beyond the regions of ionization. In the high field regions close to the point, electrons are removed very rapidly. This occurs even from the plasma of the negative glow as the new ionizing electrons introduce ever increasing charges. As these regions are left, the departing electrons move more slowly. In consequence of the presence of both O_2 and O as well as other electronegative chemical components created in the discharge regions, the electrons which are slowed up by inelastic collisions of excitation and ionization can attach to these substances to yield negative ions of low mobility. Beyond some 0.01 cm from the point, i.e., beyond B in Fig. 7, the fields are insufficient to allow *detachment* of electrons from O_2^- ions for which X/p is 90.[9] Thus negative ions could form and remain present in increasing number. It is most unlikely that free electrons will attach in any great measure to form ions as long as they have the average energy corresponding to that causing excitation and ionization, i.e. in fields where the ratio of field strength X to pressure p in mm of Hg, X/p exceeds 40. This occurs out to a, or in this case 0.04 cm. Beyond this they will attach in increasing number as energy decreases. How rapidly the electrons attach to make ions beyond a cannot be calculated since attachment coefficients in a plasma with inelastic impacts have never been studied. Some data observed by de Graffenried[10] as to intensities of the electrical wind currents from a pair of positive and negative wires with intense corona indicate a difference in the ratio of about 3 to 1 in favor of the positive point. Since the positive ions *all* effectively transfer momentum, it means that only about 1/3 of the electrons have attached to give negative ions in the high field regions. Considerable attachment does however, occur and cause a rapid building up of a negative space charge. Furthermore, this attachment must occur fairly close to the point since it must suffice to choke off the Trichel pulse after 4×10^{-7} second, when a total of 2×10^{9} ions have been created. Added evidence for this lies in the fact that it is only in ion-forming gases that one gets Trichel pulses and that further relatively low concentrations of O_2 suffice.

It is clear that the potential distribution shown in Fig. 7 is only one of a sequence of distributions existing during the pulse ranging from approximately that of Fig. 6 initiating the discharge and the Morton regime to that indicated as a possible situation as the pulse chokes off and

[9] L. B. Loeb, Phys. Rev. **48**, 684 (1935); also N. E. Bradbury, Phys. Rev. **44**, 883 (1933); F. Bloch and N. E. Bradbury, Phys. Rev. **48**, 689 (1935).

[10] A. L. de Graffenreid, personal communication to the writer, Dec. 23, 1947.

ionization ceases shown in Fig. 8. The situation in Fig. 7 represents the distribution at the height of the most active period, i.e., in the first 2×10^{-7} second. Exactly how the negative space charge builds up to break off the pulse is not clear. It must, however, be realized that all actions around the point from the first avalanche on are such as to concentrate the discharge and act to make ionization more and more effective. Such autocatalytic cumulative action cannot go on indefinitely. It is thus likely that as the pulse goes on for some 3×10^{-7} second the rate of electron generation gets ahead of the rate of electron and ion removal by the outer fields. Thus it appears that after an interval of 4×10^{-7} second in which some 2×10^{9} electrons have been created and distributed over a volume that it is impossible to define at present, the potential gradient near the point is so lowered that the ionization ceases. Such a state is indicated in Fig. 8.

The gap must then remain inactive for the time necessary to move this negative space charge well towards the anode. This takes of the order of 10^{-3} second near onset as indicated by the frequency of the regular Trichel pulses. The clearing time for positive space charges in a similar gap and with currents of the same order has been directly measured by Kip on streamer pulses and is also of this order of magnitude.[11] The rate of clearing is perhaps twice as rapid with the negative point since the electrons traverse part of the gap *as electrons* and attach to ions later. The mobilities of negative ions in air are also 30 percent greater than for positive ions. Thus the negative clearing time will be less leading to larger negative than positive currents for otherwise equivalent conditions as observed.[3] As the potential on the point is increased its chief effect is to increase the potential across the low field region thus decreasing the clearing time of the inhibitory space charge. This increases the frequency of Trichel pulses. Hence current increase runs proportional to pulse frequency.[3] Whether the pulse starts as soon as the space charge has cleared away depends on the presence of triggering electrons near the point. At onset where marginal conditions exist and clearing times are long such electrons may not be at hand. Thus Hudson[4] and also English[3] have found it essential to resort to MgO dust specks on the point in clean air to serve as triggering sources to insure regularity of pulses, for the sensitive volume for ionization by external sources is extremely small. At higher potentials where clearing times are shorter the "steady" corona does not require such sources, although even then extinction periods and fluctuations are less if they are present.

The character of the phenomena in the absence of electron attaching impurities has been studied by G. L. Weissler[8] in very pure H_2 and N_2. These gases differ radically from air. It has been indicated elsewhere that the work function of the surface and hence γ are strongly affected by absorbed gases. Recent work by Weissler[12] indicates that O_2 bombardment increases the work function of a W surface by 1.2 ev. N_2 *decreases* it about 0.3 ev below that for a clean surface outgassed by electron bombardment. A bombardment with A does not alter the surface while H_2

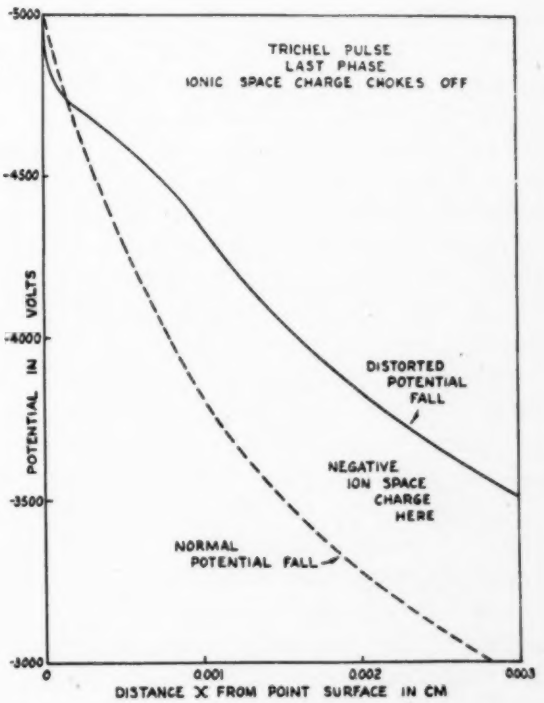

FIG. 8. Last phase of the Trichel pulse. Negative space charge backs up and reduces the potential gradient at the cathode terminating the pulse.

[11] A. F. Kip, Phys. Rev. **55**, 549 (1939).

[12] G. L. Weissler, Bulletin, Los Angeles meeting of the American Physical Society, January 3, 1948.

reduces the work functions by some 0.5 ev or more below that for an outgassed surface. Both H_2 and O_2 tend to stay in the metal and diffuse out only slowly. Thus long outgassing is required and surface readjustments take time. Again the *first* Townsend coefficient in pure H_2 is quite a bit higher than for air while in N_2 it is nearly the same as for air. Since the starting potential for the building up of space charges and thus for the corona is set by the Townsend condition that $\gamma(\exp\int_r^{a+r}\alpha dx)=1$, it is not surprising to note that the starting threshold for negative corona is very much lower for the Pt point in pure H_2 and pure N_2 than in air and that it is even lower than for the positive point in the pure gases. The potential for negative onset is 2800 volts for H_2, 3700 volts for N_2 and 3500 and 4800, respectively, for the positive onset in H_2 and N_2. Even 0.1 percent of O_2 in N_2 raises the starting potential to 4200 and 4300 volts, respectively, and yields Trichel pulses. While the very much lower threshold for H_2 relative to that for N_2 is in part only caused by the first Townsend coefficient, the lowering of the negative onset relative to the positive in N_2 is largely ascribed to γ. Once the threshold condition is reached positive space charge accumulation such as indicated above occurs and corona begins. It begins on an unconditioned surface, or else on one previously conditioned. Both pure H_2 and N_2 are relatively transparent to electrons and the discharge appears in both cases with fairly heavy currents at onset. These are of the order of a thousand-fold those at onset in air.

The corona at onset in both case starts out as diffuse appearing discharge that consists of myriads of very weak, intermittent discharges covering the point. They yield a low current of the order of the Trichel pulse current in air. With time this condition develops into a more or less concentrated glow discharge at one point which is quite steady and a thousand times more intense. If the potential is increased, concentration takes place more rapidly.

The character, intensity and number of the pulses indicate that this initial discharge operating just as the threshold is not interrupted by electron space charges, which are removed rapidly in the slightly distorted field in the absence of ion formation.**** One must ascribe this phenomena to small statistical fluctuations in the many threshold discharges all about the point with low γ. On more effective bombardment and cleaning of the surface at some point, with possible sputtering of the surface, a very effective spot of lowered work function is produced such that a really heavy discharge sets in.**** With a Pt point in N_2 this discharge is fixed and stable. In H_2 on the contrary, while the discharge concentrates at one spot the spot does not remain fixed but continuously wanders over the surface. It appears, therefore, that conditioning of the point is initially hard, but that once a clean spot develops the discharge settles down. A similar initial conditioning in H_2 is needed but once the discharge concentrates, the surface is too much altered and the spot wanders from quasi clean to quasi clean points of the surface where the emission is propitious. In any case, both shapes of discharge show the Crookes and Faraday dark spaces as well as the negative glow and column as in air and are in this respect similar in mechanism to the air corona except that they do *not extinguish themselves periodically.*

It is clear from the magnitude of the current that aside from continuity and the lack of interruptions of longer duration observed in air, the effectiveness of ion production rises above that in air. On the other hand, the fact that the current does not increase indefinitely but reaches a steady high value means that a *smoothly acting* limiting factor is present.† This cannot be due to change of surface or to negative ions and Trichel pulses. It can only be that due to *electronic* space charge accumulations largely acting in the lower field regions of the discharge.† The space charge with a thousand-fold increase in current backs up to raise the negative values of the potentials near the point so that the potential drops allowed to

**** Very recent results of C. G. Miller (Ph.D. thesis University of California, 1948), using concentric cylinders with pure N_2 indicate that in *pure* N_2 this diffuse "conditioning" discharge is continuous and with formation of a cathode spot and large γ the electron space charge limitation cannot prevent the spot going to a spark unless a limiting resistor is used. Weissler's gas was slightly contaminated by gas liberated by bombardment of the surface in running the discharge and a limiting resistor prevented a spark.

† This limiting factor in pure N_2 is either an external limiting resistor or ion formation due to traces of impurity liberated by the filament as Miller has shown.

act in the region of the point just suffice to maintain the current at a steady limited value, with, however, no interruptions or pulses.

The presence of heavy sputtering and pitting of the points even in the pure gases gives eloquent proof of the presence of very high space charge fields near the negative point surface.[4,8] Sputtering should not be noticeable in the usual time of operation of corona points if positive ion energies are 2 volts or under.[5] If the ion energies are in excess of 20 volts sputtering could be expected. The presence of notable sputtering indicates fields near the cathode of the order of 10^6 volts per cm, which over a few ionic free paths can give the ions the needed energy. Such action would, therefore, be expected in the Morton regime and is consistent with mechanisms suggested.

The equation fixing the threshold for the negative corona onset $\gamma(\exp\int_r^{a+r}\alpha dx)=1$ has recently been shown[13] to have a counterpart in the threshold of the positive point pre-onset burst pulse corona which reads $\beta f(\exp\int_r^{a+r}\alpha dx)=1$. Here f is a factor giving the number of photons produced by the electron avalanche capable of photo-ionizing the gas and β is the geometrical chance factor that these photons of absorption coefficient μ will photo-ionize the gas in such a fashion as to build up the discharge. It is seen that the Townsend integral is common to both but that γ and βf can differ. If γ is of the order of 10^{-3} or more as experience indicates while βf is 10^{-4}, which is its value in air (it could well be less in pure N_2 or H_2), it would be expected that the onset for negative Trichel pulses would be materially lower than for the pre-onset positive burst pulses. It would also be expected that the negative onset would be sensitive to the point material and condition while the positive onset depends on the gas only. Since the $(\exp\int_r^{a+r}\alpha dx)$ as related to onset potential varies very rapidly with small changes in potential, as α is a rapidly changing function of field strength, very small changes in V can mask smaller variations in γ or βf so that they may not be noted within experimental uncertainties. In pure H_2 and N_2 the negative threshold is some 700 volts lower than the positive. In air for metal points on the contrary the two thresholds are markedly close together. English[3] has noted that as a function of pressure the negative onset in air is bowed upward and crosses the linear positive threshold once at lower and again near 760 mm, differences being at all times less than 150 volts. Weissler showed that 0.1 percent of O_2 added to pure N_2 raised the negative threshold close to the positive value. Kip[4] in a hasty survey found that the thresholds appeared constant even with such different metal points at Pt, Cu and Zn.

Several explanations are possible.

a. In the absence of a suitable relation for the pre-onset positive burst pulse threshold, the writer[8] had suggested that possibly the attachment of electrons to O_2 molecules to give O_2^- ions necessitated that the fields around the point out to the distance a in the integral had to be great enough to cause the O_2^- ions to shed their electrons on molecular impact. This shedding[9] occurs at $X/p=90$ in air while the value of a conventionally used in onset calculations requires a ratio of $X/p=40$. Thus it was believed that this requirement might raise the threshold of the negative onset to equality with the positive. If one regards the *new* equation for positive onset[13] it is seen that the integral for the positive and negative points is the same unless one applies the $X/p=90$ criterion to the value of a for the negative and *not* for the positive point. Actually the electrons involved in both cases are *generated* in high field regions near the point where $X/p>40$ and under such conditions they will probably always remain free. If either case were adversely affected by attachment, it would be the *incoming carriers* to the positive point and not the electrons *leaving* the negative point. Therefore, if a is reduced for *either point* it will be so for the *positive*. Since otherwise than through a the Townsend integral is the same for both points, the writer's hypothesis cannot account for the observations in air in case βf is lower than γ.

b. If negative ion formation yielding negative space charges beyond a were invoked as an explanation, it would not suffice. Negative ion formation beyond a as seen does affect the discharge by choking off the Trichel pulses. It cannot serve to do more than act in this way after enough electrons are created by the

[13] L. B. Loeb, Phys. Rev. **73**, 798 (1948).

FIG. 9a. Photograph of positive corona near onset. Tip of hemispherical point outlined by closely adhering glow of burst pulse corona. Streamers clearly indicated in the neck of the discharge. Positive glow beyond streamer's end.

avalanches. Thus it cannot fix the onset threshold for Trichel pulses.

c. It was early suggested that for surfaces, where, possibly owing to the action of O_2 on the metal the work function was increased and γ decreased so that it was less than βf, photoelectric ionization *in the gas* might set the threshold of the negative as well as the positive corona. This suggestion was discounted because the quantity βf for a negative point with maximum ionization at some distance from the point should be very much less than for the positive point through photon dissipation. This conclusion was recently justified by the work of English[3] on the threshold potentials of negative and positive coronas from water points at low pressure. No true *negative* corona could be observed at as much as 3000 volts above positive corona onset with the water point. For such a point γ is probably vanishingly small compared to βf. Thus even with a geometrically diminished βf true negative corona did not appear at potentials 3000 volts higher than for the positive point. One can thus assume that negative onset cannot depend on ionization in the gas.

d. The only explanation remaining is that owing to the effect of O_2, and possibly also oxides of nitrogen produced by the avalanches, on the negative point γ was decreased so as to be fortuitiously equal to βf for air, or O_2-N_2 mixtures, in the case of metal points.†† English observed that for small points the negative threshold is lower and for large points the positive threshold is lower. Point material was of no influence, point condition, very important. More work is obviously needed but the general conclusion based on the relations for the thresholds of positive and negative coronas in air and other gases that γ and βf, respectively set the thresholds is unescapable.

THE POSITIVE CORONA

It is not the intention to discuss the positive point corona in detail. It is, however, expedient to present certain features of the positive point corona not hitherto clearly discerned which derive directly from the studies on the shape of the negative point corona and to contrast the differences observed. The visual and photographic observation of the positive point corona in air reveals the following phenomena. Just at the onset of the Geiger Counter regime, at a potential V_0 of closely 5050 volts, the oscilloscope shows the intermittent *burst pulse* corona of Trickel.†††[2] At this point there are no visual or

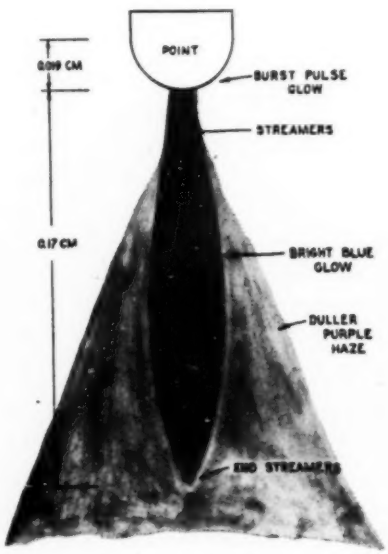

FIG. 9b. Schematic diagram of positive corona near onset.

†† Later work by W. N. English, Pasadena meetings, Am. Phys. Soc., July, 1948, and by C. G. Miller, thesis, California, 1948, have shown that the relative threshold values do shift with point radius, composition of O_2-N_2 mixtures and pressure.

††† Use of too intense a source of triggering electrons can give a simulated threshold for burst pulse corona which

photographic manifestations at the point. As the potential is raised very slightly (about 50 to 100 volts) above this potential the *pre-onset streamers, interspersed with burst pulses* are observed on the oscilloscope. The length of the streamers changes very slightly with potential and depends primarily on point radius. At still higher potentials, the streamers become less frequent and burst pulses become more frequent until all streamers vanish at the point, because of extensive space charge fouling and the intermittent burst pulses merge to give the steady corona at an *onset potential*, V_0. In what follows only the pre-onset streamers and burst pulses near onset will be discussed.

Under these conditions visually the succession of pre-onset streamers and burst pulses produce the glow shown in the photograph of Fig. 9a and in the schematic sketch of Fig. 9b on a 0.038 cm diameter point. The hemispherical point is pretty well covered by a closely adhering bluish white glow. Along the axis of the needle projected into the gap there is a bluish purple neck or stem ending fairly sharply at the point S^1 at about 1.7 mm from the point. The stem at S^1 eases itself in a fainter purple haze shaped like the bowl of an inverted wine glass. This gradually fades out at its lower end at some 3 mm from the point. It may be noted that unlike the negative corona, the flaring part of the glow is nearly limited by the lines of force emanating from the point. With smaller diameter points the lateral flare disappears[3, 14] and all that one sees is the central section of Fig. 9b except that the lower extremity beyond S^1 fades away gradually as does the axial lower extremity of Fig. 9b. In the past the flare had not been satisfactorily explained. The streamer branching observed by S. Gorrill[15] in cloud track pictures of impulsive over-volted streamers from the point had been suggested as the cause. However, branching would not be expected with *pre-onset* streamers. An adequate explanation is now at hand. The well known oscillographic records of the streamers and bursts are shown with a low speed oscilloscope in Fig. 9c. This cannot resolve the streamer pulse. The high speed oscilloscope record of the streamer is shown in Fig. 9d.[14] Such oscilloscopes can no longer record the burst pulses because of cut-off.

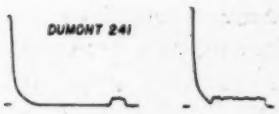

FIG. 9c. Slow speed oscillograph of streamers right in each case and burst pulses left. Duration of longer burst about 100 microseconds.

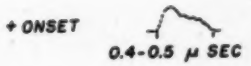

FIG. 9d. High speed oscillograph of a streamer pulse. Note the writing speed of the rise is so fast it is not observed. The rest of the pulse is probably correctly resolved.

The threshold V_g for the pre-onset positive point burst pulse corona may again[13] be represented by a threshold condition expressed by $\beta f(\exp\int_r^{a+r}\alpha dx)=1$. This threshold marks the appearance of the intermittent *burst pulse* corona at V_g. Here as before, $(\exp\int_r^{a+r}\alpha dx)$ represents the avalanche formation by ionization by collision of an initiating electron in advancing from $a+r$ in the gap, where α just begins to have a finite value, to the point surface at r. This avalanche as soon as it reaches the point loses all its electrons to the point leaving behind a positive space charge with its maximum value *right at the point surface*. Burst pulse formation, however, does *not directly* derive from this process for the positive ions do not play a direct role. However, the $(\exp\int_r^{a+r}\alpha dx)$ electrons before their absorption and during their last paths have created a proportional number of photons (*high energy* ultraviolet light quanta), $f(\exp\int_r^{a+r}\alpha dx)$ by exciting impacts with atoms. Here f, the proportionality factor, is less than unity in considerable measure (of the order of 10^{-4} in air). These energetic photons whose absorption coefficient, μ, is of the order of 10 cm^{-1} are capable of ionizing the gas molecules that absorb them. A fraction β of these photons will escape absorption by the point and will create useful electrons in the gas about the avalanche a cm beyond the point. Any of these photoelectrons absorbed beyond a distance greater than a from the point, can give a new avalanche which will perpetuate the process. If β represents the fraction of the

starts at a much lower potential. It is a statistical effect of a rapid sequence of field intensified avalanches (see reference 13).

[14] W. N. English, Phys. Rev. **71**, 638 (1947).

[15] S. Gorrill, thesis, University of California, May 1939.

photons that are absorbed beyond a from the point, then the ionization becomes self-sustaining when $\beta f(\exp\int_r^{a+r}\alpha dx)=1$ and sets the condition for corona onset V_0. Obviously β will depend on geometrical factors and μ and is given by $\beta=0.5e^{-\mu\bar{a}}$. The quantity $\bar{a}$ is an average distance traversed by photons in the zone of thickness a about the point. It is roughly given by $\bar{a}=1.86a$. Burst pulses will build up by spreading laterally along the point surface. They can also increase by electrons feeding *into* the original avalanche head. In this case they could build up to streamers as will be indicated.[16] Burst pulse ionization can spread until positive space charges lower the fields and stop the process. Thus they can last tens to hundreds of microseconds. The glow from these will lie within 2×10^{-8} cm of the point and be most intense *at* the point surface. Their glow and appearance potential contrasts with and is independent of streamer appearance.

In the case of streamer formation it has elsewhere been indicated,[17] that a streamer will form in a *uniform* gap of length δ, or greater, after the avalanche has progressed a distance such that $\epsilon fe^{\alpha\delta}=1$. Here $e^{\alpha\delta}$ is the number of electrons created by the avalanche and $fe^{\alpha\delta}$ is the number of photons produced that can ionize the gas. The quantity ϵ is the chance that one of these photons can be absorbed and create an electron in a sensitive zone of radius $\rho+\Delta x^1$ about the radius ρ of the newly created space charge so as to propagate the streamer. Δx^1 is determined by the vector field of the space charge X^1 plus the existing field, X, roughly through the relation $(\exp\int_\rho^{\rho+\Delta x^1}\alpha^1 dx)=e^{\alpha\delta}$, with α^1 the value of α in the enhanced field $X+X^1$. Thus ϵ depends on the space charge density $\alpha e^{\alpha\delta}/\pi\rho^2$ created by the avalanche which gives X^1, on X, and on the absorption coefficient μ of the gas.

In the case of the positive point corona the question of the threshold for streamer onset is not as simply defined. The primary avalanche is given by $(\exp\int_r^{a+r}\alpha dx)$. If it were the photons and space charge from this avalanche *alone* that were to *initiate the streamer* then the condition would be set by writing $\beta f(\exp\int_r^{a+r}\alpha dx)=1$ as before with β and f having the same meaning. In the case of the positive point, however, the distance of avalanche advance a is very short. Thus the volume occupied by the positive space charge which depends on ρ would be much smaller as the electron diffusion determined by the distance a is much smaller. Hence $(\exp\int_r^{a+r}\alpha dx)$ could be smaller with smaller ρ and yet yield a *propagating field*.[16] Fitzsimmons'[18] data and calculations fix the integral as 6×10^4 for pre-onset streamers while $e^{\alpha\delta}$ for a plane parallel gap is of the order of 1.2×10^7.[19] On the other hand, photon production accompanying the reduced ionization, that is $f(\exp\int_r^{a+r}\alpha dx)$ would be correspondingly reduced. The condition for *streamer* advance, namely that a *photoelectron be produced in the sensitive volume with adequate space charge distortion*, would remain the same and thus be adversely affected by reduced avalanche travel and ρ. Thus *unlike burst pulses streamers* are required to build up adequate space charge fields *plus* adequate photo-ionization. Neglecting the photo-ionization Fitzsimmons[18] showed that the data given for a 0.038 cm diameter point satisfied the Meek equation for streamer propagation. However, it is hardly conceivable that a reduction in photon producing electrons by a factor of 500 can give a sufficiently large ϵf to yield a streamer unless f increases vastly for the point. It is probable that with the *point* and its highly divergent field the absorption of the electrons together with concentration of photoelectrons converging into the point may at potentials not much higher than those for burst pulse onset cause the building up of streamer forming space charge concentrations by *successive avalanches* into the same region.[16] It must be concluded that the application of the Meek equation for such streamers from fine points is not justified and no proper theory can be evolved. We can, however, generalize as follows: *Streamer onset* cannot occur *below* the threshold for burst pulse formation. It *may* occur at fields above burst onset. With the chance for successive avalanches building up the space charge field of an initial avalanche to streamer propagating values, it is *not unlikely that streamers will begin to appear at potentials*

[16] L. B. Loeb and Robert A. Wijsman, J. App. Phys. **19**, 797 (1948).
[17] L. B. Loeb, Phys. Rev. **74**, 210 (1948).
[18] K. E. Fitzsimmons, Phys. Rev. **61**, 175 (1942).
[19] L. B. Loeb and J. M. Meek, *Mechanism of the Electric Spark* (Stanford University Press, Stanford University, California, 1941), p. 35.

not much above those setting the threshold for burst pulse formation, as is observed. This consideration then accounts for the observation of streamers at a very few hundred volts above burst pulse onset and for the simultaneous and alternate appearance of bursts and streamers at the same potentials.

After a streamer has developed, neither bursts nor streamers can form *in the same region*, until the space charge has had a chance to clear by movement of the positive space charge well beyond a into the gap. The same holds for streamers initiating from a region where a burst has just been created and died out. This does not preclude bursts or streamers appearing by photoionization, very shortly, at some neighboring region of the point which is not fouled by receding positive space charge. The number of ions needed to cause space charge fouling that chokes off the discharge is of the same order of magnitude with both positive and negative points, i.e. some 10^{10} ions.

One more point must be made concerning the movement of positive streamers from the point in contrast to that in a uniform field. The electrical field about the point decreases rapidly and in the undistorted gap it is already unable to cause ionization much beyond the distance a. Thus the streamer propagating outward from the point will soon run into fields so low that it can no longer propagate. Hence streamers will depend primarily on a and thus on point radius r for their distance of propagation, or length, in the gap, as has been experimentally observed.[14] In the gap considered the distance appears to be about 1.7 mm and it has been measured by English[14] as a function of point radius. The new concept of *streamer development by successive avalanches* explains why even with the smallest points English was able to observe streamers even though they were very short, a circumstance contrary to previous prediction. These fine point streamers were not explicable in terms of the original theory of Meek where a *single* avalanche was required to yield ions enough to build up the streamer. It had led to a false prediction by the writer that streamers would not be found for very small values of r which appeared to be substantiated by Kip's[4] observations.

One may now turn to a study of the positive corona streamer with the same sort of analysis used for the negative point. At the assumed observed onset of 5050 volts with the undistorted field, one electron avalanche starting at a cm from the positive point surface will as before produce $(\exp\int_r^{a+r}\alpha dx)$ electrons and positive ions, yielding the same number of ions, i.e., 6×10^4, corrected as for the negative point. The electrons in this case, however, enter the point and leave behind a positive space charge whose distribution is indicated by the full curve of Fig. 10. The total ionization at each point is indicated by the dashed curve. It is noted that the ions are now nearly all created within 0.01 cm of the point and that the number is greatest at the point, going from 5260 at 0.003 cm from the point to 33,600 at the point. These ions drift outward from the point with a velocity of the order of 2×10^5 cm/sec, the electrons having entered the point. The maximum luminosity is now produced right at the point surface. With this as a start and choosing a potential a little above burst pulse onset one can assume that a *sequence* of an adequate number of avalanches builds up a space charge field satisfying the Meek-Raether streamer criterion of $X=KX^1$, with $K=1$ for want of a better quantitative criterion. At this potential assuming the photo-

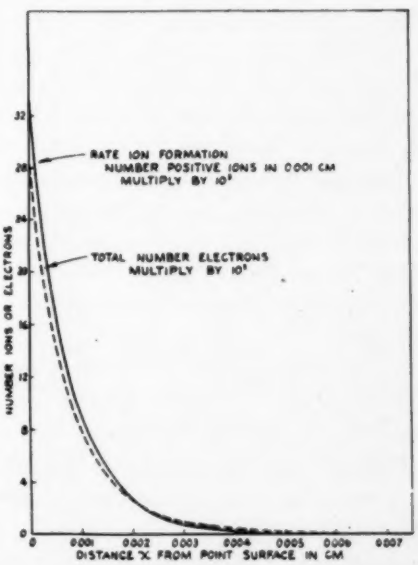

FIG. 10. Positive ion density, solid curve, and number of electrons in the avalanche as a function of distance from the positive point. Multiply scale at right by 10^3 in each case. Full curve is rate of ion formation in 10^{-3} cm.

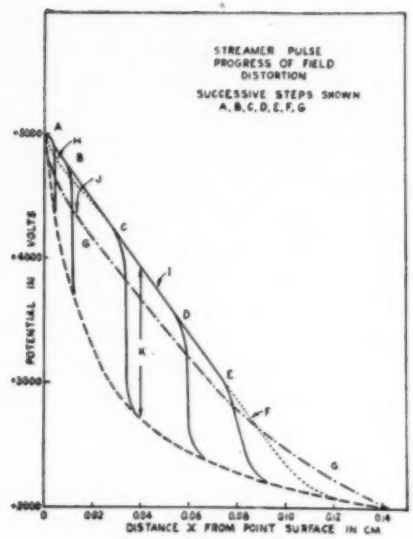

FIG. 11. Progress of Field Distortion by a Streamer pulse in successive steps shown as *A*, *B*, *C*, *D*, etc. Time scale is 2×10^{-9} sec., beyond that steps *F* and *G* about 1.1×10^{-8} sec. Full curve steps. Dashed curves undistorted field. Steps *F* and *G* shown as dotted and dot-dashed lines.

electric ionization already adequate to give burst pulses, the streamer starts its advance. This rough estimate enables us to proceed to develop Fig. 11. The dashed curve is as before that for the undistorted field. At the point *A* is represented the propagating space charge potential as the streamer advance begins, extending perhaps out to 0.005 cm with a slope dV/dx corresponding to $X+X^1=2X$. The streamer will then advance through the successive stages *B*, *C*, *D*, and *E* to its distance of propagation at about 1.2 mm. This advance occurs at a speed of some 10^8 or more cm/sec and consumes 1.7×10^{-9} second. After this point is reached, while the space charge causes some ionization in advance of itself, the ionization is no longer able to cause rapid advance as a propagating streamer. Hence the electron current i up the streamer channel from the tip to the point rapidly declines. The plasma disappears leaving a positive space charge with some electrons in it that moves in the field at about 1.6×10^4 cm/sec towards the cathode. Thus in some 4 to 8 microseconds the now defunct streamer tip is at *F* and in a similar interval later it is at *G* with a gradient so weak that ionization has practically ceased. While the streamer tip advanced with the current i flowing, the gradient down its stem of conducting plasma gave a sensible linear fall of potential as indicated by the line marked *I*. With the cessation of current at *F* and *G* and the more rapid movement of ions near the point the dotted and dot-dashed curves *H* and *J* mark the clearing of the field near the point corresponding to tips *F* and *G*. The total number of ions in the space charge channel are some 1.7×10^9. The channel is very narrow. The potential gradient between its edge and the neighboring undistorted field, at a point *K* in Fig. 11, with the channel along the point axis at 1100 volts positive to the adjoining space gives fields sufficiently high to cause heavy ionization by electrons drawn radially into the channel. Thus the channel will expand laterally and the region where it is expanding will be luminous, but with an entirely different density of light emission than in the propagating streamer itself, where gradients of the order of 10^5 volts/cm exist. The lateral spread of ionization will be confined mainly to the regions where the space charge *lingers* after extinction, since the time for much lateral ionization during rapid advance in 2×10^{-9} second is limited. The lateral spread near the point will thus be much less than that in regions near the end of the streamer advance and in the ensuing 0.13 cm or so. Most electrons created *during* advance are feeding into the advancing streamer tip with its high field.

It should be noted here that in contrast to the negative corona only positive ions and positive space charges occur. Hence the potential curve for the streamer process as well as for burst pulses will always be *above* the *undistorted* field curve. The fact that the expansion of the glow is limited approximately by the undistorted radial field lines from the point is of interest. It probably indicates that the slow electrons created and ionizing radially from the streamer channels are also moved upward by the undistorted field more or less along the lines of force. If now one superpose a large number of streamers occurring over an interval of seconds or minutes and realize that these streamers propagate from different spots near the tip of the point as the gap is fouled by one streamer or another, one can understand the mechanism of the production of the luminosity in the observed photograph of Fig. 9a.

The frequency of burst pulses, their duration and the frequency of streamers will depend on the rate of fouling; i.e. the current and the time for the space charge to clear. This is somewhat longer than for the clearing of the negative point Trichel pulses owing to the lower mobility of the positive ions compared to electrons and negative ions in the Trichel pulses. The number of ions in streamers and burst pulses is of the same order of magnitude as in the negative Trichel pulses, but the frequency is reduced some 50 percent so that near onset the negative corona currents in air are of the order of twice as great as the positive corona currents as observed.[3] In both cases the currents are limited by the low fields in the plane region leading to the Ohm's law regime near onset, V_0 and V_g, observed by Kip[1] and by English[3] for positive and negative corona.

Alloying of Metal Powders by Diffusion*

SIDNEY WEINBAUM
Jet Propulsion Laboratory, California Institute of Technology, Pasadena, California
(Received March 5, 1948)

In the preparation of alloys by sintering metal powders, the alloy is formed by the diffusion of metals into each other. The distribution of metallic powder in space is expressed by means of a triple series; this series is used to obtain the solution of the diffusion equation. The resulting formula gives the concentration of metal as a function of space, time, temperature, and particle size. Sample calculations made for one-to-one atomic proportion nickel-copper alloys are in general agreement with experimental results.

INTRODUCTION

IN the preparation of alloys by sintering metal powders, the alloy is formed by the diffusion of metals into each other. The commercial powders used in sintering consist of particles within a wide range of size, and the distribution of these particles as to size varies greatly from sample to sample. The separation of the particles by size is achieved by means of an elutriator, and when particles of one size are used in sintering, the time necessary for the process of alloying to be completed becomes a function of the temperature of sintering and of the size of the particles only.

MATHEMATICAL REPRESENTATION OF DISTRIBUTION OF PARTICLES IN MIXED POWDERS OF TWO METALS

In order to apply the diffusion equation, it is necessary to know the initial space distribution of the particles. The simplest assumption would be that of the case of cubical particles of two different metals, with the particles arranged alternately in all three directions. A one-to-one atomic mixture of equal size particles of copper and nickel (densities 8.90 and 8.92, respectively) was selected as suitable for sample calculations because partial experimental data on such a copper-nickel alloy have been obtained at the Jet Propulsion Laboratory.

Under the idealized picture of alternate arrangement of cubical particles of two different metals, it is possible to picture the distribution of these metals in one dimension as illustrated in Diagram A.

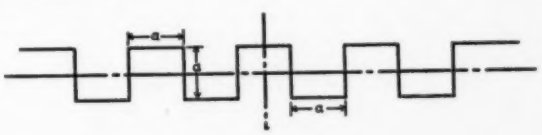

DIAGRAM A.

The positive peaks correspond to the particles of one of the metals under consideration, whereas the negative peaks represent the absence of particles of this metal, the spaces being filled with the particles of the second metal.

This picture is similar to the square wave occurring in electronics and can be represented

* This paper is a revised report of a theoretical investigation made at the Jet Propulsion Laboratory of the California Institute of Technology and was issued at Pasadena, California, in slightly different form as JPL Progress Report No. 4–51, November 18, 1947.

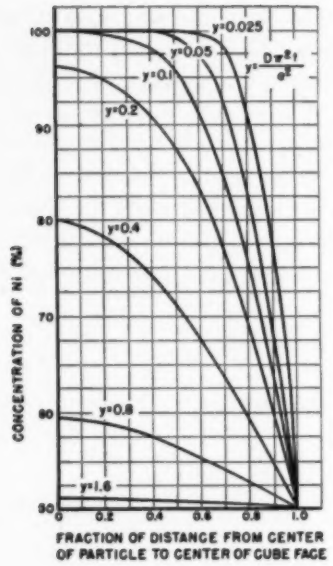

FIG. 1. Concentration along the line $(x\ 0\ 0)$.

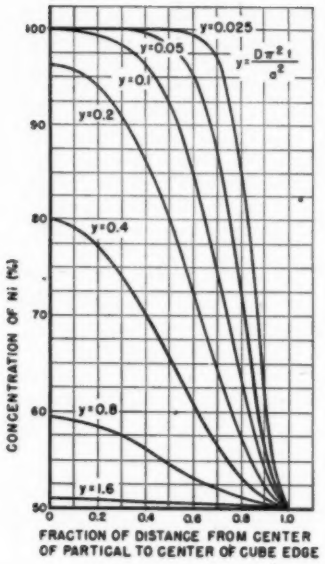

FIG. 2. Concentration along the line $(x\ x\ 0)$.

mathematically[1] by a Fourier Series:

$$F(x)=\frac{2a}{\pi}\sum_{l=0}^{\infty}\frac{(-1)^l}{2l+1}\cos\frac{(2l+1)\pi x}{a}. \quad (1)$$

Equation (1) has been successfully applied by Chevenard and Waché[2] to the study of diffusion in a solid consisting of alternate thin sheets of two metals.

Extending the square-wave picture to three dimensions, a three-dimensional series is obtained:

$$F(x,y,z)=\frac{8a^3}{\pi^3}\sum_{l=0}^{\infty}\sum_{m=0}^{\infty}\sum_{n=0}^{\infty}\times\frac{(-1)^{l+m+n}}{(2l+1)(2m+1)(2n+1)}\cos\frac{(2l+1)\pi x}{a}\times\cos\frac{(2m+1)\pi y}{a}\cos\frac{(2n+1)\pi z}{a}. \quad (2)$$

DIFFUSION EQUATION

In three dimensions, the diffusion equation[3] is

$$\frac{\partial C}{\partial t}=D\left(\frac{\partial^2 C}{\partial x^2}+\frac{\partial^2 C}{\partial y^2}+\frac{\partial^2 C}{\partial z^2}\right), \quad (3)$$

where C is concentration, D is the diffusion coefficient, and t is time. The diffusion coefficient D in this equation is considered to be constant with respect to concentration; for most metals it has the same value in all three directions.

For the case under consideration the standard solution of Eq. (3) becomes, by making use of Eq. (2),

$$C=\frac{8\alpha a^3}{\pi^3}\sum_{l=0}^{\infty}\sum_{m=0}^{\infty}\sum_{n=0}^{\infty}\frac{(-1)^{l+m+n}}{(2l+1)(2m+1)(2n+1)}\times\cos\frac{(2l+1)\pi x}{a}\cos\frac{(2m+1)\pi y}{a}\times\cos\frac{(2n+1)\pi z}{a}e^{-k^2Dt}. \quad (4)$$

Substituting this value of C in Eq. (3) results in the following expression for k^2:

$$k^2=\frac{\pi^2}{a^2}[(2l+1)^2+(2m+1)^2+(2n+1)^2]. \quad (5)$$

For $t=0$ and the values of x, y, z between 0 and $\pi/2$, the triple series in Eq. (4) becomes[4]

$$\left[\cos\frac{\pi x}{a}-\frac{1}{3}\cos\frac{3\pi x}{a}+\frac{1}{5}\cos\frac{5\pi x}{a}-\cdots\right]^3=\frac{\pi^3}{64}. \quad (6)$$

[1] F. E. Terman, *Radio Engineers' Handbook* (McGraw-Hill Book Company, Inc., New York, 1943), p. 20.

[2] P. Chevenard and X. Waché, "Etude expérimentale de la diffusion métallique par la méthode thermomagnétique appliquée à des agrégats multilames," Mémoire Révue de Metallurgie (Paris, 1945).

[3] R. M. Barrer, *Diffusion in and through Solids* (University Press, Cambridge, England, 1941), p. 2.

[4] L. B. W. Jolley, *Summation of Series* (Chapman and Hall, Ltd,. London, 1925), p. 5.

But under the same conditions, $C=1$. Hence, from Eq. (4), $\alpha=8/a^3$.

The question arises as to what should be the criterion for the completion of the alloying process. The regions around the centers of the particles are the last parts of the system to change, and hence the concentration at the point (0 0 0) can be selected as such a criterion. Another way of estimating the progress of the alloying process would be to calculate the average concentration of one of the metals in the original particle. The average concentration of the original metal is given by

$$C_{av}=\frac{8}{a^3}\int_0^{a/2}\int_0^{a/2}\int_0^{a/2}\frac{64}{\pi^3}\sum_{l=0}^{\infty}\sum_{m=0}^{\infty}\sum_{n=0}^{\infty}\left[\frac{(-1)^{l+m+n}}{(2l+1)(2m+1)(2n+1)}\cos\frac{(2l+1)\pi x}{a}\right.$$

$$\left.\times\cos\frac{(2m+1)\pi y}{a}\cos\frac{(2n+1)\pi z}{a}\right]\cdot\left[\exp\left(-\frac{\pi^2}{a^2}D[(2l+1)^2+(2m+1)^2+(2n+1)^2]t\right)dxdydz\right]$$

$$=\frac{512}{\pi^6}\sum_{l=0}^{\infty}\sum_{m=0}^{\infty}\sum_{n=0}^{\infty}\frac{\exp\left(-\frac{\pi^2}{a^2}D[(2l+1)^2+(2m+1)^2+(2n+1)^2]t\right)}{(2l+1)^2(2m+1)^2(2n+1)^2}. \quad (7)$$

The series in Eq. (4) and especially the series in Eq. (7) converge very rapidly. Using Eq. (4), the concentration as a function of $y=(D\pi^2t)/a^2$ has been calculated along the lines connecting the center of the particle with (a) the center of a cube edge, (b) the center of a face, and (c) a corner of the cube. The results of these calculations are shown in Figs. 1, 2, and 3, respectively. Results of calculations of C_{av} from Eq. (7) are shown in Fig. 4. By plotting concentration against the parameter y, the resulting curves can be used (with proper choice of the value of D) to determine the concentration as a function of time for any desired pair of metals under consideration.

ANALYSIS OF RESULTS

In considering interdiffusion of metals, it is necessary to bear in mind that at any point in the alloy only one coefficient applies, that of the particular concentration at that point. The

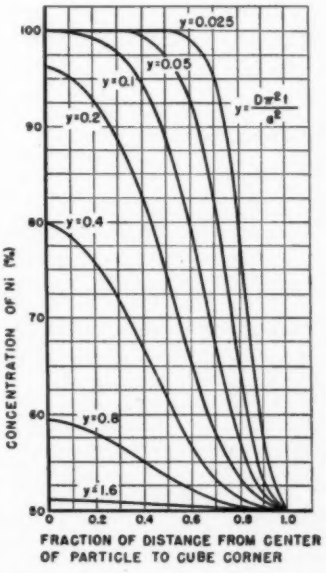

FIG. 3. Concentration along the line $(x\ x\ x)$.

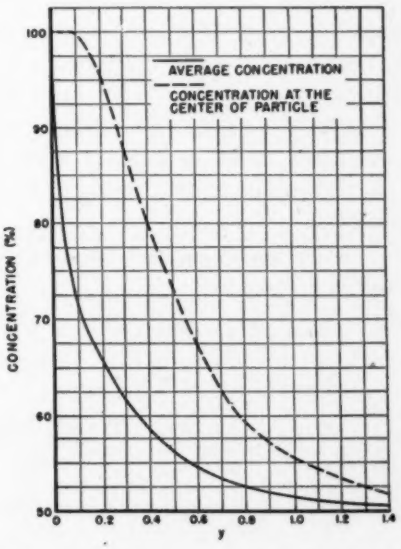

FIG. 4. Concentration as a function of $y=(D\pi^2t)/a^2$.

variation of D with the concentration in the nickel-copper alloys has been studied by Matano[5] with the interesting result that D of copper in nickel remains constant until the concentration of copper reaches about 70 percent; above this point, the value of D rises rapidly with the increase in copper content, reaching a value for D of nickel in copper more than eight times that of D of copper in nickel. Thus, if the positive peaks in the three-dimensional representation of the mixed powders are considered to be nickel, the assumption that D is constant in Eqs. (4) and (7) becomes well justified for the range $-a/2$ to $a/2$ of the variables x, y, and z. The study of Matano shows that copper moves into nickel more slowly than nickel into copper; hence, the nickel particles will be slower in losing their identity. The composition of the original nickel particle should therefore be the criterion for the completeness of the alloying process.

Equation (4), at $t=0$, gives $C=1$ for the nickel particle and $C=-1$ for the copper particle. At the interface of the particles $C=0$, which corresponds to an atomic composition of 50 percent nickel and 50 percent copper. The character of Eq. (4) is such that the interfaces will always remain at this value, though in reality some motion of the 50–50 composition region will occur because of variation of D with concentration.

The criterion for the completeness of the alloying process has to be established arbitrarily. The process may be considered completed when, say, the calculations yield $C=0.01$, which corresponds to a composition of 50.5 percent nickel and 49.5 percent copper. It may be noticed that this is a much more stringent criterion when Eq. (4) is used than when calculations are made from Eq. (7).

The time necessary to obtain a certain concentration is given by

$$t=\frac{ya^2}{D\pi^2}, \tag{8}$$

where y is the variable plotted for the two selected criteria in Fig. 4. Hence the time necessary to obtain a certain concentration $f(y)$ is proportional to the square of the edge length of the particle (or to $v^{\frac{1}{3}}$, where v is the volume of the particle) and inversely proportional to D at the temperature where diffusion takes place. Coefficient D for the diffusion of copper in nickel is given[6] by

$$D=1.04\times10^{-3}e^{-17800/T}. \tag{9}$$

Hence, knowing particle size and the temperature of sintering, the time necessary to reach a given average concentration or any given concentration at points along some of the lines in a cube can be easily computed from Figs. 1 to 4 by utilizing Eqs. (8) and (9).

The data accumulated at the Jet Propulsion Laboratory in the x-ray study of the process of diffusion in copper-nickel alloys do not lend themselves to a quantitative evaluation of the degree of the completion of the alloying process. Thus a direct check of the validity of the derived expressions is at present not available. However, the examination of the x-ray patterns of the copper-nickel alloys at different stages of the process of alloying reveals a very good qualitative correlation with the results of the calculations.

CONCLUSIONS

The expressions obtained for the concentration of individual metals in certain binary alloys prepared by sintering give concentration as a function of space, time, temperature, and particle size. The general agreement with the experimental data, which are difficult to evaluate numerically, is very encouraging and leads one to believe that the obtained results can be used for the evaluation of the completeness of the alloying process in the alloys such as in copper-nickel in a one-to-one atomic proportion, which fulfill certain conditions imposed by the mathematical expression for the distribution of particles in space.

[5] C. Matano, "On the relation between the diffusion coefficients and concentrations of solid metals (the nickel-copper system)," Jap. J. Phys. **8**, 109 (1933).

[6] Reference 3, p. 271.

Scattering of Ultrasonic Radiation in Polycrystalline Metals*

W. Roth**
Research Laboratory of Electronics, Massachusetts Institute of Technology, Cambridge, Massachusetts
(Received March 15, 1948)

A method for measuring absorption and velocity of ultrasonic radiation in the frequency range from 5 to 100 Mc by use of pulse techniques is described. Results of such measurements performed on polycrystalline magnesium and aluminum as a function of frequency and grain size show that the absorption coefficient varies linearly with frequency and inversely with grain size. The scattering power of a metal, and the fidelity with which an ultrasonic pulse is transmitted is shown to depend on the elastic constants of the single crystals. Criteria are established for evaluating the fidelity of pulse transmission in cubic and hexagonal metals, and figures of merit for many such polycrystalline metals are given.

I. INTRODUCTION

WITHIN the past decade, particularly during the war, much interest developed in the techniques for utilizing high frequency ultrasonic radiation. Although applications to methods for underwater communications have received the major share of publicity, much progress has also been made in the realm of ultrasonic propagation in solids. Researchers have employed the latter to investigate the fundamental elastic properties of matter, while engineers have employed such methods to detect and investigate macroscopic flaws in metals.

Bergmann,[1] Bär,[2] Ludloff,[3] Bhagavantam and Bhimasenacher,[4] and Huntington[5] have reported the results of both continuous wave (*CW*) and pulsed methods for determining the elastic constants of solids. Firestone,[6] Giacomini and Bertini,[7] and Trost[8] have been active in applying ultrasonics to the testing of metals. Other specialized applications using ultrasonic radiation in both liquids and solids were developed during the war at the M.I.T. Radiation Laboratory[9,10] and the U. S. Navy Underwater Sound Laboratories.

Despite the wealth of information concerning ultrasonic propagation in solids already available, there still remains a considerable void in our knowledge of the phenomena experienced in the megacycle region. This arises from two basic causes: first, the previous work on solids was restricted mainly to lower frequencies where greater thicknesses can be penetrated, and, second, the applications which did involve higher frequencies were primarily of immediate engineering need during the war, and thus could not be spared for more basic research.

Although the fact that some polycrystalline solids transmit ultrasonic pulses with less attenuation and distortion than others was recognized by those at M.I.T. Radiation Laboratory working on delay lines,[10] no verified explanations were presented. An effective change in the attenuating properties of steel as the grain size was varied was reported by Firestone,[6] but only a qualitative picture was given. Since these examples typify the state of the art at the close of the war, it was felt that research of a more fundamental nature was needed to explain some of the phenomena previously observed as well as to investi-

* This work has been supported in part by the Signal Corps, the Air Materiel Command, and O.N.R. It is a condensation of material first presented in a thesis bearing the same title submitted in partial fulfillment of the requirements for the degree of Doctor of Philosophy at the Massachusetts Institute of Technology (1947).
** Now at Harvey Radio Laboratories, 447 Concord Avenue, Cambridge, Massachusetts.
[1] L. Bergmann, *Ultrasonics* (John Wiley and Sons, Inc., New York, 1939).
[2] R. Bär, "Supersonic measurement of elastic constants of isotropic solids," Helv. Phys. Acta **13**, 61 (1940).
[3] R. F. Ludloff, "Ultrasonics and elasticity," J. Acous. Soc. Am. **12**, 193 (1940).
[4] S. Bhagavantam and J. Bhimasenacher, "Elastic constants of crystals," Proc. Ind. Acad. Sci. **A20**, 298 (1944).
[5] H. B. Huntington, *Ultrasonic Measurements on Single Crystals* (M.I.T. Research Laboratory Electronics Technical Report No. 10, March 1947).
[6] F. A. Firestone, "Supersonic reflectoscope," J. Acous. Soc. Am. **17**, 287 (1946).
[7] A. Giacomini and A. Bertini, "Supersonic Method for Testing Homogeneity of Solids," Ricerca Scientifica, **10**, 921 (1939).
[8] A. Trost, "Detecting Flaws with U.H.F. Sound Waves," Sheet Metal Industr. 255, February 1944.
[9] M. Cefola *et al*, "Application of Pulse Techniques to the Measurement of Supersonic Waves in Liquids," M.I.T. Rad. Lab. Report 963, March 1946.
[10] D. Arenberg, "Supersonic Solid Delay Lines," M.I.T. Rad. Lab. Report 932, April 1946.

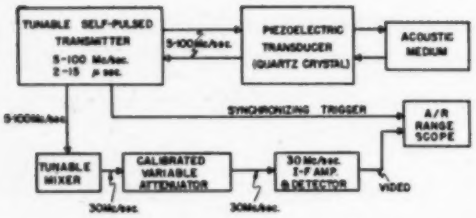

FIG. 1. Block diagram ultrasonic measuring equipment.

gate propagation in polycrystalline metals at higher frequencies.

Accordingly, apparatus for the generation and detection of ultrasonic pulses operating in the frequency band from 5 to 100 megacycles per second (Mc) was designed and constructed, and an investigation of propagation in polycrystalline metals was initiated. In particular, specimens of the desired metals were annealed so as to obtain a series with graduated grain sizes, and the velocity of propagation and absorption were measured for longitudinal waves as a function of grain size and ultrasonic frequency.

II. EXPERIMENTAL PROCEDURE

The measuring technique used to study ultrasonic absorption and velocity includes the following basic steps:

(a) generation of an electrical pulse of the desired frequency and pulse length;
(b) conversion from electrical to ultrasonic energy;
(c) transmission of the ultrasonic pulses through the metal specimen under investigation;
(d) conversion from ultrasonic to electrical energy; and, finally,
(e) interpretation of the electrical pulses to provide accurate measurement of relative intensities and time intervals.

Figure 1 illustrates in block diagram form how these functions are performed and interrelated. The electrical pulses having carrier frequencies anywhere in the band from 5 to 100 Mc with corresponding pulse widths varying from 15 microseconds (μsec.) to 2 μsec. are generated by the transmitter. The output from this unit is applied to an x cut quartz piezoelectric crystal transducer by means of a short transmission line where it is transformed into ultrasonic energy comprising a pulse packet of longitudinal elastic waves.

The crystal is acoustically loaded by a bath of distilled water in which is immersed the metal sample to be examined. The wave packet is transmitted through the water and into the metal specimen through which it propagates. After reflection from the second surface of the metal, the pulse returns through the water to the same transducer as that used for transmission. Here, it is reconverted to an electrical pulse, and is returned to the transmitter from which it is fed to the tunable mixer.

This latter element heterodynes the incoming pulse with a local oscillator (*LO*) signal and converts it to a pulse having a carrier frequency of 30 Mc regardless of its original frequency. This converted pulse is fed to a calibrated variable attenuator which is used to measure its peak power. After further amplification and detection by a standard 30-Mc intermediate-frequency (*I-F*) amplifier, the resulting video pulse is displayed on a cathode-ray oscilloscope. The scope used is a commercial instrument, including means for accurately measuring time differences. These are useful for determining the velocities of propagation of the ultrasonic pulses in the different metals. The synchronizing trigger, which is required to initiate the timing sweeps of the oscilloscope, is obtained from the transmitter.

Figure 2 is a view of the experimental equipment as arranged for a run. (*A*) is the electrical console containing the pulse generation and reception circuits. The plug-in coils (*B*) are used for band switching to provide the wide frequency

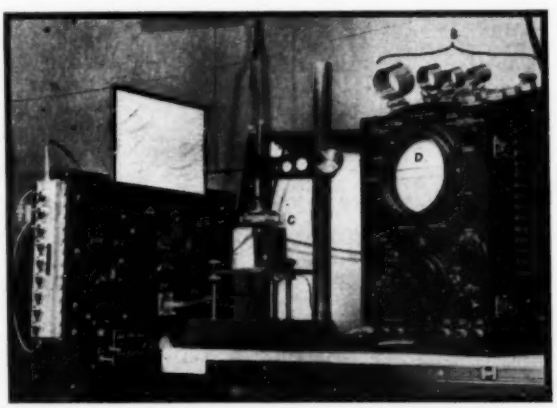

FIG. 2. Arrangement of experimental equipment.

coverage desired: tuning within each band is done with the calibrated dials observed on the panel. Peak electrical power output of 200 watts was measured at 25 Mc.

The electrical r-f pulses are fed to the quartz crystal transducer mounted at the bottom of the glass test tank (C). Here, conversion to ultrasonic energy results in a beam about $\frac{1}{4}$ in. in diameter propagating upward in a distilled water bath. The metal under test is immersed in the liquid and intercepts the beam to produce patterns on the screen of the Dumont A/R Range Scope (D). Typical patterns are shown in Figs. 3 and 4.

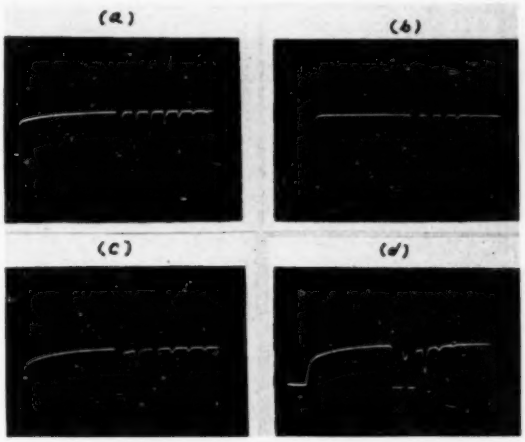

FIG. 3. (a) Fused quartz: diam. = $\frac{1}{2}$ in., length = $1\frac{3}{8}$ in., f = 28.2 Mc/sec., pulse width = 2.5 μsec., sweep length = 122 μsec. (b) Magnesium: diam. = 1 in., length = $1\frac{1}{4}$ in., D^* = 0.35 mm, f = 16.9 Mc/sec., pulse width = 3.5 μsec., sweep = 122 μsec., D/λ = 1.5. (c) Magnesium: diam. = 1 in., length = $1\frac{1}{4}$ in., D = 1.8 mm, f = 16.9 Mc/sec., pulse width = 3.5 μsec., sweep = 122 μsec., D/λ = 7.6. (d) Aluminum: diam. = $\frac{3}{4}$ in., length = $1\frac{1}{2}$ in., D = 0.21 mm, f = 16.9 Mc/sec., pulse width = 3.5 μsec., sweep = 122 μsec., D/λ = 0.88.
* D = grain size.

Figure 3a shows echoes resulting from a homogeneous rod of fused quartz. Deflection is downward, and time increases to the right. The first pulse at the left-hand edge of the sweep is the main bang. The delay before the second pulse is due to the time of propagation in the liquid before the transmitted pulse strikes the first surface of the quartz. The reflection from the first surface produces the second echo which, in this case, is of sufficient intensity to overload the receiver.

The train of pulses following that caused by the first surface results from multiple reflections between the two parallel end surfaces of the quartz. The exponential decrease in amplitude should be noted; this occurs only when materials that appear homogeneous to the beam are used. Since fused quartz of the length used here, $1\frac{3}{8}$ in., has extremely low attenuation, the absorption indicated by this exponential envelope is principally due to the reflection loss at the water-quartz interface. The reflection coefficient at this boundary is not unity; hence, not all the energy continually reflects back and forth within the quartz; a fraction is lost each round trip and the exponential decay results.

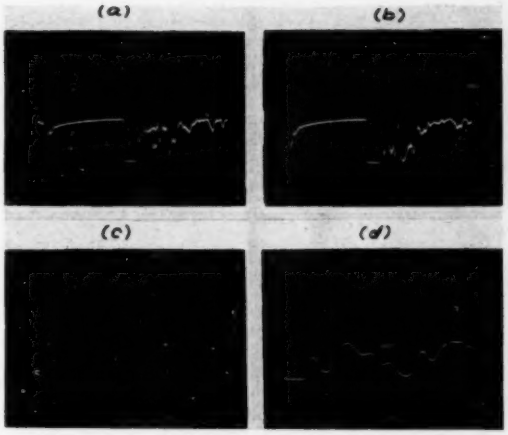

FIG. 4. (a) Brass (70–30): 1-in. cube, f = 16.9 Mc/sec., pulse width = 3.5 μsec., sweep = 122 μsec. (b) Brass (70–30): 1-in. cube, f = 16.9 Mc/sec., pulse width = 3.7 μsec., sweep = 122 μsec. (c) Magnesium: diam. = 1 in., length = $1\frac{1}{4}$ in., D^* = 0.35 mm, f = 28.2 Mc/sec., pulse width = 2.5 μsec., sweep = 12.2 μsec., D/λ = 2.5. (d) Aluminum: diam. = $\frac{3}{4}$ in., length = $1\frac{1}{2}$ in., D = 0.21 mm, f = 28.2 Mc/sec., pulse width = 2.5 μsec., sweep = 24.4 μsec, D/λ = 1.5.
* D = grain size.

Figure 3b is a similar photograph showing the pattern obtained for fine-grained magnesium. The only difference to be noted is the increased absorption in the solid as indicated by the increased slope of the exponential. Figure 3c is the result for coarse-grained magnesium. No exponential envelope is observed, because the scattering and refraction processes resulting from the non-homogeneities of the large grains introduce interference effects. Thus, one pulse may be small as a result of phase cancellation, while the next may be large as a result of phase addition.

Figure 3d is for aluminum and illustrates an effect previously absent, namely, energy return from metal grains located between the surfaces. This is indicated by the hump between the second and third pulses. A more extreme case of this

TABLE I. Description of metals tested.

Nominal composition	Forming process	Supplier
Magnesium Mg 99.95 percent Cu, Zn <0.01 Cd 0.002 Mn 0.0012 Al, Fe, Ni, Pd, Si, Sn <0.001	1-in. diam. round bar extruded at 410–450°F at a speed of 1–2 ft./min. with a reduction of 9×	Dow Chemical Company
Aluminum 2S commercially pure, Al min. 99 percent	Cold-formed round bar ½-in. diam. with a minimum of 50 percent cold work	Aluminum Company of America

phenomenon is shown in Fig. 4a. The metal here is brass, although this pattern is typical of most non-homogeneous anisotropic materials. In this case, the scattered energy from the grain boundaries is large enough to mask completely the energy reflected from the surfaces. No measurement can be made with such a pattern. Figure 4b is exactly the same except that the pulse width is slightly greater. The general pattern is similar, but the detailed fluctuations are not. This implies that the increased length of the wave train has affected the phase relationships of the interference processes, producing altered patterns. Similar variations occur for the same reason if the frequency, or alignment of the sample with respect to the beam, is changed slightly.

Figure 4c is a view of a single pulse displayed on an expanded sweep in proper position for determining its amplitude and the time elapsed with respect to the start of the sweep. No pulse distortion is evident, since fine-grained magnesium was used. Figure 4d is a similar view of aluminum, showing considerable pulse distortion. No measurements can be made with such a pulse.

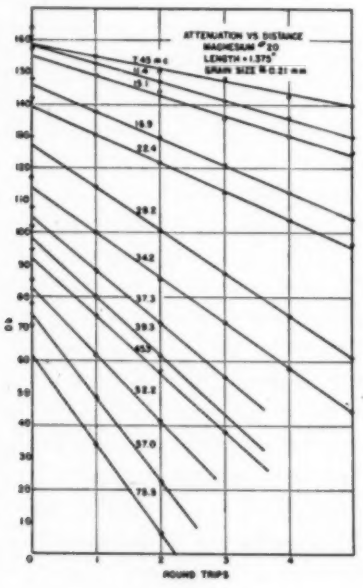

FIG. 5.

III. EXPERIMENTAL RESULTS

Six metals, magnesium, aluminum, copper, brass, nickel, and monel, were obtained in a cold-worked condition and were annealed in order to develop the desired grain sizes.[11] Of the six, only magnesium and aluminum were suitable for measuring purposes, since the pulse distortion when using the remaining four metals was prohibitive. The description of the magnesium and aluminum follows in Table I.

Attenuation

The results of measurements made on two representative magnesium specimens for different frequencies are plotted in Figs. 5 and 6. The former, for a fine-grained sample, appears to be homogeneous to the incident beam since the points on the logarithmic plots lie along straight lines that correspond to time exponentials on the

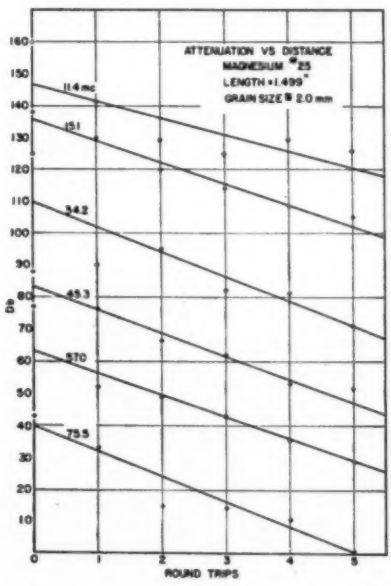

FIG. 6.

[11] The heat treating and grain counting reported here were done by Mr. D. Essman under the supervision of Professor M. Cohen, both of the M.I.T. Department of Metallurgy.

cathode-ray tube screen. The latter, for a coarse-grained sample, shows much departure from an exponential resulting from the large grains. The attenuation of the first sample can be measured accurately, whereas considerable error could be introduced in the second case. These curves are typical of both good and bad experimental runs for magnesium and aluminum.

From the slopes of these curves and the power reflection loss at the water-metal interface (see below), graphs of attenuation in the metal *vs.* frequency for different grain sizes can be plotted. Figure 7 illustrates such curves for the two samples referred to above. Although the large scatter of the individual points about the mean is disturbing, this is the nature of the processes under investigation, and cannot be avoided. The linear variation of attenuation with frequency should be noted. For grain sizes lying between the two cases shown, straight lines are also found, but the slopes assume values intermediate to those shown.

Figure 8 is a plot of the slopes of the previous curves as functions of grain size. The attenuation α is stated in terms of the amplitude absorption coefficient rather than in decibels per inch, where α is defined from the relation

$$I = I_0 \exp(-2\alpha x), \tag{1}$$

in which I = intensity in a plane wave at point x.
I_0 = intensity in a plane wave at point $x=0$, and
α = amplitude absorption coefficient.

The solid rectangles indicate the areas of error for the experimental results with magnesium, and the dotted rectangles indicate the same for aluminum. Although these areas are large, more information can be obtained from these data than is at first thought possible.

Even if a larger percent error in grain size for the uppermost point were assumed, the actual grain size limits or width of this rectangle would not be increased substantially. Similarly, a larger percent error in absorption per cycle for the point farthest to the right would not increase the height of this rectangle greatly. Therefore, the extreme limits of the curve eventually drawn are rather well defined. If we now consider the number of curves that will also pass through the center of distribution of the remaining rectangles,

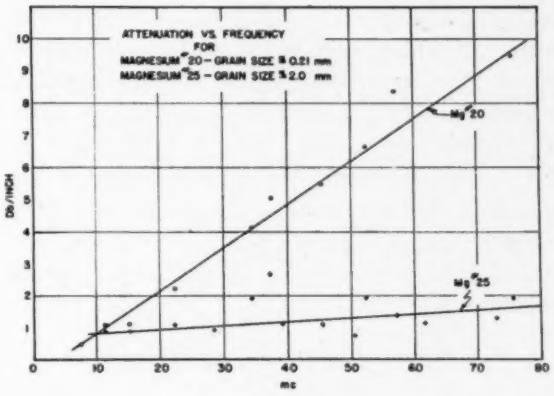

FIG. 7.

our choice is severely limited. The solid curve finally drawn is an equilateral hyperbola which gives

$$\frac{d\alpha}{df} = \frac{2\times10^{-9}}{D}, \tag{2}$$

or

$$\alpha = 2\times10^{-9}\frac{f}{D} + K(D) \text{ cm}^{-1},$$

where

f = frequency in cycles/sec.,
D = grain size in mm, and
$K(D)$ = a function independent of frequency but possibly dependent on D, in cm^{-1}.

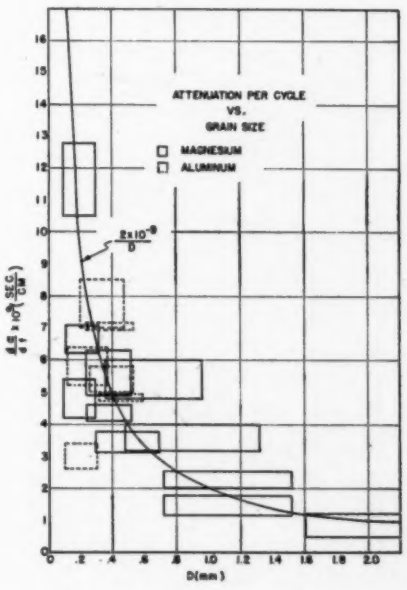

FIG. 8.

$K(D)$ is the value of α for either $f=0$ or $D=\infty$, neither of which were obtained in these experiments. However, by extrapolating the attenuation *vs.* frequency curves to $f=0$, $K(D)$ is found to lie in the region bounded by ± 0.05 cm^{-1} for all the samples tested. It should be noted that this expression refers to the frequency band from 5–100 Mc and should not be considered to apply outside this range without further experimental verification.

Power Reflection Coefficient

The power reflection coefficient for normal incidence at the interface between two semi-infinite media is given in the usual way by[1]

$$R=\left(\frac{\rho_1 V_1-\rho_2 V_2}{\rho_1 V_1+\rho_2 V_2}\right)^2, \qquad (3)$$

where ρ=density, V=velocity, and the subscripts refer to the respective media. Experimental determination of this quantity was performed by making two absorption-distance runs on each sample. The metal was completely immersed in water in one case, but only one surface was immersed in the other. Since the reflection at an air-to-metal boundary is essentially unity, the difference in the attenuation in the two cases equals the reflection loss at one metal-water interface, or $-10\log_{10}R$. Curves of these runs for the two magnesium specimens previously discussed are shown in Fig. 9. The vertical displacement between corresponding points of the two curves in each set equals $n\times 10\log_{10}R$, where n is the order of the round trip. From this measured reflection loss, R was determined for each metal and checked against the value calculated from Eq. (3). The constants for water were taken from A. B. Wood, *Textbook of Sound*. The results are:

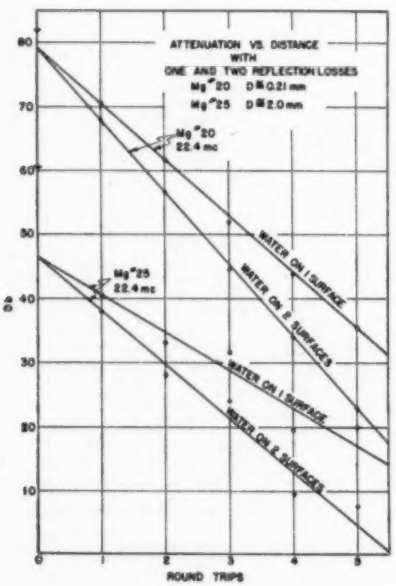

FIG. 9.

Metal	R Observed	R Calculated
Mg	0.558	0.561
Al	0.708	0.714

and the agreement is seen to be excellent.

It should be noted that this applies only for propagation from the metal to the water and not for the opposite direction. When propagating into the metal, standing waves are set up at the surface layers due to the inhomogeneities, and the conditions for application of Eq. (3) are not present. This discrepancy was observed. The departure occurs at a lower frequency for larger grains, because the inhomogeneities assume importance at a lower frequency.

Velocity

The velocity of propagation of longitudinal waves in infinite plates is given by

$$V^2=\frac{E(1-\sigma)}{\rho(1+\sigma)(1-2\sigma)}, \qquad (4)$$

where

ρ=density,
E=Young's modulus,
σ=Poisson's ratio.

This velocity is measured experimentally by dividing twice the sample length by the time difference between successive echoes. By using the known constants for the polycrystalline metal in question, Eq. (4) can be applied to check the experimental value. This was done for aluminum and is recorded below.

For magnesium, no consistent constants for the polycrystalline metal could be found, so the results of calculations giving the velocity of propagation as a function of direction in a hexagonal crystal were used. The velocity for a polycrystalline sample represents a weighted

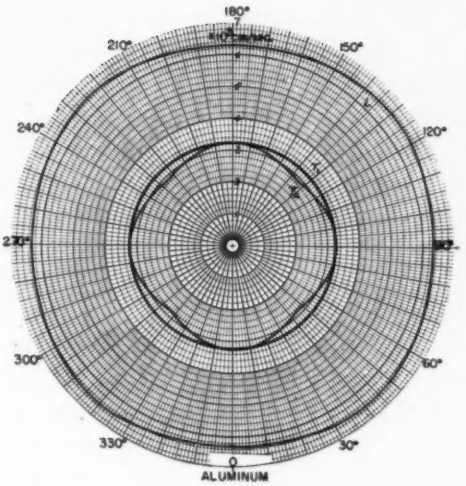

FIG. 10. Velocity in surface planes.

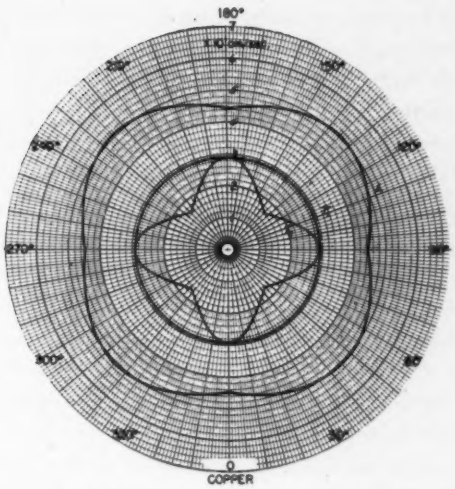

FIG. 11. Velocity in surface planes.

average of all values present in the individual crystal. These are also tabulated below. The agreement in both cases is very good and no velocity dispersion was observed.

Metal	Observed V (in units of 10^5 cm/sec.)	Calculated V (in units of 10^5 cm/sec.)	Source of elastic constants
Mg	5.77 ± 0.004	(5.61 – 5.81 for single crystal)	R. F. S. Hearmon, Rev. Mod. Phys. **18**, 409 (1946).
Al	6.31 ± 0.01	6.32	G. W. C. Kaye and T. H. Laby, *Table of Physical and Chemical Constants* (Longmans, Green, and Company, New York, 1941).

Comparison with Published Results

Mason and McSkimin[12] recently published a paper reporting results of ultrasonic absorption measurements for aluminum made in the frequency range from 2 to 15 Mc. Since the conclusions based on their work are different from those reported here, a critical comparison is in order.

Although they report results for both incident longitudinal and shear waves, only the former can be compared with those reported here, since no shear measurements have been made. Two serious disagreements and one agreement should be noted. First, they find attenuation varies with D^3 where we find a $1/D$ relation, and, second, they report a variation with wave-length of $1/\lambda^4$ at low frequencies (changing in one case to $1/\lambda^2$ at higher frequencies), while we find a $1/\lambda$ variation. The agreement concerns the velocity measurements. They obtained 6.32×10^5, and the result stated here is $6.31\pm0.01\times10^5$ cm/sec.

Unfortunately, the composition of the aluminum used in the two cases was not the same, so the two sets of experimental absorption data cannot be plotted together to give results having much significance. Aluminum 17 ST, which they used, has a nominal composition of 95 percent Al, 4 percent Cu, ½ percent Mn, and ½ percent Mg, whereas the aluminum used here is better than 99 percent pure. Although this difference in composition seems small, the attenuation found with the latter metal is about two times greater than the figure they report for the common frequency of 15 Mc and common grain size of about 0.2 mm. They do not state the mechanical or thermal treatment of the samples tested other than that "standard" rods having different grain sizes were used. It is here assumed that they were commercial stock without further annealing for strain relief or grain size control.

Two different grain sizes were used in their experiments, and they state values for D of 0.23 ± 0.01 mm and 0.13 ± 0.01 mm, respectively. Since no special annealing procedures were em-

[12] W. P. Mason and H. J. McSkimin, "Attenuation and scattering in metals and glasses," J. Acous. Soc. Am. **19**, 464 (1947).

ployed to prepare these samples, it is difficult to see how grain size errors of only ± 5 and ± 10 percent were obtained, when errors larger than ± 50 percent were found with the carefully prepared specimens used for the present work—especially since lengths up to 12 in. were reportedly used, whereas only $1\frac{1}{2}$-in. samples were employed here. Commercial stock would not be strain-free with such uniform grain structure as that indicated. As a result, the conclusion that attenuation varies with D^3, formulated after testing only two different specimens with grain-size values that are not accurately known, does not seem to be warranted.

The $1/\lambda^4$ behavior they report is in distinct contrast to the $1/\lambda$-form found here. Although no estimate of experimental errors is included in their data, it appears as if straight lines can be plotted through their points as well as the fourth power curves actually plotted. If this is done, their curves become similar to the attenuation *versus* frequency curves found in the present research. The D^3/λ^4 variation obtained by Mason and McSkimin may indeed, prove to be the case after more information is accumulated over wider frequency ranges, but from the nature of data on hand no justification for its adoption is apparent at the present time.

Explanation of Results

Since a polycrystalline metal is a tightly packed assembly of scattering elements, the theories developed by Rayleigh[13] and Morse[14] for scattering of a plane wave by an isolated single scattering element should not be expected to apply. Multiple or secondary scattering is neglected when extending the simple theory to loosely packed assemblies, but this cannot be done in the present case. The theoretical explanation of the experimentally determined expression for α given above must await more powerful techniques for handling multiple scattering from large assemblies of closely coupled elements.

An explanation of the variation in the fidelity of pulse transmission through different polycrystalline metals is furnished by examining the velocity anisotropies for the single crystals of the metals in question. By extending the method previously discussed by Christoffel,[15] Love,[16] and more recently by Mueller,[17] expressions for the velocities of propagation for the three possible modes in cubic and hexagonal crystals can be developed. For the surface planes of cubic crys-

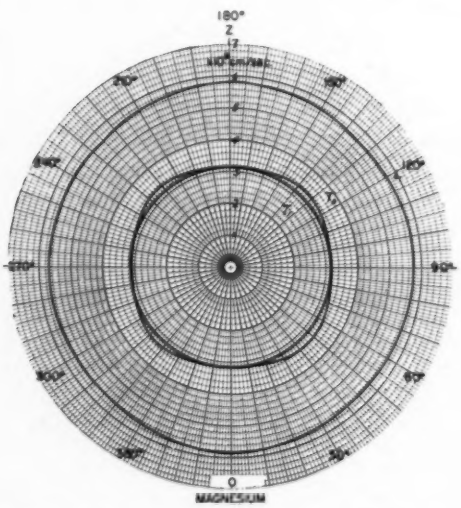

FIG. 12. Velocity in planes parallel to z axis.

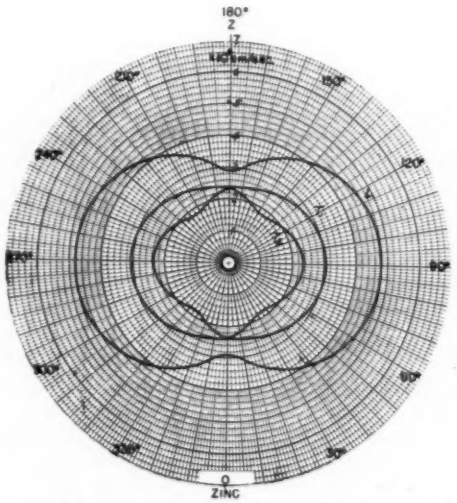

FIG. 13. Velocity in planes parallel to z axis.

[13] Lord Rayleigh, *Theory of Sound* (Dover Publications, New York, 1945), Vol. 2, pp. 420, 425.
[14] P. M. Morse, *Vibration and Sound* (McGraw-Hill Book Company, Inc., New York, New York, 1936), pp. 265, 269.
[15] E. B. Christoffel, Ges. math. Abhandlungen **Bd2**, 81 (1910).
[16] A. E. Love, *Mathematical Theory of Elasticity* (The Cambridge University Press, New York, 1920), p. 303.
[17] H. Mueller, "Intensity and polarization of light diffracted by supersonic waves in solids," Phys. Rev. **52**, 223 (1937); H. Mueller, "Determination of elasto-optical constants with supersonic waves," Zeits. f. Krist. **(A)99**, 122 (1938).

tals the equations are

$$k_{1,2}^2=\frac{(c_{11}+c_{44})\pm((c_{11}-c_{44})^2+\sin^2 2\varphi\{2c_{44}(c_{11}+c_{12})+c_{12}^2-c_{11}^2\})^{\frac{1}{2}}}{\frac{1}{2}[4c_{11}c_{44}+\sin^2 2\varphi\{c_{11}^2-c_{12}^2-2c_{44}(c_{11}+c_{12})\}]},$$

$$k_3^2=\frac{1}{c_{44}},$$

where $1/k_i(\rho)^{\frac{1}{2}}$ is the velocity of propagation, V_i, and ρ = density,

c_{jk} = elastic constants of the single crystal,
φ = angle of propagation in the surface planes with respect to the x, y, or z axis.

For the xy planes of hexagonal crystals we have

$$k_1^2=\frac{2}{c_{11}-c_{12}},$$

$$k_2^2=\frac{1}{c_{11}},$$

$$k_3^2=\frac{1}{c_{44}},$$

which are independent of the angle of propagation. The velocities in hexagonal crystals in planes parallel to the z axis are dependent upon angle and can be obtained from the equations:

$$k_{1,2}^2=\frac{b\pm(b^2-4a)^{\frac{1}{2}}}{2a},$$

$$k_3^2=\frac{1}{\frac{1}{2}(c_{11}-c_{12})\cos^2\theta+c_{44}\sin^2\theta},$$

where

$a=\frac{1}{4}\sin^2 2\theta(c_{11}c_{33}-c_{13}^2-2c_{13}c_{44})+c_{11}c_{44}\cos^4\theta+c_{33}c_{44}\sin^4\theta,$

$b=c_{11}\cos^2\theta+c_{33}\sin^2\theta+c_{44},$

θ = angle of propagation with respect to the xy plane.

Polar plots of the velocities in cubic aluminum and copper and hexagonal magnesium and zinc are given below in Figs. 10–13. The caption L refers to the quasi-longitudinal mode polarized in the plane of propagation, T_1 refers to the quasi-transverse mode polarized normal to this plane, and T_2 refers to the quasi-transverse mode polarized in the plane of propagation.

Aluminum, copper, and magnesium were tested, and, as noted above, copper was a poor transmitter, while aluminum and magnesium were good. Reference to the polar plots shows that copper is very anisotropic, while the other two are only slightly so. Although zinc was not tested, it has been included as an example of a highly anisotropic hexagonal metal which, therefore, should provide poor ultrasonic pulse transmission.

A polycrystalline solid comprising an aggregate of randomly oriented anisotropic grains scatters because discontinuities are presented to the incident pulse at the grain boundaries. The greater the anisotropy of the grain, the greater the scattering. A metal composed of isotropic grains, which have circular velocity polar plots, would not produce scattering since no discontinuities

TABLE II. Cubic system alloys.

Metal	$\frac{S_{44}}{2(S_{11}-S_{12})}$	Predicted pulse transmission
Cu_3Au	0.40	fair
72% Cu, 28% Zn	0.25	poor (observed)
β—Brass (CuZn)	0.05	very poor
5% Cu, 95% Al	0.85	good
75% Ag, 25% Au	0.35	fair
50% Ag, 50% Au	0.35	fair
25% Ag, 75% Au	0.35	fair

Cubic system elements.

Metal	$\frac{S_{44}}{2(S_{11}-S_{12})}$	Predicted pulse transmission
Al	0.81	good (observed)
Cu	0.31	poor (observed)
Au	0.35	fair
Fe	0.42	fair
Pb	0.26	poor
K	0.16	poor
Ag	0.35	fair
Na	0.14	poor
W	1.0	excellent

Hexagonal system elements (5 coefficients).

Metal	$\frac{S_{13}}{S_{12}}$	$\frac{S_{33}}{S_{11}}$	$\frac{S_{44}}{2(S_{11}-S_{12})}$	Predicted pulse transmission
Cd	6.2	2.9	2.1	fair
Mg	0.58	0.89	0.99	very good (observed)
Zn	−11.5	3.4	1.7	fair

would be introduced by grain boundaries. This concept enables us to establish a basis of comparison or figures of merit for judging the fidelity of pulse transmission for any metal.

The strains in a solid can be expressed in terms of the stresses if the elastic moduli matrix for the solid is known. The only difference between the cubic matrix and the isotropic matrix is that in the former case $S_{44}/2(S_{11}-S_{12}) \neq 1$, where S_{ik} are the elements of the matrices. The hexagonal matrix has the additional inequalities $S_{13}/S_{12} \neq 1$ and $S_{33}/S_{11} \neq 1$. If the substance were isotropic, these respective inequalities would not exist; hence this departure can be used as a figure of merit. Table II lists all cubic and hexagonal metals whose constants are given by Hearmon,[18] and the departure of the listed values from unity is a measure of the anisotropy. The experimental observations in several of the cases agree with these predictions as noted below. Tungsten is the only outstanding example of an isotropic solid included here. It should transmit pulses with little scattering and, hence, with good fidelity even at high ultrasonic frequencies.

[18] R. F. S. Hearmon, "Elastic constants of anisotropic materials," Rev. Mod. Phys. 18, 409 (1946).

ACKNOWLEDGMENTS

The author wishes to thank Professor Julius A. Stratton for his continuous interest in this research program and Professor Morris Cohen for his cooperation throughout the metallurgical phases of the work. It is with especial pleasure that he acknowledges the assistance of Professor Hans Mueller, under whose guidance this research was conducted.

The Bridge Erosion of Electrical Contacts. Part I.

J. J. Lander and L. H. Germer
Bell Telephone Laboratories, Murray Hill, New Jersey

(Received April 16, 1948)

Bridge erosion is the transfer of metal from one electrode to the other which occurs when an electric current is broken in a low voltage circuit which is essentially purely resistive. It is associated with the bridge of molten metal formed between the electrodes as they are pulled apart, and more specifically with the ultimate boiling of some of the metal of this bridge before the contact is finally broken. This paper is concerned with fundamental studies of this molten bridge and with empirical measurements of the transfer of metal.

From known physical constants one calculates that, when the melting point is reached at a current I, the diameter of the area of contact of two electrodes is about $1.5\times10^{-5}\ I$ cm for silver, copper, or gold, and about $7.5\times10^{-5}\ I$ for platinum or palladium. When the maximum temperature of the molten bridge reaches the boiling point the mean bridge diameters are roughly $4\times10^{-5}\ I$ and $20\times10^{-5}\ I$ respectively. Experimental tests have been made of relations entering into these calculations.

On breaking a contact about $6\times10^{-14}\ I^3$ cm^3 of metal is transferred from the positive to the negative electrode. This represents about 100 percent of the volume of the molten bridge for silver, copper, or gold, and about 0.5 percent for platinum or palladium. The amount of transfer can be decreased, and even its direction reversed, by heating the negative electrode, and by other means. Calculations have been made of temperature distributions in the neighborhood of a contact and a theory has been developed to account for the reversal of direction of transfer. The theory of the fundamental mechanism has, however, been reserved for later publication.

I. INTRODUCTION

WHEN an electric current is about to be broken at two separating metallic electrodes, the current density is of necessity extremely high at the last point of contact. This results in local heating and molten metal is formed much of which gets displaced from its original position.* There is, in general, a net transfer of metal between the electrodes so that with repeated operation one of them grows continuously at the expense of the other. The forma-

* These generalizations are not true if the circuit potential is lower than a certain critical value which is characteristic of the electrode metal and is of the order of 0.5 volt, nor perhaps if the current is below about 0.06 amp.

tion of a connection of molten metal between electrodes just before they separate has been called "bridging," and the net transfer of metal from one electrode to the other which accompanies this phenomenon has been called "bridge erosion." A better title for this type of erosion may emerge as soon as its nature is thoroughly understood.

In relay operation the occurrence of bridge erosion has been recognized for many years. It is accompanied, however, by other forms of erosion and in many cases its effects are masked by them so that it is not noticed. Bridge erosion must be thought of as one of many factors determining contact performance and, in a systematic attempt which we are making to isolate the various factors and to study them individually, it is the first to be investigated carefully.

Although the transfer of metal from one electrode to the other in the bridging of electrical contacts is well known, there are still on the one hand several theories regarding its cause, and on the other hand there is disagreement regarding most of the quantitative factors which can be established by empirical measurement, such as for example the variation of the rate of transfer with magnitude of the current. Even the direction of the transfer, from positive electrode to negative electrode or from negative to positive, has not been completely established. The confusion arises from variability in experimental conditions and from failure to isolate bridge erosion from other types of erosion. The problem of most immediate importance is the recognition of bridge erosion uncomplicated by other phenomena and the establishment of conditions under which it can be studied by itself.

Our work on bridge erosion splits naturally into two parts, determination of the empirical laws of bridge formation and bridge transfer, and experiments intended to discover the cause of transfer and to relate the empirically discovered laws to physical properties of matter. This paper takes up chiefly the first aspect of the work, the empirical measurements. There is, however, no perfectly sharp dividing line and there will be some encroachment here upon the more scientific aspects of the problem which were intended to be reserved for a future paper.

II. THEORY OF A STATIC BRIDGE

If the operation of a relay is sufficiently slow, thermal and hydrodynamic equilibrium will be approximately maintained while the contacts are opening. Relations can then be considered between the temperatures of various parts of the contact region, the over-all resistance, the dimensions of the bridge of molten metal, and other parameters, as if the contacts were stationary at each stage of their opening. This section is concerned with such relationships. It will be shown later that normal relays do actually operate slowly enough so that at least thermal equilibrium is quite well maintained most of the time. Calculations regarding a static bridge of molten metal are therefore actually applicable to some conditions of relay operation. The results of these calculations are important not only in the study of bridge erosion, but also in work which is not yet completed on "the short arc" between metal electrodes and in the understanding of other factors which influence contact performance.

Evidence will be presented in the next section indicating that, when a molten bridge is broken by separation of the contacts, the highest temperature reached before rupture is in the neighborhood of the boiling point of the metal. In considering the formation and destruction of a bridge, and concomitant transfer of part of the bridge metal from one electrode to the other, it is evident then that our attention must be focused primarily upon the behavior of the *molten* metal at temperatures up to the boiling point. We are interested in the interrelations of such parameters as dimensions of the bridge, resistance, current, and maximum current density. In the work to be reported here we have been concerned with five metals only, silver, copper, gold, platinum and palladium. Enough is known about the properties of these five metals to enable us to draw a few simple theoretical conclusions which are of importance to us.

If the metal is not appreciably heated by the flow of current, so that the resistivity nowhere changes from ρ_0 its room temperature value, the "spreading resistance"[1] of a contact is ρ_0/l when the area of contact is assumed to be a circle of diameter l. When there is local heating but the

[1] J. Jeans, *Electricity and Magnetism* (Cambridge University Press, Teddington), fifth ed. p. 352.

maximum temperature T_{max} is below the melting point T_m, it is clear that the over-all resistance will be less than it would be if the entire electrodes were at T_{max}, that is,

$$R<(\rho_0/l)[1+\alpha(T_{max}-T_0)+\beta(T_{max}-T_0)^2] \\ =[\rho_0+(\rho_{max}-\rho_0)]/l.$$

where α and β are temperature coefficients of resistance and ρ_{max} is the resistivity at T_{max}. It seems, on the other hand, intuitive that $R>[\rho_0+(\rho_{max}-\rho_0)/2]/l$. We express the resistance by a formula which is intermediate between these two limits, $R=[\rho_0+(\rho_{max}-\rho_0)(2/3)]/l$ or,

$$Rl=(\rho_0+2\rho_{max})/3, \qquad (1)$$

which can be proved (Section VI) to be quite a good approximation for steady heat flow.

Even when the local heating is sufficient to melt some of the metal in the contact area the total resistance can still be calculated. This is best accomplished by estimating first the resistance R_1 of the solid metal and then obtaining from it the resistance R_2 of the molten metal by means of a relation between R_1, R_2 and the maximum temperature, which comes directly from a calculation given by Kohlrausch[2] in 1900. According to this relation, the ratio of the total resistance, R_1+R_2, to R_1 is

$$\frac{(R_1+R_2)}{R_1}=\frac{V}{[V-(V^2-V_m^2)^{\frac{1}{2}}]} \\ =\frac{T_{max}}{[T_{max}-(T_{max}^2-T_m^2)^{\frac{1}{2}}]}, \qquad (2)$$

where V is the potential across the contact and V_m is the potential which would exist across the contact if the maximum temperature were T_m, *regardless of the geometrical shape which the molten metal assumes.*

In estimating R_1, we first let l represent the diameter of the circle formed by the intersection of the solid-liquid boundary with the plane surface of one of the solid electrodes. If each solid-liquid boundary were a hemisphere of diameter l and if the solid metal had a zero temperature coefficient of resistance, then R_1 would be equal[1] to $2\rho_0/\pi l$; and for a real metal, by the approximation used in Eq. (1), $R_1 l=(\rho_0+2\rho_m)(2/3\pi)$ where ρ_m is the resistivity of the solid metal at the melting point. The total resistance, R_1+R_2, would then, by the relation derived from Kohlrausch's theory, be given by,

$$Rl=(\rho_0+2\rho_m)(2/3\pi)T_{max}/ \\ [T_{max}-(T_{max}^2-T_m^2)^{\frac{1}{2}}]. \qquad (3)$$

This value is actually too high because the solid-liquid boundary is not a hemisphere, but lies somewhere intermediate between the hemisphere of diameter l and the circle of the same diameter. If the circle were truly the boundary between solid and liquid, the expression of Eq. (3) for R would be larger by the factor $\pi/2$, so that R does actually lie between the value given by Eq. (3) and a value larger by $\pi/2$. We can, however, look at Eq. (3) in a slightly different way; this equation will be true if l represents not the intersection circle by which it was defined but a dimension slightly smaller than the diameter of that circle. Now the minimum cross-sectional diameter of a molten bridge is certainly considerably smaller than the diameter of the melting circle by which l was defined above, and it is appropriate to use Eq. (3) as a reliable expression for R if we consider that l is a sort of average linear dimension of the molten bridge. Without accurate knowledge of the bridge shape any more refined calculation would probably be unjustified, if not impossible.

The dependence of R_2 upon R_1 and T_{max}, which was used above, comes from a general relationship derived by Kohlrausch between the temperatures and electrical potentials at various points in a conductor which is heated by the flow of electricity through it (see Appendix 1). It is assumed only that the conductor loses and gains electricity and heat through the same surfaces which are isothermal as well as equipotential surfaces. If the Wiedemann-Franz-Lorentz Law, $k\rho=AT$ where k is thermal conductivity, is satisfied for this conductor the Kohlrausch relation gives for the potential φ of any point in the body at the temperature T, $\varphi=\varphi^*\pm[\varphi^{*2}-A(T^2-T_0^2)]^{\frac{1}{2}}$, where T_0 is the absolute temperature at the two surfaces through which electricity and heat flow to or from the body, the potential of one of these surfaces is chosen as zero, and φ^* is the electrical potential of the hottest point.† This equation

[2] F. Kohlrausch, Ann. d. Physik 1, 132 (1900).

† See Appendix 1.

gives $\varphi^{*2}=A(T_{max}^2-T_0^2)$, and φ equals respectively zero and $2\varphi^*$ at the two equipotential surfaces at temperature T_0. From this relation the potential V across a contact is given by,

$$V^2=4A(T_{max}^2-T_0^2), \quad (4)$$

and, for $T_0 \ll T_{max}$,

$$T_{max}=V/2A^{\frac{1}{2}}=\text{approx. } 3200V, \quad (4A)$$

with V expressed in volts.[3] When the maximum bridge temperature is above the melting point, $T_{max}>T_m$, the melting point isothermal surfaces are also equipotential surfaces and their potentials are $\varphi^*-(\varphi^{*2}-AT_m^2)^{\frac{1}{2}}$ and $\varphi^*+(\varphi^{*2}-AT_m^2)^{\frac{1}{2}}$. Now, if I is the current through the contact, obviously $R_1=2[\varphi^*-(\varphi^{*2}-AT_m^2)^{\frac{1}{2}}]/I$ and $R_2=2(\varphi^{*2}-AT_m^2)^{\frac{1}{2}}/I$. The ratio $(R_1+R_2)/R_1$, which is also the number of times the rate of energy dissipation in the entire contact is greater than that in the solid part, is $\varphi^*/[\varphi^*-(\varphi^{*2}-AT_m^2)^{\frac{1}{2}}]$, which is Eq. (2).

For a contact at high temperature, but before melting, one obtains from Eqs. (1) and (4A),

$$l/I=(\rho_0+2\rho_{max})/3V$$
$$=3200(\rho_0+2\rho_{max})/3T_{max}, \quad (5)$$

and from Eqs. (3) and (4A) after the beginning of melting,

$$l/I=2(\rho_0+2\rho_m)/3\pi[V-(V^2-V_m^2)^{\frac{1}{2}}]$$
$$=6400(\rho_0+2\rho_m)/3\pi[T_{max}-(T_{max}^2-T_m^2)^{\frac{1}{2}}]. \quad (6)$$

Equation (5) can be proved to be numerically equivalent to Eq. (9) below which is derived by more rigorous methods. All of these equations are derived for the assumed condition of steady heat flow. It is proved in Section V that in the operation of standard relays steady heat flow exists after the beginning of melting, but not before. Equation (6) is therefore properly applied to relays, but Eqs. (5) and (9) must be considered as only rough approximations.

In order to make the applications of Eqs. (4), (5), and (6) to our five contact metals which we wish to make, we must have numerical values of melting and boiling points, room temperature resistivities, and temperature coefficients of resistance for the solid metals. What we have chosen as the best values of these quantities are written down in columns 2–6 of Table II as they are found in International Critical Tables, in papers by Northrup,[4] and in a book by L. F. Vines.[5] For convenience, the symbols which are used here and later in this paper are defined in Table I.

TABLE I. List of symbols.

	Units	
l	cm	Diameter of contact region, or of molten bridge
l_m		Diameter of contact for $T_{max}=T_m$
l_b		Dimension of bridge for $T_{max}=T_b$
T_0	°K	Temperature at distance from contact region
T_m		Melting point
T_b		Boiling point
T_{max}		Maximum Temperature
ρ	ohm cm	Resistivity, in general
ρ_0		Resistivity, at T_0°K
ρ_m		Resistivity of solid at T_m°K
α	°C^{-1}	Temperature coefficient of resistance of solid
β	°C^{-2}	Coefficient β in $\rho=\rho_0(1+\alpha\theta+\beta\theta^2)$ for solid
V	volts	Potential across contact
V_m		Potential across contact for $T_{max}=T_m$
V_b		Potential across contact for $T_{max}=T_b$
R	ohms	Total resistance of contact, in general
R_1		Resistance of the solid part of a contact
R_2		Resistance of the liquid part of a contact
R_m		Total resistance with $T_{max}=T_m$
R_b		Total resistance with $T_{max}=T_b$
I	amp.	Current through contact
i	amp. cm^{-2}	Current density at bridge
k	watt cm^{-1} °C^{-1}	Thermal conductivity
δ	°C^{-1}	Temperature coefficient of thermal conductivity
σ	g cm^{-3}	Density
H_f	joule/g	Heat of fusion
h	joule/g °C	Heat capacity
a	cm/sec.^{2}	Acceleration of contact separation
K	cm^2/sec.	$K=k/\sigma h$

Numerical values of various parameters of bridges of these five metals for maximum tem-

[3] This relation has often been applied to contacts, see, for example, Ragnar Holm, *Electric Contacts* (Hugo Gebers, Stockholm, 1946).

[4] E. F. Northrup, J. Frank. Inst. **177**, 1 and 287 (1914); *ibid.* **178**, 85 (1914).

[5] R. E. Vines, *The Platinum Metals and Their Alloys* (The International Nickel Company, 1941).

TABLE II.

1	Constants from I.C.T., Vines and Northrup					Parameters of bridges at melting and boiling points						
	2	3	4	5	6	7	8	9	10	11	12	13
									$l/I\times10^6$		$iI\times10^{-9}$	
	T_m	T_b	$\rho_0\times10^6$ at 20°C	$\alpha\times10^3$	$\beta\times10^6$	V_m volts	V_b volts	R_1/R_2 Boil. pt.	Melt. pt. cm/amp.	Boil. pt. cm/amp.	Melt. pt. amp.²/cm²	Boil. pt. amp.²/cm²
Ag	1233	2223	1.6	3.61	—	0.39	0.70	0.195	13	29	7.5	1.5
Cu	1356	2573	1.7	4.1	+0.43	0.42	0.80	0.132	17	49	4.4	0.5
Au	1336	2873	2.2	3.65	—	0.42	0.90	0.131	19	48	3.5	0.5
Pt	2046	4803	10.0	4.0	−0.585	0.64	1.50	0.106	70	198	0.26	0.03
Pd	1827	4253	10.0	3.61	—	0.57	1.33	0.108	82	228	0.19	0.02

perature at the melting point and at the boiling point have been calculated (Table II) from these data and the results written down in columns 7–13. In columns 7 and 8 are the over-all voltages across a contact respectively at the melting point and at the boiling point, as obtained from Eq. (4A). In column 9 are values of the ratio R_1/R_2 of the resistances of the solid and molten parts of a contact when the maximum temperature has just reached the boiling point, as obtained from Eq. (2). The values of columns 10 and 11 are calculated from Eqs. (5) and (6). Finally, one readily finds estimates of current density, i; the cross section of a bridge is roughly $\pi l^2/4$ so that $iI=4/\pi(l/I)^2$ and the values of columns 12 and 13 are gotten from those of columns 10 and 11; the values of column 12 will represent current densities at melting, but those of column 13 are slightly smaller than the *maximum* current density at the center of a molten bridge where it is most constricted.

Comparison of the different metals on the basis of the data of Table II is of immediate interest. The numbers in columns 7 and 8 are the powers put into the various bridges at a current of 1 ampere; at the melting point these powers do not differ greatly, and only by a factor of 2 at the boiling point. When the maximum temperature is near the boiling point most of the over-all resistance is in the molten part of a bridge (column 9); the contribution of the spreading resistance in the solid electrode is only from 9 to 17 percent of the total. Bridge dimensions, which are proportional to the current, are much the same for silver, copper and gold at both the melting point and the boiling point but are smaller (columns 10 and 11) than the corresponding dimensions for platinum and palladium bridges by a factor in the neighborhood of 5; expressed differently, *the volume of metal in a bridge of platinum or palladium is roughly 100 times greater than the volume of a bridge of silver, copper or gold at the same current.* Current densities are inversely proportional to the total current, and at a current of 1 ampere are of the order of 10^9 amperes per square centimeter.

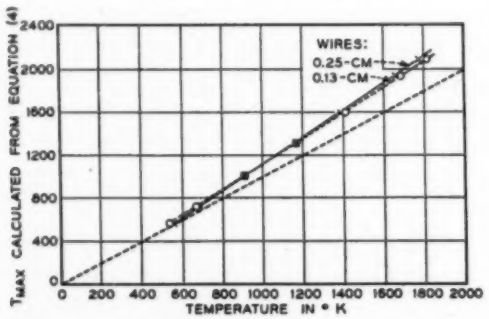

FIG. 1. Comparison of maximum temperature for a platinum wire, calculated from Eq. (4), with measured maximum temperature.

The parameters recorded in columns 7, 8, 10, and 11 of Table II have been subjected to experimental measurement, and comparisons between observed values and those of Table II are given in the following section. The agreements which have been found support the theory strongly.

III. BRIDGE MEASUREMENTS

Experimental tests of the relation between voltage and maximum temperature and of the relation between current and bridge dimensions are given below.

The Relation between Voltage and Maximum Temperature

(a) *Direct Measurement of Voltage and Temperature*

The straightforward way of testing Eq. (4) is to measure the temperature at the center of an

extremely short section of wire clamped firmly between heavy leads when the wire is heated by an electric current, and to compare this temperature with the voltage between the leads. By making the wire short it becomes a satisfactory model of an electrical contact. Experiments of this type have been carried out upon 0.036 cm platinum wires clamped between heavy water cooled copper jaws. Thermocouple wires of 0.005 cm diameter of pure platinum and platinum-10 percent rhodium alloy are welded to the center of the exposed section of the larger wire, precautions being taken to obtain symmetry of these leads so that they pick up no potential from the gradient along the wire.

The results of these experiments are represented by the plot of Fig. 1. The abscissae of this figure are temperatures of the center of the wire as determined by the thermocouple, and the ordinates are maximum temperatures as calculated by Eq. (4) from the voltage between the leads. The points indicated by crosses were obtained from a wire 0.25 cm long, and those indicated by circles from a wire 0.13 cm long. (It can be readily shown by calculation that even for wires as long as 0.25 cm the heat lost by radiation is completely negligible in comparison with the heat carried away by conduction to the water-cooled ends, as is required if the theory is to apply.) Discrepancies between true temperatures, from the thermocouples, and calculated temperatures, from the voltages between the leads, are found to increase with increasing temperature to about 260° at 1800°K which was the highest temperature of the tests. Although the reasons for the discrepancies are not understood, their magnitudes are not disturbing.**

(*b*) *Exploded Wire Experiments*

Other tests of Eq. (4) have been made by examining voltage time curves obtained from short wires which were exploded electrically. Wires of various metals were clamped at their ends and then exploded by connection to a 4-volt storage battery through a specially constructed chatter-free mercury switch. Oscilloscopic records of potential across some of these wires are reproduced in Fig. 2. Significant features of these curves are the sharp second change in slope, which evidently corresponds to the initiation of melting in a wire, and the final change in slope, representing the boiling point. That this is actually the boiling point seems to be clear from the fact that the record is discontinuous immediately after the third change of slope, jumping at once to the open circuit potential of 4 volts.

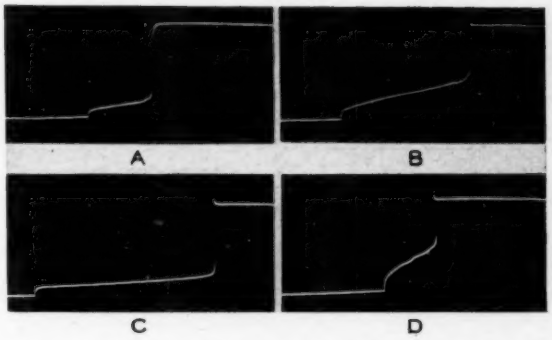

FIG. 2. Oscilloscopic records of potential across wires exploded by connection to a 4-volt storage battery. *A*-copper, *B*-platinum, *C*-silver, *D*-palladium.

It was not experimentally convenient to explode wires which were short and thick enough to make temperature radiation negligible. Tests were made therefore upon wires of various lengths. In Fig. 3 are reproduced the resulting melting and boiling point voltages, plotted for each of seven metals against length of wire, the wire diameter being indicated on each plot. The arrows at the left represent melting and boiling point voltages calculated from Eq. (4).

The experiments upon exploding wires are of intrinsic interest apart from their rough verification of Eq. (4). It is reported below that oscilloscopic records resembling those of Fig. 2 can be obtained from the breaking of a metal contact. Experience in the interpretation of these records becomes then of value.

(*c*) *Opening Contacts*

In Fig. 4 are reproduced a number of superposed traces of the potential across a pair of platinum contacts on breaking. The potential difference is zero along the base line and 4 volts along the upper line. In each of the traces there

** Numerical experimental values of electrical resistivity and thermal conductivity for platinum are available up to temperatures close to the melting point. By using these rather than the Wiedemann-Franz-Lorentz Law it has been shown that the discrepancies are not due to inaccuracy of this law. It can be proved, furthermore, that the discrepancy cannot be due to Thomson heat.

TABLE III. Observed and theoretical maximum voltages.

	Final voltage from oscilloscopic traces	Calculated V_b Table 2, column 8
Ag	0.8	0.70
Cu	0.8	0.80
Au	1.0	0.90
Pt	1.6	1.50
Pd	1.4	1.33

is an ill-defined arrest in the voltage rise at about 0.7 volt, and a complete break in the trace at 1.6 volts. From the experience with exploded wires, and by comparison with the data for platinum in columns 7 and 8 of Table II, it is clear that these two voltages represent respectively the melting and boiling points.

In column 2 of Table III are written down experimental values of the final breaking voltage for each of our five contact metals. For comparison are given in column 3 the voltages at the boiling point of a contact V_b, as calculated from Eq. (4) and given in Table II, column 8. The experimental values are as accurately measurable for separating contacts as for exploding wires, and the former are in considerably better agreement with the theoretical values than are the latter as one would expect from the fact that the requirement of only negligible heat loss by radiation is well satisfied only in the case of the contacts. The traces from which the data of Table III were obtained supply the most convincing evidence for the correctness of the picture of the formation and final boiling of a bridge whenever current is interrupted by the separation of metal contacts.

One notes that the experimental voltages tend to be higher than the theoretical. This is in line with the discrepancy shown in Fig. 1; in fact, the maximum excess of temperature calculated from the voltage in the experiment leading to Fig. 1 over the true temperature was 260°C corresponding to $260/3200 = 0.081$ volt, which is about the mean discrepancy exhibited in Table III, for considerably higher temperatures. The experimental evidence indicates then that Eq. (4) is as accurate for these five metals at their boiling points as it is for platinum just below its melting point. This check of Eq. (4) at high temperatures is a verification of the Wiedemann-Franz-Lorentz Law for *molten* metals. It is in agreement with very meager data on conductivities of molten bismuth, cadmium and aluminum which were previously available.

Bridge Dimensions

(a) *Direct Measurement of Bridge Length*

A measurement of the relation between bridge length and current at high temperatures has been made by determining the separation of electrodes under a microscope. With contacts pressed together an appropriate current is first established in a circuit containing sufficient resistance to permit only inappreciable change when a bridge is established by drawing the contacts apart. They are separated by a micrometer screw until the voltage reaches a value corresponding to a temperature somewhat below the boiling point, the separation being determined readily by microscopic observation of marks on the electrodes near their point of contact.

Measurements were made of the separation s of platinum electrodes at 5, 10, and 20 amperes for the potential of 1.0 volt, and of gold electrodes at 15 and 25 amperes for a potential of

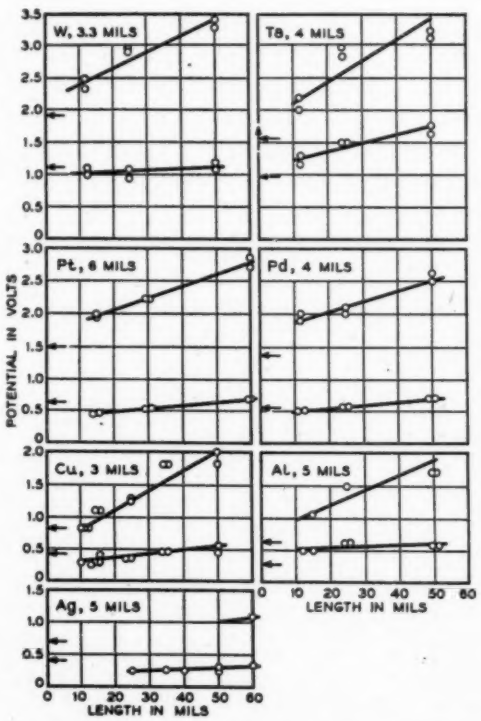

FIG. 3. Melting point and boiling point voltages for exploded wires of various lengths.

0.8 volt. The data are assembled in columns 2–5 of Table IV. Values of l/I are calculated from Eq. (6) and written down in column 6. If one makes the naive assumption that, as the boiling point is approached, the length of a molten bridge becomes approximately equal to its diameter, the quantities in columns 5 and 6 should agree.

TABLE IV. Comparison of measured bridge length with calculated bridge diameter.

1	2	3	4	5	6
	Current (amp.)	Potential (volt)	Separation s (cm)	$s/I\times10^6$ (cm/amp.) Expt. values from columns 2–4	$l/I\times10^6$ (cm/amp.) Calc. from Eq. (6)
Pt	5	1.0	0.0008	160	
	10		0.0013	130	
	20		0.0024	120	
			Average	137	124
Au	15	0.8	0.00055	36	
	25		0.00080	32	
			Average	34	42

(*b*) *Diameters of Pits Left by an Exploded Bridge*

Photographs and measurements have been made by W. G. Pfann (to be published elsewhere) of pits left on each of two electrodes after the explosion of a molten bridge drawn out between them. It is to be expected that each of these pits represents approximately the boundary between solid and liquid metal when the maximum temperature of the bridge reached the boiling point, and therefore the theory indicates that the quotient of diameter by current should be constant and only a little larger than the calculated value of l/I given in column 11 of Table II.

Pfann finds that for platinum electrodes in a 6 volt circuit the diameter of the pit is proportional to the current over the range of his measurements from 0.8 to 7.2 amp. The diameter is 185×10^{-6} cm/amp. but, correcting for the fact that the current was measured before the bridge was established and the actual *final* current when each bridge broke was smaller by the factor $(6-1.6)/6=0.73$, the true value of this quotient becomes 253×10^{-6} cm/amp. For silver and palladium contacts pits measured by Pfann at the single current of 5.3 amp. were found to have a diameter, after correction, of 44 and 244×10^{-6} cm/amp. respectively. Each of these three ratios is a little larger than the corresponding theoretical value in column 11 of Table II, and the agreements offer good support to the theory.

(*c*) *Estimates of Bridge Lengths from Oscilloscopic Records*

Still another method of finding a dimension of a liquid bridge is offered by oscilloscopic traces like those of Fig. 4. Measurements of the life times of platinum bridges in microseconds, obtained from such traces, are plotted against current in Fig. 5. In each test the contacts were separating at a velocity which was intended to be 1.2 cm/sec.,*** and therefore the slope of the line which fits the points of Fig. 5, 74 microseconds/ampere, corresponds to bridge lengths of 89×10^{-6} cm/amp. This is in poor agreement with the direct measurements of bridge length and with Pfann's measurements of diameter, but the experimental difficulties and uncertainties of the oscilloscopic observations were great and perhaps the disagreements are not beyond experimental error.†

(*d*) *Published Data*

Holm (see reference 3, p. 333) calculates very roughly that the maximum diameter and maxi-

FIG. 4. Superposed oscilloscopic records of the potential across a contact on opening a 4-volt circuit.

*** The velocity of 1.2 cm/sec. was chosen because this is about the rate of separation of conventional telephone relay contacts when they break the bridge formed on opening. The opening of usual types of telephone relays occurs at uniform acceleration which may be anywhere in the range from 5000 to 50,000 cm/sec^2. At the separation s the velocity is $(2as)^{\frac{1}{2}}$, where a is the acceleration. If we assume $s=l$ and take $l=198\times10^{-6}I_b$ for platinum contacts at the boiling point, we obtain for the velocity $v=1.4$ to 4.4 cm/sec. at 1 amp., and 0.4 to 1.4 cm/sec. at 0.1 amp. For silver or gold contacts the velocities are a little less than half these values.

† Details of the experimental procedure are given in section 4.

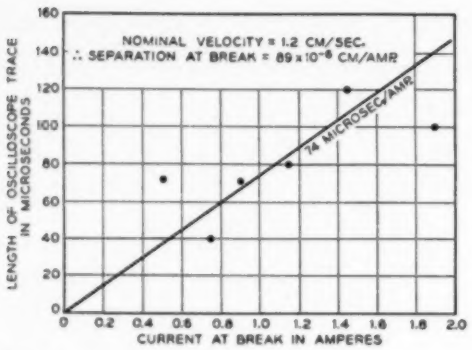

FIG. 5. Measurements of the lifetimes of molten bridges at various currents for the same velocity of contact separation.

mum length of bridges of silver, copper, and gold are about 36×10^{-6} cm/amp.—in agreement with our theoretical values of Table II, column 11.

The only measurements of bridge dimensions with which we are familiar are those of Fairweather.[6] In Fairweather's Fig. 23 he plots, without experimental points, various parameters of a platinum bridge as functions of current through the bridge. From his plots we have found that the length and diameter of a platinum bridge at a potential of 1.0 volt are respectively about 1180 and 640×10^{-6} cm at a current of about 6.8 amp. These numbers yield respectively ratios of $l/I=175$ and $s/I=94\times10^{-6}$ cm/amp. at 1.0 volt. These are to be compared with 124×10^{-6} cm/amp. calculated for platinum at 1.0 volt from Eq. (6).

(e) *Shape of a Bridge*

The diameter, l, of the contact between two solid electrodes at a high maximum temperature is given by Eq. (5). At the beginning of melting this still represents the diameter of the bridge which now begins to acquire a third dimension. When the maximum temperature is above the melting point the *maximum* bridge diameter is slightly larger than the value given by Eq. (6), and the bridge has now a third dimension s which is at first small but grows with increasing T_{max} until, as the boiling point is approached, it seems probable that the bridge length s becomes comparable with the maximum diameter.

There is at present no quantitative theory relating bridge *length* and other parameters, but the direct measurements of length reported above do indicate clearly that for both gold and platinum bridges the length actually becomes approximately equal to the maximum diameter at a temperature only a little below the boiling point. The oscilloscopic records lead to bridge lengths at the boiling point equal to about half the maximum diameter, but these observations are subject to large experimental error.

IV. TRANSFER OF METAL ON BREAK

Experimental Method

The erosion of contacts in telephone relays takes place slowly, and in many cases appreciable disturbance of the metal surfaces is observed only after the contacts have been opened and closed millions of times. If many erosion tests are to be carried out it becomes, therefore, advantageous to have some method of accelerating the destructive processes. We have found that, in most cases, the number of operations per second can be greatly increased without detectable change in the damage done to the contacts per individual operation, and this type of accelerated test has proved to be highly useful.

Conventional relay structures are not adaptable to very high rates of operation. They are, furthermore, subject to chatter on make, and even on break. Velocities and accelerations are not under good experimental control, and the usual ranges of velocities and accelerations cannot be maintained at rates of operation much higher than normal. For these, and for other reasons, standard relays are not suitable for the tests which we wished to make, and the repetitive tests of contacts which are described below were carried out upon experimental structures designed for our needs.

The most satisfactory type of test equipment has been a contact between two crossed wires, respectively of diameter 1.2 and 0.3 mm. The larger wire is rigid and the smaller wire is pressed against it and supported as a cantilever about 2.5 cm from the contact. Electrical connection between the wires is broken in the direction normal to both of their lengths when the lighter wire is struck by a vibrating rod coming against it very close (about 0.5 mm) to their point of

[6] A. Fairweather, J. Inst. Elec. Eng. 92, Part 1, 301 (1945).

contact. The rod is part of a loudspeaker unit and its amplitude and frequency can be adjusted to any desired values. The amplitude is large compared to the length of the bridge formed when the contacts separate, and the effective mass is large compared to that of the small wire. The rod strikes the wire at the center of the rod's vibration, and it is intended that it shall carry the wire along with it at its full velocity. Since the motion is a sine function of the time, the velocity with which the contacts separate is readily calculated from the frequency and amplitude; the former, which was 120 cycles per second in all of the tests described below, is known from the calibrated oscillator which supplies power to the speaker unit and the latter is determined by microscopic observation.

In all of the repetitive tests the contacts operate without chatter. During each test the plates of an oscilloscope are continuously attached to the two sides of the contact and any chatter is at once detected on the oscilloscope screen. The force between the contacts can be adjusted by means of a micrometer screw operating upon one of the supports through a cantilever bar, and this adjustment is used as one means of eliminating chatter. Other useful methods are change of frequency, change of amplitude, change of the length of the vibrating wire, and use of damping materials.

The oscilloscopic traces of breaking platinum contacts which were reproduced above as Fig. 4 were made with this apparatus. Traces of this sort are not readily obtained from conventional relays because of the disturbing effect of vibration in the relay springs. It seems clear that the simplified contacts of the present experiments are operating under more nearly ideal conditions. One is not, however, justified in assuming that the velocity of opening of these contacts is always uniform and is just that calculated from the vibration of the rod of the speaker unit. The fact that the point where the vibrating rod strikes the small wire cannot coincide exactly with the contact between the two wires makes possible the existence of a transient vibration during the very first motion of the light wire. When one examines individual traces, such as one of those making up Fig. 4, it is found that there is considerable variation in total length along the time scale from one to another. This variation is attributable, in part at least, to variation resulting from mechanical imperfections.

With repeated opening and closing of a pair of contacts of any one of a number of metals studied, in a non-inductive circuit in which the voltage is very low, there results a transfer of metal from the positive to the negative electrode. A projection or mound is formed on the negative and a corresponding pit or depression in the positive. In experiments by Pfann, to be published elsewhere, the gain in mass of the negative is found to be just equal to the loss of the positive. We have carried out tests in which, by means of an auxiliary relay, the operations of opening and closing the circuit are separated. In these tests it was discovered that in a circuit in which the potential is 4 volts at least 99 percent, and perhaps all, of the transfer of metal occurs on the break. After completing these tests it was considered unnecessary to separate make from break and the experimental equipment was considerably simplified.

The amount of metal transferred in a large number of operations is determined by optical examination of the mound which is built up on the negative electrode. The shape of the base of the mound is determined microscopically with fair accuracy, but its height and general profile above the surface of the contact wire can be obtained better from the projection of a shadow of the wire surface upon a screen. A photograph and a shadowgraph of a typical mound are reproduced as Fig. 6. These optical estimates of volumes have important advantages over weighing, the most important being the sensitivity. By these methods good estimates can be made of volumes of mounds containing as little as 0.1 microgram (5×10^{-9} cc) of metal. We are thus

FIG. 6. A photo-micrograph and shadowgraph of a mound of metal transferred to the negative electrode.

TABLE V. Amounts of platinum transferred at various currents.

1	2	3	4	5
			Volume transferred	
I (amp.)	I_b (amp.)	Operations	Shadowgraph estimate cc $\times 10^9$	Microscopic estimate cc $\times 10^9$
1.25	0.75	216,000	14.7	14.7
1.25	0.75	742,000	52.9	55.0
1.9	1.14	21,600	—	3.6
1.9	1.14	72,000	12.7	19.0
1.9	1.14	648,000	32.4	54.0
0.85	0.506	1,080,000	5.1	5.3
0.85	0.506	1,080,000	8.5	11.4
3.15	1.89	108,000	42.2	62.0
2.4	1.44	144,000	22.6	21.2
1.5	0.90	504,000	16.9	23.0
0.62	0.37	3,800,000	—	7.5
1.16	0.636	1,000,000	13.0	5.4

able to experiment with low rates of transfer of metal, corresponding to small currents in the range used in actual relay contacts, without requiring an inconveniently large number of operations for each test.

Amounts of Transfer

Preliminary tests were carried out upon the rate of formation of mounds of metal upon the negative member of two platinum electrodes as a function of their rate of separation. This rate was varied from 0.04 to 3.4 cm/sec. (which is about the extreme range in telephone relay practice) without any difference being discovered in the rate at which metal was transferred from positive to negative electrode. We have therefore concluded that the transfer is independent of velocity of separation, and all of the tests reported in the next paragraph were made at 1.2 cm/sec. which is about an average value for conventional relays at the instant the bridge is broken.

Data on the transfer of platinum in a non-inductive 4 volt circuit are given in Table V. In column 1 are values of the current with the contacts pressed together, in column 2 the current at the breaking point of the bridge, in column 3 the number of operations, and in columns 4 and 5 independent estimates by different methods of the volume of the mound formed on the negative electrode. In Fig. 7 are plotted logarithms of the volume of metal transferred per operation against logarithms of the current at break (column 2) the points appearing as circles and crosses representing the two different methods of estimating volumes.[7] The line through the experimental points represents the equation

$$\text{Volume} = 6\times10^{-14} I_b^3 \text{ cm}^3/\text{operation}, \quad (7)$$

with I_b expressed in amperes. Pfann has made transfer measurements upon platinum at two different currents, to be published elsewhere, and has obtained values which are plotted for comparison. His measurements would fit an equation $\text{Volume} = 4\times10^{-13} I_b^3$, somewhat greater than we have found.

Measurements of transfer like those of Table V and Fig. 7 have been carried out for silver, gold, and palladium also, and the results are reproduced in the plots of Fig. 8. The straight line on each of these plots is the graph of Eq. (7). The volumes of the mounds of silver, gold and palladium were obtained by microscopic estimates before the shadowgraph method was developed, and the plots of Fig. 8 represent measurements which were less careful than those for platinum in some other ways also. The lower precision of the measurements for these three metals does not, however, leave any uncertainty regarding the observation that the transfer of these metals varies with current in much the same way as does the transfer of platinum and that, for any given current, volumes of the four metals transferred per operation are much the same.††

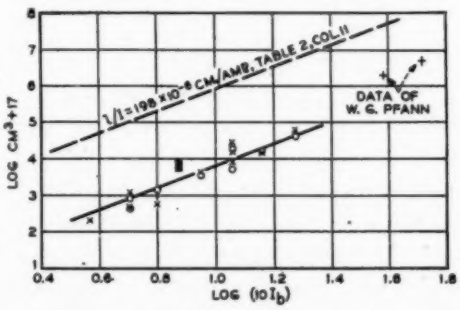

FIG. 7. Volumes of platinum transferred per operation at different currents, from the data of Table V.

[7] Bridge transfer was discovered by R. Holm and collaborators—Wiss. Veröff. Siemens-Werk 14/1, 30 (1935); 14/3, 53 (1935). They report that the amount of transfer is proportional to the square of the current with various proportionality factors for different metals, representing amounts of transfer considerably larger than we have observed in the current ranges which have been investigated.—R. Holm, *Electric Contacts*, p. 326.

†† The *shape* of the mound of metal transferred to the negative electrode is dependent upon the metal, the size of the mound, and the rate at which it was formed. Plati-

It is of interest to compare the volume of metal transferred per operation with the volume of each molten bridge. The volume of molten metal when the maximum temperature in a bridge reaches the boiling point is of the order of magnitude of l_b^3 with the value of l_b given by Eq. (6), Table II, column 11. The true volume is less than this because of constriction at the center of a bridge to a diameter considerably less than l_b, but it is on the other hand larger because there is molten metal entirely outside of the bridge proper; altogether it seems that l_b^3 is not a bad estimate of the total volume of molten metal. Values of $(l_b/I)^3$ from Eq. (6) are written down in the second column of Table VI for the four metals for which transfer measurements are available, and the corresponding line representing total bridge volume for platinum is drawn on Fig. 7. The amount of metal transferred, 6×10^{-14} cc/amp.^{3}, represents the percentages given in column 3 of the total volumes of the bridges; within experimental error, about 100 percent of a bridge of gold or of silver is transferred and about 0.5 percent of a bridge of platinum or palladium.[8] One might think that percentages greater than 100 are impossible, but this may not be so if some of the heat responsible for melting metal in the positive electrode is received *after* the contacts separate, for example from bombardment by thermionic electrons from the negative contact.

These numerical values can be interpreted as in agreement with the results obtained by Pfann who found that the pit left in the positive electrode after the explosion of a bridge of gold or of silver is much larger than the pit left in the negative electrode, and that there is no observable difference in the case of platinum or of palladium.

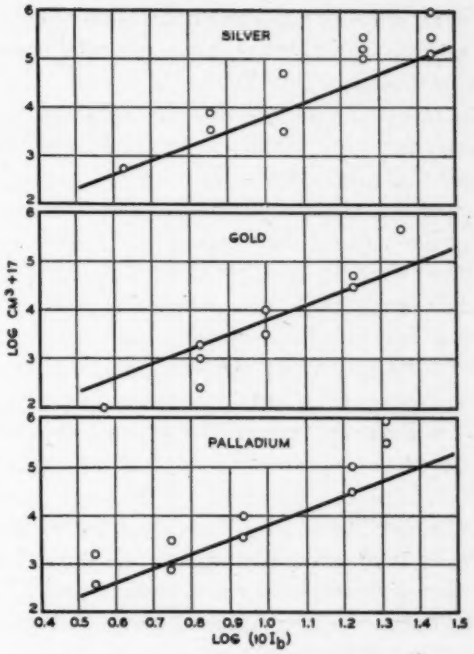

FIG. 8. Transfer measurements for gold, silver and palladium.

If the total circuit potential is lower than that corresponding to the boiling point of the metal electrodes, then boiling cannot occur and a molten bridge must be mechanically disrupted without the explosion which is its normal method of breaking. In considering the mechanism of bridge transfer it is important to know whether or not normal transfer of metal occurs if the boiling point is not reached. An experimental test of this question has proved that appreciable transfer does not occur without boiling. For gold, transfer of normal amount was found when the circuit potential was 2.0 volts and even when it was 1.0 volt, but only very slight transfer occurred in an 0.8-volt circuit. For platinum, transfer of about normal amount was found at 4.0, 3.0, and 2.0 volts, but no detectable transfer was

TABLE VI. Percentages of bridge volumes transferred.

	Bridge volume $l_b^3/I^3\times10^{14}$ cm^3/amp.^{3}	Percentage of bridge transferred
Ag	2.5	240.0
Au	11.1	55.0
Pt	780.0	0.8
Pd	1200.0	0.5

num and palladium mounds tend to be low and broad, and mounds of silver and gold tall and narrow. For platinum mounds of the same volume those formed at small currents (i.e., many operations) are taller and narrower than those formed at large currents (i.e., few operations). Finally, any platinum mound grows steadily taller relative to its breadth with increasing number of operations. At the present time we have no comprehensive understanding of these empirical observations.

[8] Holm has made a similar comparison of bridge volume and amount of transfer. He draws the following conclusion, without reference to any particular metal—"Considering the great uncertainty of the theoretical basis for the computation, we are inclined to conclude that in reality the whole bridge is transferred to the cathode"—See reference 3, p. 336.

obtained at 1.4 or 1.0 volts in 300,000 operations at a current which was 4 amperes with the contacts pressed together.¶

Equation (7) represents fantastically small volumes for very small currents. For example, at 0.6 milliampere the volume given by Eq. (7) is that of one atom of platinum, and presumably the bridge volume would be that of 200 atoms! It is clear that the relation cannot hold when the current is very small. Experimentally, it has been tested at a current as low as 0.13 amp., where it seems to be still valid although the precision of the measurement of transferred volume was low here. Oscilloscopic records of opening platinum contacts have the conventional appearance, with a well defined final break at 1.6 volts corresponding to the boiling point of the metal, for a current as low as 0.06 amp. but below this current the oscilloscopic trace becomes unstable and a well defined break voltage can often not be found. We believe that this means that a real bridge is not formed at a current below 0.06 amp. A current of 0.06 amp. corresponds by Eq. (7) to a transfer of 9×10^5 platinum atoms per operation, and the molten bridge presumably contains about 10^8 atoms. The oscilloscopic observations must be interpreted to mean that this is enough material to form a true bridge.‡

V. THERMAL EQUILIBRIUM

It was stated above that a steady condition of heat flow is maintained for most of the time during which a bridge of molten metal is being drawn out between two contacts before they finally separate. Reliance upon this statement simplified the studies of bridge formation and bridge transfer, but its justification was postponed. It will be shown below that thermal equilibrium is quite closely attained during the later history of each molten bridge, but that large departures from equilibrium occur before and immediately after the beginning of melting. The results presented up to this point depend upon later stages in the history of each bridge and do not require investigation of non-equilibrium conditions which exist earlier.

Equilibrium in a Molten Bridge

Experimental evidence that approximate thermal equilibrium obtains during the later stages of each molten bridge is afforded by the observation that the measured rate of transfer of metal is independent of the rate of separation of the contacts, and by agreement between theoretical and experimental values of bridge dimensions near the boiling point. These agreements can be supplemented by reasoning.

It is pertinent to estimate the total amount of heat energy evolved in a bridge from the beginning of melting to the time when the boiling point is reached and separation is completed, and to compare this with the heat required by the bridge itself, just to melt the metal and to raise its temperature. At the beginning of the life of a bridge the power evolved is IV_m watt and at the end of its life, which is $(2l_b/a)^{\frac{1}{2}}$ sec. later on the assumption that the electrode acceleration is uniform and that the final length is l_b, it is IV_b watt. At the beginning none of this heat is produced in the bridge itself, but at the end about 80 percent is produced here (Table II, column 9). The average power generated within the bridge will be close to IV_m and the total energy $IV_m(2l_b/a)^{\frac{1}{2}}$. Since l_b is proportional to I this energy varies with $I^{\frac{3}{2}}$; the proportionality factor, which is the energy for a current of 1 amp., is given on line 3 of Table VII for gold and for platinum, which are representative of the two types of contact metals considered in this paper. The total heat required to melt all of the final volume of the bridge, $l_b^3\sigma H_f$, plus that required to raise *half* of the final volume from 300°C to the boiling point, $l_b^3\sigma h(T_b-300)/2$, is written down on line 6. The quotient of the heat generated to that required is given on line 7. This ratio is proportional to $I^{-\frac{1}{2}}$ and is much larger for gold than for platinum. Yet even for platinum at the large current of one ampere the ratio is 1100. The largeness of this ratio means clearly that conditions of steady heat flow must obtain during at least most of the life time of a molten bridge.

¶ The various potentials used in these tests were supplied from a 2000 mf condenser across one leg of a potentiometer by means of which its voltage could be adjusted to any desired value. The time constant of the circuit was in all cases large enough to prevent significant voltage rise before each bridge was broken.

‡ It is wise to point out here that Eq. (7) according to which the volume of metal transferred to the negative electrode is proportional to the cube of the current, has been checked over only a relatively narrow range of currents. There are reasons for believing that its validity is not general.

The fact of thermal equilibrium can be established also by more direct reasoning. We assume generation of heat at the steady rate of w watts at a point source $r=0$ in an infinite solid. The differential equation of heat flow is, $\partial u/\partial t = K\partial^2 u/\partial r^2$, where r is the distance from the source, $K=k/\sigma h$ (Table I), and u is a new variable $u=rT$. With $T=0$ at $r=\infty$ this leads to the steady value temperature at r of $T'=w/4\pi kr$, and with the initial condition $T=0$ at $t=0$, the fraction of steady state temperature reached[9] at any time t is, $T/T'=1-erf\, r/2(Kt)^{\frac{1}{2}}$. Using values of k midway between room temperature and the melting point[10] and known values of σ and h, we obtain $T/T'=1-erf(0.42r/t^{\frac{1}{2}})$ for gold and $T/T'=1-erf(1.0r/t^{\frac{1}{2}})$ for platinum. From these equations have been calculated the times required to reach 0.9 of the final equilibrium temperature at a distance from the assumed point heat source equal to 5 times the maximum bridge radius $[r=5(l_b/2)]$, and these times are written down on line 8 of Table VII. These are *smaller* than the bridge lifetimes (line 2) by the factors given on line 9. In an actual contact the approach toward equilibrium is more rapid than is indicated by the result of this calculation because the generation of heat is distributed over a considerable volume, even outside of the bridge itself, rather than concentrated at a single point as assumed here.

TABLE VII. Energy relations in bridges at relay contacts.

	Gold	Platinum	
1. Average acceleration for telephone relays, a	20,000	same	cm/sec.^{2}
2. Bridge lifetime $(2l_b/a)^{\frac{1}{2}}$ (Table II, column 11)	69.0	141.0	$\times I^{\frac{1}{2}}\times 10^{-6}$ sec.
3. Total energy into bridge, $V_m I(2l_b/a)^{\frac{1}{2}}$	2.9	9.0	$\times I^{\frac{1}{2}}\times 10^{-5}$ joule
4. Heat of fusion of bridge, $l_b^3\sigma H_f$ (See Table I)	1.4	190.0	$\times I^2\times 10^{-10}$ joule
5. Heat to raise half of bridge to b.p., $l_b^3\sigma h(T_b-300)/2$	3.5	650.0	$\times I^2\times 10^{-10}$ joule
6. Heat required by bridge, (4)+(5)	4.9	840.0	$\times I^2\times 10^{-10}$ joule
7. Ratio (3)/(6)	60.0	1.1	$\times I^{-\frac{3}{2}}\times 10^5$
8. Time for $T/T'=0.9$ at $r=5(l_b/2)$	0.32	31.0	$\times I^2\times 10^{-6}$ sec.
9. Ratio (8)/(2)	0.005	0.2	$\times I^{\frac{1}{2}}$

Thermal Conditions at the Beginning of Melting

At the beginning of the motion of one electrode relative to another, which is pressed against it, the area of contact decreases rapidly, before melting, at a rate determined by the elastic properties of the metal and the velocity of relative motion. The spreading resistance increases correspondingly, with increase in the rate of evolution of heat and rise in the local temperature. When one works out the rate of temperature rise on the assumption of a condition of steady heat flow the value obtained is so high that the basic assumption of steady flow cannot possibly be correct. The calculation for the actual case is difficult and has not been attempted. From the calculation on the assumption of steady conditions we draw the conclusion that thermal equilibrium is not attained until after the beginning of melting, and this conclusion is of importance in work described in a later section.

To calculate the rate of temperature rise for the hypothetical condition of equilibrium we write $(dT_{max}/dt)=(dT_{max}/dl)(dl/dt)$. From Eq. (5) one obtains $dT_{max}/dl=-3T_{max}^2/3200\rho_0 I$ on the simplifying assumption that ρ_{max} is equal or proportional to $\rho_0(T_{max}/T_0)$ which is good enough for the present purpose. To obtain dl/dt one thinks of two contacting surfaces of radius of curvature c pressed together by the force P and being restored to the curvature c as they separate; dl/dt is equal then to $-4cv/l$, where v is the velocity of relative motion. The curvature c which is significant here is due to residual elastic deformation superposed upon plastic flow, and is related to the initial diameter l_P of the contact area by the formula for elastic deformation,[11] $l_P=(2.22)(Pc/E)^{\frac{1}{2}}$, where E is Young's modulus and l_P is determined by P and by the flow hardness of the metal H through the expression[12] $l_P=2(P/\pi H)^{\frac{1}{2}}$. Collecting these formulas together one obtains $dT/dt=5\times 10^{-4}T^2EP^{\frac{1}{2}}v/\rho_0 IH^{\frac{1}{2}}l$. For reasonable estimates of the magnitudes of quantities appearing in this expression, dT/dt is of the order $10^{12}v/I^2$ for gold or platinum at the melting point. If the contacts are opening at constant acceleration a, the velocity reached when the diameter of the area of contact has

[9] H. S. Carslaw, *The Conduction of Heat* (The Macmillan Company, New York, 1921), second edition, p. 151.

[10] Value of k for gold from I.C.T., and for platinum from R. Holm and R. Störmer, Wiss. Veröff. Siemens-Konzern 9, part 2, 312 (1930).

[11] See reference 3, p. 74.

[12] See reference 3, p. 75.

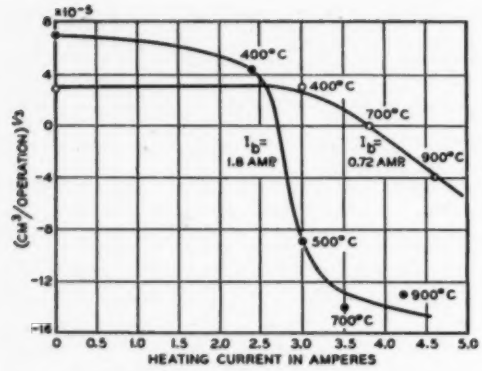

FIG. 9. Effect of heating the negative electrode upon the transfer of platinum at $I_b = 1.8$ amp. and at 0.72 amp.

decreased to l from its initial value l_P is $v = [a(l_P^2 - l^2)/2c]^{\frac{1}{2}}$, and as the melting point is approached l^2 can be neglected in comparison with l_P to give $v = l_P(a/2c)^{\frac{1}{2}}$. The numerical value of dT/dt is found to be simply enormous under any operating conditions.

VI. THERMAL ASYMMETRY

The fact of transfer of metal at the breaking of a molten bridge is most easily accounted for by assuming that more heat is dissipated upon the positive electrode than upon the negative, either within the bridge itself by thermoelectric heating, or by electron bombardment before or after the bridge breaks. Whether or not these ideas are correct, the effect of thermal asymmetry deserves investigation.

Experimental Asymmetry

(*a*) *Auxiliary Heating*

Auxiliary heating of one of the electrodes is the most straightforward method of producing thermal asymmetry. Such heating has been carried out using a modified form of the wire contact apparatus described above, in which the contacts are platinum and the heavy stationary contact is replaced by a lighter wire through which an auxiliary current can be passed. With this heated wire the negative member of the contact pair, the amount of platinum transferred per operation was found to be reduced or even reversed in sign. In Fig. 9 the abscissae represent the heating current in the negative wire, and the ordinates the volume of metal transferred per operation plotted as the cube root in order to make the figure more compact. Measurements were made at $I_b = 0.72$ and 1.8 amp., and optically estimated temperatures of the negative wire near the contact are indicated for each experimental point. One sees that no measurable transfer occurs at some heating current in the neighborhood of 3 amp. (variously estimated as a temperature of 400 to 700°C), and that for higher heating currents the direction of transfer is reversed with the mound appearing on the positive electrode rather than the negative.

One must not conclude from this experiment that thermal asymmetry is necessarily the cause of transfer. The observations do, however, confirm one's intuition that this can be an adequate cause.

(*b*) *Carbon-Silver Contact Pair*

Temperature asymmetry, additional to that occurring between contacts of the same metal, is produced automatically whenever two electrodes are of different substances which do not have the same thermal and electrical conductivities, for example silver and carbon. Since the thermal and electrical conductivities of carbon are much lower than those of silver, the maximum temperature must always occur in the carbon but melting must occur only in the silver. One expects, however, that silver will never be transferred to carbon because the surface of the latter is much too hot.

Experiments with silver against carbon bear out these predictions. In repetitive tests in a 4 volt circuit it has been found that there is no detectable transfer of silver, or of carbon, for either direction of the electric current. Some roughening of the silver surface is observable under the microscope, but if there is any transfer of metal at all it is smaller than would occur between two silver surfaces for the same current by a factor of at least 100. Some cracking of the carbon surface is observable which is attributable to thermal shock. The electrical and thermal conductivities of carbon can be increased by impregnation with silver, and contacts between silver and silver-impregnated carbon should show less thermal shock and may have interesting possibilities.

Carbon against carbon contacts in a 4-volt circuit give also no determinable transfer of ma-

terial on repeated operation, but here again the thermal shock appears to be severe as crevasses are produced in the surfaces.

(c) *Platinum-Gold Contact Pair*

Pfann has discovered (to be published elsewhere) that when a current of 5.3 amp. is interrupted in a 6-volt circuit there is no appreciable erosion if the positive contact is gold and the negative contact platinum. At the beginning of repetitive tests a little platinum is transferred to the *positive* electrode, but then the transfer stops and the current can be interrupted repeatedly without further effect. For a time which is apparently indefinitely long the contact surfaces remain unchanged, the platinum on the positive being in the form of a thin layer lying upon the massive gold electrode.

Further experiments have shown that, when current is broken in a low voltage circuit between a positive gold electrode and a negative platinum electrode at various currents and various velocities of separation, under some conditions the behavior is that just described, but under other conditions there is a continuous transfer of gold to the negative resulting in a mound of gold, as if both contacts were of gold. One can say that the contacts are "stable" against erosive transfer under some conditions, but "not stable" under others. Stability occurs at high currents and low velocities and transfer of gold to platinum, in the normal positive to negative direction, at low currents and high velocities. On a map on which the coordinates are velocity and current the area can be divided into a region of normal transfer and a region of "stability." On this plot, reproduced as Fig. 10, the points represented by circles give the results of experiments in which the electrodes were gold and platinum, the solid circles corresponding to experiments in which gold mounds were built upon the negative platinum electrode and the open circles to experiments in which the contacts became stable with only a trifling film of platinum showing on the positive. The few circles which are partly solid and partly open represent intermediate conditions in which there was some transfer of gold to the negative electrode and at the same time some platinum film on the positive.

One can explain the phenomena readily enough in qualitative fashion. Because the thermal and electrical conductivities of gold are much higher than those of platinum the temperature must be higher on the platinum side of each final contact area than on the gold side. Without quantitative information one cannot guess whether melting will occur first at the interface in gold, which has a lower melting point than platinum, or at the location of the maximum temperature which lies in the platinum. In the former case the resistivity of the molten gold will increase by a factor of about 2 over that of solid gold so that more gold will melt at once and a bridge composed of gold alone will be formed, with resulting transfer from the gold electrode to the platinum electrode. In the latter case the molten platinum resistivity will increase by a factor of 2 and a platinum bridge will be formed, with resulting transfer of platinum *from negative to positive;* but this transfer of platinum to gold can go on to only a very limited extent, because we soon have two platinum electrodes between which it is now well known that transfer is from positive to negative. There must, therefore, be a position of stability at which the normal transfer is exactly neutralized by cooling of the positive platinum surface by the gold upon which it lies.

Which of these two conditions, "stability" or normal transfer, will obtain is determined by the

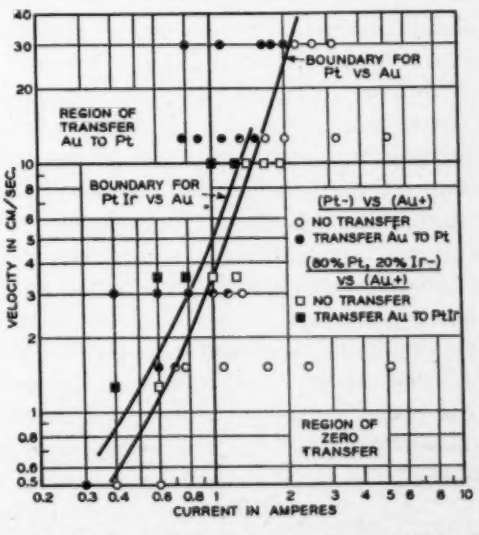
BOUNDARY FOR Pt VS Au
REGION OF TRANSFER Au TO Pt
BOUNDARY FOR Pt Ir VS Au
(Pt-) VS (Au+)
NO TRANSFER
TRANSFER Au TO Pt
(80% Pt, 20% Ir-) VS (Au+)
NO TRANSFER
TRANSFER Au TO Pt Ir
REGION OF ZERO TRANSFER
VELOCITY IN CM/SEC.
CURRENT IN AMPERES

FIG. 10. Regions of "transfer" and of "stability" of a negative platinum electrode against a positive gold electrode, and of a negative platinum-iridium electrode against a positive gold electrode.

current and the velocity. It has been proved above that a condition of steady heat flow does not exist before the beginning of melting, and therefore one sees intuitively that increasing the departure from equilibrium by increased velocity favors higher temperature at the most constricted area, the gold-platinum interface, relative to the maximum temperature, in the platinum; high velocity, therefore, favors melting of gold and low velocity melting of platinum, transfer and "stability" respectively. Large currents correspond to a large scale factor of the entire contact region, and therefore greater temperature difference between the interface and the maximum temperature isothermal, favoring stability. More precise thinking regarding these matters is clearly required.

Since platinum iridium alloy (20 percent iridium) has higher resistivity than platinum, one predicts that in the operation of this alloy against gold the minimum current for stability will be displaced toward lower currents. Tests of gold against platinum-iridium have been carried out with the alloy negative, and the results are indicated on Fig. 10 by the solid and open squares. One sees that the boundary between stability and transfer lies, for all velocities of separation, at lower currents than the same boundary for platinum against gold, as predicted, although the difference is not great. To obtain protection under all conditions one requires two metals of sufficiently different thermal and electrical conductivities which have melting points not too widely different.

It is to be expected that if a gold-platinum contact pair is operated with the *platinum positive*, rather than negative, there will as before be ranges of currents and of velocities for which stability will occur, and the dividing line between the region of stability and the region of transfer will be identical with the dividing line of Fig. 10; the two regions will simply be reversed. A few confirmatory tests of this have been carried out but the experiments have not been as extensive as those made with the platinum electrode negative.‡‡

‡‡ After contacts have been operated for a time in the region of stability with platinum positive, a discoloration of platinum is found upon the *negative* gold electrode but no gold upon the positive. This is a surprising result which the theory in its simplest form is unable to account for.

Thermal Asymmetry Theory

Some calculations have been made regarding thermal relations at a solid contact before melting starts. It is assumed that the contact area is a circle of diameter l between two semi-infinite conductors, and that we have a condition of steady heat flow. The calculation is possible because of the simplicity of this model. Since steady heat flow is, in fact, not established in general before melting occurs, the results, although informative, do not satisfy our requirements completely. Calculations for non-equilibrium conditions have not been attempted, nor have calculations regarding conditions in a molten bridge where the geometry is not simple.

In Appendix 1 is deduced the relation of Eq. (8) between the temperatures T_1 and T_2 at any two points in our model, the maximum temperature $T_{\max}$, and the geometrical parameters μ_1 and μ_2 which define the T_1 and T_2 isothermals;

$$\pm\sin(T/T_{\max})\Big|_{T_1}^{T_2} = (IA^{\frac{1}{2}}/\pi\bar{k}l)\tan^{-1}(2\mu^{\frac{1}{2}}/l)\Big|_{\mu_1}^{\mu_2}. \quad (8)$$

Here A is the constant of the Wiedemann-Franz-Lorentz Law, $\bar{k}$ is the mean thermal conductivity between T_0 and $T_{\max}$, and μ is equal to z^2 along a line normal to the circular contact area at a distance z from its center. It is not assumed that the entire contact is composed of one metal only, but if there are two or more metals their boundaries must be isothermal and equipotential surfaces. Furthermore, it is not assumed that the temperatures at great distances are the same on the two sides.

Three cases are of interest:

1. *A contact composed of one metal only with symmetrical temperatures on the two sides.*

Substituting $T_1 = T_0$ at $\mu_1 = \infty$ into Eq. (8) one obtains an expression for the temperature T_2 at any isothermal μ_2 in the contact area.

For $\mu_2 = 0$ the temperature T_2 is $T_{\max}$ and one obtains,

$$l/I = (A)^{\frac{1}{2}}/2\bar{k}\cos^{-1}(T_0/T_{\max}), \quad (9)$$

which can be considered a more sophisticated form of Eq. (5). It can be proved that Eqs. (5) and (9) give almost identical numerical values of l/I. For example, for $T_0 = 300$ and values of $\bar{k}$ ob-

tained from the literature[13] one gets from Eq. (9) values of l/I at the melting point of 15×10^{-6} cm/amp. for Ag, 20×10^{-6} for Cu, 16×10^{-6} for Au, 63×10^{-6} for Pt and 54×10^{-6} for Pd; these are in good agreement with calculations from Eq. (5) written down in column 10 of Table II, except for palladium for which there are sound reasons for believing that the published values of thermal conductivity are inaccurate.

2. *A contact between two different metals with temperatures the same at great distances on the two sides.*

In general, the temperature maximum will not be at the circle of contact. Equation (8) can be applied separately in three different regions, (a) in metal A which does not contain the temperature maximum, (b) in metal B between the circle of contact and the maximum temperature isothermal, and (c) in metal B beyond the maximum temperature isothermal. For these regions the boundary conditions are respectively,

(a) $T_1=T_0$ at $\mu=\infty$ and $T_2=T_i$ at $\mu=0$,
(b) $T_1=T_i$ at $\mu=0$ and $T_2=T_{\max}$ at $\mu=\mu^*$,
(c) $T_1=T_{\max}$ at $\mu=\mu^*$ and $T_2=T_0$ at $\mu=\infty$,

where T_i is the interface temperature and μ^* defines the location of the maximum temperature isothermal. These boundary conditions yield three simultaneous equations containing the five parameters T_0, $T_{\max}$, T_i, l/I, and μ^*/l.

From these equations one can determine, for the condition of steady heat flow to which they apply, whether melting occurs first in metal A at the interface or in metal B at the maximum temperature isothermal. By the simple qualitative theory of stability given above, these two situations correspond respectively to transfer and to "stability" for metal B negative to metal A, and conversely to "stability" and to transfer for metal B positive to metal A. The equations, which correspond to steady heat flow and therefore to sufficiently low velocity of separation, predict that whether or not stability occurs will be independent of current.

It is interesting to apply the equations to a gold-platinum contact. Using the numerical values $\bar{k}=3.56$ for gold, $\bar{k}=0.87$ for platinum and $A=2.4\times10^{-8}$, one obtains for $T_{\max}=2046°$K, the melting point of platinum, $T_i=1416°$K, $l/I=39\times10^{-6}$ cm/amp. and $\mu^*/l=0.33$. The value obtained for T_i is slightly above the melting point of gold and indicates therefore that stability will occur for platinum positive but not for platinum negative. The trend of the experimental boundary line in Fig. 10 is toward stability at all currents for sufficiently low velocity when the platinum is *negative*, and exactly disagrees therefore with the result of the calculation. The result calculated from Eq. (8) is, however, highly dependent upon the values of $\bar{k}$ which are used; very slight changes in the conductivities could lead to a prediction of stability for platinum negative rather than for platinum positive. It is probable that the mean conductivity values are not very accurate, and it is also possible that the use of constant average conductivities introduces appreciable error.

It is interesting to compare the calculated value $l/I=39\times10^{-6}$ cm/amp. in a gold-platinum contact at approximately the melting points of gold and of platinum with 16×10^{-6} and 63×10^{-6} calculated from the same equation respectively for a gold contact and for a platinum contact each at its melting point.

3. *A contact between electrodes of the same metal with one electrode heated.*

When one electrode is heated the maximum temperature isothermal is no longer at the contact. By an application of Eq. (8) one can work out μ^* the distance of this isothermal from the contact area and the volume of metal between it and the surface of the electrode in which it lies. A simple theory of the way in which heating the negative electrode can neutralize or reverse the normal direction of transfer would predict that the entire volume of metal between the maximum temperature isothermal and the surface is transferred to the positive electrode, and net transfer will be just zero when this volume is equal to normal transfer in the reverse direction, which is approximately $6\times10^{-14}I_b^3$ cm^3 (Eq. (7)).

When the suggested calculation is carried out by substituting the appropriate boundary conditions into Eq. (8) one obtains $\mu^*=$approx. $\pi\pm A^{\frac{1}{2}}T_m(T_0'-T_0)/4\bar{k}(\pi T_m-T_0'-T_0)^2$, where T_0 and T_0' are the temperatures at great distances

[13] Thermal conductivity data for Pt from Holm and Störmer, see footnote 10, for other metals from I.C.T.

on the two sides of the contact, and the significant volume = approximately $\pi^2 A^{\frac{1}{2}} I^3 T_m^3 (T_0' - T_0)/24\bar{k}^3(\pi T_m - T_0' - T_0)^4$. For platinum, the volume given by this expression for $T_0 = 300°\text{K}$ and $T_0' = 900°\text{K}$ is $1.6 \times 10^{-14} I^3$ which is of the order of magnitude required (Eq. (7)). The experimental observation that transfer of platinum is reversed by heating the negative electrode to a few hundred degrees can thus be accounted for by this simple theory.

The expression for the volume between the maximum temperature isothermal and the electrode surface is roughly proportional to $(T_0' - T_0)/\bar{k}^3 T_m$, where $\bar{k}^3 T_m$ is about 30 times larger for gold than for platinum. Since normal transfer is about the same for these two metals one concludes at once that for gold contacts it will be quite impossible to reverse the direction of transfer by heating the negative electrode, because this would require a temperature of about $2 \times 10^{4°}\text{C}$.

APPENDIX I

Steady State Temperature Distribution in the Neighborhood of a Solid Contact

We assume that electricity and heat are conducted to, and removed from, a metal across surfaces which are both isothermals and equipotentials. It can then be shown that throughout the metal all equipotential surfaces are also isothermals.[14] It is assumed now that the metal is made up of two conductors of infinite extent which meet at a plane but are in contact only at a circle of diameter l in this plane. Choosing rectangular coordinates with the z-axis normal to this circle and with the origin at its center, the quipotential surfaces in each conductor are semi-ellipsoids having the equation, $x^2/[(l/2)^2+\mu] + y^2/[(l/2)^2+\mu] + z^2/\mu = 1$, with each value of the parameter μ defining a semi-ellipsoid which corresponds to a particular potential and a particular temperature.[15] The resistance between two ellipsoids μ_1 and μ_2 is $R = \rho/4\pi C$ where C is the capacity[16] between two conductors having the form of these ellipsoids, given by

$$1/C = \int_{\mu_1}^{\mu_2} d\mu/[(l/2)^2+\mu]\mu^{\frac{1}{2}}.$$

The rate of change of potential with μ is,

$$d\varphi/d\mu = I dR/d\mu = I\rho/4\pi[(l/2)^2+\mu]\mu^{\frac{1}{2}}.$$

If we can determine the relation between potential φ and temperature T, this will suffice for finding T at all points.

The desired general relation between φ and T was derived in a notable paper by Kohlrausch,[2] who obtained $-2\int k\rho dT = \varphi^2 + c_1\varphi + c_2$. With the Wiedemann-Franz-Lorentz Law $k\rho = AT$, and the boundary condition $\varphi = 0$ at $T = T_0$, this becomes $\varphi^2 + c_1\varphi + A(T^2 - T_0^2) = 0$. For a maximum temperature $T_{\max}$ occurring at φ^* where $dT/d\varphi = 0$, we find $c_1 = -2\varphi^*$, and this equation is then,

$$\varphi^2 - 2\varphi^*\varphi + A(T^2 - T_0^2) = 0.$$

By differentiation with respect to μ and equating the two expressions for $d\varphi/d\mu$, one obtains a differential equation which could be integrated except for the presence of the resistivity ρ. Since thermal conductivity k is known to vary only slightly with temperature it is appropriate to use the Wiedemann-Franz-Lorentz Law to replace ρ by AT/k, and then to write for k its mean value between T_0 and $T_{\max}$, $\bar{k}$. When $\bar{k}$ is brought outside of the integral sign and the integration is carried out we get

$$\pm\sin^{-1}(T/T_{\max})\Big|_{T_1}^{T_2} = (IA^{\frac{1}{2}}/\pi\bar{k}l)\tan^{-1}(2\mu^{\frac{1}{2}}/l)\Big|_{\mu_1}^{\mu_2}.$$

This is the desired general relation giving the temperature T at each point in the contact region. The positive sign applies in the region $\varphi > \varphi^*$ and the negative sign in the region $\varphi < \varphi^*$.

[14] Disselhorst, Ann. d. Physik **4** Series 1, 316 (1900).

[15] See reference 3, p. 15.

[16] Kottler, *Handbuch der Physik* Vol. 12, p. 462.

Twinning in Tetragonal Alloys of Copper and Manganese*

FRANCIS T. WORRELL**
Institute for the Study of Metals, University of Chicago, Chicago, Illinois
(Received May 17, 1948)

Studies have been made of an alloy 88 percent Mn–12 percent Cu. This alloy when annealed at 925°C and quenched to room temperature has a tetragonal structure of axial ratio 0.97. It has been suggested that such a structure would show twinning along the 101 and 011 planes. Verification of this suggestion is presented.

ALLOYS of copper and manganese possess a number of unusual properties which make them of some interest. One of these properties, an unusually high internal friction, has been the subject of some research at this laboratory recently. In the process of these investigations the herein reported structural details were unearthed.

Copper exists in a face-centered cubic form with lattice parameter, $a_0 = 3.608$A. Manganese is known to exist in four allotropic modifications: α, a body-centered cubic structure with 58 atoms per unit cell;[1] β, a simple cubic structure with 20 atoms per unit cell;[2] γ, a face-centered tetragonal structure;[1b] and δ, whose structure is unknown. These forms are listed in Table I, along with the lattice parameters. Also listed are the transition temperatures as found by Dean and his co-workers[3] at the United States Bureau of Mines.

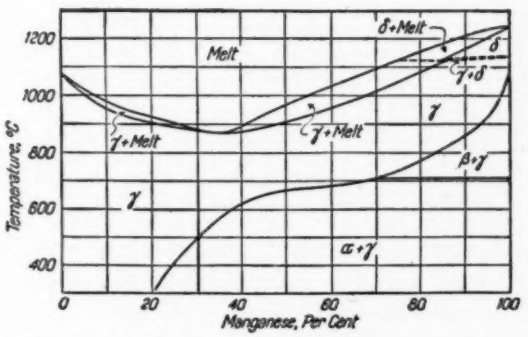

FIG. 1. Equilibrium diagram for the system copper-manganese (after Dean).

The equilibrium diagram has been investigated by various workers, notably Persson,[4] Grube *et al.*,[5] and Dean *et al.*[3] The results of these investigations have been quite different, partly because of the great sluggishness of the phase transformations. The equilibrium diagram found by Dean and his co-workers is presented in Fig. 1 as being probably the best available at the present time.

The recent work on the system copper-manganese indicates that copper and γ-manganese form a continuous series of solid solutions. As manganese is added to the face-centered copper the alloy remains cubic, but the lattice expands to a maximum value of about 3.76A at about 60 percent manganese, then apparently contracts slightly to a minimum at 82 percent manganese. At this composition the lattice becomes, in an apparently continuous fashion, tetragonal. Beyond this point it changes gradually to the lattice of γ-manganese. The lattice parameter *versus* composition is plotted in Fig. 2.

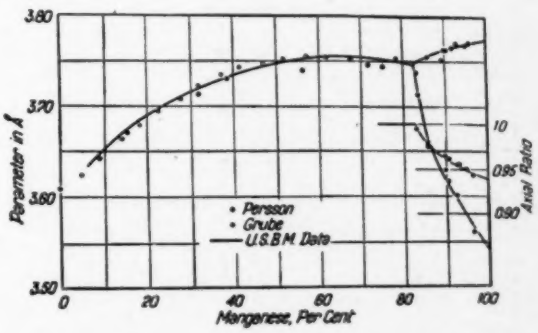

FIG. 2. Lattice parameter as a function of composition of the γ-phase (after Dean).

* This research was supported by the Office of Naval Research, USN (Contract N-6ori-20-IV).
** Now at the Department of Physics, Rensselaer Polytechnic Institute, Troy, New York.
[1] (a) G. D. Preston, Phil. Mag. **5**, 1198 (1928); (b) cf. also Westgren and Phragmen, Zeits. f. Physik **33**, 777 (1925).
[2] G. D. Preston, Phil. Mag. **5**, 1207 (1928).
[3] R. S. Dean, J. R. Long, T. R. Graham, E. V. Potter, and E. T. Hayes, Trans. A.S.M. **34**, 443 (1945).
[4] E. Persson, Zeits. f. physik. Chemie **B9**, 25 (1932).
[5] G. Grube, E. Ostreiche, and O. Winkler, Zeits. f. Electrochemie **10**, 770 (1939).

TABLE I. Allotropic forms of manganese.

Phase	Symmetry	a_0 (A)	c/a	Transition temperature (°C)
α	b.c. cubic	8.894		705±5
β	s. cubic	6.29		1092±3
γ	f.c.t.	3.774	0.937	1133±2
δ	?	?	? m.p. 1246	

It should be noted that these determinations of the structure of the γ-alloys were not made at the elevated temperatures at which these alloys exist, but were made on samples which had been quenched to room temperature from these temperatures. The structure of γ-manganese has not been determined by this method, since it has not been found possible to retain pure γ-manganese by quenching. However, alloys of about 97 percent manganese will retain the γ-structure on quenching, so the curves in Fig. 2 are extrapolated from the last point to 100 percent manganese. The parameters thereby found agree with those for freshly made electrolytic manganese, historically called γ-manganese; the high temperature form is therefore assumed to be γ-manganese.

The particular alloy on which the work herein reported was done had a composition 88 percent manganese and 12 percent copper. When this alloy is annealed at 925°C for several hours and quenched in water to room temperature it has a high internal friction at temperatures around room temperature. In connection with an investigation of the origin of this internal friction, Zener[6] has pointed out that this alloy, being tetragonal, could readily twin along the 101 and 011 planes. The arrangement of the atoms in such a twin structure is shown in Fig. 3, which represents a section of the crystal in the 010 plane.

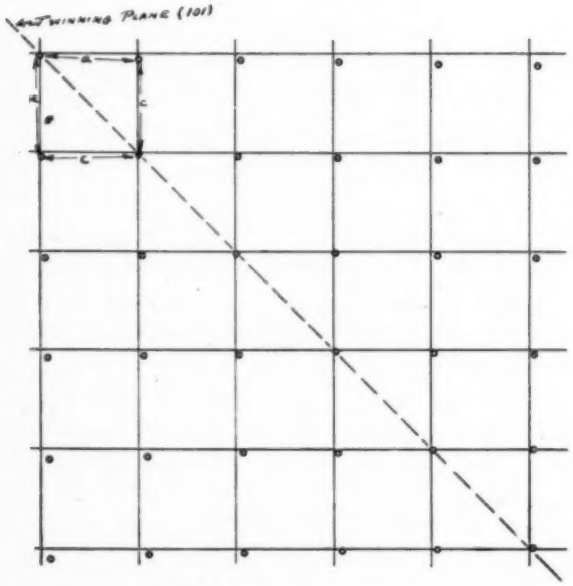

FIG. 3. Section in the 010 plane across the 101 twinning plane of a slightly tetragonal crystal. The gridwork is a cubic axis system; the circles are the atoms of the tetragonal lattice.

Previous work has not shown this postulated twin structure to exist. The reason may possibly be found in the technique for etching the samples for metallographic examination. It can be seen from examination of Fig. 3 that the two halves of the twin are at an angle of almost 90° to one another, say, $90°-\delta$, where δ is a small angle. If one regards this structure to be approximately cubic, then this orientation of $90°-\delta$ is equivalent to a relative orientation of δ. Since δ is small, the slightly different orientations of the regions on either side of the twin boundary may not show up if too vigorous an etchant is used. The conventional etching technique for these alloys apparently suffers from this difficulty. Fortunately, the twins were found by us on a sample of composition 88 percent manganese, 12 percent copper, which had been mechanically polished by the usual method, then etched with 5 percent citric acid. In Fig. 4 is a 250× picture of what was found on this one sample. This picture was taken in a Bausch and Lomb metallograph, using the "sensitive tint." The fine banded structure which is visible here was later shown to be the twin structure that was sought.

Subsequent attempts to get better patterns by similar etching techniques resulted in a failure even to duplicate what had already been done. Apparently, our etchant was too vigorous. However, when electrolytic techniques were used the results were considerably better. The samples were polished electrolytically after having had an initial mechanical polishing down to 4/0 paper, since it was feared that the effects of mechanical polishing might go down to a greater depth than our etchant would reach. The elec-

[6] C. Zener, *Elasticity and Anelasticity of Metals* (University of Chicago Press, Chicago, 1948).

trolyte consisted of one part each of 85 percent H_3PO_4 and glycerine, and two parts of methyl alcohol. A current density of around 0.5 amp./cm^2 was used for 15 minutes. After polishing the sample was removed from the cell as quickly as possible and washed in alcohol. Apparently some etching took place along with the polishing, or perhaps between the time when the current was shut off and the sample was washed, because when the sample was examined under the microscope, it was seen to have a polished surface covered by a stain which delineated the various crystal grains and the twins in different colors.

A picture of a typical area from a sample of the 88 percent manganese alloy is shown in Fig. 5. This picture was taken at a magnification of 250× under polarized light. Note that in the grain occupying roughly the left and center of the picture there appear to be two types of twins: a large twin extending across the grain, and numerous small twins oriented in several directions and superposed on the large twin pattern. The large twin structure resembles that seen in alpha-brass, and is shown later to be twinned along the same plane as those in brass. It would appear that the small twins are along a different plane than the large ones.

The orientation of these twins has been determined by examination of the photomicrographs of the surface, and by x-ray methods. Analysis of the photomicrographs was done using a stereographic net. For each analysis a grain was selected which had a large twin and three sets of the fine twins. The boundary of the large twin was assumed to be the trace of a {111}*** plane, and the boundaries of the fine twins to be traces of {110} planes. Thus, one had to satisfy four boundary conditions to verify the assumption.

The directions of each of these traces were measured. Diametral lines were laid out on a piece of tracing paper superposed on a meridional

FIG. 4. Photomicrograph of 88 percent Mn–12 percent Cu. Quenched from 900°C; mechanically polished; 5 percent citric acid etch, 250×.

stereographic net, each line being normal to the direction of one of the traces in the photograph. Each of these lines is the locus of the poles of all possible planes which could have given rise to the corresponding trace. Then a standard projection with the [001] (or sometimes the [110] direction) normal to the plane of the paper was superposed on the first plot and on the net. The three plots were rotated relative to one another about the axis normal to the plane of the papers till, by a process of trial, a relative orientation could be found such that rotation of the standard projection about the vertical axis of the net would simultaneously bring a ⟨111⟩ pole into coincidence with the line representing the family of supposed {111} planes, and three ⟨110⟩ poles into coincidence with the three lines representing families of supposed {110} planes. As a further check in the case of a crystal having a set of {110} twins across a {111} boundary from those {110} traces already plotted, a line was drawn on the graph representing these planes. This line was then reflected across the

*** Since the structure under discussion is tetragonal, not cubic, it is, of course, not correct to consider (110) exactly equivalent to (101), e.g., {110}, implying that the 110 and the 101 planes, for example, are equivalent. However, the structure is so nearly cubic ($c/a=0.97$), that this seems justifiable. The following graphical analysis was made using a standard projection for a cubic crystal, since it was found to differ so slightly from the tetragonal case, and introduced only small errors.

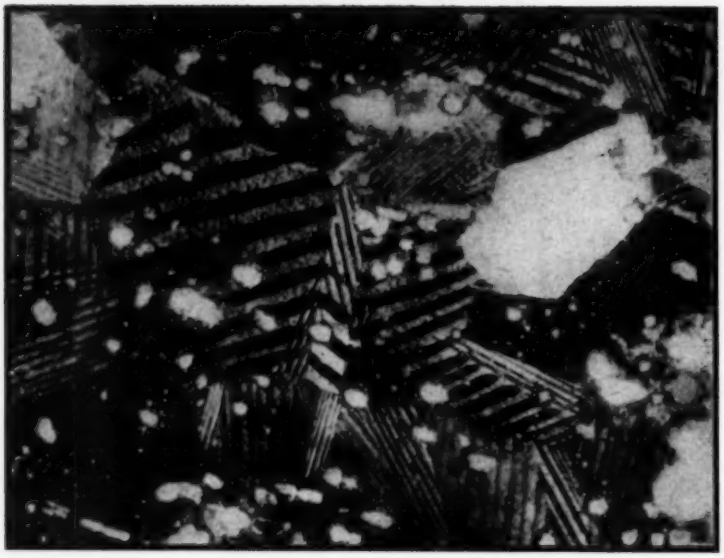

FIG. 5. Photomicrograph of electropolished and etched sample of 88 percent Mn–12 percent Cu. Quenched from 925°C; 250×; polarized light.

line representing the {111} plane, and was found to contain one of the ⟨110⟩ poles.

This procedure was followed in analyzing ten different areas selected from both a transverse and a longitudinal section of a $\frac{1}{4}$-in. bar of the same alloy, to eliminate possible false results from a preferred orientation in the specimen. A solution was possible in all cases. In Fig. 6 is shown a typical solution.

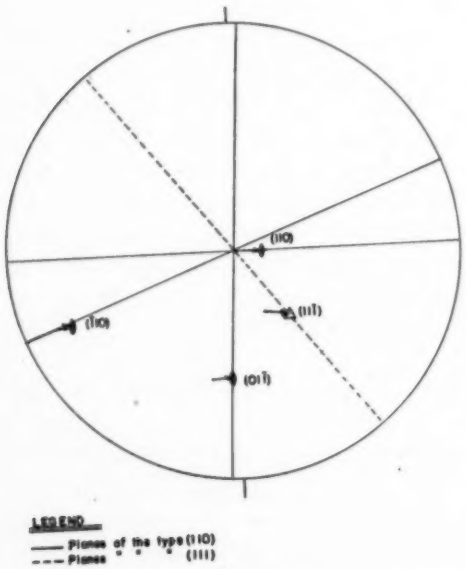

FIG. 6. Typical solution of twin boundary orientation problem. Arrows show the 14° rotation about the vertical axis of the stereographic net required to bring the poles into coincidence with the lines, as shown.

The possibility that the twinning planes of the small twins could be {111} or {211} was explored on three of the plots, but no solution was found for either possibility.

A further test of the existence of these twins can be made by x-ray methods.† As has been shown earlier, a given plane, say the (100) plane, will be at an angle of $90°-\delta$ with the same plane on the other side of a twinning plane of the type {110}. Or, the (110) plane will be at an angle of δ with another plane of the same type, say the (001) plane, across the boundary. If one takes a rotation or oscillation picture of a polycrystalline sample, one will get a picture with a series of spots arranged along the lines that would appear in a powder photograph of the same material. Since the structure is not cubic, but slightly tetragonal ($c/a=0.97$) in this case, certain of the lines, e.g., (110), will be doubled. If the sample were completely untwinned (i.e., no {110} twins), the spots would be randomly arranged, but with the type of twinning which exists here one will find certain spots in pairs adjacent to one another in the two lines of the doublet. These spots correspond to reflections from two planes of the same type at an angle δ with one another.

One of the specimens used in the previous

† The author is indebted to Dr. C. S. Barrett, of this laboratory, for suggesting this method and taking the pictures.

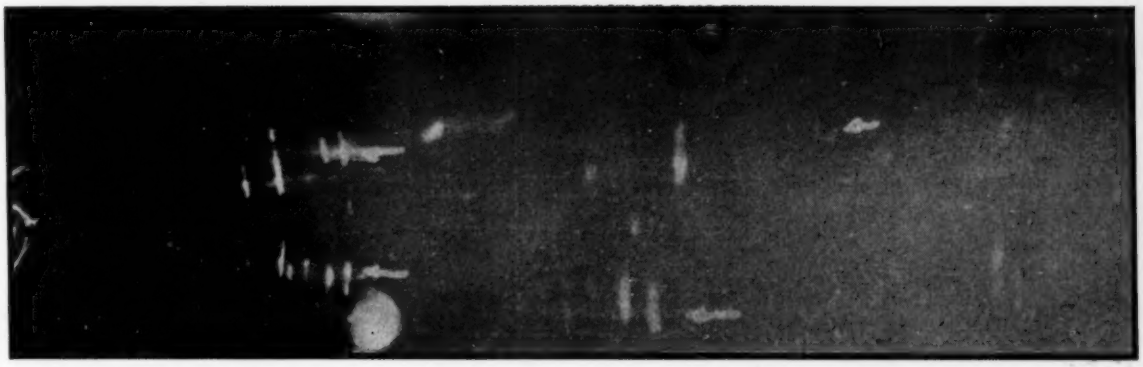

FIG. 7. X-ray oscillation photogram of Cu-Mn alloy. Arrows indicate pairs of spots.

studies was mounted in a cylindrical Debye camera of 71.6-mm diameter, as shown in Fig. 7. The specimen was a piece from a $\frac{1}{4}$-in. cylindrical bar. The beam was incident on the edge of the piece. A picture could not be taken of a single grain because of the small grain size. So an area was chosen which had the smallest possible number of grains, so that the doubled spots could be certainly located. The sample was oscillated through about 30° during the exposure. Copper Kα-radiation was used.

A typical photogram is shown in Fig. 7. The lines along which the spots were expected to fall were indexed by comparison with a powder photogram of the same material. Arrows indicate the doubled spots that were being sought. Several pictures of different parts of the specimen yielded similar results. In all, 5 experiments of this kind yielded 23 pairs of spots, a number far in excess of the normal expectancy from chance coincidence. This evidence leaves no doubt that the plane of twinning is of the type {110}, as postulated.

ACKNOWLEDGMENT

The author wishes to acknowledge the help of Dr. Clarence Zener who suggested the structure which is herein reported, and who was always helpful during the course of the work; also the interest and encouragement of Dr. Cyril S. Smith, Director of the Institute. The x-ray photograms were taken and interpreted by Dr. C. S. Barrett. The sample shown in Fig. 4 was prepared and photographed by Miss Thelma Barkin. Other members of the Institute have helped in ways too numerous to mention.

Figures 1 and 2 are reproduced by permission of the American Society for Metals.

Cavity Drag in Two and Three Dimensions*

MILTON S. PLESSET** AND PHILIP A. SHAFFER, JR.
U. S. Naval Ordnance Test Station, Pasadena, California

(Received May 17, 1948)

The free streamline theory has been applied to the computation of the cavity drag of symmetrical wedges of arbitrary angle. The drag coefficients and cavity widths and lengths are tabulated for a range of both cavitation parameter and internal angle. The pressure distributions computed for two-dimensional wedges have been taken to be approximately correct for cones of revolution of the corresponding internal angles. Under this assumption, drag coefficients for right circular cones of arbitrary internal angle have been computed and are tabulated for a range of both cavitation parameter and internal angle.

INTRODUCTION

IN an earlier paper,[1] the authors showed that Riabouchinsky's[2] theory of the drag of a flat plate in two-dimensional cavitating flow may be extended to symmetrical wedges of arbitrary angle. The evaluation of drag coefficients, pressure distributions, and cavity shapes from the extended theory must be carried out numerically; the results of these computations are presented here. It was also proposed to evaluate the drag of cones of revolution on the assumption that the pressure distribution along a generator of the cone is the same as that along the two-dimensional wedge of the same internal angle. A few drag coefficients computed on this basis were found to be in good agreement with experimental values given by Reichardt.[3] A complete tabulation of calculated values of drag coefficients for a series of cones of revolution will be given here.

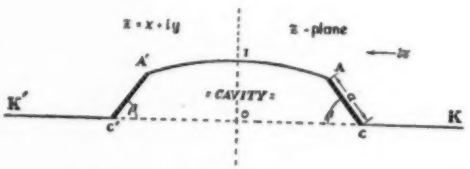

FIG. 1.

THE DRAG COEFFICIENT FOR TWO-DIMENSIONAL WEDGES

The general character of the flow of a liquid past a body with the formation of a vapor or gas cavity is determined by the value of the cavitation parameter, σ, which is defined by

$$\sigma=(p_0-p_1)/(\rho v_0^2/2), \tag{1}$$

where p_0 and v_0 are the static pressure and velocity in the undisturbed liquid stream, and p_1 is the static gas pressure in the cavity. The classical solutions[4] of the free stream lines enclosing a cavity correspond to $\sigma=0$; the corresponding cavity wake is infinite in extent. A solution for $\sigma>0$ was first given for a two-dimensional flat plate by Riabouchinsky. His method for obtaining a finite cavity consisted in placing an "image" plate downstream from the true plate. This same procedure is used here for the symmetric wedge with half-angle β; the geometry is shown in Fig. 1, which represents the $z=x+iy$ plane. Only the upper half of the flow is considered. If $W=U+iV$ is the complex potential (cf. Fig. 2) so that

$$u=-\partial U/\partial x=-\partial V/\partial y,$$
$$v=-\partial U/\partial y=\partial V/\partial x, \tag{2}$$

where u, v are the x, y components of the fluid velocity, and U and V are the velocity potential

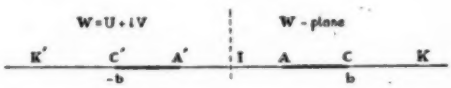

FIG. 2.

* This study was supported by the Office of Naval Research.

** Present address: California Institute of Technology, Pasadena, California.

[1] M. S. Plesset and P. A. Shaffer, Jr., Rev. Mod. Phys. **20**, 228–231 (1948).

[2] D. Riabouchinsky, Proc. Lond. Math. Soc. (Ser. 2) **19**, 206–215 (1920).

[3] H. Reichardt, *Reports and Translations No. 766*, Ministry of Aircraft Production, August 15, 1946; distributed by Office of Naval Research, Navy Department, Washington, D. C.

[4] H. Lamb, *Hydrodynamics* (Dover Publications, New York, 1945), sixth edition, Ch. IV, pp. 73–78; and U. Cisotti, *Idromeccanica Piana*, Part 2 (Tamburini, Milan, 1921–22).

TABLE I. The cavitation parameter. $\sigma(\alpha,\beta)$.

α	β 15°	30°	45°	60°	75°	90°	105°	120°	135°	150°	165°
0°	0.0000	0.0000	0.0000	0.0000	0.0000	0.0000	0.0000	0.0000	0.0000	0.0000	0.0000
5	0.0296	0.0600	0.0913	0.1236	0.1568	0.1910	0.2262	0.2624	0.2997	0.3381	0.3777
10	0.0602	0.1241	0.1918	0.2635	0.3396	0.4203	0.5058	0.5965	0.6926	0.7945	0.9026
15	0.0923	0.1931	0.3032	0.4235	0.5549	0.6984	0.8551	1.0264	1.21 4	1.4177	1.6408
20	0.1261	0.2682	0.4281	0.6083	0.8112	1.0396	1.2969	1.5866	1.9129	2.2803	2.6940
25	0.1622	0.3506	0.5697	0.8242	1.1201	1.4639	1.8635	2.3279	2.8676	3.4948	4.2237
30	0.2009	0.4423	0.7321	1.0801	1.4981	2.0000	2.6028	3.3267	5.1962		
35	0.2431	0.5453	0.9210	1.3880	1.9685	2.6902	3.5873				
40	0.2896	0.6630	1.1445	1.7655	2.5663	3.5989					
45	0.3415	0.7996	1.4142	2.2387	3.3447						

TABLE II. Drag coefficients for two-dimensional wedges. $C_D(\alpha,\beta)$.

α	β 15°	30°	45°	60°	75°	90°	105°	120°	135°	150°	165°
0°	0.2838	0.4885	0.6370	0.7448	0.8230	0.8798	0.9207	0.9498	0.9703	0.9845	0.9939
5	0.2927	0.5185	0.6959	0.8375	0.9528	1.0482	1.1293	1.1993	1.2613	1.3176	1.3694
10	0.3029	0.5521	0.7624	0.9443	1.1057	1.2522	1.3885	1.5180	1.6436	1.7674	1.8914
15	0.3146	0.5901	0.8385	1.0688	1.2880	1.5016	1.7142	1.9297	2.1514	2.3825	2.6259
20	0.3281	0.6330	0.9258	1.2148	1.5073	1.8097	2.1279	2.4676	2.8346	3.2346	3.6741
25	0.3436	0.6826	1.0278	1.3889	1.7754	2.1966	2.6621	3.1825	3.7695	4.4364	5.1975
30	0.3618	0.7401	1.1481	1.5993	2.1080	2.6898	3.3634	4.1497	5.0738		
35	0.3829	0.8076	1.2922	1.8574	2.5274	3.3308	4.3031				
40	0.4080	0.8880	1.4676	2.1803	3.0676	4.1830					
45	0.4378	0.9853	1.6852	2.5927	3.7806						

and the stream function, respectively, one has

$$dW/dz=\zeta=-u+iv. \tag{3}$$

The mathematical problem consists in finding the conformal transformation which takes the ζ-plane into the W-plane. The required transformation is given by the following sequence:

$$\eta=\zeta^{\pi/2\beta}; \tag{4}$$

$$t=i/2(1/\eta-\eta); \tag{5}$$
$$t=W\tan\alpha/(b^2-W^2)^{\frac{1}{2}};$$

$$W=bt/(\tan^2\alpha+t^2)^{\frac{1}{2}}. \tag{6}$$

The parameter b fixes the cavity length CC'. The parameter α is defined as follows:

$$v_0{}^{\pi/2\beta}=(1-\sin\alpha)/\cos\alpha. \tag{7}$$

Further, with the fluid velocity normalized to unity along the free streamline AIA', one has from Eq. (1)

$$1+\sigma=1/v_0{}^2, \tag{8}$$

so that

$$1+\sigma=\{(1+\sin\alpha)/\cos\alpha\}^{4\beta/\pi}. \tag{9}$$

The drag coefficient is readily expressed in the form

$$C_D=(1/v_0{}^2)\frac{\int_{AC}(1-|\zeta|^2)dy}{\int_{AC}dy}. \tag{10}$$

For the purpose of evaluating these integrals it is desirable to replace dy by

$$dy=(dy/dz)(dz/dW)(dW/dt)dt. \tag{11}$$

Along AC, these derivatives have the values

$$\begin{aligned} dy/dz&=-e^{i\beta}\sin\beta,\\ dz/dW&=1/\zeta=(1/|\zeta|)e^{-i\beta},\\ dW/dt&=b\tan^2\alpha/(\tan^2\alpha+t^2)^{\frac{1}{2}}. \end{aligned} \tag{12}$$

When these values are substituted in (8), the result is

$$dy=-(\sin\beta/|\zeta|)b\tan^2\alpha/(\tan^2\alpha+t^2)^{\frac{1}{2}}dt. \tag{13}$$

The evaluation of the integrals is further simplified if the substitution $t=\sec\phi$ is made; in particular, in those cases in which the integrals can be evaluated by analytical methods this substitution leads to known elliptic integrals. The substitution is valid only along the path AC; under this restriction, one obtains the following

relations:

$$\eta = i(1-\sin\phi)/\cos\phi;$$
$$|\zeta| = [(1-\sin\phi)/\cos\phi]^{2\beta/\pi}. \quad (14)$$

In order to make the expressions for the drag coefficient and related quantities more compact, the following abbreviations will be used:

$$P(\phi,\beta) = 1-[(1-\sin\phi)/\cos\phi]^{4\beta/\pi}, \quad (15)$$

$$\Delta(\phi,\alpha) = (1-\sin^2\alpha\,\sin^2\phi)^{-\frac{1}{2}}, \quad (16)$$

$$\Delta'(\phi,\alpha) = (1-\cos^2\alpha\,\cos^2\phi)^{-\frac{1}{2}}, \quad (17)$$

$$Q(\phi,\beta) = \cos\phi\,\sin\phi[(1+\sin\phi)/\cos\phi]^{2\beta/\pi}, \quad (18)$$

$$dY(\phi,\alpha,\beta) = Q(\phi,\beta)\Delta(\phi,\alpha)d\phi, \quad (19)$$

$$Y(\phi',\alpha,\beta) = \int_{\phi'}^{\pi/2} dY(\phi,\alpha,\beta). \quad (20)$$

Here the limits are understood to be the limiting values of ϕ. In terms of these functions the cavity drag coefficient for a two-dimensional wedge may be written

$$C_D(\alpha,\beta) = (\sigma+1)\frac{\int_0^{\pi/2} P(\phi,\beta)dY(\phi,\alpha,\beta)}{Y(0,\alpha,\beta)}, \quad (21)$$

where $1/v_0^2$ has been replaced by the equivalent quantity $\sigma+1$. Numerical values of σ are given for a range of values of both α and β in Table I. The results of numerical integration of (21) leading to the drag coefficient for two-dimensional wedges are presented in Table II for wedge angles from 15° through 165° at 15° intervals.

CAVITY SHAPE IN TWO-DIMENSIONAL FLOW

The free stream line AIA' will be determined only so far as is necessary to fix the length and width of the cavity. Along this stream line, $V=0$ and $dU/ds=-1$, where s is the length of arc along the stream line measured from an arbitrary origin. Thus $U=-s$, if $s=0$ where $U=0$ (the point I). Since

$$W(AIA') = U(AIA') = bt/(\tan^2\alpha+t^2)^{\frac{1}{2}},$$

one has

$$s = -bt/(\tan^2\alpha+t^2)^{\frac{1}{2}}.$$

If $\theta=\arg\zeta$, then

$$t = \sin(\pi\theta/2\beta) = \sin\psi,$$

for points on AIA'. Finally, the x and y co-

TABLE III. $\bar{x}/a$.

α	β 15°	30°	45°	60°	75°	90°	105°	120°	135°	150°	165°
0°	∞	∞	∞	∞	∞	∞	∞	∞	∞	∞	∞
5	195.195	162.091	132.584	106.541	83.794	64.154	47.440	33.428	21.908	12.653	5.432
10	53.645	44.439	36.226	28.983	22.674	17.254	12.668	8.856	5.754	3.292	1.399
15	23.812	19.656	15.947	12.682	9.850	7.432	5.404	3.736	2.398	1.353	0.567
20	13.041	10.719	8.648	6.830	5.261	3.933	2.829	1.933	1.225	0.682	0.282
25	8.056	6.587	5.279	4.136	3.156	2.333	1.658	1.117	0.697	0.382	0.155
30	5.356	4.353	3.463	2.689	2.030	1.483	1.039	0.690	0.423		
35	3.732	3.012	2.376	1.826	1.363	0.983	0.679				
40	2.680	2.145	1.676	1.274	0.939	0.667					
45	1.960	1.554	1.201	0.902	0.656						

The half-length of the cavity measured from the vertex of the wedge of slant height a is $\bar{x}+a\cos\beta$.

TABLE IV. $\bar{y}/a$.

α	β 15°	30°	45°	60°	75°	90°	105°	120°	135°	150°	165°
0°	∞	∞	∞	∞	∞	∞	∞	∞	∞	∞	∞
5	2.730	4.551	5.551	5.937	5.824	5.336	4.589	3.682	2.704	1.728	0.813
10	1.414	2.349	2.860	3.048	2.976	2.712	2.318	1.847	1.346	0.853	0.398
15	0.858	1.420	1.724	1.828	1.774	1.606	1.361	1.075	0.775	0.486	0.224
20	0.588	0.968	1.171	1.235	1.191	1.071	0.901	0.705	0.504	0.320	0.143
25	0.428	0.702	0.845	0.886	0.849	0.757	0.631	0.490	0.346	0.212	0.096
30	0.323	0.527	0.630	0.656	0.624	0.552	0.456	0.350	0.244		
35	0.248	0.403	0.478	0.494	0.466	0.408	0.333				
40	0.193	0.311	0.366	0.375	0.350	0.303					
45	0.151	0.240	0.280	0.284	0.262						

The half-width of the cavity measured from the vertex of the wedge of slant height a is $\bar{y}+a\sin\beta$.

TABLE V. Drag coefficients for cones of revolution. $C_D(\alpha,\beta)$.

α	β 15°	30°	45°	60°	75°	90°	105°	120°	135°	150°	165°
0°	0.2045	0.3758	0.5181	0.6350	0.7296	0.8053	0.8646	0.9101	0.9442	0.9693	0.9874
5	0.2108	0.3990	0.5664	0.7143	0.8450	0.9599	1.0609	1.1495	1.2276	1.2972	1.3604
10	0.2184	0.4255	0.6213	0.8064	0.9817	1.1477	1.3054	1.4559	1.6004	1.7407	1.8792
15	0.2275	0.4557	0.6849	0.9147	1.1459	1.3787	1.6140	1.8527	2.0966	2.3478	2.6097
20	0.2379	0.4906	0.7586	1.0429	1.3445	1.6653	2.0072	2.3725	2.7649	3.1891	3.6525
25	0.2501	0.5311	0.8456	1.1969	1.5892	2.0274	2.5171	3.0655	3.6817	4.3779	5.1686
30	0.2648	0.5788	0.9494	1.3847	1.8950	2.4918	3.1898	4.0061	4.9635		
35	0.2818	0.6355	1.0749	1.6173	2.2835	3.0988	4.0950				
40	0.3022	0.7039	1.2296	1.9110	2.7882	3.9109					
45	0.3270	0.7875	1.4236	2.2899	3.4593						

ordinates of I measured from A are

$$\bar{y}=\int_0^\beta \sin\theta|ds|\,;\quad \bar{x}=\int_0^\beta \cos\theta|ds|\,.$$

If the distance along the wedge face CA is a, then

$$\bar{x}/a=-\frac{\int_0^{\pi/2}\cos(2\beta\psi/\pi)\cos\psi\,\Delta'(\psi,\alpha)d\psi}{Y(0,\alpha,\beta)}, \quad (22)$$

$$\bar{y}/a=\frac{\int_0^{\pi/2}\sin(2\beta\psi/\pi)\cos\psi\,\Delta'(\psi,\alpha)d\psi}{Y(0,\alpha,\beta)}. \quad (23)$$

These quantities are tabulated in Tables III and IV.

DRAG COEFFICIENTS FOR CONES OF REVOLUTION

If one assumes that the pressure distribution along the surface of a right circular cone is the same as that along the side of the two-dimensional wedge of the same internal angle, drag coefficients for cavity flow are readily obtained. The wedge pressure distribution is integrated over the surface of the cone and the result is divided by the dynamic pressure $\rho v_0^2/2$ times the base area of the cone. In terms of the abbreviations (15) through (20), the expression for the cavity drag of a cone of half-angle β may be written:

$$C_D(\alpha,\beta)=2(\sigma+1)\times\frac{\int_{\phi=0}^{\phi=\pi/2}P(\phi,\beta)\,Y(\phi,\alpha,\beta)d\,Y(\phi,\alpha,\beta)}{\{Y(0,\alpha,\beta)\}^2}. \quad (24)$$

Drag coefficients have been evaluated for cones by numerical integration; Table V presents the results of these calculations for cone half-angles, β, from 15° through 165° at 15° intervals. The parameter α is related to the value of the cavitation parameter σ as numerically defined in Table I.

In support of the assumption of the two-dimensional pressure distribution for use in the three-dimensional case, one may cite the necessary agreement of the assumed pressure function with the actual pressure function at the stagnation point at the apex of the cone and at the separation point. It is evident that the error in this approximation arises from differences at intermediate points between the detailed shape of the assumed pressure distribution and the actual distribution.

The calculated pressure distributions for two-dimensional wedges are shown for $\sigma=0$ in Fig. 3. The ordinate corresponds to the net pressure at a given point on the body divided by the stagnation pressure, and the abscissa is the y coordinate divided by the maximum value of y for given β.

CAVITY DRAG OF A CIRCULAR DISK

For arbitrary values of β, the integrations of (18), (22), (23), and (24), cannot be performed in terms of tabulated functions. For $\beta=\pi/2$, however, the expressions simplify and are readily integrated to yield results in closed form. Riabouchinsky has given both the drag coefficient and the maximum dimensions of the cavity for flow about a two-dimensional lamina; his results are summarized as follows:

$$C_D(\alpha)=(\sigma+1)(\mathbf{E}-\cos^2\alpha\mathbf{K})/(\sin^2\alpha+\mathbf{E}-\cos^2\alpha\mathbf{K}), \quad (25)$$

$$\bar{x}/a=(\mathbf{E}'-\sin^2\alpha\mathbf{K}')/(\sin^2\alpha+\mathbf{E}-\cos^2\alpha\mathbf{K}), \quad (26)$$

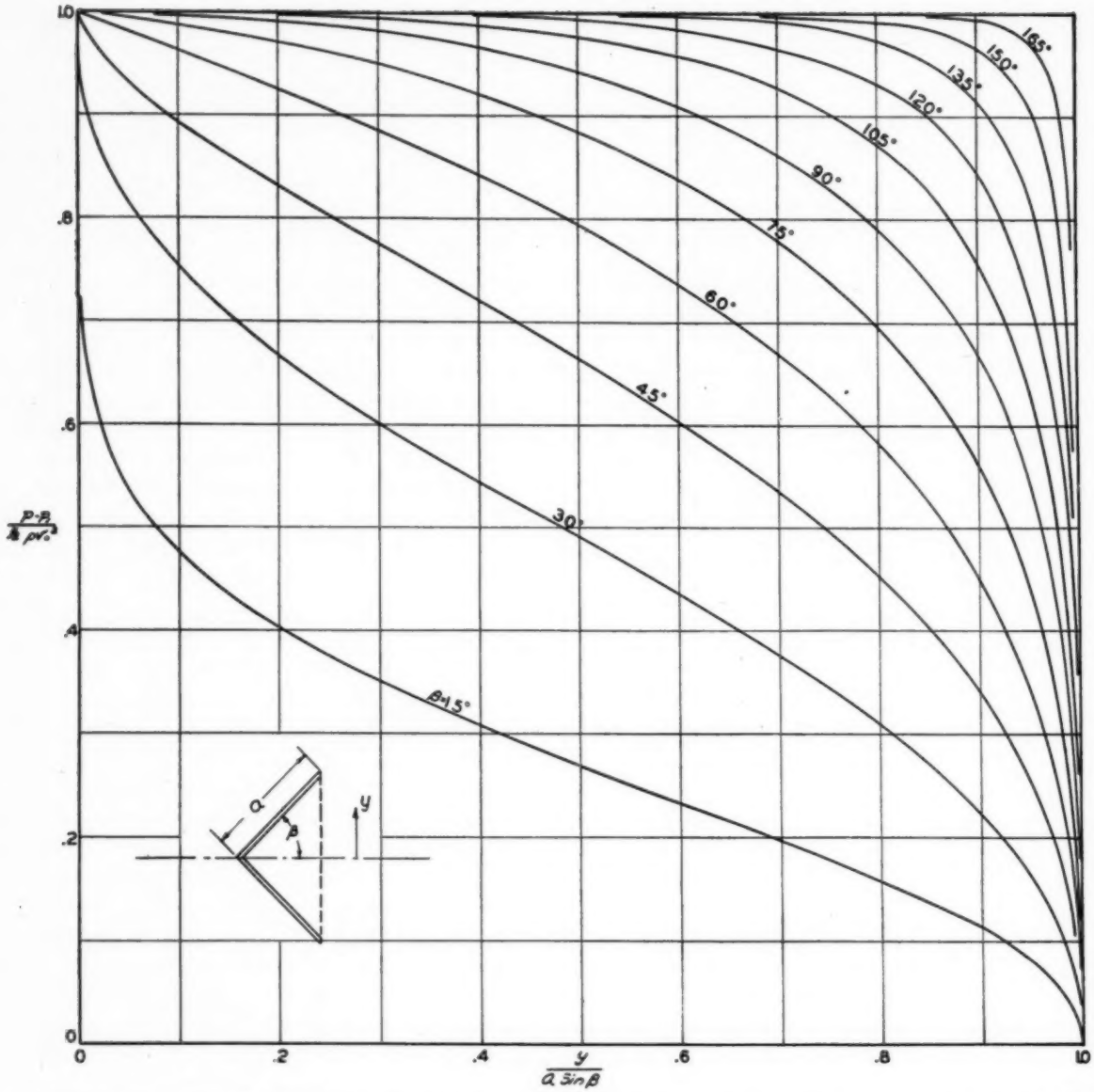

FIG. 3. The pressure coefficient $(p-p_1)/(\rho v_0^2/2)$ is plotted as ordinate against the normalized ordinate $y/a\sin\beta$ of position on the face of the wedge. The value of the pressure on the face of the wedge is p, the constant pressure in the cavity is p_1, v_0 is the liquid velocity at infinity, and ρ is the liquid density. The slant height of the wedge is a, the internal half-angle of the wedge is β, and the vertical position of a point on the wedge face is given by y. These pressure curves correspond to the case of zero cavitation parameter.

and

$$\bar{y}/a=\sin\alpha(1-\sin\alpha)/(\sin^2\alpha+\mathbf{E}-\cos^2\alpha\mathbf{K}), \quad (27)$$

where $\mathbf{E}$, $\mathbf{K}$, and the corresponding primed quantities are complete elliptic integrals.[5]

[5] The notation for the complete elliptic integrals $\mathbf{E}$, $\mathbf{K}$, $\mathbf{E}'$, $\mathbf{K}'$, and $\mathbf{B}$, and for the incomplete elliptic integrals $F(\alpha,\phi)$ and $D(\alpha,\phi)$ is that defined by E. Jahnke and F. Emde in *Tables of Functions* (Dover Publications, New York, 1945).

In the evaluation of the approximate drag coefficient for the circular disk, two additional steps must be taken. The first of these, the determination of the general form of Y, leads to[5]

$$Y(\phi,\alpha)=\sec^2\alpha\{\cos\phi(1+\sin\phi)/(1-\sin^2\alpha\sin^2\phi)^{\frac{1}{2}} +\mathbf{B}(\alpha)-F(\alpha,\phi)+D(\alpha,\phi)\}. \quad (28)$$

Secondly, the integration of the assumed pressure distribution, (15), over the surface of the

cone can be carried out using this function Y. The resulting drag coefficient is

$$C_D(\alpha)=\frac{2(\sigma+1)\left\{\dfrac{1}{\sin^2\alpha}-\dfrac{ln(1+\sigma)}{(2\sin\alpha\tan^2\alpha)}+\mathbf{B}^2(\alpha)\right\}}{\{1+\mathbf{B}(\alpha)\}^2}. \tag{29}$$

NUMERICAL PROCEDURES

The function $Q(\phi,\beta)$ which occurs in the integrals involved in the expression of the drag coefficients becomes infinite at $\phi=\pi/2$ when $\beta>\pi/2$. Further, for $\beta<\pi/2$, while $Q(\phi,\beta)$ vanishes at $\phi=\pi/2$, the function cannot be approximated conveniently for numerical integration. It is necessary, therefore, to restrict the numerical integration to a region removed from $\phi=\pi/2$ and to continue the integration up to $\phi=\pi/2$ by analytical integration of appropriate approximations in this region.

The numerical integration was carried out using an interval of 7.5° from $\phi=0°$ to $\phi=82.5°$, and an interval of 1.5° from 82.5° to 88.5°. The integration coefficients were computed using the tables of Lowan and Salzer.[6] The remaining portions of the several integrals were evaluated in a manner exemplified as follows: the integrals are of the form

$$\int_{59\pi/120}^{\pi/2}\cos\phi\sin\phi\left(\frac{1+\sin\phi}{\cos\phi}\right)^{2\beta/\pi}F(\phi)d\phi, \tag{30}$$

where $F(\phi)$ denotes the factor of $Q(\phi,\beta)$ in a typical integral, and Q has been written explicitly. If the substitution $x=\pi/2-\phi$ is made, and if $\sin x$ and $\cos x$ are approximated by the first terms only of their respective power series, the integral (30) becomes

$$2^{2\beta/\pi}\int_0^{\pi/120}F(\pi/2-x)x^{(1-2\beta/\pi)}dx, \tag{31}$$

with an error of approximately 0.1 percent. To facilitate the computation, $F(\pi/2-x)$ is approximated by a Newton interpolational polynomial of three terms, and the integration (31) is carried out. The process yields an expression for the integral in terms of the values of $F(\pi/2-x)$ at $x=0$, $\pi/120$, $\pi/60$; the coefficients are functions of the angle β.

The numerical computation of the integrals was carried out by means of punched card equipment manufactured by the International Business Machines Corporation. The values of Q, Δ, P and the several integration coefficients, all of which were first computed and compiled in tabular form, were punched into cards; IBM machines were then employed to form the necessary products and to sum the products in the required manner. The results of intermediate stages of the calculation were summary-punched into new cards which were used in subsequent computational operations. The use of these machines permits the computation of many discrete problems simultaneously; in the present case the 110 computations corresponding to all combinations of 10 values of α with 11 values of β for a single integration, four of which are required, can be performed in one operation. This procedure not only lessens the computing time by a very large factor, but also greatly diminishes the probability of error in the many computational steps involved.

Many of the available numerical tabulations have been omitted here for the sake of brevity; the omitted details will be found elsewhere.[7]

ACKNOWLEDGMENT

The authors wish to express their appreciation to Miss Reba Beeler and to Miss Ina Squire for their assistance in the numerical computations, and to Mr. W. C. Chaplin of the Southern California Cooperative Wind Tunnel for his work in the IBM computations.

[6] A. N. Lowan and H. E. Salzer, J. Math. and Phys. **24**, 1–21 (1945).

[7] Naval Ordnance Report No. 1014.

Energy Losses of Sound Waves in Metals Due to Scattering and Diffusion

W. P. Mason and H. J. McSkimin
Bell Telephone Laboratories, Murray Hill, New Jersey
(Received June 7, 1948)

When high frequency longitudinal and transverse sound waves are sent through a multicrystalline rod of metal, attenuation losses result because of scattering and diffusion of sound waves by the grains. When the grain size is less than one-third of the wave-length, these losses are due to Rayleigh fourth power law scattering and are proportional to the grain volume. The scattering factor depends on the anisotropy of the elastic constants. Two different factors are obtained, one for shear waves and one for longitudinal waves. These factors have been evaluated for cubic and hexagonal metals. From the measured elastic constants the only metals with a low loss are aluminum, magnesium, and tungsten. The calculations indicate that the losses for aluminum and magnesium are about equal for longitudinal waves, but for shear waves magnesium has a very low shear loss. It has been found experimentally that magnesium has nearly as low a loss as fused quartz.

Experiments with higher frequencies show that when the wave-length is one-third of the grain size or less, the transmission process becomes a diffusion process similar to the propagation of a heat wave. The grain sizes determine the mean free path, and the loss becomes inversely proportional to the grain diameter. An approximate formula for diffusion losses has been obtained which agrees closely with the experimental values.

I. INTRODUCTION

WHEN high frequency longitudinal and transverse sound waves are sent through a multicrystalline rod of metal, attenuation losses result, caused by reflection and scattering of the waves by the individual grains of the metal. In a former paper[1] measurements were made in the frequency region from 2 to 15 megacycles, which indicated that a scattering loss was the principal source of attenuation and that this loss was proportional to the grain volume and the fourth power of the frequency in agreement with Rayleigh's calculation for the scattering of sound by an obstacle. Further calculations of scattering factors for cubic and hexagonal metals have been made which show that the scattering is determined by the anisotropy of the elastic constants. Two different factors are obtained, one for shear waves and one for longitudinal. The calculations indicate that the only metals having low scattering losses are aluminum, magnesium, and tungsten. The calculations indicate that the losses for aluminum and magnesium are about equal for longitudinal waves, but for shear waves magnesium has a very low shear loss.

Experiments in the scattering range check these calculations and show that the loss in magnesium for shear waves is about $\frac{1}{10}$ that of aluminum. As the frequency is increased it was found that the loss changed from a condition determined by scattering to a condition determined by diffusion for which the loss is inversely proportional to the grain diameter and independent of the frequency. Scattering formulae are valid when the grain size is less than a third of a wave-length, while diffusion formulae appear valid when the wave-length is about $\frac{1}{3}$ of the grain size. Between these limits no adequate theory exists for determining the loss. The measurements presented here agree well with those made by Roth,[2] which are in the frequency range of diffusion.

II. EXPERIMENTAL METHODS

The experimental method used in the former paper[1] was to attach shear and longitudinal crystals to the squared ends of a rod of the material to be measured and to transmit longitudinal or shear waves through the wax joints. Reflection amplitudes from the ends of the rod determine the attenuation, and the spacing of the reflections on the oscillograph determine the velocity of transmission. By taking several length rods the loss caused by the wax joints can be evaluated.

Another method for measuring longitudinal waves in metals that has recently been employed by Roth[2] is to immerse the metal rod on one end

[1] W. P. Mason and H. J. McSkimin, "Attenuation and scattering of high frequency sound waves in metals and glasses," J. Acous. Soc. Am. 19, 464 (1947).

[2] W. Roth, *Quarterly Progress Report* (Research Laboratory of Electronics, M.I.T., October 15, 1947).

in a water bath. The crystal generates a wave in the water which in turn generates a longitudinal wave in the rod. A series of reflections is picked up by the receiving crystal due to metal-water interface reflections and due to reflections in the metal rod. By changing the length of the water path, the reflections from the metal-water face and the reflections in the metal are easily separated, and the series resulting from reflections within the metal can be determined. This series has to be corrected for the loss caused by the energy transmitted into the water, but this loss can be evaluated by calculation or by putting water on the free end of the rod. For aluminum this loss was 1.5 db per reflection. With this correction the attenuation in the metal can be evaluated. Losses by this method have been compared with those obtained by the wax joint method, and they come out quite accurately the same. The water bath method is probably superior for very high frequencies but is limited to longitudinal waves.

For very high frequencies it is difficult to transmit shear waves through a wax joint. To get around this difficulty use is made of the recently discovered fact[3] that very viscous liquids have a shear elasticity. Since by heating the liquid and pressing the crystal on the metal surface a very thin layer of liquid can be obtained, the losses through such a joint are considerably less than through a wax joint. The liquid principally used for this purpose is a 5600 molecular weight polyisobutylene (trade name Vistac II). Previous measurements[4] from 20 to 100 kilocycles indicated that this liquid had a shear elasticity of about 3×10^7 dynes per square centimeter at room temperature. Some further measurements were made in the range from 10 to 30 megacycles, by a method that will be described in a forthcoming paper.[5] which show that the shear stiffness has increased to 3×10^9 dynes/cm^2 in this frequency region. Using a thin layer of polyisobutylene the junction loss is very small up to 30 megacycles.

[3] W. P. Mason, "Measurement of the viscosity and shear elasticity of liquids by means of a torsionally vibrating crystal," Trans. A.S.M.E. **69**, 359 (1947).

[4] Mason, Baker, McSkimin, and Heiss, "Mechanical properties of long chain molecule liquids at ultrasonic frequencies," Phys. Rev. **77**, 1074 (1948).

[5] Mason, Baker, McSkimin, and Heiss, "Measurement of shear elasticity and viscosity of liquids by means of ultrasonic waves," to be presented at the VII International Congress of Applied Mechanics, September 7, 1948, London.

III. EXPERIMENTAL RESULTS

In the previous paper two aluminum rods having grain sizes of 0.23 mm and 0.13 mm, and with the spread in grain size from 0.5 to 1.7 times these figures, were measured for longitudinal and shear waves and for frequencies for which the grain size was $\frac{1}{3}$ or less the wavelength; the attenuation can be represented by the equation

$$A=B_1f+B_2f^4, \tag{3}$$

where A is the attenuation in nepers per centimeter and B_1 and B_2 are constants. This indicates that the attenuation contains a hysteresis term proportional to the frequency and a fourth power scattering term. An evaluation of the constant B_2 for longitudinal and shear waves is given in the next section. For the rods of 0.23 mm and 0.13 mm the B_2 terms for longitudinal waves were

$$\begin{aligned} &\text{Longitudinal}\\ &B_2=3.74\times10^{-30}\ \text{neper/cm/cycle}^4,\\ &\quad 0.23\text{-mm grain}\\ &0.695\times10^{-30}\ \text{neper/cm/cycle}^4\\ &\quad 0.13\text{-mm grain} \end{aligned} \tag{4}$$

For shear waves

$$\begin{aligned} &B_2=50.2\times10^{-30}\ \text{neper/cm/cycle}^4,\\ &\quad 0.23\text{-mm grain}\\ &9.4\times10^{-30}\ \text{neper/cm/cycle}^4\\ &\quad 0.13\text{-mm grain} \end{aligned} \tag{5}$$

By the use of the water bath method the losses of these rods have been extended up to 30 megacycles, with the results shown in Fig. 1. As the

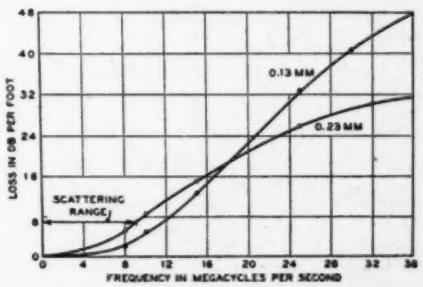

FIG. 1. Measured attenuation for longitudinal waves for two aluminum rods having grain sizes of 0.13 mm and 0.23 mm plotted as a function of frequency. Diffusion range about 80 megacycles.

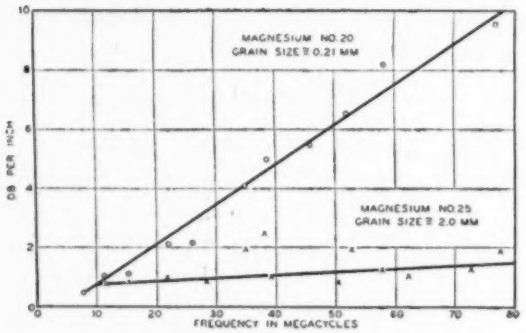

FIG. 2. Measured attenuation for longitudinal waves for two magnesium rods having grain sizes of 0.21 mm and 2 mm plotted as a function of frequency (after Roth).

frequency increases, the losses of the large grain size material become less than that for the small grain size material, and at high frequencies the relative loss is nearly inversely proportional to the grain size. This type of loss is also obtained for magnesium, as shown by Fig. 2 taken from data by Roth.[2] This figure shows the loss in db per inch as a function of frequency for two different grain size materials, 0.21 mm and 2.0 mm. The losses are about 10 times as large for the small grain size materials as for the large and show that diffusion conditions are determining the losses in the high frequency range. The loss for the 0.21-mm grain material of 5.75 db per foot at 8 megacycles indicates that the scattering loss for magnesium for longitudinal waves is about the same as for aluminum for the 0.23-mm grain size material.

Figure 3 shows the measured loss for shear and longitudinal waves for a magnesium rod plotted as a function of frequency. The grain size for this rod has been determined as 0.12-mm diameter.

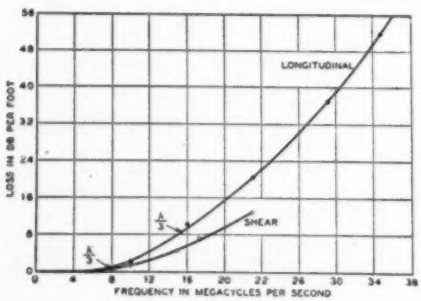

FIG. 3. Measured attenuation for longitudinal and shear waves of a magnesium rod having a grain size of 0.12 mm plotted as a function of frequency. (Dow Metal FS-1).

The loss[6] is exceptionally low and up to 10 megacycles is less than 1.5 db per foot. This is the lowest high frequency loss measured for any metal. The reason for this very low loss is the very nearly isotropic modulus for shear as discussed in the next section.

The velocities of propagation for longitudinal and shear waves for these two metals were independent of frequency and had the values

Metal	Velocity for longitudinal waves	Velocity for shear waves
Aluminum	6.32×10^5 cm/sec.	3.13×10^5 cm/sec.
Magnesium	5.77×10^5 cm/sec.	3.05×10^5 cm/sec.

IV. CALCULATION OF SCATTERING LOSSES FOR LONGITUDINAL AND SHEAR WAVES

As shown in the previous paper,[1] the cause of the scattering loss in metals is the fact that the grain direction is distributed at all angles with respect to the direction of the acoustic wave, and since the elastic constant varies with orientation, a reflection or scattering occurs at intersections between grain boundaries. The longitudinal elastic constants for a cubic crystal for any orientation are given by the equations

$$c_{11}' = c_{11}(l_1^4+m_1^4+n_1^4) + (2c_{12}+4c_{44})(l_1^2m_1^2+l_1^2n_1^2+m_1^2n_1^2), \quad (6)$$

$$c_{44}' = c_{11}(l_1^2l_2^2+m_1^2m_2^2+n_1^2n_2^2) + 2c_{12}[l_1l_2m_1m_2+n_1n_2(l_1l_2+m_1m_2)] + c_{44}[(l_1l_2+m_1m_2)^2+(l_1l_2+n_1n_2)^2 + (m_1m_2+n_1n_2)^2], \quad (7)$$

where l_1 to n_3 are the direction cosines between the new set of axes and the crystallographic axes x, y, and z according to the relations

	x	y	z
x'	l_1	m_1	n_1
y'	l_2	m_2	n_2
z'	l_3	m_3	n_3.

For aluminum

$$c_{11}=10.76\times10^{11}\ \text{dynes/cm}^2,\quad c_{12}=6.18\times10^{11},\quad c_{44}=2.84\times10^{11}. \quad (8)$$

From these equations it can be shown that c_{11} (which should correspond to $(\lambda+2\mu)$ the bulk

[6] The low loss for magnesium for shear waves seems to have been first determined by D. L. Arenburg (Radiation Laboratory, M.I.T.) in his study of solid materials for delay lines.

TABLE I. Elastic constants of cubic metals (s constants in cm²/dyne, c constants in dynes/cm²).

Metal	s_{11}	s_{12}	s_{44}	c_{11}	c_{12}	c_{44}	$\langle c_{11}' \rangle_{Av}$	$\langle c_{44}' \rangle_{Av}$
				Face-centered cubic				
Al	1.59×10^{-12}	-0.58×10^{-12}	3.52×10^{-12}	10.76×10^{11}	6.18×10^{11}	2.84×10^{11}	11.20×10^{11}	2.75×10^{11}
Au	2.33	−1.07	2.38	19.6	16.45	4.20	21.7	3.76
Ag	2.32	−0.993	2.29	11.9	8.94	4.37	14.21	3.89
Cu	1.49	−0.625	1.33	17.02	12.3	7.51	21.14	6.65
Pb	9.30	−4.26	6.94	4.85	4.09	1.44	5.67	1.27
				Body-centered cubic				
Fe	0.757	−0.282	0.862	23.7	14.1	11.6	29.15	10.47
Na	48.3	−20.9	16.85	0.615	0.469	0.592	1.03	0.506
K	83.3	−37.0	38.0	0.416	0.333	0.263	0.593	0.226
W	0.257	−0.073	0.660	50.2	19.9	15.15	50.2	15.15

wave modulus for an isotropic body) can vary from 10.76×10^{11} dynes/cm² to 11.49×10^{11}, while the shear constant can vary from 2.84×10^{11} dynes/cm² to 2.27×10^{11}.

The average value of c_{11}' can be determined from the equation

$$c_{11}'=c_{11}+[2(c_{12}-c_{11})+4c_{44}]\times[l_1^2m_1^2+l_1^2n_1^2+m_1^2n_1^2]. \quad (9)$$

If we let the radius vector be in a plane through z making an angle φ from the x axis, the vector making an angle θ from z, it is readily shown that the direction cosines are

$$l_1=\sin\theta\cos\varphi, \quad m_1=\sin\theta\sin\varphi, \quad n_1=\cos\theta.$$

Hence if all orientations are equally probable, the average space value of c_{11}' will be

$$\langle c_{11}' \rangle_{Av}=c_{11}+[2(c_{12}-c_{11})+4c_{44}]\frac{\int_0^{2\pi}d\varphi\int_0^{\pi}[\sin^4\theta\sin^2\varphi\cos^2\varphi+\sin^2\theta\cos^2\theta]\sin\theta d\theta}{4\pi}$$

$$=c_{11}+\frac{[2(c_{12}-c_{11})+4c_{44}]}{5}. \quad (10)$$

Since $l_1l_2+m_1m_2+n_1n_2=0$, the shear modulus of Eq. (7) can be put into the form

$$c_{44}'=2(c_{12}-c_{11})[l_1l_2m_1m_2+l_1l_2n_1n_2+m_1m_2n_1n_2]+c_{44}[(m_1n_2+n_1m_2)^2+(n_1l_2+l_1n_2)^2+(l_1m_2+m_1l_2)^2]. \quad (11)$$

The shear modulus can be averaged in all directions by taking the direction cosines

$$\begin{aligned} l_1&=\cos\theta\cos\varphi, & m_1&=\cos\theta\sin\varphi, & n_1&=-\sin\theta,\\ l_2&=-\sin\varphi, & m_2&=\cos\varphi, & n_2&=0,\\ l_3&=\cos\varphi\sin\theta, & m_3&=\sin\varphi\sin\theta, & n_3&=\cos\theta, \end{aligned} \quad (12)$$

where θ measures the angles of the normal z' with respect to z and φ is the angle of the zz' plane with respect to x. Inserting these values in (11), the average value of c_{44}' is

$$\langle c_{44}' \rangle_{Av}=c_{44}+\frac{[2(c_{11}-c_{12})-4c_{44}]}{4\pi}\int_0^{2\pi}d\varphi\times\int_0^{\pi}\cos^2\theta\sin^2\varphi\cos^2\varphi\sin\theta d\theta \quad (13)$$

$$=c_{44}+\frac{[c_{11}-c_{12}]-2c_{44}}{12}.$$

Table I gives the elastic constants of a number of cubic metals and their average $\langle c_{11}' \rangle_{Av}$ and $\langle c_{44}' \rangle_{Av}$ constants.

It is obvious from this table that the only cubic metals that approximate isotropic materials are aluminum and tungsten.

The other metal of interest for high frequency ultrasonic work is magnesium, which is a hex-

TABLE II. Elastic constants of hexagonal metals (s constants in cm²/dyne, c constants in dynes/cm²).

Metal	s_{11}	s_{12}	s_{13}	s_{33}	s_{44}	c_{11}	c_{12}	c_{13}
Mg	2.21×10^{-12}	-0.77×10^{-12}	-0.49×10^{-12}	1.97×10^{-12}	6.03×10^{-12}	5.86×10^{11}	2.49×10^{11}	2.08×10^{11}
Zn	0.84	+0.11	−0.78	2.87	2.64	16.35	2.64	5.19
Cd	1.23	−0.15	−0.93	3.55	5.40	12.12	4.81	3.84

	c_{33}	c_{44}	$\langle c_{11}'\rangle_{Av}$	$\langle c_{44}'\rangle_{Av}$
Mg	6.6×10^{11}	1.65×10^{11}	5.88×10^{11}	1.66×10^{11}
Zn	5.31	3.78	13.17	4.80
Cd	4.45	1.85	8.51	2.45

agonal crystal. For a hexagonal crystal there are five elastic constants. For a hexagonal crystal, the c_{11}' and c_{44}' elastic constants for any orientation take the form

$$\begin{aligned} c_{11}' &= c_{11}(l_1^2+m_1^2)^2+c_{33}m_1^4 \\ &\quad +(2c_{13}+4c_{44})n_1^2(l_1^2+m_1^2), \\ c_{44}' &= c_{11}\left[(l_1l_2+m_1m_2)^2\right. \\ &\quad \left.+\left(\frac{l_1m_2-m_1l_2}{2}\right)^2\right]-\frac{c_{12}}{2}[l_1m_2-m_1l_2]^2 \\ &\quad +2c_{13}n_1n_2(l_1l_2+m_1m_2)+c_{33}n_1^2n_2^2 \\ &\quad +c_{44}[(m_1n_2+n_1m_2)^2+(n_1l_2+l_1n_2)^2]. \end{aligned} \tag{14}$$

Inserting the direction cosines of Eqs. (10) and (13) and averaging over the sphere, we find

$$\begin{aligned} \langle c_{11}'\rangle_{Av} &= \frac{8}{15}c_{11}+\frac{3}{15}c_{33}+\frac{2}{15}(2c_{13}+4c_{44}), \\ \langle c_{44}'\rangle_{Av} &= \frac{1}{3}\left(\frac{c_{11}-c_{12}}{2}\right)+\tfrac{2}{3}c_{44}. \end{aligned} \tag{15}$$

Table II shows the elastic constants and average values of $\langle c_{11}'\rangle_{Av}$ and $\langle c_{44}'\rangle_{Av}$ for three hexagonal metals. From this table it is obvious that magnesium is the most isotropic hexagonal metal and that it is more nearly isotropic for shear than for the longitudinal constants.

As shown in the previous paper,[1] the Rayleigh scattering law leads to a scattering term for longitudinal waves equal to

$$A_{\text{nepers/cm}}=\frac{2\pi^3Tf^4}{v^4}\left\langle\left[\frac{c_{11}'-\langle c_{11}'\rangle_{Av}}{\langle c_{11}'\rangle_{Av}}\right]^2\right\rangle_{Av}. \tag{16}$$

Where T is the grain volume, f the frequency, v the velocity, and $[c_{11}'-\langle c_{11}'\rangle_{Av}]/\langle c_{11}'\rangle_{Av}$ is the average change in the elastic constant from grain to grain. For shear waves the scattering term is

$$A_{\text{nepers/cm}}=\frac{8}{3}\frac{\pi^3Tf^4}{v^4}\left\langle\left[\frac{c_{44}'-\langle c_{44}'\rangle_{Av}}{\langle c_{44}'\rangle_{Av}}\right]^2\right\rangle_{Av}. \tag{17}$$

To determine these space average values of the square of the elastic anisotropy we have from Eqs. (9) and (11)

$$\begin{aligned} c_{11}' &= c_{11}+[2(c_{12}-c_{11})+4c_{44}] \\ &\quad \times[l_1^2m_1^2+l_1^2n_1^2+m_1^2n_1^2], \\ \langle c_{11}'\rangle_{Av} &= c_{11}+\left[\frac{2[c_{12}-c_{11}]+4c_{44}}{5}\right]. \end{aligned} \tag{18}$$

Hence

$$\begin{aligned} &\left[\frac{c_{11}'-\langle c_{11}'\rangle_{Av}}{\langle c_{11}'\rangle_{Av}}\right]^2 \\ &\quad =A-B[\sin^4\theta\sin^2\varphi\cos^2\varphi+\sin^2\theta\cos^2\theta] \\ &\qquad +C[\sin^4\theta\cos^2\varphi\sin^2\varphi+\sin^2\theta\cos^2\theta]^2, \end{aligned} \tag{19}$$

where

$$A=\left[\frac{[2(c_{12}-c_{11})+4c_{44}]}{5c_{11}+2(c_{12}-c_{11})+4c_{44}}\right]^2,$$

$$B=10A, \quad C=25A.$$

Integrating this equation over all orientations, we have

$$\begin{aligned} \left\langle\left[\frac{c_{11}'-\langle c_{11}'\rangle_{Av}}{\langle c_{11}'\rangle_{Av}}\right]^2\right\rangle_{Av} &= A\left[1-2+\frac{25}{21}\right] \\ &= \frac{4}{21}\left[\frac{2(c_{12}-c_{11})+4c_{44}}{5c_{11}+2(c_{12}-c_{11})+4c_{44}}\right]^2. \end{aligned} \tag{20}$$

The value of the shear anisotropy constant for cubic metals is obtained by integrating the

expression

$$\left\langle\left[\frac{c_{44}'-\langle c_{44}'\rangle_{Av}}{\langle c_{44}'\rangle_{Av}}\right]^2\right\rangle_{Av}=\left[\frac{2(c_{11}-c_{12})-4c_{44}}{\langle c_{44}'\rangle_{Av}}\right]^2 \times\frac{\int_0^{2\pi}d\varphi\int_0^{\pi}\left[\cos^2\theta\sin^2\varphi\cos^2\varphi-\frac{1}{24}\right]^2\sin\theta d\theta}{4\pi}$$

$$=\frac{17}{5760}\left[\frac{2(c_{11}-c_{12})-4c_{44}}{\langle c_{44}'\rangle_{Av}}\right]^2. \quad (21)$$

The scattering factors for the hexagonal metals were calculated from Eqs. (15) and (16) by introducing the direction cosines of Eqs. (10) and (13) and averaging over the sphere. The results are

$$\left\langle\left[\frac{c_{11}'-\langle c_{11}'\rangle_{Av}}{\langle c_{11}'\rangle_{Av}}\right]^2\right\rangle_{Av}=\frac{4}{1575}\left[\frac{48c_{11}^2-64c_{11}c_{33}+28c_{33}^2-16c_{11}(2c_{13}+4c_{44})+4c_{33}(2c_{13}+4c_{44})+3(2c_{13}+4c_{44})^2}{\langle c_{11}'\rangle_{Av}^2}\right], \quad (22)$$

$$\left\langle\left[\frac{c_{44}'-\langle c_{44}'\rangle_{Av}}{\langle c_{44}'\rangle_{Av}}\right]^2\right\rangle_{Av}=\frac{1}{45}\left[\frac{c_{11}-c_{12}-2c_{44}}{\langle c_{44}'\rangle_{Av}}\right]^2.$$

TABLE III. Scattering factor for longitudinal and shear waves.

Metal	$\left\langle\left(\frac{c_{11}'-\langle c_{11}'\rangle_{Av}}{\langle c_{11}'\rangle_{Av}}\right)^2\right\rangle_{Av}$	$\left\langle\left(\frac{c_{44}'-\langle c_{44}'\rangle_{Av}}{\langle c_{44}'\rangle_{Av}}\right)^2\right\rangle_{Av}$
Al	3×10^{-4}	1.95×10^{-3}
Au	1.78×10^{-3}	2.3×10^{-2}
Ag	5×10^{-3}	2.7×10^{-2}
Cu	7.4×10^{-3}	2.9×10^{-2}
Pb	4.2×10^{-3}	3.4×10^{-2}
Fe	6.7×10^{-3}	2.0×10^{-2}
Na	2.9×10^{-2}	5.1×10^{-2}
K	1.7×10^{-2}	4.6×10^{-2}
W	0	0
Mg	9×10^{-4}	4×10^{-5}
Zn	5.6×10^{-3}	3.6×10^{-2}
Cd	2.8×10^{-2}	4.8×10^{-2}

The scattering factors for the metals listed above are given in Table III. From the table it is obvious that the metals having the least scattering loss will be tungsten, magnesium, and aluminum.

The measured values for aluminum and magnesium agree quite well with these calculated scattering factors. For the particle size of 0.13 mm for aluminum the theoretical value of scattering attenuation is

$$B_2=0.134\times10^{-30}\ \text{neper/cm/cycle}^4, \quad (23)$$

compared to a measured value of $B_2=0.695\times10^{-30}$ which agrees as closely as could be expected, considering that the particles scatter shear as well as longitudinal waves and that since the shear waves are shorter they are more efficient sources of scattering. The ratio of scattering loss for the two grain size aluminum rods should be

$$(0.23)^3/(0.13)^3=5.5, \quad (24)$$

and this agrees quite exactly with the experimental ratio of 5.4. For magnesium grain size of 0.21 mm the scattering loss at 8 megacycles should be 2.6 db per foot compared to a measured value of 5 db per foot.

The agreement in the case of shear waves is somewhat better. For aluminum with 0.13-mm grain size the theoretical attenuation is

$$B_2=6.1\times10^{-30}\ \text{neper/cm/cycle}^4, \quad (25)$$

compared to a measured value of $B_2=9.4\times10^{-30}$. This is a good agreement, since the spread of particle sizes tends to make the loss larger than would be calculated from a single particle size. The ratio between the shear scattering losses for the two rods is again 5.5 theoretically compared to the experimental value of 5.4.

For magnesium the small shear scattering factor of 4×10^{-5} shows that the loss from scattering should be small. The theoretical value is

$$B_2=2.09\times10^{-31}\ \text{neper/cm/cycle}^4, \quad (26)$$

compared to an experimental value of

$$B_2=4.6\times10^{-31}\ \text{neper/cm/cycle}^4. \quad (27)$$

The experimental value for the term proportional to the frequency is

$$A_{\text{neper/cm}}=1.06\times10^{-10}f.$$

This corresponds to a low frequency Q of

$$Q=\frac{B}{2A}=\frac{(2\pi f/v)}{2(1.06\times10^{-10})f}=100{,}000,$$

which is higher than that measured for any other metal.

V. DIFFUSION LOSSES AT HIGH FREQUENCIES

As the wave-length of the acoustic wave becomes equal or less than the grain size, the Rayleigh type of scattering loss gives way to a diffusion type of wave propagation similar to the mechanism for heat transfer. Here the attenuation is controlled by the mean free path, i.e., the distance that the wave can traverse without reflection or refraction. For the case of a sound wave in metal the mean free path is obviously determined by the grain diameter since free transmission occurs in the crystal but reflection occurs at the boundary between grains.

A rough estimate of diffusion losses can be made as follows: The receiving crystal is very directional and hence all that will be picked up are waves that are normal to the surface. When the frequency is so high that the wave-length is small compared to the grain size, the loss is caused by reflection between grains and to the change in direction caused by these reflections. These two losses, since they are both caused by reflections, are comparable, and hence we calculate the losses by reflection at normal incidence, and assume the change in direction loss is of the same order of magnitude. If the wave goes from one grain to another at normal incidence across the boundary, one part is transmitted and the other reflected. Since the amount lost by reflection is small, the transmitted part is in terms of pressure

$$p=p_0[1-R_1]=p_0\exp(-R_1), \tag{28}$$

where R_1 is the reflection coefficient. For n such reflections in a length l, the terminal pressure becomes

$$p=p_0\exp(-[R_1+R_2+\cdots+R_n]) \\ =p_0\exp(-n\bar{R}), \tag{29}$$

where $\bar{R}$ is the average reflection coefficient. Now if the average particle diameter is D, then

$$nD=l \quad \text{or} \quad n=l/D, \tag{30}$$

where l is the total path length. Hence

$$p=p_0\exp\left(-\frac{\bar{R}l}{D}\right), \tag{31}$$

and the loss should be inversely as the grain diameter for a diffusion process. Multiplying the exponent by 2 to take account of the loss by change in direction (which should be the same order of magnitude as the reflection loss), the loss in nepers per centimeter should be in the order of

$$A=\frac{2\bar{R}}{D}. \tag{32}$$

To evaluate the average reflection coefficient, we have

$$R=(Z_1-Z_2)/(Z_1+Z_2) \\ =\left(\frac{c_{11}'}{\rho}\right)^{\frac{1}{2}}-\left(\frac{\langle c_{11}'\rangle_{Av}}{\rho}\right)^{\frac{1}{2}}\Bigg/ \\ \left(\frac{c_{11}'}{\rho}\right)^{\frac{1}{2}}+\left(\frac{\langle c_{11}'\rangle_{Av}}{\rho}\right)^{\frac{1}{2}}, \tag{33}$$

where c_{11}' is the elastic constant in any direction and $\langle c_{11}'\rangle_{Av}$ the elastic constant average over all directions. Since $(c_{11}'-\langle c_{11}'\rangle_{Av})/\langle c_{11}'\rangle_{Av}$ is a small quantity, this reduces to

$$R=\frac{1}{4}\left|\frac{c_{11}'-\langle c_{11}'\rangle_{Av}}{\langle c_{11}'\rangle_{Av}}\right|. \tag{34}$$

In evaluating this we have to take the absolute value since energy is lost no matter what the sign of the reflection coefficient. This makes it a difficult integration, and since only an approximate calculation has been made it is sufficiently accurate to take one-fourth the average of the two extremes of reflection coefficient. For magnesium the average value of $\langle c_{11}'\rangle_{Av}$ is 5.88×10^{11}. The maximum value is $c_{33}=6.6\times10^{11}$, while the minimum value is 5.75. Hence the average reflection coefficient is in the order of 0.0075. The indicated loss for the magnesium bar with 2-mm grain size is 0.075 neper per cm, or 1.6 db per inch, which checks reasonably well with the data of Fig. 2 for the 2-mm grain size magnesium.

Fourth power scattering holds up to a frequency for which the grain size is about a third of a wave-length, while diffusion processes result when the grain size is 3 wave-lengths or larger. No adequate theory exists for the transition region.

Probability That a Meteorite Will Hit or Penetrate a Body Situated in the Vicinity of the Earth*

G. GRIMMINGER
Douglas Aircraft Company, Inc., Santa Monica, California
(Received June 14, 1948)

When a body is situated at sufficiently great altitudes (about 200 km or above) it is exposed to impact by the meteorites which enter the earth's atmosphere. A preliminary attempt is made to estimate the probability that a body situated in the vicinity of the earth will be hit by a meteorite and, when hit does occur, to estimate the metal plate thickness necessary to prevent perforation by the impact of meteorites of different sizes. For stainless steel skin thicknesses ranging from 0.05 to 0.02 inch it is necessary to consider meteorites as small as those corresponding to magnitude 8 to 11, respectively. In general, however, it is found that for meteorites which are large enough to present a perforation hazard the probability of a hit is negligibly small, particularly if the body is not exposed to meteoritic impact for excessively long periods of time.

INTRODUCTION

AS a result of the great development in recent years of rocket motors and large size rocket powered vehicles, the idea of sending a body to extremely high altitudes or even into interplanetary space may now be thought of with considerable seriousness. In this connection the question always arises as to the probability that the body will be hit and damaged by a meteorite.** This would be the case, for example, if one should consider a body which revolves about the earth as a satellite. An attempt will be made here to answer some of these questions, at least in a preliminary way.

I. METEORITES

Number, Size, and Velocity

It is well known that a great many meteorites enter the earth's atmosphere each day. If a body should be situated at great heights above the earth, the question arises as to what are the chances that the body will be hit by a meteorite and if a hit does occur, what are the probabilities that the meteorite will seriously damage or otherwise interfere with the motion of the body.

Meteorites[1] are discrete masses of matter from outer space which enter the earth's atmosphere. Judging from those which are large enough to survive the journey through the air and reach the ground, and which are then called fallen meteorites, they are composed mainly of stony matter (similar to igneous rock) and metallic nickeliferous iron. Like fallen meteorites, the relative amount of iron and stony matter in the meteorites may be expected to vary greatly, ranging from almost all iron to almost all stone. However, it is quite likely that the stony meteorites are more prevalent than iron meteorites by a factor of more than ten, although a stony meteorite itself may contain some 25 percent iron by mass. It will be assumed that the meteorites consist mainly of stony matter.[2]

Meteorites vary greatly in size, ranging from something smaller than a pin head or grain of sand up to the large meteoritic masses found on the earth which weigh 10 or 20 tons or more. According to Leonard,[1] meteorites may be of any magnitude whatever, from the size of the tiniest solid particle to that of a mass of planetary dimensions, and are the smallest discrete astronomical bodies. The term meteor is properly used to denote the luminous phenomenon which results from the motion of a meteorite through the earth's atmosphere. It is estimated that the weight of the average fallen meteorite is 220 pounds before entering the atmosphere and that this reduces to about 44 pounds by the time the

* Originally prepared as a Douglas Aircraft Company Report dated May, 1946.

** See Willy Ley, *Rockets—The Future of Travel Beyond the Stratosphere* (Viking Press, New York, 1944).

[1] F. C. Leonard, "Meteorites: Immigrants from Space," Publications of the Astronomical Society of the Pacific, 57, 5, (1945).

[2] F. G. Watson, *Between the Planets* (The Blakiston Company, Philadelphia, 1941), pp. 140, 177.

TABLE I. The number, mass, and size of meteorites entering the atmosphere each day.*

Visual mag. M	Observed No.	True No. N	Total No. from −3 up to and including mag. M S_M	Mass m, grams	Mass m, lb.**	Diam. of equiv. sphere*** d, ft.	Diam. of equiv. sphere d, in.	Diam. of equiv. sphere d, cm
−3	28,000	28,000	2.84×10^{4}	4.0	8.72×10^{-3}	4.27×10^{-2}	5.12×10^{-1}	1.30
−2	71,000	71,000	9.94×10^{4}	1.6	3.53×10^{-3}	3.17×10^{-2}	3.80×10^{-1}	9.66×10^{-1}
−1	180,000	180,000	2.79×10^{5}	0.630	1.39×10^{-3}	2.32×10^{-2}	2.78×10^{-1}	7.07×10^{-1}
0	450,000	450,000	7.28×10^{5}	0.250	5.51×10^{-4}	1.705×10^{-2}	2.046×10^{-1}	5.20×10^{-1}
1	1,100,000	1,100,000	1.88×10^{6}	0.100	2.20×10^{-4}	1.257×10^{-2}	1.508×10^{-1}	3.83×10^{-1}
2	2,800,000	2,800,000	4.72×10^{6}	0.040	8.72×10^{-5}	9.22×10^{-3}	1.11×10^{-1}	2.81×10^{-1}
3	6,400,000	7,100,000	1.18×10^{7}	0.016	3.53×10^{-5}	6.83×10^{-3}	8.20×10^{-2}	2.08×10^{-1}
4	9,000,000	18,000,000	2.98×10^{7}	0.0063	1.39×10^{-5}	5.00×10^{-3}	6.00×10^{-2}	1.52×10^{-1}
5	3,600,000	45,000,000	7.47×10^{7}	0.0025	5.51×10^{-6}	3.67×10^{-3}	4.40×10^{-2}	1.12×10^{-1}
6		110×10^{6}	1.88×10^{8}	0.0010	2.20×10^{-6}	2.705×10^{-3}	3.246×10^{-2}	8.24×10^{-2}
7		280×10^{6}	4.72×10^{8}	0.00040	8.72×10^{-7}	1.986×10^{-3}	2.383×10^{-2}	6.05×10^{-2}
8		710×10^{6}	1.18×10^{9}	0.00016	3.53×10^{-7}	1.471×10^{-3}	1.765×10^{-2}	4.48×10^{-2}
9		18×10^{8}	2.98×10^{9}	0.000063	1.39×10^{-7}	1.078×10^{-3}	1.294×10^{-2}	3.29×10^{-2}
10		45×10^{8}	7.47×10^{9}	0.000025	5.51×10^{-8}	7.93×10^{-4}	9.52×10^{-3}	2.42×10^{-2}
15		45×10^{10}	7.47×10^{11}	2.5×10^{-7}	5.51×10^{-10}	1.705×10^{-4}	2.046×10^{-3}	5.20×10^{-3}
20		45×10^{12}	7.47×10^{13}	2.5×10^{-9}	5.51×10^{-12}	3.67×10^{-5}	4.40×10^{-4}	1.20×10^{-3}
25		45×10^{14}	7.47×10^{15}	2.5×10^{-11}	5.51×10^{-14}	7.93×10^{-6}	9.52×10^{-5}	2.42×10^{-4}
30		45×10^{16}	7.47×10^{17}	2.5×10^{-13}	5.51×10^{-16}	1.705×10^{-6}	2.046×10^{-5}	5.20×10^{-5}

* Based on Watson, reference 2.
** lb = grams $\times 2.205\times10^{-3}$.
*** Based on a specific gravity of 3.4. See reference 5.

earth's surface is reached. However, meteorites which are large enough to reach the earth's surface occur with such low frequency, 5 or 6 a day for the whole earth, that they need not be considered here.

The values used for the number, size, and mass of meteorites entering the atmosphere each day are given in Table I, which is based on a table given by Watson.[3] While it is realized that the values shown in Table I may be subject to considerable error, it is believed that they represent the best estimate available at the present time.

The visual magnitude of a meteor is expressed in terms of a scale in which algebraically large magnitudes represent faint bodies. Two meteors which differ by five magnitudes have a 100-fold difference in brightness and, since the brightness is directly proportional to the mass, they represent a 100-fold difference in mass. A meteor just visible to the naked eye has magnitude of 5, while the full moon has a magnitude of −12.55. Also it will be noticed from Table I that when the magnitude differs by five units, the number of meteors changes by a factor of 100. In this way the table may be extended to include smaller and smaller meteorites (numerically larger magnitudes). However, according to Watson,[4] there is a limiting magnitude beyond which there can be few, if any, meteorites, and this limiting size is a meteorite of magnitude 30. This is explained by the fact that for a particle smaller than this the solar radiation pressure is sufficient to repel any particle to such an extent that it could not remain in the solar system. In Table I, figures are included for meteorites down to the smallest possible size, magnitude 30. The diameters given are obtained on the basis that the meteorite is a sphere composed mainly of stony matter which, according to Whipple,[5] has a specific gravity of 3.4. The variation of size with magnitude is also shown in Fig. 1.

Before leaving the question of the frequency of meteorites, it is believed worth while to point our the following consideration. In estimating the probability that a meteorite will hit an exposed body in space, one may consider either the total number of meteorites of all sizes, or only the total number of a certain size, or else the total number of a certain size plus all those of larger size. In considering the probabilities of a hit by a meteorite we are not especially concerned with the entire total number of meteorites

[3] See reference 2, p. 115.

[4] See reference 2, p. 116.

[5] F. L. Whipple, "Meteors and the earth's upper atmosphere," Rev. Mod. Phys. **15**, 252 (1943).

of all possible sizes since many of these are too small to do any damage. On the other hand, we are concerned with meteorites of a certain given size and especially those sizes which can cause damage and at the same time occur with considerable frequency. Furthermore, since when considering a certain size the total number of all larger sizes may be appreciable, this suggests also the consideration of the total number of meteorites down to and including those of given size.

The total number of meteorites in this case may be obtained from the basic consideration used in Table I that when the magnitude increases by 5, the number increases by 10^2 and therefore for a change of 1 magnitude the number changes by a factor of 2.5. Thus, if there are N' meteors of magnitude M' in each 24-hour period, there will be

$$N = N' \times (10)^{2/5(M-M')} \tag{1}$$

meteors of magnitude M in the same period. Meteors of magnitude less than -3 need not be considered since they occur too infrequently to be of any importance. The sum of all those of magnitude -3, up to and including magnitude M, is given by

$$S_M = N' \times (10)^{-2/5M'} \sum_{-3}^{M} (10)^{2/5M}. \tag{2}$$

Using the relation for the sum of a geometric series, this reduces to the form

$$S_M = \frac{10^{2/5}}{10^{2/5}-1} \times N' \times (10)^{2/5(M-M')} \times [1-(10)^{-2/5(M+4)}]. \tag{3}$$

Choosing a meteor of magnitude 0 as a basis for the computation, $M'=0$, $N'=450{,}000$, the numbers are then determined from the relation

$$N = 4.5 \times 10^5 \times (10)^{2M/5}, \tag{4}$$

and

$$S_M = 7.47 \times 10^5 [(10)^{2M/5} - 0.025]. \tag{5}$$

The values of S_M are shown in Table I.

Consideration must now be given to the meteorite velocity and, in particular, to any effect which the outer atmosphere may have in decreasing the velocity. If it is assumed that the meteorites move in parabolic orbits at the same distance from the sun as the earth, a meteorite encountering the earth head-on will enter the outer atmosphere with a speed of 250,000 ft./sec., while one overtaking the earth will enter the atmosphere with a speed of only 43,300 ft./sec.[1] According to Watson[2] most meteors appear at a height of about 300,000 feet, regardless of their brightness, and may be taken to have an average atmospheric velocity of about 150,000 ft./sec. This is in agreement with the observational data presented by Whipple (see Table II of reference 5), which also indicate that the amount of deceleration experienced by a meteorite in its travel through the atmosphere above 100 km is probably quite small. Further conclusions on this point may be obtained from the following considerations.

Neglecting the acceleration of gravity, the atmospheric deceleration of a meteorite is determined from the relation

$$\frac{dV}{dt} = -C_D \frac{\rho A}{2m} V^2, \tag{6}$$

where

V = velocity,
m = mass of meteorite,
A = maximum cross-section area of meteorite,
ρ = atmospheric density,
C_D = drag coefficient,
t = time.

If the meteorite is assumed to be a sphere of diameter d and density ρ_m, and if the relation $dV/dt = (dV/dh)(dh/dt) = V dh/dV$ is used, where

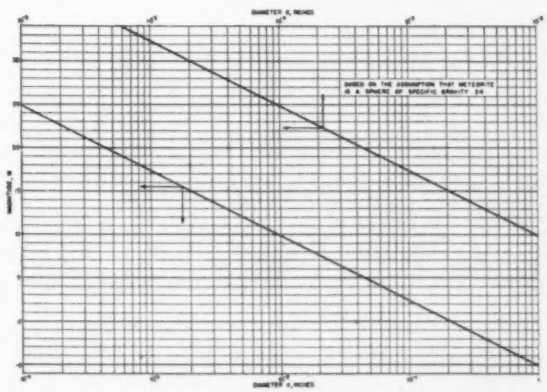

FIG. 1. Size of meteorite corresponding to meteor magnitude. See Table II.

TABLE II. Effect of atmosphere on meteorite velocity. (V_i = meteorite velocity outside of atmosphere.)

Alt. h km	Scale height H km	Density of atmosphere ρ g/cm³	Magnitude, M −3	0	5	10	15	20	25	30
			V/V_i							
50	10.66	1.02×10^{-6}	0.8312*	0.6295*	0.1165*	0.0001*	0.0000+*	0.0000+*	0.0000+*	0.0000+*
100	9.90	3.98×10^{-9}	(0.9993)*	(0.9983)*	(0.9923)*	(0.9647)*	(0.8461)*	(0.4603)*	(0.0275)*	(0.0000+)*
100	9.90	3.98×10^{-9}	0.9986	0.9967	0.9846	0.9307	0.7160	0.2119	0.00076	0.0000+
150	18.09	5.82×10^{-11}	0.99996	0.99991	0.9996	0.9981	0.9911	0.9593	0.8251	0.4091
200	25.82	4.13×10^{-12}	1.0000−	1.0000−	0.99995	0.9998	0.9991	0.9958	0.9807	0.9135
250	33.80	5.93×10^{-13}	1.0000−	1.0000−	1.0000−	0.99996	0.9999	0.9992	0.9963	0.9831
300	42.01	1.29×10^{-13}	1.0000−	1.0000−	1.0000−	1.0000−	0.99995	0.9998	0.9990	0.9954
400	99.83	1.20×10^{-14}	1.0000−	1.0000−	1.0000−	1.0000−	1.0000−	0.99995	0.9997	0.9990
500	130.5	3.69×10^{-15}	1.0000−	1.0000−	1.0000−	1.0000−	1.0000−	1.0000−	0.9999	0.9996
600	162.8	1.54×10^{-15}	1.0000−	1.0000−	1.0000−	1.0000−	1.0000−	1.0000−	0.99995	0.9998
700	182.6	8.00×10^{-16}	1.0000−	1.0000−	1.0000−	1.0000−	1.0000−	1.0000−	1.0000−	0.9999

* Based on $C_D=1$. All other values based on $C_D=2$.

h denotes height, the deceleration equation becomes

$$\frac{dV}{V}=-\frac{3}{4}\frac{C_D}{d}\frac{\rho}{\rho_m}dh. \tag{7}$$

Considering the highly rarefied gas conditions existing in the upper atmosphere above 100 km, the drag of the meteorite must be calculated on the basis of free molecule flow rather than from gas dynamics, and the drag coefficient may be taken to have the constant value[6–8] $C_D=2$. Below 100 km the high Mach number value (see reference 13) $C_D=1$ is probably more appropriate. Although the atmospheric density ρ varies greatly with the height h, as far as the total deceleration of a meteorite is concerned, this is determined not particularly by the vertical distribution of density but rather by the total mass of atmosphere through which the meteorite must travel. Assume, for simplicity, that the flight path of the meteorite lies in the vertical, and consider the total mass of atmosphere in a vertical direction through which a meteorite must pass in order to reach an altitude h above the earth's surface. For this purpose it is convenient to introduce the concept of homogeneous atmosphere and scale height. An atmosphere, or any portion thereof, is said to be homogeneous if it has the same composition and density throughout. If the atmosphere above a certain height h is treated as homogeneous, the thickness of this portion of the atmosphere is equal to the scale height H defined by the relation[9]

$$H=\frac{R_u T}{Mg'}, \tag{8}$$

where

R_u = universal gas constant,
T = absolute temperature of the atmosphere at the height h,
M = molecular weight of the atmosphere at the height h, and
g' = apparent acceleration of gravity at the height h.

Introducing the scale height H, the deceleration equation, (7), may be written

$$\frac{dV}{V}=-\frac{3}{4}\frac{C_D}{d}\frac{\rho}{\rho_m}dH, \tag{9}$$

which may be integrated to yield the result

$$\frac{V}{V_i}=\exp\left(-\frac{3}{4}\frac{C_D}{d}\frac{\rho}{\rho_m}H\right), \tag{10}$$

where V_i is the meteorite velocity before entering the atmosphere and V is the velocity when the meteorite has descended to an altitude h.

Values for ρ and H at all heights in the atmosphere are given in another report.[10] Using $\rho_m=3.4$ g/cm³ for the meteorite density and using the values in Table I for the meteorite

[6] A. F. Zahm, "Superaerodynamics," J. Frank. Inst. **217**, 153 (1934).
[7] E. Sänger, "Gaskinetik sehr hoher Fluggeschwendikeiten," Luftfahrtforschung (Munich), Report 972, (1938).
[8] H. S. Tsien, "Superaerodynamics, mechanics of rarefied gases," J. Aero Sci. **13** (Dec. 1946).
[9] S. Chapman and J. Bartels, *Geomagnetism* (Oxford University Press, London, 1940) Vol. I, pp. 488–493.
[10] G. Grimminger, *Analysis of Temperature, Pressure, and Density in the Atmosphere Extending to Extreme Altitudes* (to be published).

diameter d, the effect of atmospheric deceleration as obtained from Eq. (10) is shown in Table II. For meteorites corresponding to magnitude 5 or less it is seen that the deceleration caused by the atmosphere is negligible above 100 km. For the smallest meteorites it is necessary to go to altitudes of the order of 200 km before the deceleration becomes negligible. If gravity effects were considered, the deceleration would be slightly less. However, the gravity effect cannot be large, for, even when gravity acts continuously on a particle traveling to the earth from infinity, the resulting increase in velocity is only about 36,000 ft./sec. (11 km/sec.), which is quite small compared to the velocities to be considered here (150,000 to 250,000 ft./sec.). Actually (reference 1, p. 9), the maximum increase in the meteorite velocity which can be caused by gravity is only 14,000 ft./sec. In the present discussion it will be assumed that the body is sufficiently distant from the earth (at least above 200 km) that the atmospheric deceleration of the meteorites may be neglected. The average meteorite velocity will be taken as 150,000 ft./sec. and the maximum velocity as 250,000 ft./sec.

II. THE PENETRATION OF METAL PLATE BY A METEORITE

In view of the extremely high velocity of the meteoric particles it is conceivable that even a very small particle might be able to penetrate the metal skin of the body it strikes. There is very little information available concerning the penetration of metal plate by very small but extremely high speed particles. However, the indications are that in the case of normal impact on metal plate of a small but very high speed particle in which the speed of the particle is large compared to the velocity of propagation of plastic deformation[11] in the plate, the particle penetrates as though the plate were perfectly deformable like a fluid.[12] In this case the differential equation for the motion of the particle through the plate is

$$m\frac{dV}{dt} \equiv \frac{m}{2}\frac{d(V^2)}{ds} = -C_D\frac{\rho_p}{2}\frac{d^2}{4}V^2 \qquad (11)$$

where

m = mass of particle $= \frac{4}{3}\frac{d^3}{8}\rho_m$ (assumed spherical),

d = diameter of particle,

s = distance of penetration into the plate,

ρ_p = density of the plate—$2.8\frac{g}{cm^3}$ for dural, $7.9\frac{g}{cm^3}$ for stainless steel,

ρ_m = density of particle—$3.4\frac{g}{cm^3}$ for a meteorite,

$\sigma = \frac{\rho_p}{\rho_m}$, and

C_D = drag coefficient.

Equation (11) may be written in the form

$$ds = -\frac{\frac{2}{3}}{C_D\sigma}\frac{d\,d(V^2)}{V^2}. \qquad (12)$$

Since the penetration of the particle into the plate is being treated as though the plate were a compressible fluid, the value of the drag coefficient may be taken from gas dynamics. It must be pointed out, however, that since Eq. (11) is assumed to be valid only when the speed of the particle in the plate has a high "Mach number" (based on the material of the plate, i.e., the plastic deformation velocity), the value used for the drag coefficient must likewise correspond to a high Mach number. In the ordinary usage of gas dynamics the Mach number is defined by the ratio V/c, where V is the speed of the moving object and c is the speed of sound (velocity of propagation of small pressure waves) in the fluid medium. In the Mach number analogy used here for plate penetration, c is replaced by the velocity of propagation of plastic deformation. The drag of a projectile at high Mach numbers has been considered by Epstein,[13] and if his formula (27) be evaluated for a sphere, it will be found that $C_D = 1$. This value is also substantiated to some extent by the results of Charters and Thomas.[14] Using

[11] T. von Karman, "On the Propagation of Plastic Deformation in Solids," NDRC Report A-29 (OSRD Report No. 365), Jan. 1942.

[12] It is understood that J. L. Synge of the Carnegie Institute of Technology has analyzed this concept theoretically in an unpublished paper.

[13] P. Epstein, "On the air resistance of projectiles at high mach numbers," Proc. Nat. Acad. Sci. **17**, 546 (1931).

[14] A. C. Charters and R. N. Thomas, "The aerodynamic performance of small spheres from subsonic to high supersonic velocities," J. Aero. Sci. **12**, 468 (1945).

$C_D=1$, Eq. (12) becomes

$$ds=-\frac{2}{3}\frac{d}{\sigma}\frac{d(V^2)}{V^2},$$

which gives the result

$$s=\frac{4}{3}\frac{d}{\sigma}\log\frac{V_i}{V}, \tag{13}$$

where V_i is the velocity of the particle as it first strikes the plate and V is its velocity after it has penetrated a distance s. When the speed V of the particle has dropped to about 5 times the plastic deformation velocity V_1, it will be assumed that this law of penetration is no longer valid. In the range in which it is to be used the equation is then written

$$s=\frac{4}{3}\frac{d}{\sigma}\log\frac{V_i}{5V_1}, \tag{14}$$

When the speed of the particle is less than 5 times the plastic deformation speed it will be assumed that the penetration takes place according to one of the armor penetration formulas.*** One such formula is

$$t=F\frac{mV^2}{d^2}, \tag{15}$$

where

t = thickness penetrated,
m = mass of projectile,
F = Thompson coefficient,
d = diameter of projectile, and
V = velocity of projectile.

The work of Duwez and Clark[15] on the penetration of copper by high speed small caliber bullets directly verifies the velocity squared relation for speeds of the order of 4000 ft./sec. Their results can be expressed by the relation

$$\frac{t}{d}=5.9\times10^{-7}V^2, \tag{16}$$

where V is expressed in feet per second. Thus the experimental data in the ballistic range give rise to penetration formulas proportional to V^2. Since the results of Duwez and Clark are considered the best to use in the present study, a formula corresponding to Eq. (16) will be used in the ballistic range. Since the ultimate strengths of dural and copper are of the same order of magnitude, and since the ballistic penetration is closely connected with this property of the metal, it will be assumed that the results for copper also apply to dural within the degree of approximation of the equations.

Equation (16) was obtained from experiments with 0.224-inch diameter projectiles. It is now desired to find the equivalent formula for the case in which the projectile is a sphere. If it is assumed that the kinetic energy loss per unit penetration distance is proportional to the frontal area A of the projectile and also is constant over the ballistic range (as shown in reference 14), it follows that $\Delta KE/t=\frac{1}{2}mV^2/t=CA$, where ΔKE is the change in kinetic energy when the projectile is brought to rest, and C is a constant. In the tests, the projectile weight was 69 grains† and was brought to rest from a velocity of 3870 ft./sec. in about 2 inches of copper. This gives $\frac{1}{2}mV^2/t=13.8\times10^3$ (ft.-lb./ft.), and therefore $C=\frac{1}{2}mV^2/tA=5.03\times10^7$ (ft.-lb./ft.^{3}). The corresponding penetration formula for a sphere of diameter d and density ρ_m would be

$$\frac{C\pi d^2}{4}=\frac{\frac{1}{2}\rho_m\frac{\pi}{6}d^3V^2}{t}, \quad \text{or} \quad \frac{t}{d}=\frac{\rho_m}{3C}V^2.$$

Taking $\rho_m=3.4\frac{\text{g}}{\text{cm}^3}=6.6\frac{\text{slug}}{\text{ft.}^3}$ and $C=5.03\times10^7$, as determined above from the firing tests on copper, the ballistic formula for the penetration of a spherical projectile in dural becomes

$$\frac{t}{d}=4.4\times10^{-8}V^2. \tag{17}$$

*** The writer is indebted to R. D. Park of the Douglas Research Laboratory for this approximate analysis of the penetration in the ballistic range leading to Eqs. (17) and (18).

[15] P. E. Duwez and E. S. Clark, *A Preliminary Investigation of the Mechanism of Penetration from the Standpoint of Strain Propagation*, NDRC Report No. M-317 (OSRD Report No. 3957), 1944.

† 7000 grains = 1 lb.

Since the velocity V_1 of plastic deformation in compression is known[16] to be around 1000 ft./sec., the limiting speed used in the fluid-flow Eq. (14) will be taken to be 5000 ft./sec. This corresponds to a "Mach" number of 5. Thus to determine the total penetration for a particle (meteorite), Eq. (14) is first used to compute the penetration s at which the speed is slowed down to 5000 ft./sec. The remainder of the penetration t is then computed from Eq. (17) using $V=5000$ ft./sec. The total penetration is then given by the sum $s+t$. Letting $T=s+t$ and joining Eqs. (13) and (17) at $V=5V_1(=5000$ ft./sec.), the total penetration T is then given by

$$\frac{T}{d}=\frac{4}{3\sigma}\log\frac{V_i}{5V_1}+4.4\times10^{-8}(5V_1)^2, \text{ or}$$

$$\frac{T}{d}=1.62\log\frac{V_i}{5000}+1.10, \text{ for dural.} \qquad (18)$$

For stainless steel the ultimate tensile strength is taken as twice that of copper, which gives the value 10.06×10^7 ft.-lb./ft.^{3} for the constant C and $t/d=2.2\times10^{-8}V^2$ for the ballistic penetration. Using $\rho_p=7.9$ g/cm^3 for stainless steel, the total penetration is expressed by

$$\frac{T}{d}=\frac{4}{3\sigma}\log\frac{V_i}{5V_1}+2.2\times10^{-8}(5V_1)^2, \text{ or}$$

$$\frac{T}{d}=0.58\log\frac{V_i}{5000}+0.55, \text{ for stainless steel.} \qquad (19)$$

By using the values of d from Table I, the penetration T may be expressed directly as a function of meteor magnitude as shown in Fig. 2. The penetration is given both for the average velocity 150,000 ft./sec. and for the maximum velocity 250,000 ft./sec. It is seen that with such high velocities the penetration is not very sensitive to the exact value of the velocity. On the other hand, the penetration is directly proportional to the density of the meteoritic particle, and, if this were composed mainly of iron—which might easily be the case, the penetration would be about twice as large as shown in Fig. 2.

[16] P. E. Duwez, E. S. Clark, and H. E. Martens, *The Propagation of Plastic Strain in Compression*, NDRC Report No. M-302 (O.S.R.D. Report No. 3886), 1944.

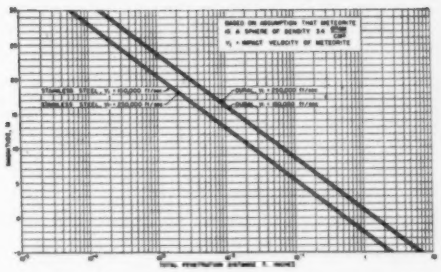

FIG. 2. Penetration of metal plate by impact of meteorites.

For metal skin thicknesses of the order of 0.02 to 0.05 inch, which are conceivable values on the basis of practice in aircraft design, Fig. 2 indicates that as far as perforation hazard is concerned it is necessary to consider meteorites up to corresponding magnitude 14 for dural and magnitude 11 for stainless steel. If the meteorite is composed mainly of iron, these values become about 16 and 13, respectively. Although the penetration formulas are based on ideas of a somewhat qualitative nature, and upon the extrapolation of rather meager ballistic data to the small sizes of meteorites, it is believed that the results may serve to give an indication of the order of magnitude of the penetration resulting from impact.

From the way in which the penetration is treated here, Eq. (11), it is seen that the mechanical work done in the penetration process is derived from the kinetic energy of the meteorite, which is assumed to undergo no physical changes as a result of impact. Thus the possibility that the heating effects occurring during impact might be sufficient to melt the meteorite has not been considered. Since we are dealing with a closed system and since the kinetic energy imparted to the body is entirely negligible, it is clear that practically all of the original kinetic energy of the meteorite must eventually appear as heat. However, since the transfer of momentum occurs more rapidly than the transfer of heat, it seems likely that the penetration by impact will have been completed by the time the full effects of the heating are felt.

III. THE METEORITE

Hit Probabilities

Having arrived at an estimate for the penetration of metal plate by meteorites of different

TABLE III. Probability of a meteorite hit.* (Based on the number N of meteorites of given size only.)

Magnitude M	−3	0	5	8	10	12	14	16	18	20	22	24	26	28	30
Average hits per hour, n_1	1.84×10^{-10}	2.95×10^{-9}	2.95×10^{-7}	4.66×10^{-6}	2.95×10^{-5}	1.84×10^{-4}	1.18×10^{-3}	7.22×10^{-3}	4.66×10^{-2}	2.95×10^{-1}	1.84	1.18×10	7.22×10	4.66×10^{2}	2.95×10^{3}
Average number of hours between hits	5.44×10^{9}	3.38×10^{8}	3.38×10^{6}	2.14×10^{5}	3.38×10^{4}	5.44×10^{3}	8.46×10^{2}	1.38×10^{2}	2.14×10	3.38	5.44×10^{-1}	8.46×10^{-2}	1.38×10^{-2}	2.14×10^{-3}	3.39×10^{-4}
p_{1+} for 24 hours	4.41×10^{-9}	7.09×10^{-8}	7.09×10^{-6}	1.12×10^{-4}	7.09×10^{-4}	4.42×10^{-3}	0.0280	0.1591	0.6734	0.9992	1.0000	1.0000	1.0000	1.0000	1.0000
$T(0.5)$ hours	1.57×10^{8}	9.78×10^{6}	9.78×10^{4}	6.20×10^{3}	9.78×10^{2}	1.57×10^{2}	2.44×10	4.00	6.20×10^{-1}	9.78×10^{-2}	1.57×10^{-2}	2.44×10^{-3}	4.00×10^{-4}	6.20×10^{-5}	9.78×10^{-6}
$T(0.99)$ hours	2.28×10^{8}	1.42×10^{6}	1.42×10^{4}	8.98×10	1.42×10	2.28	3.54×10^{-1}	5.80×10^{-2}	8.98×10^{-3}	1.42×10^{-3}	2.28×10^{-4}	3.54×10^{-5}	5.80×10^{-6}	8.98×10^{-7}	1.42×10^{-7}
$T(0.999)$ hours	2.27×10^{8}	1.41×10^{6}	1.41×10^{4}	8.94	1.41	2.27×10^{-1}	3.53×10^{-2}	5.77×10^{-3}	8.94×10^{-4}	1.41×10^{-4}	2.27×10^{-5}	3.53×10^{-6}	5.77×10^{-7}	8.94×10^{-8}	1.41×10^{-8}

* Exposed area = 1000 sq. ft.; p_{1+} = probability of at least 1 hit; $T(0.50)$ = time interval to give a 50 to 50 chance of no hit; $T(0.99)$ = time interval to give a 100 to 1 chance of no hit; $T(0.999)$ = time interval to give a 1000 to 1 chance of no hit.

sizes, it remains to estimate the probability that the body will be hit by a meteorite. The meteorites will be assumed to have a random distribution both as regards their distribution over a spherical surface surrounding the earth and as regards their occurrence with time. It is further assumed that in the event of a meteorite hit, the meteorite makes normal impact with the surface of the body. It is not difficult to see that neither the meteorite velocity nor the horizontal velocity of the body are involved in determining the probability of a hit. This follows essentially from the assumption that the distribution of the meteorites is random with respect to surface area and time. Thus there will be a certain number N of meteorites of specified size which enter the spherical surface surrounding the earth in each 24-hour period, and for any exposed body area A_b, lying on this surface, it is equally likely that this area will be hit regardless of where it may be situated on the surface. If A_r is the area of the spherical surface and if the unit of time is one hour, the average number of hits per hour n_1 by meteorites of specified size (M) is

$$n_1=\frac{NA_b}{24A_r}. \tag{20}$$

When a hit occurs on the average once in the time $\bar{t}$, the average number of hits $\bar{n}$ in the time T is

$$\bar{n}=\frac{T}{\bar{t}}=\frac{NA_b}{24A_r}T=n_1T, \tag{21}$$

when the unit of time is the hour. From the Poisson distribution[17] the probability p_r that a hit will occur *exactly* r times in the time interval T is

$$p_r=\frac{\bar{n}^r e^{-\bar{n}}}{r!}. \tag{22}$$

It follows that the probability p_0 that a hit will not occur in the time T is

$$p_0=p(0)=e^{-\bar{n}}. \tag{23}$$

If p_{1+} is used to denote the probability that a hit will occur *at least once* in the time T, since

[17] J. F. Kenney, *Mathematics of Statistics* (D. Van Nostrand Company, Inc., New York, 1941), Part 2, p. 29.

$p_{1+}+p_0=1$ it follows that

$$p_{1+}=1-e^{-\bar{n}}. \tag{24}$$

Although p_{1+} does not refer to the exact number of hits in the time T, it is considered to represent the probability of most significance as far as the hit by a meteorite is concerned.

Certain probability-based time intervals of interest are as follows:

(1) The time interval for which the body has a 50 to 50 chance of not being hit. For this case $p_0=0.5$, and if the time interval is denoted by $T(0.5)$ it follows from (23) that

$$T(0.50)=-\frac{1}{n_1}\log 0.50=\frac{0.69315}{n_1}. \tag{25}$$

(2) The time interval for which the body has a 100 to 1 chance of not being hit. In this case $p_0=0.99$, and the time interval is

$$T(0.99)=-\frac{1}{n_1}\log 0.99=\frac{0.01005}{n_1}. \tag{26}$$

(3) The time interval for which the body has a 1000 to 1 chance of not being hit. In this case $p_0=0.999$, and the time interval is

$$T(0.999)=-\frac{1}{n_1}\log(0.999)=\frac{0.0010005}{n_1}. \tag{27}$$

To form an idea of the order of magnitude of the probabilities, it may be assumed, for example, that the body is moving as a satellite in a circular orbit about the earth at a height of 300 miles above the earth's surface—well above the levels where atmospheric effects would be of any consequence. Using 20.89×10^6 feet as the radius of the earth, this gives $A_r=4\times(22.47)^2\times10^{12}=6.3448\times10^{15}$ ft.^{2}. The planform area A_r of the body exposed to impact by meteorites will be taken as 1000 ft.^{2}. The resulting probabilities are given in Table III as a function of meteorite size. If S_M—Eq. (5)—is used instead of N, the probabilities are as shown in Table IV.

The appropriate values to be obtained from these tables depend upon how long the body is to remain exposed to meteoritic impact, and upon the size (magnitude) of the smallest meteorite presenting a perforation hazard, that is, upon the thickness of the metal skin. For a stainless steel skin of thickness 0.05 inch, Fig. 2 shows that the smallest size that need be considered corresponds to magnitude $M=8$. It is seen from Table IV, for example, for $M=8$ that the average time interval between hits is 1.29×10^5 hours,

TABLE IV. Probability of a meteorite hit.* (Based on the number S_M of meteorites of a given size plus all those of larger size.)

Magnitude M	−3	0	5	8	10	12	14	16	18	20	22	24	26	28	30
Average hits per hour, n_1	1.86×10^{-10}	4.78×10^{-9}	4.90×10^{-7}	7.75×10^{-6}	4.90×10^{-5}	3.10×10^{-4}	1.96×10^{-3}	1.23×10^{-2}	7.75×10^{-2}	4.90×10^{-1}	3.10	1.90×10	1.23×10^{2}	7.75×10^{2}	4.90×10^{3}
Average number of hours between hits	5.36×10^{9}	2.09×10^{8}	2.04×10^{6}	1.29×10^{5}	2.04×10^{4}	3.23×10^{3}	5.11×10^{2}	8.10×10	1.29×10	2.04	3.23×10^{-1}	5.11×10^{-2}	8.10×10^{-3}	1.29×10^{-3}	2.04×10^{-4}
p_{1+} for 24 hours	4.47×10^{-9}	1.15×10^{-7}	1.18×10^{-5}	1.86×10^{-4}	1.18×10^{-3}	7.42×10^{-3}	0.0459	0.2564	0.8442	1.0000	1.0000	1.0000	1.0000	1.0000	1.0000
$T(0.5)$ hours	3.72×10^{8}	1.45×10^{6}	1.41×10^{4}	8.95×10²	1.41×10^{2}	2.24×10^{1}	3.58×10	5.62×10	8.95	1.41	2.24×10^{-1}	3.58×10^{-2}	5.62×10^{-3}	8.95×10^{-4}	1.41×10^{-4}
$T(0.99)$ hours	5.39×10^{7}	2.10×10^{5}	2.05×10^{3}	1.30×10^{2}	2.05×10^{1}	3.24×10	5.18	8.14×10⁻¹	1.30×10^{-1}	2.05×10^{-2}	3.24×10^{-3}	5.18×10^{-4}	8.14×10^{-5}	1.30×10^{-5}	2.05×10^{-6}
$T(0.999)$ hours	5.37×10^{6}	2.09×10^{4}	2.04×10^{2}	1.29×10^{1}	2.04×10	3.23	5.16×10⁻¹	8.11×10^{-2}	1.29×10^{-2}	2.04×10^{-3}	3.23×10^{-4}	5.16×10^{-5}	8.11×10^{-6}	1.29×10^{-6}	2.04×10^{-7}

* Exposed area = 1000 sq. ft.; p_{1+} = probability of at least 1 hit; $T(0.50)$ = time interval to give a 50 to 50 chance of no hit; $T(0.99)$ = time interval to give a 100 to 1 chance of no hit; $T(0.999)$ = time interval to give a 1000 to 1 chance of no hit.

or about 15 years. Thus the probability of a hit in this case is inconsequential. For a 24-hour period the probability p_{1+} that the body will be hit at least once does not become of any significance until $M=16$ or 18. However, the penetration corresponding to this magnitude is so small (about 0.003 inch for stainless steel, Fig. 2) that even though the probability of a hit becomes high it does not matter as far as damage to the body is concerned. Considering the probability-based time intervals, it is seen from Table IV, for example, that for a 1000 to 1 chance that the body will not be hit by a meteorite of corresponding magnitude 10 or less, the body may safely remain aloft for 20 hours. If the probability number is relaxed down to a 50 to 50 chance of no hit, the time increases to 14,100 hours. In general, the probability tables indicate that for meteorite sizes which are large enough to present a perforation hazard (about magnitude 8 or 10) the probabilities of a hit are quite small and may usually be neglected if the time interval is not excessively large.

Further improvements in the results would require more accurate data of the frequency of meteorites as a function of their size, a more accurate theory of the penetration of metal plate by small high speed particles, and a consideration of the effects upon the penetration process of the heat generated during impact.

Calendar of Meetings

October

18–22 American Institute of Electrical Engineers (Midwest General Meeting), Milwaukee, Wisconsin
20–22 American Standards Association (Annual Meeting), New York, New York
21–23 Optical Society of America (Annual Meeting), Detroit, Michigan
24–27 American Institute of Mining and Metallurgical Engineers, El Paso, Texas
25–28 Technical Association of the Pulp and Paper Industry, Buffalo, New York
25–29 American Society for Metals, Philadelphia, Pennsylvania
25–29 Society of Motion Picture Engineers, Washington, D. C.
26 Association of Consulting Chemists and Chemical Engineers, New York, New York
27–29 Gas Discharge Conference, Brookhaven National Laboratory, Upton, Long Island, New York
30 American Mathematical Society, New York, New York

November

3–5 American Institute of Electrical Engineers (Southern District Meeting), Birmingham, Alabama
4–5 Society of Automotive Engineers (National Fuels and Lubricants Meeting), Tulsa, Oklahoma
4–6 Acoustical Society of America, Cleveland, Ohio
4–6 National Electronics Conference, Inc. (Annual Technical Forum), Chicago, Illinois
5–6 Society of Rheology, New York, New York
7–10 American Institute of Chemical Engineers, New York, New York
8–10 Institute of Radio Engineers, Rochester, New York
11–13 Geological Society of America (Annual Meeting), New York, New York
13–15 Conference on Applied Spectroscopy, Pittsburgh, Pennsylvania
15–17 American Oil Chemists Society, New York, New York
15–17 National Academy of Sciences, Berkeley, California
19–20 X-Ray and Diffractionists Conference (Southeast Section), Detroit, Michigan
26–27 American Physical Society, Chicago, Illinois
28–December 3 American Society of Mechanical Engineers (Annual Meeting), New York, New York

December

5–8 American Society of Refrigerating Engineers, Washington, D. C.
12–13 American Chemical Society (Southwestern Regional Meeting), Houston, Texas
26–31 American Association for the Advancement of Science, New York, New York
26–31 Mathematical Association of America, Columbus, Ohio
29–30 American Chemical Society (Division of Industrial and Engineering Chemistry), Chicago, Illinois

January, 1949

27–29 American Physical Society, New York, New York

On the Canonical Form of the Equations of Steady Motion of a Perfect Gas

MAX M. MUNK AND ROBERT C. PRIM
Naval Ordnance Laboratory, Washington, D. C.
(Received June 25, 1947)

The equations for general steady motion of a perfect gas are expressed in terms of a reduced number of basic dependent variables. Neither constant entropy nor constant flow energy is assumed throughout the flow, but only along individual streamlines. The basic dependent variables used are the "reduced velocity" vector

$$\mathbf{w}\equiv\mathbf{v}\Big/\left(\frac{2\gamma}{\gamma-1}\frac{p}{\rho}+v^2\right)^{\frac{1}{2}}$$

and the logarithm of the pressure, $\ln p$. The resulting form of the dynamic equation is

$$(\mathbf{w}\cdot\text{grad})\mathbf{w}+\frac{\gamma-1}{2\gamma}(1-w^2)\,\text{grad}\ln p=0,$$

and that of the continuity equation is

$$\text{div}[(1-w^2)^{1/\gamma-1}\mathbf{w}]=0,$$

representing four equations in four unknowns. The fundamental characteristic and shock relations are also expressed in terms of these reduced variables.

INTRODUCTION

THE following analysis relates to the steady motion of a perfect gas as ordinarily defined: that is, of a gas with constant specific heats in which viscosity and heat conduction are negligible except within infinitely thin shock regions. Absence of body forces is assumed.

The study of such motions involves basically eight variables. There are three independent variables, namely, the three space coordinates. There are five dependent variables, namely, the three components of the velocity vector $\mathbf{v}$ and two variables of state, such as the pressure p and the density ρ of the gas. Consequently the number of independent equations available must also be five. There is the equation of continuity

$$\text{div}(\rho\mathbf{v})=0 \tag{1}$$

and there are also the three equations of dynamic equilibrium

$$(\mathbf{v}\cdot\text{grad})\mathbf{v}+(1/\rho)\,\text{grad}p=0. \tag{2}$$

The necessary fifth equation follows from the fact that in an inviscid, non-conducting gas the flow along any streamtube is necessarily adiabatic. However, it must not be assumed that any single adiabatic expansion relation holds throughout the entire flow, but merely that along each individual streamline the particles expand and contract adiabatically. A different adiabatic expansion curve will, in general, be associated with each different streamline. These considerations result in the so-called "weak" Bernoulli equation

$$a^2=v^2+(2\gamma/\gamma-1)(p/\rho), \tag{A}$$

where $a^2\equiv$the square of the ultimate flow velocity, and $\gamma\equiv$the ratio of the specific heat at constant pressure to that at constant volume. It has the attribute "weak" because a^2, the square of the "ultimate velocity," is constant along each individual streamline, but does not necessarily have the same values at two different streamlines. This limitation is introduced into the mathematical analysis by means of the equations:

$$\mathbf{v}\cdot\text{grad}a^2=\mathbf{v}\cdot\text{grad}(v^2+(2\gamma/\gamma-1)(p/\rho))=0, \tag{3}$$

the dot denoting, as usual, scalar multiplication.

REDUCTION OF THE SYSTEM OF EQUATIONS

These five equations (1) to (3) involving five dependent variables will now be reduced to a system of four equations involving four dependent variables. This reduction is carried out by means of the substitution

$$\mathbf{v}=\mathbf{w}a \tag{4}$$

"a" denoting the positive root of a^2 in Eq. (A). It is noted that the local Mach number of the

flow is immediately connected with the reduced velocity (4) by means of

$$M^2=(2/\gamma-1)(w^2/1-w^2). \tag{5}$$

The transformation of (1) and (2) making use of (3) is straightforward and yields

$$(\mathbf{w}\cdot\text{grad})\mathbf{w}+(\gamma-1/2\gamma)(1-w^2)\ \text{grad}\ \ln p=0 \tag{6}$$

and

$$\text{div}[(1-w^2)^{1/\gamma-1}\mathbf{w}]=0. \tag{7}$$

Equation (7) is in a familiar form but has a much more general meaning than the similar equation often found in the literature in connection with potential flows. Equations (6) and (7) constitute the canonical form of the most general system of equations for the steady motion of a perfect gas.

CHARACTERISTICS

The characteristic relations are generally of interest for two-dimensional problems only. Since the equations of motion have been reduced together with the number of variables so that only one variable of gas state, namely, the pressure, occurs, it follows that the conditions holding along characteristics can also be written in terms of only pressure and geometric quantities. Indeed, the well-known[1] relations reduce to the following form

$$\frac{1}{\gamma}d\ \ln p\mp\frac{1}{\sin\mu\ \cos\mu}d\theta+\frac{\sin\theta}{\cos\mu\ \sin(\theta\mp\mu)}d\ \ln r=0, \tag{8}$$

where $\mu\equiv$the Mach angle$\equiv$arc sin $1/M$, $\theta\equiv$the streamline inclination angle, and $r\equiv$the distance from axis of symmetry ($d\ \ln r=0$ for plane two-dimensional flow).

SHOCK WAVES

Across shock fronts, the ultimate velocity a is conventionally assumed to preserve its magnitude. Hence Eq. (3) expresses a relation extending even across shock waves.

For a normal shock front the direct relation between the ratio of the pressures p_1 and p_2 in front of and behind the shock and the corresponding reduced velocities w_1 and w_2 are well known

$$\frac{p_2}{p_1}=\frac{\left(\frac{\gamma+1}{\gamma-1}\right)^2 w_1^2-1}{\frac{\gamma+1}{\gamma-1}(1-w_1^2)}, \tag{9}$$

$$w_1w_2=\frac{\gamma-1}{\gamma+1}. \tag{10}$$

With oblique shock waves, having the two shock angles σ_1, and σ_2, the equations become

$$\frac{p_1}{p_2}=\frac{\left(\frac{\gamma+1}{\gamma-1}\right)^2 w_1^2\sin^2\sigma_1-1}{\frac{\gamma+1}{\gamma-1}(1-w_1^2\sin^2\sigma_1)}, \tag{9a}$$

$$w_1\sin\sigma_1\cdot w_2\sin\sigma_2=\frac{\gamma-1}{\gamma+1}, \tag{10a}$$

together with

$$w_1\cos\sigma_1=w_2\cos\sigma_2. \tag{11}$$

It becomes thus apparent that the reduction of the number of basic variables is not restricted to regions between shock waves, but relates to the entire flow including shock waves.

CONCLUSION

The reduction of the number of equations and of the number of variables thus presented illustrates an important feature of the gas motion problem. Clearly then, each streamline pattern serves for a great many gas flows, all of which have their basic mathematical features in common.[2] The general problem does not go beyond the apparently specialized problem of studying gas motions with constant ultimate velocity throughout the entire flow. All possible steady motions of a perfect gas can be reduced to such flows. Potential flows, however, are truly special and lead to reduced velocities likewise having a potential. Indeed, in any case of uniform total enthalpy the reduction carried out in this paper becomes trivial.

Authors' Note: It has been brought to our attention that many of the results in this paper have been arrived at independently by B. Hicks, P. Guenther, and R. Wassermann (Quar. App. Math. 5, 357–361 (1947)).

[1] R. Meyer, "The Method of Characteristics for Problems of Compressible Flow Involving Two Independent Variables," presented at the Sixth International Congress of Applied Mechanics, Paris (1946).

[2] M. Munk and R. Prim, "On the Multiplicity of Steady Gas Flows Having the Same Streamline Pattern," Proc. Nat. Acad. Sci., May 1947.

Letter to the Editor

Production of Ice Crystals by the Adiabatic Expansion of Gas

BERNARD VONNEGUT
General Electric Research Laboratory, Schenectady, New York
July 15, 1948

IN experiments on a supercooled cloud produced in a home freezer, V. J. Schaefer[1] showed that at temperatures of −38.9°C or lower water vapor spontaneously forms ice crystals in very large numbers. By the adiabatic expansion of air in a Wilson cloud chamber, B. M. Cwilong[2] found, similarly, that ice crystals were produced at temperatures below −35°C. Simple and interesting experiments can be performed by a combination of these two techniques.

A child's pop gun fired into a supercooled cloud in a cold chamber produces very large numbers of ice crystals. The adiabatic expansion of the air as it is released from the gun reduces its temperature to below −38.9°C, with the consequent production of large numbers of ice crystals. If the cork is not put into the gun tightly enough, the temperatures produced are above −38.9°C and no ice crystals result.

In order to rule out the possibility that the loud noise from the pop gun might have caused nucleation, a mixture of potassium chlorate and sulfur was exploded in the supercooled cloud. Although the report was far louder than the pop gun, no ice crystals were observed.

A bottle of carbonated beverage having sufficient pressure produces large numbers of ice crystals when it is suddenly opened in a supercooled cloud. Bottles of carbonated drinks kept in the freezing compartment of a household refrigerator often become supercooled. Frequently, these bottles do not freeze until the cap is removed. If such a bottle is watched as the cap is removed, many ice crystals can be seen to form at the surface of the liquid and spread throughout the bottle. A miniature snow storm produced in the gas in the neck of the bottle starts the crystallization of the contents. It has been observed that a bottle of supercooled beverage can be caused to freeze by tapping the surface of the container. Such a tap undoubtedly causes adiabatic compression and expansion of any minute bubbles in the liquid which could momentarily reduce their temperature to below −38.9°C, thus starting the formation of ice crystals.

The vapor trails which sometimes stream off the propeller tips and wings of airplanes flying at low temperatures probably are similar to the foregoing phenomena. As the propeller or wing passes through the air, it causes adiabatic expansion of the air in certain regions. If the temperature of the atmosphere is sufficiently low, this expansion will momentarily reduce the temperature to a value at which ice crystals form spontaneously. If the atmosphere is supersaturated with respect to ice, these ice crystals will grow into a visible vapor trail.

The surprisingly large number of ice crystals produced by the rapid expansion of even a small quantity of air can be shown by bursting a small rubber balloon in a supercooled cloud. A balloon about 1.5 mm in diameter when burst in a supercooled cloud at −20°C produces at least 3×10^7 snow crystals, or about 1.6×10^{10} crystals per cc of expanded air.

Experiments under carefully controlled conditions are being conducted in this laboratory by V. J. Schaefer to determine quantitative relationships between the number of crystals produced and the temperature, pressure, volume, and humidity of the expanded air.

[1] (a) V. J. Schaefer, "The production of ice crystals in a cloud of supercooled water droplets," Science **104**, 457 (1946); (b) V. J. Schaefer, "The production of clouds containing supercooled water droplets or ice crystals under laboratory conditions," Bull. Am. Meteorolog. Soc. **29**, 175 (1948).
[2] B. M. Cwilong, Nature **155**, 361 (1945).

Recent Books

Pure and Applied Mathematics

METHODS OF ALGEBRAIC GEOMETRY. VOLUME I

BY W. V. D. HODGE AND D. PEDOE. Pp. 440+viii. Cambridge University Press, Teddington, and The Macmillan Company, New York, 1947. Price $6.50.

The first part of the book is devoted to the basic notions of pure algebra and the development of the theory of matrices. Book II, the major portion of the volume, discusses the algebraic and synthetic definitions of projective space, through Grasman coordinates, collineations, and correlations. Complete proofs are given for most theorems; however, in a number of special cases the proofs are not noted in detail when sufficiently simple. The theory of algebraic varieties and the study of certain loci will be treated in Volume II, to be announced.

ADVANCED CALCULUS

BY DAVID V. WIDDER. Pp. 432+xvi. Prentice-Hall, Inc., New York, 1947. Price $5.00.

Theoretic problems are introduced after the problems of elementary calculus have been reviewed. The Stieltjes integral and the Laplace transform are dealt with in three chapters. Included are an index of symbols as well as a full subject index.

INTRODUCTION TO MATHEMATICAL STATISTICS

BY PAUL G. HOEL. Pp. 258+x. John Wiley and Sons, Inc. New York, 1947. Price $3.50.

A comprehensive, well-written introduction to important work in the field, this book was designed to serve as a college text for a two-semester course in mathematical statistics. It includes both the classical and modern methods. The majority of the large-sample methods are concentrated in the first part of the book to give students taking only

one semester of work a fairly unified treatment. Topics include sampling inspection, design of experiments, analysis of variance, sequential analysis, and non-parametric methods of analysis. Numerous examples and exercises illustrate the material.

FUNCTIONS OF A COMPLEX VARIABLE

Third edition. By Thomas M. Macrobert. Pp. 390+xv. The Macmillan Company, New York, 1947. Price $4.50.

Enlarged in scope to include an appendix on generalized hypergeometric functions and miscellaneous examples, the book otherwise remains unchanged from the second edition.

VECTOR AND TENSOR ANALYSIS

By Louis Brand. Pp. 439+xvi. John Wiley and Sons, Inc., New York, 1947. Price $5.50.

The author discusses vectors and tensors as applied to mechanics, hydrodynamics, and electrodynamics, with an introduction to the algebra of motors. It may be used as a college text, since there are problems in each chapter showing applications of material covered. The most important results are given as theorems, with essential conditions clearly stated.

MATRIX AND TENSOR CALCULUS; WITH APPLICATIONS TO MECHANICS, ELASTICITY, AND AERONAUTICS

By Aristotle D. Michal. Pp. 132+xiii. John Wiley and Sons, Inc., New York, 1947. Price $3.00.

An outgrowth of a series of lectures on the subjects given under the sponsorship of the Engineering, Science, and Management War Training Program in 1942–43, this book is divided into two parts. The first deals with matrix calculus, an analytic and algebraic subject, as distinguished from tensor calculus, which is discussed in the second part. The author attempts to give a working knowledge of the subjects applicable to engineering and theoretical research.

APPLIED MATHEMATICS FOR ENGINEERS AND PHYSICISTS

By Louis A. Pipes. Pp. 618+xiii. McGraw-Hill Book Company, Inc., New York, 1946. Price $5.50.

The mathematics used in electrical, mechanical, and civil engineering, as well as in classical physics, is dealt with in this book. Specifically the material covers the Laplace transforms, matrices, finite differences and conformal mapping. The techniques of applied mathematics are stressed and problems are taken from all engineering fields, particularly in electronics.

LECTURES ON THE CALCULUS OF VARIATIONS

By Gilbert A. Bliss. Pp. 296+ix. University of Chicago Press, Chicago, 1946. Price $5.00.

Divided into two parts—The Simpler Problems and The Problem of Bolza—this book is based on selected material from numerous courses given by the author. Few illustrative examples have been given for the first six chapters, dealing with problems in three dimensions. A bibliography on the problem of Bolza has been included for the first time in book form.

MANUAL OF MATHEMATICS AND MECHANICS

Second edition. By Guy Roger Clements and Levi Thomas Wilson. Pp. 349+x. McGraw-Hill Book Company, Inc., New York, 1947. Price $3.75.

The section of mechanics has been revised, as well as new material added on the mathematics of electrical engineering. Useful as a reference tool for the engineer. The paper and print make for ease in reading, and a glossary and tables for physics courses have been appended.

INTRODUCTION TO THE DIFFERENTIAL EQUATIONS OF PHYSICS

By L. Hopf. Translated by Walter Nef. Pp. 154+v. Dover Publications, Inc., New York, 1948. Price $1.50.

Written in a style which is direct and easily understood, this little volume is aimed at those readers whose mathematical training is limited to elementary calculus. Beginning with the basic concept of the equation, the author develops the differential principle through solutions by eigenfunctions, change of variables, and the use of singularities. Subject index for important terms and equations.

SEQUENTIAL ANALYSIS

By Abraham Wald. Pp. 212+xii. John Wiley and Sons, Inc., New York, 1947. Price $4.00.

In presenting the theory of sequential analysis as a method of statistical inference, this book deals with the sequential probability test. The mathematical development is designed for the reader who is limited to college calculus. The book is divided into three parts: general theory, application of general theory to special cases, and the problem of multivalued decisions and estimation, with an appendix containing sections of two papers on the subject published by the author in 1944 and 1945.

PROCEEDINGS OF A SYMPOSIUM ON LARGE-SCALE DIGITAL CALCULATING MACHINERY

Jointly sponsored by the Navy Department Bureau of Ordnance and Harvard University at the Computation Laboratory, January 7–10, 1947. Pp. 302+xxix. Harvard University Press, Cambridge, Massachusetts, 1948. Price $10.00.

This is Volume XVI of the Annals of the Computation Laboratory of Harvard University. The papers presented here bring together for the first time the widely divergent opinions of the best methods of further increasing the adaptability of large-scale digital calculating machinery. Speakers from industry and research make this the most advanced statement of the future development of this field. The material covers existing calculators, storage devices, numerical methods, sequencing, coding, and input and output devices.

NOMOGRAPHY

By Alexander S. Levens. Pp. 176+viii. John Wiley and Sons, Inc., New York, 1948. Price $3.00.

Originally published in 1937 as *Alignment Charts*, this new edition has been revised and the bibliography brought up to date. The material is based on nomography courses given by the author, dealing with alignment charts of straight line scales and more complex forms of four or more variables, including curved scales and combinations of Cartesian coordinate charts with alignment charts. Each chapter is followed by exercises based on the explanatory material. Chapters are devoted to miscellaneous forms, practical short cuts, and the use of determinants. A bibliography and an appendix illustrating useful forms are included. The index covers subjects and form equations.

TABLES OF INTEGRALS AND OTHER MATHEMATICAL DATA

Revised edition. By Herbert Bristol Dwight. Pp. 250+x. The Macmillan Company, New York, 1947. Price $2.50.

To the fundamental and advanced definitions in the first edition have been added new integrals, material on inverse functions and on Bessel functions. A probability table has been included. No derivations are shown in this synopsis of compact results. A full list of references and an index are given.

ELEVEN- AND FIFTEEN-PLACE TABLES OF BESSEL FUNCTIONS OF THE FIRST KIND, TO ALL SIGNIFICANT ORDERS

By Enzo Cambi. Pp. 154+vi. Dover Publications, Inc., New York, 1948. Price $3.95.

A contribution to the field of Bessel functions of the high order. The main table gives $J_n(x)$ for x varying from 0 to 10.5 at intervals 0.01, and for $n=0$ (1) 29, to eleven places. Values of $J_n(x)$ for x varying from 0 to 0.5, at interval 0.001 to fifteen places and $n=0$ (1) 11 are given in a supplementary table.

A LOCUS WITH 25,920 LINEAR SELF-TRANSFORMATIONS

By H. F. Baker. Pp. 107+xi. Cambridge University Press, Teddington, and The Macmillan Company New York, 1947. Price $2.00. Cambridge Tracts in Mathematics and Mathematical Physics No. 39.

This booklet is concerned with a locus exhibiting the structure of the group of the lines of a cubic surface, regarded as the group of the tritangent planes of the surface. Substitutions of 4, 5, and 6 objects are explained in detail.

Mechanics, Fluid Dynamics, and Materials

AN INTRODUCTION TO MECHANICS

By J. W. Campbell. Pp. 372+xviii. Pitman Publishing Corporation, New York, 1947. Price $4.50.

Based on the principle of teaching mechanics by emphasizing the physical problems, the book introduces calculus and the vector calculus in its mathematics section, assuming the student to have a background of calculus or to be taking it simultaneously with a course in mechanics. Particle dynamics, gravitation, an introduction to Lagrange's equations, and catenary calculations are dealt with in separate chapters. Appendices cover standard forms of calculus, Simpon's Rule, hyperbolic functions, and bracketing. Tables, answers to example problems, and an index follow.

RELATIVITY: THE SPECIAL AND GENERAL THEORY

By Albert Einstein. Pp. 168+xiii. Reprinted by Hartsdale House, Inc., New York, 1920. Price $2.50.

This reprint is the same edition that was published in 1920, authored by the then "unknown" physicist. It is directed to the reader who has only a high school education, and the book is a straightforward explanation of the theories and principles.

LES TENSEURS EN MÉCANIQUE ET EN ÉLASTICITÉ

By Leon Brillouin. Pp. 364+x. Dover Publications, Inc., New York, 1946. Price $3.75.

This book, written in French, is an exposition of tensor analysis and its applications in theoretical physics. The material covers vector geometry, pseudo-tensors and pseudo-scalars, the principal differential operators, parallelism, Riemann space, elasticity, and waves in elastic solids. Hamilton's equations and the adiabatic invariant of Ehrenfest are discussed in the use of Riemannian geometrics in analytical mechanics.

ANALYTICAL METHOD IN DYNAMICS

By H. O. Newboult. Pp. 81. Oxford University Press, London, 1946. Price $2.50.

The author considers the motion of bodies in accelerated reference systems, and applies to specific problems the basic laws of motion derived from Newton's laws or Lagrange's equations. He deals with the motions of a rigid body and a top, the motion relative to the rotating earth, Euler's dynamical equation, and the motion of an inextensible flexible chain.

ELEMENTARY MECHANICAL VIBRATIONS

By Austin H. Church. Pp. 200+ix. Pitman Publishing Corporation, New York, 1948. Price $3.25.

This text will enable students to handle vibration problems from the standpoint of a physical explanation of the phenomena. The author does not attempt to cover self-excited vibrations, nonlinear systems, or vibrations of more than one degree of freedom. The bibliography is limited to the references used. Problems at the end of each chapter.

THE ESCALATOR METHOD IN ENGINEERING VIBRATION PROBLEMS

By Joseph Morris. Pp. 270+xv. John Wiley and Sons, Inc., New York, 1947. Price $4.50.

Dealing with the methods developed by the author for working with strength and vibration problems, particularly in aircraft engineering, this book is an explanation of the "escalator" process whereby it is possible to make Lagrangian frequency equations numerically tractable. It attacks a complicated system by eliminating linking coordinates or reactions.

ELEMENTS OF MECHANISM

Sixth edition, revised and rewritten by Venton Levy Doughtie. By Peter Schwamb, Allyne L. Merrill and Walter H. James. Pp. 428+xi. John Wiley and Sons, Inc., New York, 1947. Price $4.00.

This revision continues the original approach of the authors, but recent data and laboratory problems illustrating practical applications of theory have been added. A quantitative and extensive treatment covers motion analysis, linkages, cams, gears, worms, trains, etc., with analyses of motion, vectors, and acceleration.

PHOTOELASTICITY. VOLUME II

By Max M. Frocht. Pp. 505+xvii. John Wiley and Sons, Inc., New York, 1948. Price $10.00.

A continuation of Photoelasticity, Volume I, published in 1941. Consisting of fourteen chapters, the book may be divided into three parts covering the theory of elasticity for engineers, isopachic patterns, and the theory and applications of three-dimensional photoelasticity. New material is presented in print for the first time, discussing comparative stress patterns and new aspects for the numerical solutions of Laplace's Equation. Emphasis is on simplicity and clarity, with unusual detail. An appendix deals with the discussion of general characteristics and quantitative tests of Fosterite. Contains indexes for names and subjects.

WIND-TUNNEL TESTING

By Alan Pope. Pp. 319+xii. John Wiley and Sons, Inc., New York, 1947. Price $5.00.

"Students, tunnel engineers, and those engaged in low-cost wind-tunnel design" will find this book is an attempt to correlate in one source data which heretofore has appeared in various reports as well as the author's own work. All phases of wind-tunnel testing are covered, from their construction through the procedures for testing and the interpretation of results. Problems and references are at the end of each chapter.

MECHANICS OF MATERIALS

Second edition. By Philip Gustave Laurson and William J. Cox. Pp. 422+x. John Wiley and Sons, Inc., New York, 1947. Price $4.00.

Changes in the second edition include additional topics and problems. Data in the old problems has been changed and new examples given. The book emphasizes the physical behavior of the stressed bodies as well as the usual mathematical treatment. The presentation of the material is in a clear, understandable manner, and extreme conciseness has been avoided.

RESISTANCE OF MATERIALS

Third edition. By Fred B. Seely. Pp. 486+xiv. John Wiley and Sons, Inc., New York, 1947. Price $4.00.

Emphasis is from the engineering standpoint, not merely the mathematical methods. This edition introduces changes in the treatment of the subject by the recent trends in the use of lightweight metals, plastics, and high-strength materials, as well as welds and the use of metals at low temperatures. Devoted to engineering problems in general rather than any particular field, those features that made the previous editions valuable as ready references have been retained, with new problems and figures added.

FLIGHT ENGINEERING AND CRUISE CONTROL

By Harris G. Moe. Pp. 209+xi. John Wiley and Sons, Inc., New York, 1947. Price $4.00.

Although designed as an aid to pilots and crew-men desiring a background of technical knowledge necessary for a true understanding of airplane and engine operations, this volume will also prove helpful to engineers and students of aeronautics. The material covers altimeters and types of altitude, air speed, propellers, cruising techniques, flight planning and control, weight balance. A chapter on jet propulsion discusses its principles and probable future developments. Not unnecessarily technical, it is clear and well-written.

Heat, Thermodynamics, and Heat Engines

HEAT

By Archie G. Worthing and David Halliday. Pp. 522+xii. John Wiley and Sons, Inc., New York, 1948. Price $6.00.

This book is designed as a text for an undergraduate course, covering "classical heat," and emphasizing experimental methods. The authors have attempted to keep definitions and terms consistent throughout, thereby eliminating causes for confusion. Each chapter has a short introduction followed by theory, experiments, and problems. There are author and subject indexes.

A TEXTBOOK OF HEAT

By G. R. Noakes. Pp. 469+viii. MacMillan and Company, Ltd., London, 1947 (c1945). Price $3.00.

The author is a professor of engineering at the University of Sheffield. He stresses an understanding of the principles of the study of heat rather than the mathematical work. Chapters deal with measurement, expansion, vapour, heat engines, and heat phenomena in the atmosphere. Answers to problems are given at the end of the book.

CONDUCTION OF HEAT IN SOLIDS

By H. S. Carslaw and J. C. Jaeger. Pp. 386+viii. Oxford University Press, London, 1947. Price $8.00.

Because of the many advances in the subject, this book, although based on the author's previous work, *Introduction to the Mathematical Theory of the Conduction of Heat in Solids*, is intended to supersede it. Chapters 1–10 follow the plan of the older book in discussing the Fourier mathematics, but the later chapters replace the method of contour integration with that of the Laplace transformation, where applied to more difficult problems. Footnote references provide a guide to the literature of the subject.

TIME AND THERMODYNAMICS

By A. R. Ubbelohde. Pp. 110+vii. Oxford University Press, London, Price 6s.

A description, in non-technical terms, of the historical development of the concept of entropy, for its significance in measuring the trend of events in time. Beginning with the notion of systems, illustrations of statistical equilibria are given for a fundamental understanding of time. Radiation equilibrium and its relation with the Primacy of Vison are dealt with, followed by chapters showing that the laws of thermodynamics are derived from studies on inanimate matter.

MICROCALORIMETRY

By W. Swietoslawski. Pp. 199+x. Reinhold Publishing Corporation, New York, 1946. Price $4.75.

As the first book on microcalorimetry, this work should prove useful as an introduction to the field. The author, who has published numerous reports on this subject while at the Institute of Technology in Warsaw, discusses methods and types of measurements, particularly those he has used himself.

GAS DYNAMICS FOR AIR

By Howard W. Emmons. Pp. 46. Dover Publications Inc., New York, 1947. Price $1.75 (booklet).

This little booklet presents four tables and their graphs, produced for use in research at Harvard University. The tables include isentropic gas dynamics for air, gas dynamic functions for normal shocks, a characteristic table, and an acoustic velocity-temperature table.

HEATING, VENTILATING, AND AIR CONDITIONING GUIDE. VOLUME XXVI, 1947

Pp. 1280 (+144)+xxiv. American Society of Heating and Ventilating Engineers, New York, 1948. Price $7.50.

This edition contains an expanded Technical Data Section covering theory and current practice in the field. Many chapters have been revised, but the order is the same as in previous editions. Important changes were made in the chapters on heating and cooling, automatic control and air distribution and a new chapter has been added on corrosion. A Manufacturers' Catalog section is included.

INDUSTRIAL ELECTRIC FURNACES AND APPLIANCES. VOLUME II

By V. Paschkis. Pp. 320+xiv. Interscience Publishers, Inc., New York, 1948. Price $8.00.

The second volume of this work on industrial furnaces discusses a field in which diversity of design is more pronounced than in those types of furnaces covered in the first volume, which was published in 1945. The material is grouped in three chapters, namely, resistance furnace and appliances, induction and high frequency capacitance heating, and the selection of furnaces. It emphasizes the thermal aspects and the relationship between electrical and thermal problems. A classification of furnaces is introduced to help simplify design and nomenclature. It contains a subject index.

JET PROPULSION PROGRESS; THE DEVELOPMENT OF AIRCRAFT GAS TURBINES

By Leslie E. Neville and Nathaniel F. Silsbee. Pp. 232+xii. McGraw-Hill Book Company, Inc., New York, 1948. Price $3.50.

A detailed account of the development and potentialities of the gas turbine. Comprehensive in scope, it draws upon the experience of Germany and the Allies, describing and evaluating the various designs as applied to aircraft. Since highly technical discussions have been omitted, this book should prove useful, as well as interesting, to executives and professional men who wish to have a general survey in one volume. A glossary and bibliography will make this usable as a reference to more technical material.

PRINCIPLES OF JET PROPULSION AND GAS TURBINES

By M. J. Zucrow. Pp. 563+xiv. John Wiley and Sons, Inc., New York, 1948. Price $6.50.

This text for students is a comprehensive volume covering the basic principles of jet engines. It discusses "the workings of the continuous combustion gas turbine, the three basic types of air compressors, the axial flow turbine, the combustion chamber, and high-temperature metallurgy." Equations introduced in chapters are applied by examples and solutions. A bibliography concludes each chapter, supplementing the material used. The author is Professor of Gas Turbines at Purdue University. This book is an expansion of a course taught by him under sponsorship of the ESMWT project.

Acoustics

MUSICAL ACOUSTICS

Second edition. By Charles A. Culver. Pp. 215+xiv. The Blakiston Company, Philadelphia, 1947. Price $3.00.

The book has been revised and a chapter added on the recording and reproduction of music. It is comprehensive

but concise, and is a readable book for those interested in the physics of music. Since the mathematics is limited, it will serve as a text for music majors in college. The author considers the concepts of music, tone propagation of several instruments, and acoustics of rooms.

VISIBLE SPEECH

By Ralph K. Potter, George A. Kopp, and Harriet C. Green. Pp. 441+xvi. D. Van Nostrand Company, Inc., New York, 1947. Price $4.75.

This book deals with a new form of visible speech obtained by recording, and analyzes speech in a manner similar to that performed by the ear. It is written in a non-technical language for those readers working with the deaf, teaching languages, or interested in phonetics, speech, and vocal music. A description of the electronic principles involved, the results of experimental training of individuals in understanding speech by eye, instructions in reading Visible Speech, and the practical applications are included. Many illustrations supplement the text.

Electricity, Magnetism, and Electronics

ELECTRONIC TRANSFORMERS AND CIRCUITS

By Rueben Lee. Pp. 282+vii. John Wiley and Sons, Inc., New York, 1947. Price $4.50.

Here is a reference book on the design of electronic apparatus and effects of transformer characteristics on electronic circuits. Written for the designer of electronic equipment, but it will be useful to anyone who is interested in this field and is acquainted with circuit theory and transformer principles. Mathematical proofs are minimized, the treatment throughout being quantitative. Wartime development of video and pulse transformers is dealt with in detail. An appendix of formulas, bibliography, and an index are included.

UNDERSTANDING VECTORS AND PHASE

By John F. Rider and Seymour D. Uslan. Pp. 153+vi. John F. Rider Publisher, Inc., New York, 1947. Price $0.99.

Written for the radio technician, amateur, or student who has not had an engineering background. Beginning with the definition and elementary concepts, the book is developed through multiple representation, resolution and mathematics of vectors, and radio circuit problems.

ELECTRONIC CIRCUITS AND TUBES

By the Electronics Training Staff of the Cruft Laboratory, Harvard University. Pp. 948+xxiv. McGraw-Hill Book Company, Inc., New York, 1947. Price $7.50.

Emphasis is on applications in the fields of electronic control, although the book covers the basic theory of electron tubes and circuits. It is an outgrowth of a wartime training course but much new material has been added, including correlating response curves, filters, and power tubes. Individual chapters have been written by various authors and are very detailed, making the book a reference tool for electronic work. Appendices contain supplementary material on mathematics, electricity, and magnetism. A subject index is included.

VACUUM TUBES

By Karl R. Spangenburg. Pp. 860+xvii. McGraw-Hill Book Company, Inc., New York, 1948. Price $7.50.

Based on a course in vacuum-tube design given at Stanford University, this volume is a comprehensive survey of physical laws and their applications in this field. The author emphasizes the internal factors contributing to the operating characteristics of most tube types, and discusses the fundamental techniques of analysis necessary for understanding tube behavior. Except in the case of ultra-high-frequency tubes, circuits and tube applications have been omitted. Magnetrons, klystrons, and special tubes are covered, and recent material, including that not previously in book form, pertaining to space charge, flow, noise, characteristics of triodes, tetrodes, and pentodes, is given. The appendices contain problems, design charts, nomographs. The name and subject index are extensive.

ELECTRONICS: AND THEIR APPLICATION IN INDUSTRY AND RESEARCH

Edited By Bernard Lovell. Pp. 660+xvi. The Pilot Press, Ltd., London, 1947. Price 42s.

The objective of this book is to provide a survey of the major developments of electronic devices over the last ten years. In fourteen chapters by various authors, it is essentially a series of monographs on various subjects in electronics; however, there is little duplication, and very few errors. Concentrating on the war-time advances, the material covers the klystron, betatron, electron microscopy, and television. A bibliography is included in each chapter, and the subject index is most complete.

A SURVEY OF THE PRINCIPLES AND PRACTICE OF WAVE GUIDES

By L. G. H. Huxley. Pp. 328+xi. The Macmillan Company, New York, 1947. Price $4.75.

An introductory survey of the recent developments of wave guides, this book is an outgrowth of courses given in the Radar School at the Telecommunications Research Establishment. It is a clear and accurate account, with many explanatory diagrams, containing much material which heretofore has been classified and secret. The mathematics of the field are treated in the last chapter, allowing readers with limited mathematical background to understand the contents more easily.

ELECTRONIC ENGINEERING PRINCIPLES

By John D. Ryder. Pp. 397+x. Prentice-Hall, Inc., New York, 1947. Price $5.00.

Although designed to present electronics to students, the text is clear and complete enough to serve the reader

studying alone, or useful as a reference to the engineer in the field. Dealing with electronics as an independent field, the author applies it to all phases of electrical engineering. Supplying the fundamentals of electron tubes, it assumes a background knowledge of the alternating-current network theory.

RADAR ENGINEERING

By Donald Fink. Pp. 644+xii. McGraw-Hill Book Company, Inc., New York, 1947. Price $7.00.

Collected in a single volume is all the information on radar necessary to describe the special applications used in radio detecting and ranging of objects to engineers in radio and electronics. Part I covers the theory of radar technology, and Part II the components, structure, and the various types of circuits used in radar equipment. Although this is not an overly mathematical book, a knowledge of calculus and harmonic functions would be of help to the reader.

TELEVISION, VOLUME III; TELEVISION, VOLUME IV

Edited By Alfred N. Goldsmith and others. Vol. III. Pp. 486+xii. Radio Corporation of America, Princeton, New Jersey, 1946. Price $2.50. Vol. IV: Pp. 510+xiv. Radio Corporation of America, Princeton, New Jersey. Price $2.50.

These two volumes follow the pattern of the first two in the Television series. Volume III surveys the years 1938–1941, and Volume IV, 1942–1946. The arrangement of both covers pick-up, transmission, and reception, with the addition of parts covering color and military television in Volume IV. A summary of the paper is presented at the beginning of each monograph. An appendix in Volume III summarizes the monographs in Volumes I and II.

FREQUENCY MODULATION, VOLUME I

Edited By Alfred N. Goldsmith, and others. Pp. 515+x. Radio Corporation of America, Princeton, New Jersey, 1948. Price $2.50.

This volume is the seventh in the RCA Technical Book Series and the first on the subject of FM. The material is presented in abstract form only, in four sections: general, transmission, reception, and miscellaneous. It contains papers that have appeared in various publications in the period 1936–1947. References and bibliographies are numerous, with two appendices listing papers on FM and station placement.

NEW DEVELOPMENTS IN FERROMAGNETIC MATERIALS

By J. L. Snoek. Pp. 136+viii. Elsevier Publishing Company, Inc., New York and Amsterdam, 1947. Price $2.50. No. 19 of Monographs on the Progress of Research in Holland.

Discusses the two conceptions of crystal anisotropy and magnetostriction as applied to the theory of ferromagnetic hysteresis. In three parts, it covers the statics of ferromagnetism, the dynamics and the development of magnetic materials, especially of the "ferroxcube" type.

PARAMAGNETIC RELAXATION

By C. J. Corter. Pp. 127+vii. Elsevier Publishing Company, Inc., New York and Amsterdam, 1947. Price $2.25.

The author is a professor of experimental physics at the University of Leyden. This work is a survey, in English, of his own observations with those of Brons, Teunissen, DuPré, Dijkstra, Volger, and especially Broer. An introductory chapter presents the explanatory background for this field, covering normal paramagnetism, various magnetic ions, and dispersion and absorption. Later chapters deal with experimental methods, an evaluation of their results, and the theories of lattice relaxation, spin relaxation, and a discussion of the values of results by experimentation.

KLYSTRON TUBES

By A. E. Harrison. Pp. 271+x. McGraw-Hill Book Company, Inc., New York, 1947. Price $3.50.

The theory and application of klystron tubes, with data on their operation, power supply considerations, modulation methods, timers and measurement methods, are covered. Although mathematical explanations are used, the text is so arranged that they may be omitted by the reader with little mathematical background. Useful design information and new material on multiple resonator tubes are included.

BROADCAST OPERATOR'S HANDBOOK

By Harold E. Ennes. Pp. 265+xiii. John F. Rider Publisher, Inc., New York, 1948. Price $3.30.

As an attempt to fill the gap between the field of radio engineering and practical broadcasting operations, this book, a comprehensive treatment of control-room operation, suggests standards for modern operating technique. Control-room practice, master and remote controls, and transmitters are discussed in the first four parts, while the last two parts are devoted to technical data. The appendix gives a detailed description of a noise meter, a phase monitor, an antenna-current indicator, and a limiting amplifier. Index is included.

Atomic and Nuclear Physics

STATISTICAL THERMODYNAMICS

By Erwin Schrodinger. Pp. 88+v. Cambridge University Press, Teddington, and The Macmillan Company, New York, 1946. Price $1.50.

Originally a course of seminar lectures, this is not a book for those without some background in the subject. As a survey it covers the Nernst theorem, fluctuations, the method of mean values, the n-particle problem, and the problem of radiation and evaluation of formulae.

KINETIC THEORY OF LIQUIDS

By J. Frenkel. Pp. 488+xi. Oxford University Press, London, 1946. Price $13.00.

The title of this book does not indicate its complete scope, since the author discusses all types of disorder in solids, the thermal displacements of the atoms, and the motion of interstitial atoms and ions. The theory of transitions from an ordered to a disordered state is treated at length. The references are taken from papers which have appeared in many journals. Some of the material is already superseded, since the book was written in Moscow in 1942. However, these faults are minor in this valuable contribution to the subject.

ELECTRONS (+ AND −); PROTONS, PHOTONS, NEUTRONS, MESOTRONS, AND COSMIC RAYS

Revised edition. By Robert A. Millikan. Pp. 642+x. University of Chicago Press, Chicago, 1947. Price $6.00.

Although the first 400 pages have been scarcely changed from the 1924 edition, except for new values, the last 200 pages are almost entirely new material, including studies on cosmic rays and the mesotron. While not directed toward the physicist because of the non-mathematical presentation, it is authoritative and will appeal to the layman with some background. The scope of the contents amounts to a survey of atomic study in the 20th century, with the last chapter in the greatest detail covering the atom-annihilation hypothesis as to the origin of cosmic rays.

THE ATOM

By Sir George Thompson. Pp. 196+vii. Oxford University Press, London, 1947. Price $2.00.

This non-mathematical treatise on atomic structures has been revised to bring into account the recent developments in the release of atomic energy. In a readable style, the author explains the early backgrounds and theories of atoms, progressing through methods and results of experiments to a discussion of their structures, atom splitting and nuclear energy. It will appeal to laymen because of its simplicity of description and omission of difficult equations.

DISSOCIATION ENERGIES AND SPECTRA DIATOMIC MOLECULES

By A. G. Gaydon. Pp. 239+xi. John Wiley and Sons, Inc., New York, 1947. Price $5.00.

Heretofore, the various problems connected with the determination of dissociation energies have not appeared in book form. The present work is an attempt to clear up inconsistencies of previous results, while introducing recent developments and summarizing numerical results. Although written from the spectroscopic viewpoint, chapters on thermal methods and controlled electron impact have been included. A full discussion of the theory, as well as new material for CO and N_2, is given. Appendices tabulate low-lying atomic energy terms and the atomic heats of some polyatomic molecules. Author and subject index.

INDEX TO THE LITERATURE ON THE SPECTROCHEMICAL ANALYSIS. PART II, 1940-1945

By Bourdon F. Scribner and William F. Meggers. Pp. 180+iii. American Society for Testing Materials, Philadelphia, 1947. Price $3.00 (paper).

Brief abstracts of articles appearing in foreign journals have been added, since many libraries will have a gap during the war years. Abstracts from *Chemical Abstracts* are in most cases quoted verbatim. A detailed subject index is included.

PRINCIPLES OF QUANTUM MECHANICS

Third edition. By P. A. M. Dirac. Pp. 312+ii. Oxford University Press, London, 1948. Price $9.00.

A third edition of this well-known work has been revised to include results of research since 1935. Improvements in writing have been made; the most notable is the author's use of the notation of bracket vectors. A new treatment of the theory of systems with similar particles has been introduced, as well as a further development of quantum electrodynamics.

THE INTERPRETATION OF SPECTRA

By William Mayo Venable. Pp. 200+v. Reinhold Publishing Corporation, New York, 1948. Price $6.00.

The author offers a point of view on numerical relationships between atomic structure and light which is quite contrary to the usual concepts of atomic and nuclear physics. In the last chapter he speculates on the structure of atomic nuclei. Tables at the end of the book contain data regarding these relationships.

NUCLEAR PHYSICS TABLES AND AN INTRODUCTION TO NUCLEAR PHYSICS

By Josef Mattauch and S. Fluegge. Translated by E. P. Gross and S. Bargmann. Pp. 173, 8 plates. Interscience Publishers, Inc., New York, 1946. Price $12.00.

These Tables, compiled by Mattauch, contain data collected at the Kaiser Wilhelm Institute up to 1941. The first 104 pages of the book are "Introductory and will be especially useful for a brief presentation of the fundamentals of experimental nuclear physics." No literature references are given.

ELEMENTARY NUCLEAR THEORY

By H. A. Bethe. Pp. 147+vii. John Wiley and Sons, Inc., New York, 1947. Price $2.50.

"A short course on selected topics." Emphasis is on discussion of nuclear forces, rather than nuclear physics as a field. It contains a concise account of the descriptive theory of nuclei with the greater body of the book discussing quantitative theory of nuclear forces. Beta-disintegration and the compound nucleus are dealt with briefly; however, nuclear systems of 3 to 60 particles are omitted. Due to its limited scope, this work is not particularly suitable as a text on atomic nuclei. An appendix includes a table of nuclear species. The index is excellent.

MESON THEORY OF NUCLEAR FORCES

By Wolfgang Pauli. Pp. 69. Interscience Publishers, Inc., New York, 1946. Price $2.00.

This book is primarily a survey of the recent literature of the past decade for those who are familiar with the elements of quantum mechanics. Emphasizing the provisional state of the problems, the material is mathematically and descriptively presented with no attempts at explanatory detail.

NUCLEAR PHYSICS IN PHOTOGRAPHS

By C. F. Powell and G. P. S. Occhialini. Pp. 124+xii. Oxford University Press, London, 1947. Price $6.00.

Subtitled "Tracks of charged particles in photographic emulsions," the bulk of the book is made up of photographs with a minimum of descriptive material. Special cases are described at greater length in the appendix. Subjects include natural radio-activity, nuclear transmutations, and disintegrations due to cosmic-ray particles.

Solid State and High Polymers

PREPARATION AND CHARACTERISTICS OF SOLID LUMINESCENT MATERIALS

Edited By Gorton R. Fonda and Frederick Seitz. Pp. 459+xv. John Wiley and Sons, Inc., New York, 1948. Price $5.00.

The book is composed of papers read at a symposium of the Division of Electron Works of the American Physical Society held at Cornell University in 1946. The editors are well-known authorities in the field of luminescent phenomena. The arrangement of contents is by general characteristics, recent developments in theory and experiment, factors affecting fluorescence characteristics, storage of luminescence energy, and miscellaneous aspects of fluorescence.

FOURIER TRANSFORMS AND STRUCTURE FACTORS

By Dorothy Wrinch. Pp. 95+x. The American Society for X-Ray and Electron Diffraction, 1946. Price $4.00. ASXRED Monograph No. 2.

The author is Lecturer in Physics at Smith College. Her monograph is a contribution to the study of structure factors of atomic grouping occurring in crystals, and to the x-ray analysis of megomolecular crystals.

RADIOGRAPHY IN MODERN INDUSTRY

Pp. 122. Eastman Kodak Company, Rochester, New York, 1947. Price $3.00.

This text provides fundamental knowledge necessary for efficient radiographic practice. Theory, principles, procedure, and special techniques are discussed. A bibliography and index are included.

FERROUS METALLURGICAL DESIGN; DESIGN PRINCIPLES FOR FULLY HARDENED STEEL

By John H. Hollomon and Leonard D. Joffe. Pp. 346+x. John Wiley and Sons, Inc., New York, 1947. Price $5.00.

The authors apply scientific principles to metallurgical processes, believing that the design of steels should be based upon the knowledge of the transformations occurring in steel during heat treatment. The mechanical behavior and properties of metals, heat flow, quenching, and hardenability are discussed from the data available at the present time. A full bibliography of the field is given. An index is included.

ESSAYS IN RHEOLOGY

Compiled By British Rheologists Club. Pp. 103+viii. Pitman Publishing Corporation, New York, 1947. Price $3.00.

These essays are based upon papers given at a conference of the British Rheologists Club in 1944. Together they discuss the rheology of metals, polymers and liquids, compression and shear tests, time-variations of stress and strain, and the relationship of the field to medical science, naval problems and the fine arts. A name index is included.

MECHANICAL BEHAVIOR OF HIGH POLYMERS

By Turner Alfrey, Jr. Pp. 581+xiv. Interscience Publishers, Inc., New York, 1948. Price $9.50. Vol. VI of the High Polymers Series.

The author has given most of his attention to the minority of polymers of already known mechanical properties, since it is his aim to show how the fundamental principles underlying mechanical behavior are correlated with the molecular structures involved. In analyzing the behavior of each type of polymer, a phenomenological description and a molecular interpretation have been used. The structures "are classified and treated as amorphous linear, cross-linked, and crystalline polymers, and polymers admixed with components of low molecular weight."

PLASTIC MOLDS; DESIGN, CONSTRUCTION, USE

Third edition. By Gordon B. Thayer. Pp. 272. Huebner Publications, Cleveland, Ohio, 1946. Price $5.00.

To keep in pace with this rapidly growing industry, this third edition has been revised and enlarged to cover the latest improvements in the design, manufacture, and use of molds. Remaining specific throughout, it classifies for study compression mold types, describes transfer and jet molding, and adds a new chapter in estimating plastics molds. A "Nomenclature of Plastics Molding" is included. The table of contents, with a list of chapter sections and a cross-referenced index will make this a useful reference.

CONTRIBUTION TO THE PHYSICS OF CELLULOSE FIBERS

By P. H. Hermans. Pp. 221+xvi, III plates. Elsevier Publishing Company, Inc., New York, 1946. Price $4.00. No. 21 of Monographs on the Progress of Research in Holland.

A study of sorption, density, refraction power and orientation in two parts—theoretical and experimental. This is a summary of the work of the author and his colleagues at the Institute of Cellulose Research at Utrecht. Much of the contents has not been published elsewhere, and includes new material on rayon and natural fibers. A detailed table of contents compensates for lack of an index.

POWDER METALLURGY, ITS PHYSICS AND PRODUCTION

By Paul Schwarzkopf. Pp. 379+xii. The Macmillan Company, New York, 1947. Price $8.00.

The entire field of power metallurgy is covered in this book for metallurgists, machine and tool designers, and experts in the electric, magnetic, and electronic fields who make use of the products of the powder metallurgist. Each of the four sections—processing, products, theoretical principles, and future developments—contains its own extensive bibliography. Presenting his own knowledge of over 30 years in the field, the author discusses the latest developments and future trends. Complete author and subject indexes are given.

Chemical Physics and Chemistry

SURFACE CHEMISTRY FOR INDUSTRIAL RESEARCH

By J. J. Bikerman. Pp. 464+ix. Academic Press, Inc. New York, 1948. Price $8.00.

Surface science adapted to industrial research is the subject of this work. The author stresses the importance of several factors often disregarded, such as the miscibility of "inmiscible" liquids, etc. It should prove useful to research workers and graduate students since the author presents fundamental knowledge rather than the procedures of any industry. Surface physics are also dealt with. References are at the end of each chapter, and author and subject indices at the end of the book.

SMALL WONDER; THE STORY OF THE COLLOIDS

By Gessner G. Hawley. Pp. 220+xxi. Alfred A. Knopf, New York, 1947. Price $3.50.

The new science of the colloids is discussed in nontechnical language, in a brief survey of the principles, problems and achievements in the field. Definitely written for the layman desiring a better understanding of colloids, but the chemist will find it entertaining as an integration of the various aspects of the science.

CURRENTS IN BIOCHEMICAL RESEARCH

Edited By David E. Green. Pp. 486+viii. Interscience Publishers, Inc., New York, 1946. Price $5.00.

"Thirty-one essays charting the present course of biochemical research and considering the intimate relationship of biochemistry to medicine, agriculture, and social problems." There is no index.

THE CORROSION HANDBOOK

Edited By Herbert H. Uhlig. Pp. 1188+xxxiii. Sponsored by The Electrochemical Society, Inc. John Wiley and Sons, Inc., New York, 1948. Price $12.00.

A comprehensive survey of corrosion knowledge with emphasis on quantitative information. Covers corrosion protection and the behavior of metals and alloys at ordinary and elevated temperatures, touching briefly on theories of corrosion and testing. It includes sections on corrosion in liquids, gases, high-temperatures and special agents dealing with metals and non-metallic substances.

CHEMICAL PROCESS PRINCIPLES: PART III, KINETICS AND CATALYSIS

By Olaf A. Hougen and Kenneth M. Watson. Pp. 302+xviii. John Wiley and Sons, Inc., New York, 1947. Price $4.50.

Two professors of chemical engineering at the University of Wisconsin show ways of solving industrial chemical problems through the application of the principles of physical chemistry, by integrating these principles to arrive at optimum economic results from a minimum of pilot plant data. The book presents new methods for dealing with equilibrium problems in extraction, adsorption, dissolution, and crystallization. Problems on chemical and physiochemical processes follow each chapter. Useful conversion tables, author and subject indexes are appended at the end of the book.

PHENOPLASTS, THEIR STRUCTURE, PROPERTIES, AND CHEMICAL TECHNOLOGY

By T. S. Carswell. Pp. 267+xii. Interscience Publishers, Inc., New York, 1947. Price $5.50. Vol. VIII of the High Polymer Series.

Chemists and advanced workers in plastics will find this book is authoritative and accurate. It describes the technique of manufacture, molding methods, and miscellaneous applications of resins. New information not previously published in one volume has been collected, making this a valuable compendium of research in the field.

ENCYCLOPEDIA OF CHEMICAL TECHNOLOGY. VOLUME I

Edited By R. Kirk and D. Othmer. Pp. 982+xxiv. Interscience Publishers, Inc., New York, 1947. Price $20.00.

This encycolpedia is to meet the demand for a work covering, in English, modern American practice in chemical engineering. It will be complete in ten volumes appearing

in two or three volumes per year. The articles have been written by authorities in their respective fields; each volume will have a list of contributors. The editors are the Heads of the Department of Chemistry and the Department of Chemical Engineering at the Polytechnic Institute of Brooklyn. Presenting the entire field of chemical technology, the subject matter includes technological materials, methods, and phenomena. The bibliographies are not extensive and are meant as selected reading lists.

FRONTIERS IN CHEMISTRY. VOLUME V, CHEMICAL ARCHITECTURE

By R. E. Burk and O. Grummitt. Pp. 202. Interscience Publishers, Inc., New York, 1948. Price $4.50.

This is the fifth volume of lectures in chemistry sponsored by Western Reserve University, and deals with the study and determination of intermolecular forces interpreting the architecture of the molecule. The lectures cover (1) applications of molecular geometry in the field reaction mechanism, (2) dipole moment, resonance and molecular structure, (3) structure of coordination compounds, (4) x-ray studies of randomness in various materials, (5) light scattering in polymer solutions, and (6) the nature of inorganic gels.

THE KINETICS OF REACTIONS IN SOLUTION

Second edition. By E. A. Moelwyn-Hughes. Pp. 424. Oxford University Press, London, 1948. Price $8.50.

Advances made in the field between the publication of the first edition (1933) and the outbreak of war are included in this revision. The nature of the interaction energy is the basis of the classification of chemical reactions. Emphasizing experimental rather than theoretical aspects, the author devotes chapters to catalysis, equilibria, the frequency of molecular collisions, and to high pressure experiments. Statistical formulation of velocity constants is dealt with in an appendix. Author and subject indexes are included.

General Physics Texts

FROM GALILEO TO THE NUCLEAR AGE

By Harvey Brace Lemon. Pp. 451+xviii. University of Chicago Press, Chicago, 1946. Price $5.00.

This is the second and revised edition of *From Galileo to the Cosmic Age*. Chapters have been rewritten and new material added in this humanistic, but authoritative, approach to the study of physics.

INTERMEDIATE PHYSICS

Third edition. By C. J. Smith. Pp. 1033+xii. Edward Arnold and Company, London, and Longmans, Green and Company, Inc., New York, 1947. Price $5.00.

In this third edition of his textbook, the author attempts to explain the more elementary parts in greater detail, adds material, dealing with advanced work, and gives definitions and dimensionally correct equations. The portions of the chapters considered above elementary needs are in small print, and may be omitted by the instructor. The book covers general properties of matter, heat, optics, acoustics, electricity and magnetism. Problems are to be found at the end of each chapter, and answers printed on a separate sheet at the end of the book. Tables of trigonometric ratios and logarithms of numbers are included.

COLLEGE PHYSICS

Fourth edition. By Arthur L. Foley. Revised by J. L. Glathart. Pp. 703+xvi. The Blakiston Company, Philadelphia, 1947. Price $4.25.

A slight rearrangement of material and major revisions, notably in the first three chapters, have been made in this well-known text for liberal arts physics courses. New chapters have been added in modern physics, covering the quantum theory, radioactivity and atomic energy. Illustrative problems have been included in the text. Problems for selected chapters are at the end of the book.

COLLEGE PHYSICS

By E. F. Burton, H. Graydon-Smith, and F. M. Quinlan. Pp. 724+xxvii. Pitman Publishing Corporation, New York, 1948. Price $4.50.

The authors, members of the faculty of the University of Toronto, have designed this book for the college student who will not specialize in the sciences. However, fundamental concepts are completely dealt with and mathematical developments of physical theory given in full when they are within the scope of second-year students. Chapters on modern physics are added to the latter part of the book without disturbing the usual order of classical physics. Material of interest in medicine and household science has been fully developed. It includes detailed table of contents and index.

ESSENTIALS OF APPLIED PHYSICS

By Royal Merrill Frye. Pp. 322+xi. Prentice-Hall Inc., New York, 1947. Price $4.35.

More concise than the average physics text, this book is designed for the evening engineering college, where physics is a prerequisite for other courses. Following the usual arrangement of mechanics, sound, heat, electricity, and light, the material is presented without the use of calculus. An appendix provides the minima of algebra, geometry, and trigonometry. The author uses the electron current, mKS system, and the kilogram-calorie throughout.

COLLEGE TECHNICAL PHYSICS

By Robert L. Weber, Marsh W. White, and Kenneth V. Manning. Pp. 761+x. McGraw-Hill Book Company, Inc., New York, 1947. Price $4.50.

A text for science and engineering students at the college level. The basic ideas of physics are developed in the classical order. Algebra and trigonometry are used, but concepts of calculus are avoided. Solved examples are given, with the English system of units being stressed. A

summary concludes each chapter, with questions for class discussion. The appendix provides a brief discussion of trigonometric functions and a systematic plan for the solution of problems.

History, General Science, and Meteorology

COMBAT SCIENTISTS

By Lincoln R. Thiesmeyer and John E. Burchard. Edited by Alan T. Waterman. Pp. 412+xviii. Little, Brown and Company, Boston, 1947. Price $5.00. Science in World War II Series.

The story of the Office of the Field Service of the OSRD, and especially the work of the scientists located in all the theaters of combat during the war; their problems, solutions, and battles with the necessary military "red tape." Written authoritatively by men who were themselves combat scientists, this book will be enjoyed by those who served this branch at home or abroad, and all other readers who want the story behind the scenes. A personnel index is included.

NEW WEAPONS FOR AIR WARFARE

Edited By Joseph C. Boyce. Pp. 292+xviii. Little, Brown and Company, Boston, 1947. Price $4.00. Science in World War II Series

Radar fire-control equipment, proximity fuzes for rotating projectiles, rockets, bombs and mortars, and guided missiles are discussed in this comprehensive technical account of work done under the supervision of the Office of Scientific Research and Development. The book is written in an interesting, readable style.

THE STRANGE STORY OF THE QUANTUM

By Banesh Hoffman. Pp. 239+xi. Harper & Brothers, New York, 1947. Price $3.00.

"An account for the general reader of the growth of ideas underlying our present atomic knowledge." From the beginnings of the quantum theory the author traces the development of atomic research, introducing the work of Planck, Bohr, and others, and gives an historical sequence leading to nuclear fission. It is for popular consumption and deals primarily with personalities rather than mathematical principles.

THE EVOLUTION OF MODERN PHYSICS

By Carl Trueblood Chase. Pp. 203+ix. D. Van Nostrand Company, Inc., New York, 1947. Price $2.50.

This history of the development of physical thought from the earliest theories and experiments to conjectures on trends in the future does not include purely mathematical investigations, astronomy, or philosophical and theological aspects. It will have some appeal for the engineer as well as the layman because of the non-technical development of the physical sciences.

THE PROBLEM OF REDUCING VULNERABILITY TO ATOMIC BOMBS

By Amley J. Coale. Pp. 116+xvi. Princeton University Press, Princeton, New Jersey, 1947. Price $2.00.

Originally prepared for the Committee on Social Aspects of Atomic Energy, this information is now addressed to the general public. In simple, non-technical language, it explains the many problems of present and future defense, technical considerations involved, and the need for further research. A definite solution is not attempted, but the questions that must be answered are fully analyzed.

TIME, KNOWLEDGE AND THE NEBULAE

By Martin Johnson. Pp., 189. Dover Publications, Inc., New York, 1947. Price $2.75.

"An introduction to the meanings of time in physics, astronomy, and philosophy, and the relativities of Einstein and of Milne." The author surveys the backgrounds leading to modern concepts of "physical time," stressing Milne's new Relativity and explaining the problems confronting philosophy in formulating the question of the reality of time in human destiny. A background in mechanics, electronics, etc., is furnished in an appendix.

GERMAN RESEARCH IN WORLD WAR II

By Leslie E. Simon. Pp. 218+xi. John Wiley and Sons, Inc., New York, 1947. Price $4.00.

"An analysis of the conduct of research" by the Germans, the book is written by the Director of the Ordnance Department's Ballistic Research Laboratory (U.S.). In summarizing important projects, especially in ballistics, fire control and aerodynamics, the author reveals the lack of coordination between civilian and military research. He believes the development of rocket weapons and the gas-turbine to be their most outstanding achievement, but also describes work on wind, super guns, wind tunnels, tanks, and the use of sound as a weapon.

YALE SCIENCE: THE FIRST HUNDRED YEARS, 1701-1801

By Louis W. McKeehan. Pp. 82+x. Henry Schuman, Inc., New York, 1947. Price $2.50.

A survey of science and scientists at Yale, tracing their development through the first century of the college. The author, an authority on the history of magnetism and electricity, is Director of the Sloane Physics Laboratory.

TROPICAL AND EQUATORIAL METEOROLOGY

By Maurice A. Gardell. Pp. 237+xvi. Pitman Publishing Corporation, New York, 1947. Price $12.00.

The author has expanded a group of lecture notes to include the latest concepts and findings. The first part of the book presents a comprehensive survey of fundamental aspects of meteorology and new theories. An interpretation of typical weather phenomena in the tropical regions is

dealt with in the second part. Numerous maps, charts, and graphs are included, with mathematics being kept to a minimum.

TECHNIQUES OF OBSERVING THE WEATHER

By B. C. Haynes. Pp. 272+xvi. John Wiley and Sons, Inc., New York, 1947. Price $4.00.

Mr. Haynes is Chief, Observations Section of the U. S. Weather Bureau, and has written this book for all non-technicians who watch the weather as an occupation or hobby. It is suitable for high school or college courses. It is simple and readable. Many photographs and diagrams accompany the explanatory text.

METEOROLOGY FOR ALL

By Irving Kohn. Pp. 162+vii. Barnes and Noble, Inc., New York, 1946. Price $2.00.

Here is a small volume written in a popular, easily readable style giving facts about the atmosphere, air travel, weather forecasting, clouds, wind, storms, and how to read a weather map. The print is large and many diagrams and charts will help the reader understand the text.

PATENT NOTES FOR ENGINEERS

Pp. 165+vi. Radio Corporation of America, Princeton, New Jersey, 1947. Price $2.50.

This is the first volume of a new Engineering Book Series which will present material of a less technical nature than that now covered in the Technical Book Series published by the RCA Laboratories. Chapters deal with statutory invention, records of invention, prosecution of patent applications, interferences, ownership and use of patents. The procedures, terms, and legal aspects of patents are fully treated. Many illustrative cases are cited to help explain the text.

SUMMARY OF TECHNICAL AND PATENT ASSETS

Pp. 223+xv. Phillips Petroleum Company, Bartlesville, Oklahoma, 1948.

A list and description of the technical and patent assets of the company, including motor fuels, chemicals, synthetic rubber, lubricants, oil and gas production, etc. An index of patents and patentees is given.

New Booklets

Andrew Technical Service, 111 East Delaware Place, Chicago 11, Illinois, recently announced publication of the following new bulletins: No. 7481, *Timing Devices*, No. 7482, *Hot Plates*, No. 7483, *Tumble-Jars*, and No. 1482, *Voltage Control Apparatus*.

Electrical Testing Laboratories, Inc., 2 East End Avenue, New York 21, New York, publishes at intervals a 4-page bulletin called *The ETL M-ode*, of interest to power enterprises and manufacturers.

Dow Corning Corporation, Midland, Michigan, recently issued a 16-page pamphlet entitled *Dow Corning Silicone Mold Release Agents*. Available upon request.

Bausch and Lomb Optical Company, Rochester 2, New York, has published a new catalog describing Model L of its photomicrographic equipment. 24 pages.

Corrosion Publishing Company, Pittsburgh 12, Pennsylvania, has published the Proceedings of the Pittsburgh International Conference on Surface Reactions, held June 7–11, 1948. 236 pages. $6.50 for those attending the Conference; to all others, $10.00.

Here and There

Personnel

M. J. Kelly, Executive Vice President of Bell Telephone Laboratories, Inc., has been named chairman of the newly constituted Committee on Navigation, which was formed after a six-months study by the Research and Development Board of over-all problems related to land, marine, and air navigation.

Ladislaus Marton, who as Chief of the Electron Physics Section is in charge of electron-optical research at the National Bureau of Standards, spent the summer in Europe surveying current work in the field of electron microscopy.

Necrology

Harry Diamond, Chief of the Electronics Division of the National Bureau of Standards, died suddenly at his Washington home on June 21, at the age of 48.

Symposium on Luminescence

The Electronics Division of the Electrochemical Society is making preparations for a symposium on luminescence, to be held during its meeting in Philadelphia, May 5 to 7, 1949. This will be the fourth meeting of its kind sponsored by the Society. Interested persons are invited to attend and to take part in the discussions. Anyone wishing to contribute a manuscript should send it to Dr. R. M. Burns, Secretary, The Electrochemical Society, 235 West 102 Street, New York 25, New York, before January 15. The title and abstract should be submitted by December 15, 1948. Additional information about the symposium can be obtained from H. C. Froelich, General Electric Company, Nela Park, Cleveland 12, Ohio.

Foundry Congress

The 1941 Foundry Congress of the American Foundrymen's Society, international technical organization of the castings industry, will be staged in St. Louis, May 2–5, 1949.

Physics Fellowships

The Microwave Laboratory of the Physics Department, Stanford University, announces a number of fellowships, research assistantships, research associateships, and post-doctorate research associateships available for the academic year 1948–1949. For information and application address Professor William W. Hansen, Director, Microwave Laboratory, Stanford University, Stanford, California.

Conference on Electronic Instrumentation in Nucleonics and Medicine

A conference on electronic instrumentation in nucleonics and medicine sponsored jointly by the American Institute of Electrical Engineers and the Institute of Radio Engineers will be held at the Engineering Societies Building, 29 West 39th Street, New York, November 29–December 1, 1948.

Variable-Resistance Spring Transducer

A highly sensitive mechano-electrical transducer, which transforms slight displacements into large changes of resistance, current, or voltage, is being developed by W. A. Wildhack and his associates of the National Bureau of Standards. The active element of the device is a helical or conical spring wound in such a way that the initial tension varies slightly along its length. Thus, when the ends of the spring are pulled apart, the turns separate one by one rather than simultaneously.

When the spring is entirely closed, it has an electrical resistance approximately that of a cylindrical tube. When it is completely open, its resistance is that of the total length of the coiled wire. Resistance can thus be varied over a wide range by stretching the spring. As the percentage change in resistance may be hundreds of times greater than the percentage change in length, displacements as small as 1/100,000 of an inch can be easily measured without the use of electrical amplifying devices. The spring transducer thus provides a sensitive means for conversion of any mechanical displacement to a change in an electrical quantity that can be precisely determined. When connected to another transducer which gives a mechanical displacement output (a bimetallic strip responding to temperature changes, for example), the combination gives an easily measurable electrical output. This type of use suggests numerous scientific and industrial applications, including strain gauges, pressure elements, accelerometers, electric weighing devices, automatic temperature controls, d.c.-a.c. inverters, and voltage regulators.

The preferable construction for the transducer is a four-arm bridge of which each arm is a variable-resistance spring. An increase in applied tension elongates one pair of springs and shortens the other pair. The resistive unbalance of the bridge, as indicated by a galvanometer, thus gives a measure of the displacement that has occurred. With this arrangement, since the voltage can be nearly reversed through the bridge, the output voltage can be theoretically twice the input voltage.

The variation of the initial tension of the spring along its length may be accomplished in several ways: by conical winding, by varying the angle of feed of the wire on a uniform mandrel, or by varying its tension as it is wound. For greatest sensitivity the variation in initial tension is made quite small. To decrease contact resistance between successive turns of the closed spring, a high average initial tension is built into the spring, and the turns are coated with 0.0001 inch of gold. Thus far, nickel-alloy wire has been mainly used, because of its high resistivity and small change of mechanical properties with temperature.

The new transducer is undergoing further development at the National Bureau of Standards as part of a project on basic instrumentation for scientific research supported by the Office of Naval Research.